DETECTION AND ATTRIBUTION OF CARBON CYCLE PROCESSES FROM ATMOSPHERIC O_2 AND CO_2 MEASUREMENTS AT HALLEY RESEARCH STATION, ANTARCTICA AND WEYBOURNE ATMOSPHERIC OBSERVATORY, U.K.

BY

THOMAS BARNINGHAM

A THESIS SUBMITTED IN PARTIAL FULFILMENT OF THE REQUIREMENTS FOR THE DEGREE OF

DOCTOR OF PHILOSOPHY

UNIVERSITY OF EAST ANGLIA, U.K.

SCHOOL OF ENVIRONMENTAL SCIENCES

2018

For Mum, Dad, Laura and Chris

And the dogs…

ABSTRACT

Atmospheric oxygen (O_2) measurements represent an important tool for investigating carbon cycle processes that determine the magnitude of the fluxes of carbon dioxide (CO_2) to and from the atmosphere. By combining atmospheric O_2 and CO_2 measurements, one can derive the tracer Atmospheric Potential Oxygen, (APO = O_2 +1.1CO_2) which is a conservative tracer with respect to terrestrial O_2 and CO_2 exchange processes and therefore primarily represents ocean exchange processes.

The primary aim of this research was to assess the spatial and temporal variability of atmospheric O_2, CO_2 and APO at two contrasting locations: The Halley Research Station, Antarctica and the Weybourne Atmospheric Observatory, U.K. The measurements collected at Halley were made possible by establishing a high precision, continuous, *in situ,* atmospheric O_2 and CO_2 measurement system at the station, which I built, tested and installed as part of this research. The aim of the new measurement system was to fill in the observational O_2 gap in the South Atlantic sector of the Southern Ocean; a key region with respect to the global oceanic sink for anthropogenic CO_2 emissions.

At the Weybourne Atmospheric Observatory, I have extended and re-evaluated an existing atmospheric O_2 and CO_2 measurement record (2008-2015). The inter-annual variability of the seasonal cycles and growth rates of atmospheric O_2, CO_2 and APO were examined to assess the temporal variability of the carbon cycle processes that control them. The data were also compared to other O_2 monitoring stations in the northern hemisphere to understand the spatial variability of the processes.

Throughout this thesis, I have used a range of analysis techniques, including model-observation comparisons, to assess what drives the variability of atmospheric O_2, CO_2 and APO observed at these two locations.

TABLE OF CONTENTS

List of Figures

List of Tables

PREFACE

I have been incredibly fortunate to have spent some of my time in the last four years working in two atmospheric observatories in very contrasting, yet equally beautiful, locations:

The Clean Air Sector Laboratory at the Halley Research Station, Antarctica, looking south towards the Hinge Zone, where land ice leaves the continent and forms the floating Brunt ice shelf, upon which the station sits.

The Weybourne Atmospheric Observatory on the North Norfolk coast of the United Kingdom, looking west along the coast that borders the North Sea.

I will cherish the memories of my time spent in these places; working with the people who make the atmospheric measurements possible, and enjoyable, for the rest of my life.

ACKNOWLEDGEMENTS

There are many people I wish to thank who have helped me over the last four years as I have undertaken this Ph.D. research. However, for me, this thesis represents the culmination of ten years of study within academic institutions. There are therefore a couple of people I must thank first who ultimately, and probably unknowingly, set me on the path to where I am now.

Firstly, I began my academic career at the University of Edinburgh studying for a BSc in Environmental Geoscience. I was fortunate enough to have been assigned an inspiring supervisor: Thor Thordarson, an Icelandic volcanologist now at the University of Iceland. I went to him with the naïve and rather lofty idea of doing my undergraduate thesis on methane ebullition from the permafrost regions of northern Siberia. Clearly a little more than young undergraduate student could handle, he instead persuaded me to undertake a study of environmental and climatic change in Iceland by examination of soil profiles dated with tephra deposits from the multitude of eruptions on the island. This was my first real insight into what it takes to plan and implement fieldwork research in an unforgiving environment. I enjoyed every single minute of it.

Upon completing my degree and at a loss of what to do next, Thor kindly took me under his wing and gave me a job as a research assistant to him. It is through working with him that I learnt the importance of gathering careful and detailed observations of the natural world in order to understand the processes that underpin it. Through fieldwork and laboratory work, Thor was the one who made me realise that I could go on and make a career in scientific research. Although I came close to following a volcanology research path, I ultimately decided to again go back to university and study for a Master degree that would open up the world of climate sciences to me; an interest I had held throughout my undergraduate studies.

Consequently, the second person I must thank is Claire Reeves at the University of East Anglia (UEA). I later learnt during my Ph.D. research that Claire was on the selection panel for the awarding of the Simon Wharmby Postgraduate Scholarship in Environmental Sciences, which I was offered upon my application to the university. This scholarship is one of the reasons I chose to come to UEA to undertake further study and has hence led me on to where I am now. Claire subsequently joined my supervisory panel for my Ph.D. and she always provided the encouragement and reassurance that the research I was doing was scientifically sound. I also had the pleasure of playing with and

against her in our lunch time football sessions. I see her as one of the key people in my development as a researcher, even if she was not always directly involved in my work.

I also wish to thank the other members of my supervisory team. Firstly, Parv Suntharalingam. I've had many discussions with Parv on the modelling aspects of climate science. Given that my thesis research was primarily measurement based, the addition of the modelling knowledge that Parv provided was very welcome. In particular, she checked over my interpretation of the model output presented in Chapter 4 of this thesis. I am grateful for the comments and reassurance she gave.

Secondly, I must thank Anna Jones and Neil Brough of the British Antarctic Survey (BAS).I first met Anna and Neil at a greenhouse gas measurement meeting at Royal Holloway in London. The focus of this meeting was to build collaboration between institutions that make measurements within the vicinity of the Atlantic Ocean region. It was at this meeting that I first learnt about the Clean Air Sector Laboratory at the Halley Research Station, Antarctica that both Anna and Neil are responsible for. Consequently, it was from this meeting that I proposed that I install the O_2 and CO_2 measurement system at the CASLab, given its ideal location with respect to the Southern Ocean. It is through many meetings and discussion with Anna and Neil that it became logistically feasible to install at Halley. Their guidance and encouragement throughout the whole process was most welcome.

The installation at Halley was made possible by so many people within BAS that are too numerous to mention: The logistical team, for arranging shipment of my equipment to the base via the RRS Ernest Shackleton; the Estates team, who are responsible for keeping the base operational; and the science team, who performed the weekly and monthly maintenance tasks on the measurement system throughout the 2016 Antarctic winter. In particular, I must thank Amy Corbett, who was the primary person responsible for my system and who was in constant contact with me detailing various issues relating to power downs and such.

The time I spent at Halley was one of the most enjoyable experiences of my life and every single member of the 2015-2016 summer team I must thank for making it so. I made many friendships during my time there. Now, upon the completion of this thesis, I will begin working for BAS as the new wintering atmospheric scientist. I am looking forward to maintaining many of those friendships, both personal and professional, in the coming years.

Here at UEA, there are many people I must thank who have both helped me in some aspect of my work and have kept me smiling through what seems like an incredibly long four year journey. Firstly, I must thank Phil Wilson, Andy Macdonald and Ben Mcleod. Phil was finishing his own Ph.D. research as I began studying for my Master's degree at UEA. He subsequently worked for a year in our research group as a postdoc before going on to assume a role as a departmental technician. His expertise on the theory and design of the measurement system were most helpful in the first year of my research and he also filled the calibration cylinders for the system installed at Halley.

Andy has always been a help with various logistical aspects of my work throughout the last four years, whether it be arranging shipment of cylinders or ensuring I had the correct personal protective equipment whenever I did fieldwork at the Weybourne Atmospheric Observatory or elsewhere. Ben, on the other hand, only joined our group a year ago, yet in that time he has worked hard filling cylinders for me and so I must also thank him.

When I was working out at Weybourne it would often be with the Observatory Manager, Grant Forster. Grant has an incredible sense of humour that always kept me grounded when aspects of the research were getting tough. I hope I will collaborate with him in future as the Weybourne Atmospheric Observatory grows and becomes an ever more impressive research facility. This is in no small part thanks to the work Grant does.

James France is another person I have enjoyed getting to know and working with over the last two years that he has been with us a UEA. In particular, James gave me a quick last minute statistics 101 that gave me confidence in the significance of some of my results. James will also be working at BAS over the next few years and so I look forward to working with him again.

With respect to the build and testing phase of the measurement system, I learnt a great deal from Alex Etchells, Nick Griffin and Dave Blomfield. The knowledge I have gained in the last four years with respect to fault finding on my measurement system is down to them. We'd often spend afternoons together on a "quest" to determine what was behind a particular technical issue Furthermore, Nick was responsible for the building of the electronics box that is critical in the automation of the system and so a great deal of thanks must go to him. Alex, on the other hand was responsible for writing the software that controls the automation and without his expertise this project would never have been possible.

Alex also deserves a particularly special mention. Throughout the last four years Alex has become a close friend of mine. He joined me on my voyage to Antarctica to install the measurement system. Not only was I grateful for his expertise as an I.T. (International Troubleshooter…) specialist when installing at Halley, I was also grateful for his companionship. We shared an incredible experience together that was full of laughter and he is someone that I will always look up to and seek advice from as I continue in my professional career. In the latter stages of my Ph.D. he also kept me sane as we sometimes went out for a cheeky beer at lunchtime on Fridays, thereby helping to alleviate the end of week exhaustion.

I have been lucky to have been a part of an excellent research group in my time at UEA: the Carbon Related Atmospheric Measurement Lab (CRAM Lab) whom Andrew Manning is responsible for. Within our small group, I must firstly thank Marica Hewitt. Although not a researcher herself, she is the one who makes it all happen. She has helped with all of the logistical aspects of my work, from chasing up orders that had gone astray, to sorting out insurance for my equipment and further informing me when something had gone awry on the measurement system at Weybourne. She is a wonderful person to work with and some of the Maltese culinary delights she often brought in to work were always welcome.

With respect to my research, the only person who has had a similar experience to me is Penelope Pickers. Penelope began her Ph.D. a year before I did with a similar goal: to build, test and install an automated atmospheric O_2 and CO_2 measurement system on a cargo ship that crisscrosses the Atlantic Ocean. Penelope's advice on all aspects of my work has always been welcome and she provided a brilliant sounding board for my own ideas and understanding of our research topic. I hope to collaborate further with her in the future.

There are many other people I have collaborated with throughout my time at UEA whom I must also thank. Firstly, Ingrid van der Laan-Luijkx, who provided the CarbonTracker 2016 Halley model output to me. She always answered my emails with the many questions I had on the model set up and I hope to collaborate with her further in this area in the future. Secondly, I must also thank her husband Sander van der Laan. He worked with our research group form a far in the Netherlands, but he joined us occasionally for field work and conferences. I always appreciated his enthusiasm for our science and his humour.

I must also thank Sara-Mikaloff-Fletcher who provided the Earth System Model output presented in Chapter 4 to me. Again, Sara also took the time to answer many of my email questions on the topic and gave me the encouragement to take the modelling work further. The same goes for Britton Stephens and Gordon Brailsford. Britt has provided encouragement and also answered many O_2 related questions, whilst Gordon is someone who helped calm my nerves before my first presentation at the APO workshop at the Scripps Institution of Oceanography in September 2015. I look forward to working closely with all three of them in the future as I progress my atmospheric O_2 research.

Outside of university, there are many friends who have kept my feet on the ground and who have provided many endless nights of entertainment. In particular, I must thank the friends I first made at The University of Edinburgh, the majority of whom now live down in London. I often visited them every now and again for a catch up, a yoga session, a bike ride, a music festival, a camping trip or just a good-old afternoon pub session. They have always provided a welcome respite from my research, even if the following Monday mornings were a little hard to bear in the office.

The same goes for the friends I first made in Norwich when I moved here five years ago. In particular, the friends I made whilst working at Pizza Hut and although I don't work there now, I still regularly see many of them. The friends I made at university are too numerous to mention, but they know who they are and they will no doubt be celebrating with me when I finally hand in this thesis. I must however, give special mention to my two house mates and fellow Ph.D. researchers, Osgur and Rich. In many ways we have shared this Ph.D. journey together despite us all researching very different topics. From our mid-week Champions League football sessions, to the Saturday morning fry ups and the Sunday evening Pizzas, these are two friends that I know I have made for life. Although, we are all beginning to go our separate ways now that our research has finished, I know that we will make the effort to see each other and stay in touch, and this means a great deal to me.

The biggest thanks of all must go to my Ph.D. supervisor Andrew Manning. It was Andrew's Carbon Cycle and Climate Change course that I took during my Masters degree that inspired me to take up a Ph.D. position with him in this areas of research. Andrew's knowledge and enthusiasm for the subject really shone through during those lectures and has continued to do so in my time working with him. His technical expertise and knowledge of the components that go into to an atmospheric O_2 measurement system really are second to none. I am grateful that some of these expertise have now been passed

on to me. Despite his incredibly hectic schedule, he would always find the time to answer my questions and guide me through what has been a demanding four years of research. I am grateful for the times when I would go to his office with a quick five minute question, only to find myself still there two hours later, as he would explain the details and many nuances of atmospheric O_2 research (although I'd often leave the office not knowing what I had initially gone in there for…). I have enjoyed working for Andrew immensely over the last four years and I look forward to future collaborations with him.

Finally, I must thank the most important thing to me in my life, my family, to whom this thesis is dedicated. It has been a long ten years since I left home to begin my academic career. In that time I have seen my little sister, Laura, grow up and become incredibly well established within her own career. She has married a wonderful, loving and kind husband, Chris, who is now an integral member of our family. Throughout the last ten years and in the nineteen years prior to that, my Mum and Dad have always been there for me, no matter what. Coming home to them in the Dales is always something that I cherish. I am able to put my mind at ease and forget about the things that bother me in my professional life, simply relax and enjoy being their Son. The university life is something of an alien experience to them and I've always enjoyed explaining the many ups and downs that it has brought and I know they have enjoyed the fact that they have been able to live it through me. They never pushed me to follow a certain path, but instead encouraged, guided and supported me to find my own way in life. They have always encouraged me to do what I enjoy, try my hardest and just simply do my best. Regardless of how great or small the task ahead is, that is all that I can ever ask of myself. Over the last four years, the task has been this thesis. This is the result.

CHAPTER 1 INTRODUCTION TO ATMOSPHERIC O_2 AND THE GLOBAL CARBON CYCLE

1.1. The global carbon cycle

The global carbon cycle **(Figure 1.1)** consists of four major reservoirs: the atmosphere, the oceans, the terrestrial biosphere and the geosphere. Carbon exchanges between these reservoirs on timescales that range from between a few hours (e.g. photosynthesis) to many millions of years (e.g. the sedimentation of organic matter on the seabed and its subsequent subduction into the Earth's interior) (Berner, 1998). The carbon cycle is intimately linked to global climate due to the properties of the major atmospheric carbon species: primarily carbon dioxide (CO_2) and to a lesser, but still significant extent, methane (CH_4), carbon monoxide (CO) and the halocarbons.

During the 19th century, at a time when scientists were first grappling with the theory of the Ice Ages and what may have caused them, Joseph Fourier (1827) calculated that the Earth was warmer than it should be based on a simple radiation balance and he assumed that this must be owing to some property of the atmosphere. John Tyndall (1864) built upon Fourier's work and was the to first consider the radiative effects of atmospheric CO_2 (that is, its ability to absorb and subsequently re-emit long-wave, infrared radiation) upon the surface temperature of the Earth. This is commonly referred to as the 'greenhouse effect' and is also caused and amplified by other atmospheric constituents; primarily water vapour, CH_4 and nitrous oxide (N_2O). The greenhouse effect is critical to the habitability of Earth and results in an average surface temperature of ~15°C; without it the surface temperature would be closer to -18°C (Hansen et al., 1984). The average surface temperature of the Earth throughout geological history, however, has been far from constant (e.g. Zachos et al., 2001). Even seemingly miniscule variations in the relative abundance of the major greenhouse gases have the ability to significantly alter the temperature of the planet.

Analysis of ice core records from the Vostok ice core, Antarctica, have shown the co-variation of atmospheric CO_2 mole fraction and surface temperature through the glacial-interglacial cycles of the Quaternary period (~2.6 – 0.01 Million years ago (Ma)) (Petit et al., 1999; Siegenthaler et al., 2005). Both temperature and the CO_2 mole fraction fluctuated with periodicities between 20 and 100 thousand years (ky) as a result of natural, orbital induced changes to the amount of solar radiation reaching the Earth's surface (Milankovitch, 1941). Although these initial changes in temperature were forced by changes in solar radiation reaching the Earth's surface, the magnitude of the total temperature change between these orbital cycles cannot be accounted for unless they are

amplified by changes to the relative abundance of greenhouse gases, which are controlled by complex carbon-climate feedback mechanisms (for a review, see Sigman and Boyle (2000)). The CO_2 mole fraction was relatively low during the glacial periods (180 parts per million (ppm)) and relatively high during inter-glacial periods (280 ppm) (Siegenthaler et al., 2005). The Southern Ocean in particular is believed to have exerted a critical control over these glacial-interglacial atmospheric CO_2 variations, through changes to both the rate at which the deep ocean is "ventilated" and in the pervasiveness of biological productivity within the region (Watson and Naveira Garabato, 2006).

Following the end of the last glacial (~11.7 ky ago), atmospheric CO_2 remained relatively stable, varying between 260-280 ppm throughout the Holocene (Indermuhle et al., 1999). At the beginning of the industrial era (~1750 AD) the CO_2 mole fraction began to rise (Barnola et al., 1995).

Arrhenius (1896) was the first to recognise the influence that the industrial revolution could have on the atmospheric CO_2 mole fraction: "*The enormous combustion of coal by our industrial establishments suffices to increase the percentage of carbon dioxide in the air to a perceptible degree.*", and even made a prediction that a doubling

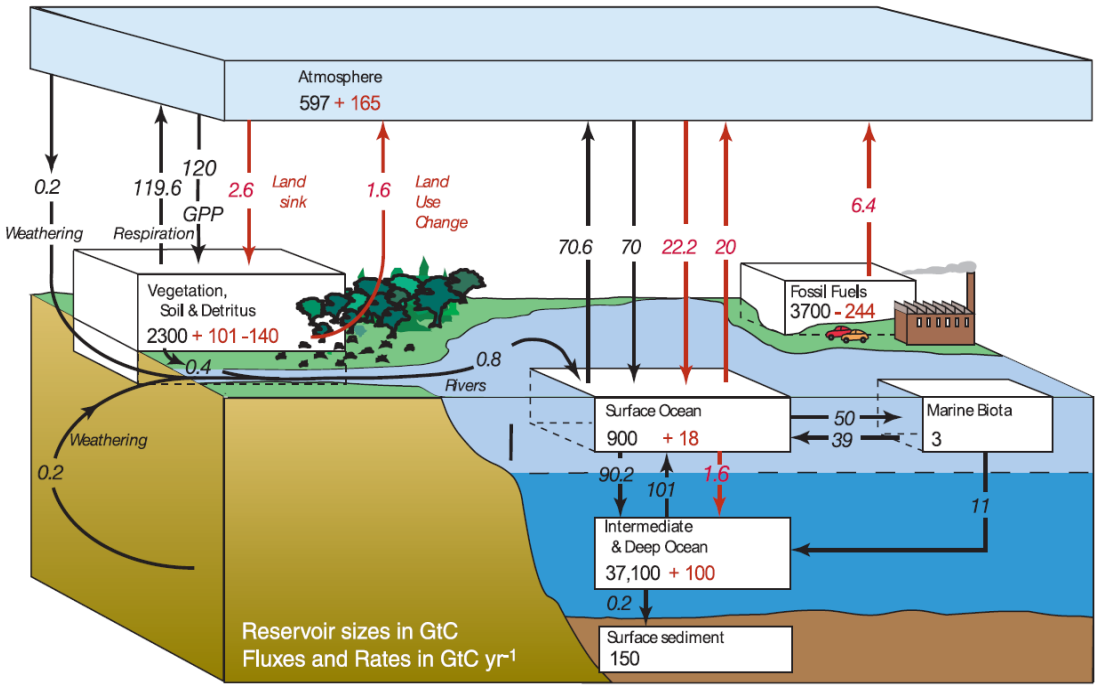

Figure 1.1. The global carbon cycle and the relative fluxes of carbon (C) between the reservoirs in Giga (10^9) tonnes of C (equivalent to Peta (10^{15}) grams of C) per year. Reservoir size (numbers inside the boxes) are given in Pg C. Black arrows and numbers indicate natural fluxes whilst red arrows and numbers indicate anthropogenically induced fluxes (Reproduced from IPCC (2007a)).

of atmospheric CO_2 would lead to an average global temperature increase of 3-4˚C (this is now known as climate sensitivity), but he postulated that this would not occur for another 500 years.

The pioneering predictions of Arrhenius (1896) were not recognised until the first reliable and continuous measurements of atmospheric CO_2 (precision of < 1.0 ppm) were made by Charles Keeling at the Mauna Loa atmospheric observatory, Hawaii, in 1958 (Keeling, 1960). The CO_2 mole fraction was observed to be ~315 ppm with a seasonal amplitude of ~5 ppm (Keeling, 1960). The atmospheric CO_2 mole fraction is now ~407 ppm (2017[1]), fast approaching the "doubled" pre-industrial mole fraction (560 ppm). It is now widely recognised and accepted that this increase is almost entirely due to the burning of fossil fuels, cement production and land use changes, such as deforestation, biomass burning, crop production and conversion of grassland to cropland (IPCC, 2013). The most recent estimates from sophisticated Earth system models of the climate sensitivity lie in the range of 1.5-4.5˚C (IPCC, 2013), making the prediction of Arrhenius (1896) all the more remarkable. The exceptionally high (relative to the last few million years) present-day CO_2 mole fraction has been unequivocally warming our climate over recent decades (0.2˚C decade^{-1}) (Hansen et al., 1997; Hansen et al., 2006; IPCC, 2007b), and will continue to do so unless the above anthropogenic activities are curtailed (IPCC, 2014).

Despite continuous warnings from the scientific community on the potential short-term, centennial scale consequences of rising CO_2 emissions to the Earth's climate system (IPCC, 2001, 2007a, 2014), we appear to be stubbornly sticking to the "business as usual" scenario (CO_2 emissions from fossil fuel combustion and cement production in 2016 = 9.9 ± 0.5 Pg C yr^{-1}) first set out by the Inter-governmental Panel on Climate Change (IPCC) in 1992 (Pepper, 1992).

The atmospheric increase in CO_2 mole fraction however, is much less than that predicted from that of fossil fuel combustion alone (approximately 57% of the expected trend (Gloor et al., 2010)). This is because CO_2 is removed from the atmosphere by the Earth's terrestrial and oceanic carbon sinks (1.27 ± 0.84 Pg C yr^{-1} and 2.50 ± 0.60 Pg C yr^{-1}, respectively for the 10 year period 2000-2010, (Keeling and Manning, 2014b)). The exact magnitude of the sinks vary from year to year due to the inter-annual variability of

[1] https://www.esrl.noaa.gov/gmd/ccgg/trends/global.html

the carbon cycle, which itself will likely be influenced by climate change. If we are to reliably predict future climatic changes, mitigate and adapt to them, it is essential that we characterise and monitor the efficiency of both the terrestrial and ocean carbon sinks' ability to withdraw anthropogenic CO_2 from the atmosphere and further reduce the uncertainty in our understanding of how these sinks will respond to future climatic changes (Le Quéré et al., 2009; Le Quéré et al., 2007).

1.2. The carbon cycle and climate change

In order to understand how the efficiency of both the terrestrial and oceanic carbon sinks will be impacted by future climatic changes, it is firstly important to consider what the natural state of these systems are prior to any anthropogenic influence. **Figure 1.1** shows both the natural and anthropogenic stores and fluxes in and between the Earth's major carbon reservoirs.

1.2.1. The terrestrial carbon cycle

In the natural, pre-industrial state, the terrestrial biosphere fixes CO_2 from the atmosphere via photosynthesis. The total amount of carbon fixed by this process is termed Gross Primary Production (GPP) and equates to approximately 120 Pg C yr^{-1} (Houghton, 2007). However, roughly half of this carbon is returned to the atmosphere via respiration (on daily to annual timescales). The remaining carbon is termed Net Primary Production (NPP, approximately 60 Pg C yr^{-1}). This carbon is then distributed amongst the living plant biomass and within the litter and soils. Again, much of this short-term carbon store is respired back to the atmosphere (~50 Pg C yr^{-1}) through autotropic and heterotrophic respiration. The remaining carbon is termed Net Ecosystem Production (NEP, approximately 10 Pg C yr^{-1}). Much of NEP is then lost through disturbance, such as natural fires, storm damage or pestilence on longer-term timescales. If the terrestrial biosphere is in equilibrium with the atmosphere, then all of the return processes to the atmosphere at the different ecosystem levels will exactly balance GPP.

The influence of the above mentioned processes can be observed in the seasonal cycle of atmospheric CO_2. For example, in the northern hemisphere, where much of the global land mass is distributed, the seasonality of atmospheric CO_2 is particularly evident (e.g. Bolin and Keeling, 1963; Pearman and Hyson, 1980; Randerson et al., 1997). Whereas natural climate variability, such as the El Niño Southern Oscillation (ENSO), can impact on all of the above mentioned levels of carbon storage within the terrestrial

biosphere which can then control the fluxes of carbon to and from the atmosphere on inter-annual timescales. This is evident in the inter-annual variability observed in the rate of change of atmospheric CO_2 (Bacastow, 1976).

Anthropogenic activities have disturbed this natural state through land use change (primarily deforestation) and through the emission of CO_2 to the atmosphere from fossil fuel burning and cement production (IPCC, 2013). As such, the terrestrial biosphere-atmosphere system is no longer in balance, with the terrestrial biosphere currently acting as a carbon sink for anthropogenic CO_2 from the atmosphere (1.27 ± 0.84 Pg C yr^{-1} for the 10 year period 2000-2010) (Keeling and Manning, 2014b).

The influence of anthropogenic CO_2 emissions on the terrestrial carbon cycle can be broadly split into two effects: 1. the direct influence of CO_2 fertilisation on photosynthetic rates (e.g. Schimel et al., 2015; Wenzel et al., 2016) and 2. the influence of climatic change (e.g. temperature and water availability) on photosynthesis (GPP), respiration (NPP and NEP) and disturbance (NBP) (e.g. Nemani et al., 2003; Zhou et al., 2001a). Understanding the impact of these processes on the terrestrial carbon cycle and any subsequent changes to the terrestrial carbon sink is complex. For example, these two influences can have synergistic effects on broader or more specific aspects of the terrestrial carbon cycle such as vegetation dynamics (Forkel et al., 2016) and ecosystem-scale light use efficiency (Thomas et al., 2016).

Coupled carbon cycle-climate models allow investigation of these processes and what effect they may have on the future of the terrestrial carbon cycle under different emissions and warming scenarios (Friedlingstein and Prentice, 2010). Model simulations show that the CO_2 fertilisation effect will increase the amount of carbon stored within the terrestrial carbon sink in the future, whereas the impact of climate change on the biosphere will tend to decrease it (Friedlingstein and Prentice, 2010). There is, however, a large amount of disagreement between the models as to how the efficiency of the net terrestrial carbon sink will evolve in the future (Friedlingstein and Prentice, 2010)

The now relatively long record of global atmospheric CO_2 observations, in conjunction with model simulations and laboratory based experiments, have allowed investigation of the terrestrial carbon cycle response to these anthropogenic changes (e.g. Bacastow et al., 1985; Barichivich et al., 2012; Forkel et al., 2016; Graven et al., 2013; Keeling et al., 1996a; Myneni et al., 1997; Pearman and Hyson, 1981; Piao et al., 2008; Randerson et al., 1997). All of these studies demonstrate an increase in the peak to trough seasonal amplitude of CO_2 in northern latitudes (>45˚N) of up to 50% since the earliest

records began in the 1960's (Graven et al., 2013; Keeling et al., 1996a). Two of these studies also reported an advance of the spring downward zero crossing of approximately 1 week since the 1950's, pointing to an increase in the length of the biosphere growing season in response to spring warming (Keeling et al., 1996a; Myneni et al., 1997). Piao et al. (2008), however, also demonstrated a trend towards an earlier autumn upward zero crossing that was significantly negatively correlated with increasing autumn temperatures, resulting in a shorter carbon uptake period, in contrast to the studies mentioned above. The Piao et al. (2008) work was corroborated by Barichivich et al. (2012), who note that despite the increase in the thermal growing season driven by an earlier spring onset and a later autumn zero crossing day, the increased temperatures in autumn actually lead to an earlier termination in the carbon uptake period. Conversely, more recent work has suggested a weakening temperature control, or at least a decoupling between increasing productivity and temperature.

The contrasting findings on the current state of the terrestrial biosphere, and it's response to current climatic change, indicate a large amount of uncertainty within this subject area and therefore merits further work. Nevertheless, at a fundamental level photosynthesis has an optimum temperature at which the reactions are favoured, whereas the amount of respiration will increase in line with increasing temperatures (Schulze, 2006). If global surface temperatures continue to rise unabated, and ignoring the effects of changes to the hydrological cycle, then one can expect the terrestrial biosphere to become a net carbon source to the atmosphere.

1.2.2. The ocean carbon cycle

In the atmosphere and ocean carbon system (**Figure 1.1**), approximately 600 Pg C naturally resides in the atmosphere whilst approximately 38,000 Pg C resides in the ocean. Thus, 98.5% of the carbon in the atmosphere-ocean system resides in the ocean whilst only 1.5% resides in the atmosphere. Henry's Law states that, at equilibrium, for a weakly soluble gas, such as CO_2, the dissolved concentration ($CO_{2\,(aq)}$) will be proportional to the partial pressure of the gas ($CO_{2\,(g)}$) in the overlying atmosphere. One would therefore expect carbon to be equally distributed between the atmosphere and the ocean. The reason why the distribution is not equal and why the majority of the carbon instead resides in the ocean is due to the chemical properties of CO_2 within seawater.

When CO_2 dissolves in sea water, it rapidly dissociates into bicarbonate (HCO_3^-) and carbonate ions (CO_3^{2-}) **(Equation 1.1)**:

$$CO_{2(g)} \leftrightarrow CO_{2(aq)} + H_2O \leftrightarrow H_2CO_{3(aq)} \leftrightarrow H^+ + HCO_3^-{}_{(aq)} \leftrightarrow 2H^+ + CO_3^{2-}{}_{(aq)} \quad (1.1)$$

The production and consumption of H^+ ions indicate that these reactions have a pH dependence. A Bjerrum plot (**Figure 1.2**) shows the distribution of dissolved CO_2, HCO_3^- and CO_3^{2-} ions (together defined as Dissolved Inorganic Carbon (DIC)) in solution as a function of pH. At a typical pH of seawater (8.2), 86.6% exists as HCO_3^-, 13.0% as CO_3^{2-} and 0.4% as dissolved CO_2. From Henry's Law, therefore, the atmospheric portion of the carbon in the atmosphere ocean system should be the same as the dissolved portion, which suggests that ~3% of the carbon should exists in the atmosphere, and 97% in the ocean (Jacob, 1999). The reason for this difference between the theoretical fraction of carbon in the ocean due to carbonate chemistry (3%) and the observed fraction (~1.5%),

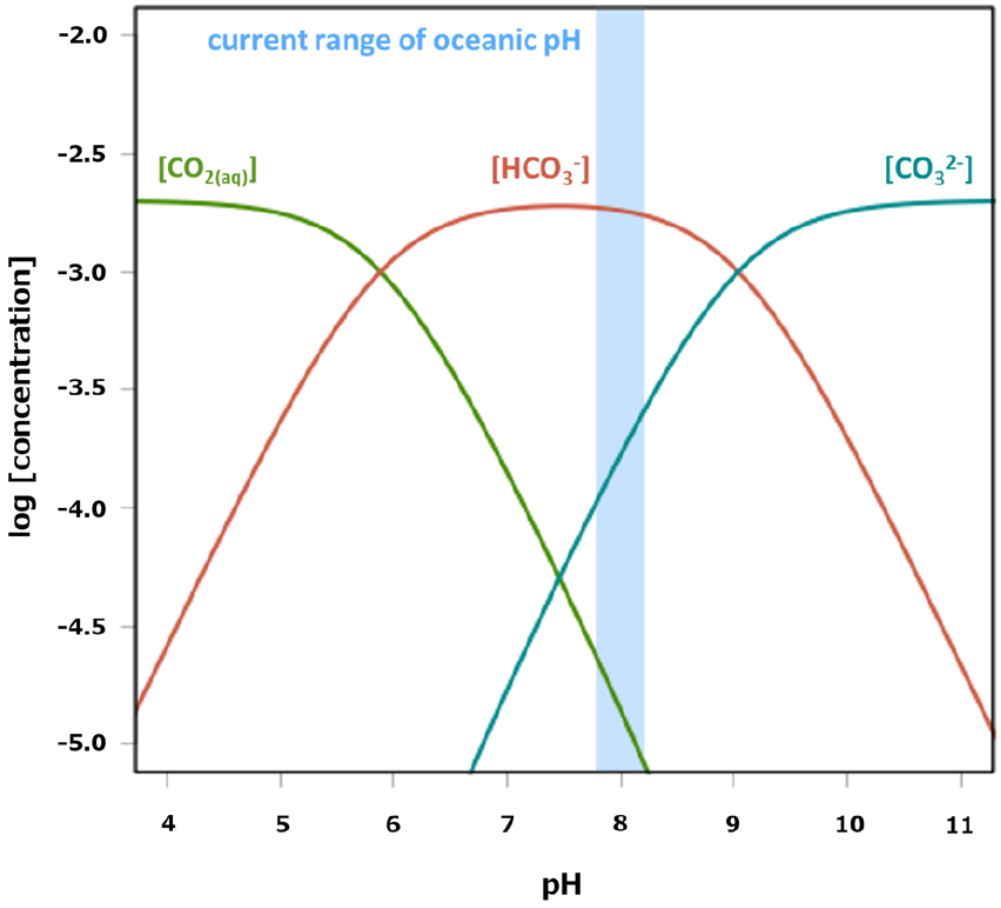

Figure 1.2. A Bjerrum plot showing the relationship between the concentrations of the ions that make up the carbonate chemistry system in the ocean and pH. The current range of oceanic pH is shown by the shaded blue bar (From Heinze et al., 2015).

is due to a combination of ocean circulation and the ocean's solubility and biological pumps.

Deep water formation occurs in the high latitude oceans (e.g.Marshall and Speer, 2012). These waters are relatively cold and the solubility of any gas (including CO_2) is therefore increased. These high DIC waters are then transported to the deep ocean which creates a gradient of DIC from the surface ocean to the deep ocean. This is known as the "solubility pump" and maintains a gradient in DIC that therefore allows more CO_2 to be absorbed from the atmosphere via Henry's Law.

This gradient is also maintained by the "biological pump". There are two biological pumps that oppose each other in the surface ocean. Firstly, primary productivity in the surface ocean consumes $CO_{2\,(aq)}$ converting it into organic carbon (~48 Pg C yr^{-1} (Houghton, 2007)). Most of this carbon is respired back into the surface ocean (~37 Pg C yr^{-1} (Houghton, 2007)). However, when the organisms die, some of this carbon is transported out of the surface ocean into the deep ocean (~11 Pg C yr^{-1} (Houghton, 2007)), either as particulate organic carbon (POC), which following microbial respiration is converted to dissolved organic carbon (DOC) and DIC. This process is known as the soft tissue pump and, with the solubility pump, keeps the deep ocean relatively high in DIC compared to the surface and the consumption of $CO_{2\,(aq)}$ thus allows more $CO_{2\,(g)}$ to be drawn in from the atmosphere than there otherwise would be if the oceans were sterile.

Additionally, the calcium carbonate pump acts to increase the concentration of DIC in the deep ocean through remineralisation. However, in the surface ocean, the calcium carbonate pump acts to increase the concentration of $CO_{2\,(aq)}$ **(Equation 1.2)**. Many marine organisms produce calcium carbonate ($CaCO_3$) shells. The production of these shells and the subsequent increase in $CO_{2\,(aq)}$ when HCO_3^- is consumed is shown by the following equation:

$$Ca^{2+}{}_{(aq)} + 2HCO_3^-{}_{(aq)} \leftrightarrow CaCO_{3\,(s)} + H_2O + CO_{2\,(aq)} \qquad \textbf{(1.2)}$$

Overall, the soft tissue pump dominates in the surface ocean and the net effect is to reduce the concentration of $CO_{2\,(aq)}$ in the surface ocean. The solubility pump is the key process that governs how effectively the ocean takes up anthropogenic CO_2, that is to say, how quickly surface waters are transported and mixed into the deep ocean. When considering the evolution of the anthropogenic ocean carbon sink, one must therefore consider how changes in ocean circulation, temperature and salinity, stratification and ice

cover may impact the efficiency of the solubility pump and hence the efficiency of the ocean as a carbon sink. (Houghton, 2007).

The biological pump does not cause an anthropogenic CO_2 sink in itself (IPCC, 2013) because productivity in the oceans is limited by the availability of nutrients, such as nitrate, phosphate (macronutrients) and trace amounts of iron (micronutrients). However, changes in the biological pump may be brought about by climate change impacts on the ocean, and may therefore affect the ability of the pump to regulate the surface to deep ocean gradient in DIC (IPCC, 2013).

One further key point to consider is the impact of the uptake of anthropogenic CO_2 has on the ocean carbonate system. As anthropogenic CO_2 is absorbed by the ocean, the equilibrium in **Equation 1.1** shifts to the right, increasing the amount of bicarbonate, carbonate and H^+ ions. Importantly, the production of H^+ ions decreases the pH, which then alters the ratio of $CO_{2(aq)}$:HCO_3^-:CO_3^{2-}, such that more of the DIC exists as $CO_{2(aq)}$ (see also **Figure 1.2**) This was first recognised by Roger Revelle and is known as the Revelle Factor or the carbonate buffering effect (Revelle and Suess, 1957). Thus, although the pre-industrial ocean holds 98.5% of the carbon in the combined atmosphere-ocean system, the reduced buffering capacity of the ocean as it takes up more CO_2 means that approximately 80% of anthropogenic carbon will reside in the ocean within the combined atmosphere-ocean system (the exact percentage is dependent on how much fossil fuel is burnt) (Broecker et al., 1979; Houghton, 2007)

1.2.2.1. The Southern Ocean carbon cycle and climate change

The Southern Ocean has long been recognised as a major influence on global climate (e.g. Imbrie et al., 1992; Knox and McElroy, 1984; Siegenthaler and Wenk, 1984; Sigman and Boyle, 2000; Toggweiler, 1999; Watson and Naveira Garabato, 2006). It is unique in terms of its geography, compared to other ocean basins, in that the absence of a land barrier in the vicinity of the Drake Passage (56-65˚S) allows a circumpolar current to exist (known as the Antarctic Circumpolar Current (ACC)) (Toggweiler and Samuels, 1995). The unimpeded flow of the ACC connects all of the Earth's major ocean basins and closes the global meridional overturning circulation (MOC) that is responsible for the storage and transfer of heat, freshwater, nutrients and carbon around the globe (Lumpkin and Speer, 2007).

The Southern Ocean is thought to currently account for ~40% of the net global ocean uptake of anthropogenic CO_2 (~0.7 Pg C yr^{-1}) (Mikaloff Fletcher et al., 2007; Sabine et al., 2004). When attempting to understand the Southern Ocean carbon cycle however, one first needs to consider oceanic transport within the region (**Figure 1.3**). Strong westerly winds that encircle the Antarctic continent exert a significant stress upon the surface of the ocean centred along the axis of the eastward flowing ACC (Rintoul, 2011). To the south of the ACC, Ekman transport creates a divergence that allows the

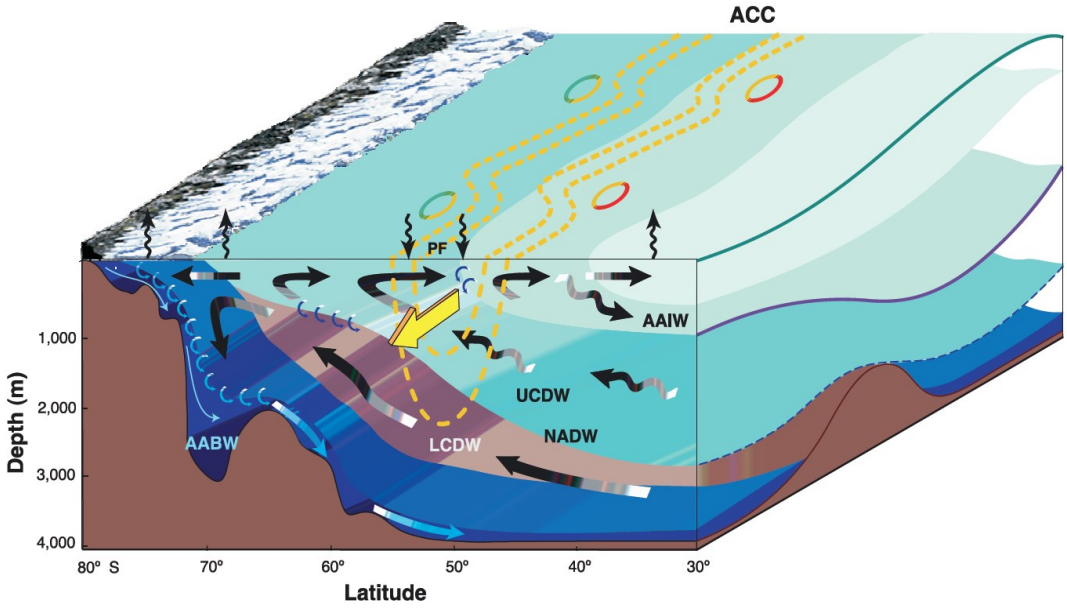

Figure 1.3. Diagram depicting general oceanic transport within the Southern Ocean. Antarctica is shown on the left of the diagram. The eastward flowing ACC is shown by the yellow arrow. Ekman transport causes a divergence at ~ 65˚S that allows the upwelling of Lower Circumpolar Deep Water (LCDW), North Atlantic Deep Water (NADW) and Upper Circumpolar Deep Water (UCDW). As surface waters flow north of the Polar Front (PF) they are subducted as Antarctic Intermediate Water (AAIW). Close to the Antarctic coast, brine rejection in the formation of sea-ice forms Antarctic Bottom Water (AABW). Wiggly vertical arrows at the surface indicate buoyancy loss or gain. Curly arrows along water mass boundaries (isopycnals) indicate eddy mixing (Olbers et al., 2004).

upwelling of deep waters rich in DIC (Rintoul, 2011). Ventilation of these waters at the surface therefore constitutes a significant source of 'natural' CO_2 to the atmosphere (Mikaloff Fletcher et al., 2007). Furthermore, the upwelling of these deep waters brings nutrients, formed by the decomposition of "old" organic matter within the water column, to the surface, stimulating "new" biological production which decreases the CO_2 concentration of the surface waters such that there is a flux of CO_2 from the atmosphere to the ocean (Takahashi et al., 2012). As these waters are transported north of the ACC, Ekman transport is convergent and surface waters are subducted into the ocean interior as Sub-Antarctic Mode Water and Antarctic Intermediate Water (Rintoul, 2011),

sequestering the carbon (Takahashi et al., 2012). It is the formation of these water masses that are thought to constitute the largest contribution to the uptake and storage of anthropogenic CO_2 within the Southern Ocean (0.42 ± 0.2 Pg C yr^{-1}) (Sabine et al., 2004; Sallee et al., 2012).

Monitoring the variability of these ocean processes is an inherently difficult task and even more so given the scarcity of observations in this isolated region of the Earth (Bakker et al., 2016). Consequently, the role of the Southern Ocean in the global carbon cycle and thus climate change is the source of much recent scientific debate (e.g. Landschützer et al., 2015; Law et al., 2008; Le Quéré et al., 2007; Le Quere et al., 2008; Metzl et al., 2006; Roy et al., 2003; Zickfeld et al., 2008).

Le Quéré et al. (2007) using an inverse method combined with observed atmospheric CO_2 mole fractions, concluded that the overall efficiency if the Southern Ocean sink for CO_2 had declined by 0.08 Pg C yr^{-1} $decade^{-1}$ for the period 1981-2004, relative to the trend that would otherwise be expected based on the increased atmospheric CO_2 burden. The model of Le Quéré et al. (2007) suggested that this was due to an increase in the ventilation of natural carbon south of the ACC as a result of strengthening winds over the Southern Ocean that are thought to be the result of human activities (Le Quéré et al., 2007; Shindell and Schmidt, 2004; Thompson and Solomon, 2002). However, both Law et al. (2008) and Zickfeld et al. (2008) contested these findings. The former suggested that the results were very much dependent on both the choice of ocean model and the network of atmospheric CO_2 observations employed (Law et al., 2008). This therefore provides a clear incentive to establish more atmospheric CO_2 monitoring stations in the region, as undertaken by my thesis. The latter argued that the altered Southern Ocean winds, coincident with rising atmospheric CO_2 mole fraction will likely increase (not decrease) the Southern Ocean carbon sink in the 21st century (Zickfeld et al., 2008). Conversely, Lovenduski et al. (2008) using output from hindcast simulations of an ocean circulation model with embedded biogeochemistry, found a similar decrease in the efficiency of the Southern Ocean carbon sink as Le Quéré et al. (2007) and also concluded strengthening of the westerly winds were a likely cause.

The increase in the westerly wind strength has been attributed to a trend towards a more persistent positive phase in the Southern Annular Mode (SAM) (Thompson and Solomon, 2002), which is characterised by a trend toward decreasing atmospheric pressure at the pole and a corresponding increase in pressure over the mid-latitudes. Moreover, atmospheric inverse models (Butler et al., 2007) and ocean biogeochemistry

models (Lenton and Matear, 2007; Lovenduski et al., 2007) suggest anomalous Southern Ocean CO_2 outgassing of ~0.1 Pg C yr^{-1} per standard deviation of the SAM index.

Whilst the above mentioned studies established that the strength of the Southern Ocean carbon sink throughout the decade of the 1990's may have decreased, more recent studies using data from the 2000's have suggested that the sink has now strengthened again (Landschützer et al., 2015; Munro et al., 2015). Using a novel neural network technique to interpolate sparse ocean dissolved CO_2 observations in both space and time within the Southern Ocean regions, Landschützer et al. (2015) confirmed the weakening efficiency of the sink in the 1990s suggested by Le Quéré et al. (2007) but determined that since 2002, the sink has strengthened substantially to a net uptake of ~1.2 Pg C yr^{-1} in 2011. The uncertainty in the future evolution of the Southern Ocean carbon sink demonstrates an imperative to use continuous, *in situ* observations to observe and quantify biogeochemical processes that influence CO_2 exchange between the Southern Ocean and the atmosphere.

1.3. Estimating the terrestrial and oceanic carbon sinks using atmospheric O_2 measurements

Different techniques have been employed to estimate the uptake of anthropogenic CO_2 by both the terrestrial and oceanic carbon sinks. These include the use of surface ocean dissolved CO_2 data (Takahashi et al., 2009) $^{13}CO_2/^{12}CO_2$ data (e.g. Gruber et al., 1996) and the application of inverse atmospheric transport models (e.g. Peylin et al., 2013). Although these techniques provide estimates of both regional and global carbon sinks, they do have their disadvantages. For example, dissolved CO_2 data are sparse, particularly in the Southern Ocean, and are sensitive to gas transfer velocities, which have been shown to be increasingly uncertain at the high wind speeds that are typical in the Southern Ocean (Wanninkhof et al., 2009). Whereas inverse transport models are sensitive to the choice of atmospheric stations used in the model runs, and in the choice of model itself (Law et al., 2008). Another approach to this problem, involves the measurement of atmospheric O_2, as first outlined by (Machta, 1980b). Ralph Keeling advanced these techniques in his first papers on the subject (Keeling, 1988a, b) and in those that followed (Keeling et al., 1993; Keeling et al., 1996b; Keeling and Shertz, 1992).

Keeling (1988b) demonstrated the insight atmospheric O_2 measurements could give to global carbon cycle studies by highlighting the fact that the sources and sinks of

CO_2 and O_2, to and from the atmosphere, are stoichiometrically linked through the oxidation and reduction of organic matter, whereby a sink for O_2 will have a corresponding CO_2 source and vice versa: firstly through the processes of photosynthesis and respiration **(Equation (**1.**3**):

$$\boldsymbol{CO_2 + H_2O \leftrightarrow CH_2O + O_2} \quad \textbf{(1.3)}$$

Where CH_2O is the approximate composition of organic matter, and secondly through combustion of fossil organic matter (i.e. coal, oil and gas) (Keeling, 1988b) **(Equation (**1.**4)**:

$$\boldsymbol{CH_x + \left(1 + \frac{1}{4}x\right) O_2 \rightarrow CO_2 + \frac{1}{2}xH_2O} \quad \textbf{(1.4)}$$

The ratio of the exchange (moles of O_2 consumed to moles of CO_2 released (O_2:CO_2)) depends on the oxidation state of the organic matter in question (Keeling, 1988b). For photosynthesis and respiration this ratio has a value of 1.10 ± 0.05 (Severinghaus, 1995), whereas for fossil fuel combustion the globally weighted average is 1.39 (Manning and Keeling, 2006b) but varies depending on the fossil fuel used (for example, 1.95 for gaseous fuels and 1.17 for solid fuels).

Both O_2 and CO_2 exchange between the atmosphere and ocean too, however the stoichiometric coupling breaks down due to differences in their seawater chemistry and in the timescale of air-sea exchange (Bender and Battle, 1999; Keeling, 1988b; Keeling et al., 1993). When CO_2 dissolves in seawater it rapidly reacts with water to form carbonic acid which then dissociates into bicarbonate and carbonate ions according **Equation 1.1** This reaction, specifically the production of H^+ ions, is the reason for ocean acidification being one consequence of increasing the atmospheric CO_2 mole fraction (Doney et al., 2009). Importantly, this sink for CO_2 does not have a corresponding source of O_2, and the lack of a similar seawater chemistry for O_2 results in a much smaller effective solubility in seawater than for CO_2 (Broecker and Peng, 1982a; Keeling, 1988b) Although CO_2 and O_2 are stoichiometrically linked in marine biological production (Redfield et al., 1963) (O_2:CO_2 = 1.4, (Anderson, 1995)), the resulting changes in seawater CO_2 is heavily

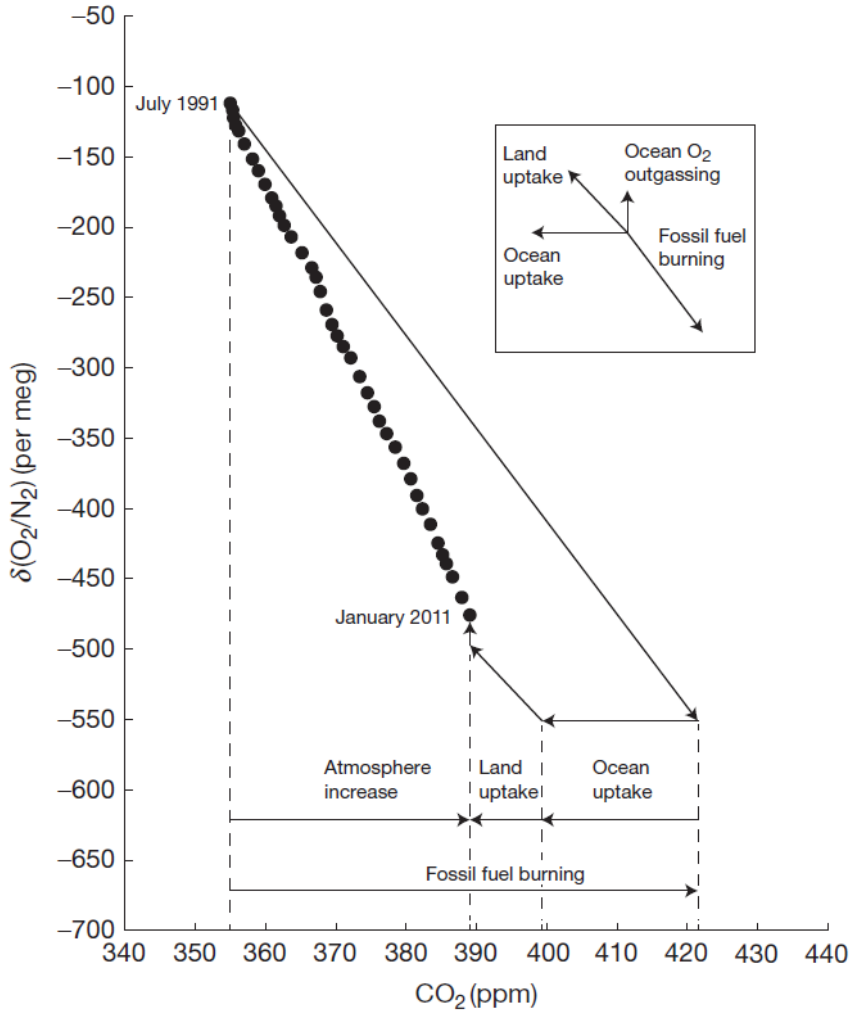

Figure 1.4. $\delta(O_2/N_2)$ (y-axis) versus CO_2 (x-axis) (both globally and annually averaged) over the period July 1991 through January 2011, computed every six months (solid circles). The expected influence on $\delta(O_2/N_2)$ and CO_2 from fossil fuel combustion alone is shown by the long downward arrow. The difference between this and the observed trend is accounted for by both the land and ocean carbon sinks. Firstly, one accounts for the small amount of O_2 outgassing due to the solubility effect from ocean warming over the time period (small vertical arrow). Secondly, since the oxidative ratio for the terrestrial biosphere is known (molar ratio of 1.1/1.0), one can compute the land carbon sink (where the gradient of the upward diagonal arrow shown is equal to 1.1) The remainder must therefore be equivalent to the ocean carbon sink, which is shown by the horizontal arrow since this has no (long term) $\delta(O_2/N_2)$ component (from(Keeling and Manning, 2014b)).

suppressed due to the carbonate chemistry reaction. The decoupling between these two species in air-sea exchange driven by their differences in seawater chemistry results in differences in their equilibration timescales. This is approximately 1 year for CO_2, whereas O_2 equilibrates much faster, on timescales of a few weeks (Broecker and Peng, 1982a).

Although the increase in the atmospheric CO_2 mole fraction due to fossil fuel burning drives a flux of CO_2 into the ocean, as described above, the corresponding decrease in the O_2 mole fraction does not drive a flux of O_2 out of the oceans. This is

because the oceans' capacity for O_2 is too small, since 99% of the total amount of O_2 in the atmosphere-ocean system resides in the atmosphere (Bender and Battle, 1999; Keeling, 1988b). Hence, by removing the fossil fuel component from the long term atmospheric O_2 signal, one knows that the residual must be due to terrestrial biosphere exchange (although a small correction must be made to account for ocean outgassing of O_2 due to thermal solubility changes (see below) (Keeling et al., 2006)). One can then estimate the corresponding terrestrial CO_2 sink from the oxidative ratio of 1.1 for the terrestrial biosphere (Severinghaus, 1995) and hence, by deduction, estimate the oceanic carbon sink (e.g. Bender et al., 1998; Keeling, 1988b; Keeling et al., 1993; Keeling et al., 1996b; Keeling and Shertz, 1992; Manning and Keeling, 2006b; Tohjima et al., 2008). This concept can be expressed quantitatively in the following **Equations (1.5** and **1.6** by deriving an atmospheric budget for CO_2 and O_2:

$$\Delta \boldsymbol{CO_2 = F - O - B} \qquad \textbf{(1.5)}$$

$$\Delta \boldsymbol{O_2 = -\alpha_F F + \alpha_B B + Z} \qquad \textbf{(1.6)}$$

ΔCO_2 and ΔO_2 represent the global atmospheric change in these species over a period of time; F represents a source of CO_2 to the atmosphere from the anthropogenic activities of fossil fuel combustion and cement production, typically estimated from fossil fuel inventories; O represents the ocean carbon sink; B represents the net terrestrial biosphere carbon sink, (the sum of biomass burning, land use change and terrestrial biosphere uptake); αF and αB represent the global average O_2:CO_2 molar exchange ratio for fossil fuels and the terrestrial biosphere (1.4 and 1.1, respectively, see above), and Z represents O_2 outgassing due to changes in both the solubility and biological pumps (Manning and Keeling, 2006b), which can typically be modelled (Bopp et al., 2002) or estimated from observations of changes in the ocean heat content (Plattner et al., 2002). All terms are defined in the units of moles per year, apart from the molar exchange ratios, which have dimensionless units.

By solving **Equation (1.6** for the terrestrial biosphere sink, B, one can then determine the ocean sink, O, from **Equation 1.5**. This is demonstrated in the vector diagram shown in **Figure 1.4**. Keeling and Shertz (1992) were the first to attempt this analysis and estimated that the oceans and terrestrial biosphere each removed approximately 30% of fossil fuel CO_2.

1.4. Seasonal variability of atmospheric O_2

On seasonal timescales, atmospheric observations of the CO_2 mole fraction are characterised by a seasonal variation driven primarily by the terrestrial biosphere (e.g. Bolin and Keeling, 1963; Pearman and Hyson, 1980; Randerson et al., 1997). There is little seasonal influence from the ocean, since, as stated above, the equilibration timescale for CO_2 between the ocean and atmosphere is of the order of 6 months to a year due to the carbonate buffering capacity of sea water (Broecker and Peng, 1982a). Observations of the atmospheric O_2 mole fraction, on the other hand, have a seasonal variation driven by the terrestrial biosphere and oceanic exchange, since atmosphere-ocean O_2 equilibration timescales are on the order of a few weeks (Broecker and Peng, 1982a). This is driven by spring/summer marine biological production, by winter ventilation of deep O_2-deficient, (carbon-rich) subsurface waters as the seasonal thermocline breaks down and a subsequent seasonal thermal solubility component (Bender and Battle, 1999). Therefore, on seasonal timescales, one can remove the seasonal atmospheric O_2 component driven by the terrestrial biosphere by taking the product of the atmospheric CO_2 seasonal amplitude and the factor αB, and summing it with the atmospheric O_2 seasonal amplitude, assuming the seasonal cycles of CO_2 and O_2 are in perfect anti-phase. The residual O_2 component is therefore solely driven by oceanic processes (Bender and Battle, 1999; Keeling et al., 1993; Keeling and Shertz, 1992). Using three years of O_2 flask sample data from Alert, Canada, La Jolla, U.S.A., and Cape Grim, Australia from 1989 to 1992, Keeling and Shertz (1992) discovered that the residual seasonal O_2 signal (after removing the terrestrial biosphere influence) was largely driven by marine biological production (85%) in the summer with a smaller but still significant thermal outgassing signal (15%), and driven by the seasonal break down of the thermocline in winter months, leading to ventilation of O_2 deficient waters. This work was later corroborated (Bender et al., 1996) on O_2 flask sample data from Cape Grim, Tasmania and Baring Head, New Zealand.

1.5. Atmospheric Potential Oxygen

In attempt to more easily distinguish the marine O_2 signal from that of the terrestrial biosphere, Stephens et al. (1998) derived the atmospheric tracer Atmospheric Potential Oxygen (APO) which is the weighted sum of atmospheric O_2 and CO_2 mole

fraction, with an adjustment made to account for terrestrial biosphere exchange processes. Hence, a change in APO (in moles) is defined as **(Equation (1.7)**:

$$\Delta APO = \Delta O_2 + \alpha_B \Delta CO_2 \quad \textbf{(1.7)}$$

ΔO_2 and ΔCO_2 represent the change of the species (in moles) and, as before, the factor αB is equal to 1.10 ± 0.05 and accounts for the O_2:CO_2 stoichiometric ratio for terrestrial biosphere photosynthesis and respiration (Severinghaus, 1995). Hence APO, by definition, is conservative to terrestrial biosphere influences (Stephens et al., 1998). Variability in APO is therefore influenced by fossil fuel combustion, which drives a decrease in APO values since the oxidative ratio for combustion is >1.1 and oceanic processes, which drive the seasonal and intern-annual variability in APO (Hamme and Keeling, 2008; Stephens et al., 1998).

There are two key assumption in the derivation of APO. Firstly, the oxidation of CH_4 and CO to CO_2 in the atmosphere has a negligible impact on the O_2 mole fraction compared to fossil fuel combustion and the terrestrial biosphere exchange processes (Stephens et al., 1998). Whilst this assumption must be considered for the assessment of global APO gradients, it does not significantly impact APO on seasonal to inter-annual timescales. Secondly, the oxidative ratio for terrestrial biosphere processes (1.10 ± 0.05) is constant across all vegetation types. Whilst this may not be strictly true, it is only relevant for studies interested in very local scale APO studies. At the regional to global level this ratio holds true (Severinghaus, 1995).

The seasonal variability in APO is driven by the ocean carbon cycle process of biological production in the spring/summer months and the subsequent breakdown of the thermocline leading to deep mixing in the winter months; both of these processes are further amplified by seasonal thermal solubility changes in the surface ocean (Bender et al., 1996; Keeling et al., 1993; Keeling and Shertz, 1992). The variability in these processes from year to year hence drives the global inter-annual variability of APO (Hamme and Keeling, 2008).

Observations of APO provide a useful independent method to test the reliability of atmosphere-ocean model predictions of air-sea O_2 and CO_2 fluxes. For example, using fortnightly samples of atmospheric O_2 and CO_2 collected on the Scripps Institution of Oceanography (SIO) O_2 flask sampling network (10 stations, established in the early 1990's) (Manning and Keeling, 2006b), Stephens et al. (1998) calculated the inter-

hemispheric gradient in APO observations and compared the results to three ocean circulation plus biogeochemistry models (OCBMs) of air-sea fluxes (Sarmiento et al., 1995; Six and Maier-Reimer, 1996) coupled to an atmospheric transport model (ATM) (Heimann, 1995). The authors discovered the models significantly underestimated the inter-hemispheric gradient of APO (decreasing towards the north) and proposed that the models must be underestimating the net southward oceanic transport of the sum of O_2 and CO_2. Conversely, Gruber et al. (2001) performed a similar study but used an inverse modelling technique that is independent of air-sea fluxes. Through their analysis, Gruber et al. (2001) discovered that the inter-hemispheric gradient of O_2 can be described by the existence of two closed ocean-atmosphere asymmetric circulation cells of O_2 transport. Whereby O_2 uptake occurs in the mid to high latitude oceans, is transported towards the tropics, where it is outgassed from the ocean at the equator and then transported back to the poles through the atmosphere. The northern hemisphere cell is stronger than that in the southern hemisphere, resulting in increased O_2 uptake in northern temperate regions (Gruber et al., 2001). This asymmetry in the two circulation cells, combined with the asymmetry in fossil fuel emissions (greater in the northern hemisphere) can account for the inter-hemispheric APO gradient more accurately than the analysis proposed by Stephens et al. (1998) (Gruber et al., 2001).

Furthermore, the modelling studies of Stephens et al. (1998) and Gruber et al. (2001) implied a strong equatorial outgassing of O_2 that produces an equatorial "bulge" in APO that could not be confirmed due to a lack of observations in this region. Tohjima et al. (2005b) subsequently confirmed this prediction using shipboard flask measurements of O_2 and CO_2 collected across the western Pacific Ocean between Japan and the United States and Japan and Australia.

A comprehensive review of how APO can be used to evaluate atmosphere-ocean models can be found in Naegler et al. (2007). The major finding of this work was that the ability of the current suite of ATMs to correctly reproduce the amount of vertical mixing observed in the atmosphere (also known as the rectifier effect) hinders efforts to use APO in the evaluation of ocean biogeochemical models, particularly on seasonal timescales.

This is less of an issue on inter-annul timescales, however. Consequently, Rödenbeck et al. (2008) performed the first atmospheric inversion of global APO observations to assess the influence in the variability of ocean CO_2 and O_2 fluxes on the APO anomaly. The authors found that tropical APO fluxes were significantly correlated with the El Niño Southern Oscillation (ENSO) Multivariate ENSO Index (MEI) index

whereby ENSO induced changes in upwelling in the central Pacific, and therefore the ventilation of O_2 poor deep waters, could explain the variability seen. The relationship between ENSO and the inter-annual variability in APO was later confirmed by Eddebbar et al. (2017).

Moreover, a modelling analysis by Verdy et al. (2007) on simulated inter-annual atmosphere-ocean O_2 and CO_2 fluxes in the Southern Ocean demonstrated that both the SAM and the ESNO significantly impacted both of the CO_2 and O_2 anomalies. Whereas, Hamme and Keeling (2008) found that a significant amount of the APO variability, particularly in the northern hemisphere, could be explained by ventilation of deep water masses within the North Atlantic and Western North Pacific ocean basins. The authors also examined the variability in APO with the Arctic Oscillation (AO) index and, although the variability was only weakly correlated, a large negative excursion in the AO index in 2001 corresponded with a negative excursion in the APO anomaly, indicative of ocean ventilation driven changes.

These analyses demonstrate the insight long term APO observations can provide on how large scale atmosphere-ocean couplings (such as the ENSO and the AO), impact the ocean carbon cycle.

Despite ATM uncertainties (Naegler et al., 2007) the seasonal cycle of APO can be used to test our understanding of the seasonality of marine carbon cycle processes. For example, Nevison et al. (2012) presented a unique analysis on the seasonal cycle of APO in the Southern Ocean. In their analysis, the authors were able to separate the thermal and ventilation components of the APO seasonal cycle using atmospheric Ar/N_2 and N_2O data, respectively. The remaining component is equal to the biological signal, representing Net Community Production (NCP) within the Southern Ocean. Using a satellite ocean colour observations of net primary productivity (NPP) (Behrenfeld and Falkowski, 1997), combined with a model to estimate export production (EP) (Laws, 2004) which is approximately equal to NCP (Nevison et al., 2012) and an atmospheric transport model (MATCH (Mahowald et al., 1997; Rasch et al., 1997)), they were able to independently verify the APO NCP component. This analysis provides an encouraging comparison of two independent data-sets that also confirms the reliability of the biogeochemical models used in their analysis.

Building upon this work, Nevison et al. (2015) used global observations of the APO seasonal cycle to evaluate six Earth system models that participated in the fifth phase of the Coupled Model Inter-comparison Project (CMIP5) (Taylor et al., 2012). The

authors attempted to account for the uncertainty in atmospheric transport, described by Naegler et al. (2007), by using a matrix method that took account of the uncertainty across 13 different ATMs to translate the ocean model air sea fluxes into an APO field. Of the six models tested, only three were able to reproduce the observed seasonal APO cycles at most of the observation sites (Nevison et al., 2015). Following this, Nevison et al. (2016) performed a similar test of global OCBMs against APO, but with a specific focus on Southern Ocean APO monitoring stations. This unique study used the models to assess Southern Ocean carbon uptake in 2100 under the RCP 8.5 scenario. The models with a better performance at reproducing the present day APO seasonal cycle predicted a smaller net carbon uptake in the Southern Ocean than those that did not (Nevison et al., 2016).

Clearly, APO observations have the unique capability of reconciling OCBMs with observations and vice versa; advancing our understanding of the atmosphere-ocean system (Battle et al., 2006).

1.6. Summary and aims of thesis

In this chapter, I began with a comprehensive review of the global carbon cycle. I discussed in detail aspects of the terrestrial carbon cycle and how current observations of the atmospheric CO_2 mole fraction are indicative of hemispheric wide responses of the

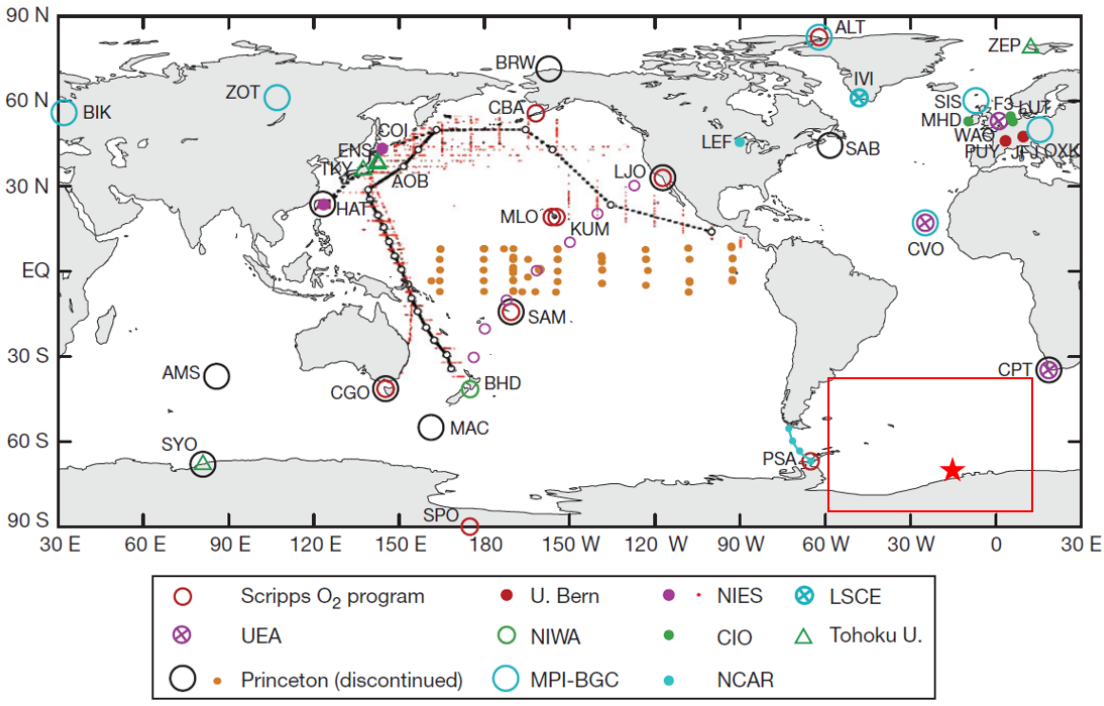

Figure 1.5. Current and historic sampling sites for atmospheric O_2. The red box shows the South Atlantic and Weddell Sea O_2 observation gap. The red star represents the location of the Halley Research Station. (from Keeling and Manning, 2014b).

terrestrial biosphere to current climate change. I then detailed the complexity of the ocean carbon cycle and how the Southern Ocean is a key region with respect to atmosphere-ocean carbon exchange, yet there is still much debate surrounding the current efficiency of the Southern Ocean carbon sink.

I have outlined the applicability of atmospheric O_2, CO_2 and APO measurements as a tool for understanding the global carbon cycle. These measurements can be used to understand both how the terrestrial biosphere is responding to current climate variability and also test our knowledge and understanding of carbon cycle processes in the Southern Ocean through model-observation comparisons.

However, modelling studies involving atmospheric APO observations are limited by the lack of global monitoring stations, particularly in the Southern Ocean region. Moreover, whilst there is a large amount of research into the seasonal and inter-annual variability of atmospheric CO_2, there is a limited amount of research into the inter-annual variability of the seasonal cycles and growth rates of atmospheric O_2 and APO. Furthermore, the current body of atmospheric O_2 and APO research stems from flask observations. Whilst this is suffice for studies of the carbon cycle at the global scale, flask observations may miss the finer details of what drives O_2 and APO variability at the regional level, such as variations driven by a combination of local scale carbon cycle processes and atmospheric transport. Consequently, the over-arching aim of this thesis was to investigate the processes that control the variability of atmospheric CO_2, O_2 and APO on different spatial and temporal scales at two contrasting coastal locations from continuous observations.

The Weybourne Atmospheric Observatory (WAO) is an existing mid-latitude atmospheric O_2 and CO_2 measurement station on the north Norfolk coast of the U.K. established in 2008 (Wilson, 2012). To investigate the variability of atmospheric O_2, CO_2 and APO on seasonal and inter-annual timescales I have chosen to extend and revise this observational dataset. I will compare the derived seasonal cycles and growth rates to the original analysis of the Wilson (2012) and to other northern hemisphere monitoring stations, in order to understand the regional variability of the species across the northern hemisphere. Following this, this I will quantify the inter-annual variability of the seasonal cycles and growth rates of atmospheric CO_2, O_2 and APO at WAO. This analysis will therefore address following questions:

1. How do the results of the analysis compare to published literature on the topic (in the case of CO_2) and, with respect to all species, how do the results at WAO compare to other northern hemisphere stations? With this, I will then assess what can be learnt about the carbon cycle processes that influence the seasonal variability of O_2 and APO, in addition to CO_2.
2. Is there a statistical relationship between the quantified variability in the seasonal cycles and growth rates of the species and the variability of the climate, characterised by temperature, precipitation and climate indices?

Whilst this work will assess whether the WAO atmospheric CO_2 mole fraction displays similar trends in the seasonal cycle and growth rate to other CO_2 observation sites, it will represent the first time such an analysis has also been applied to atmospheric O_2 and APO observations (with respect to the inter-annual variability of the seasonal cycle). Moreover, studies of the inter-annual variability of the O_2 and APO growth rate are very limited (Eddebbar et al., 2017; Hamme and Keeling, 2008; Rödenbeck et al., 2008) and this analysis will be the first to use a station situated in northern Europe.

The Halley Research Station (HBA) is a high latitude, Antarctic coastal site that measures a suite of atmospheric trace gases. Here, I will build and install a fully automated O_2 and CO_2 measurement system, largely based on the system previously built at WAO by Wilson (2012), in order to fill in the O_2 observational gap in the South Atlantic sector of the Southern Ocean (**Figure 1.5**). The South Atlantic and Weddell Sea are key regions of atmosphere-ocean exchange and represent a significant area of carbon export from the surface to the deep ocean (Bakker et al., 2008; Evans et al., 2017). Whilst this measurement system will represent the first continuous atmospheric O_2 and CO_2 measurement system in the South Atlantic sector of the Southern Ocean, it also represents only the third such measurement system in the wider Southern Ocean region (the others being at Syowa Station, Antarctica (Ishidoya et al., 2012) and Baring Head, New Zealand (Manning, 2001)). The primary aim of this work was to determine the extent with which carbon cycle processes in the South Atlantic sector of the Southern Ocean control the variability of atmospheric CO_2, $\delta(O_2/N_2)$ and APO observations at the Halley Research Station, Antarctica. This will be achieved through the following objectives:

1. Determine what carbon cycle processes control the seasonality of atmospheric CO_2 from flask observations collected at the HBA using an atmospheric inversion scheme.

2. Investigate synoptic scale variability and determine to what extent the variability can be explained by local to regional scale carbon cycle processes.
3. Compare the seasonal cycle of APO observed at HBA to that observed at other Southern Ocean stations and assess what can be learned about the spatial and temporal variability of carbon cycle processes within the Southern Ocean region.
4. Do HBA APO observations highlight deficiencies or strengths in OCBMs that are otherwise overlooked with fewer stations to compare against?

1.7. Outline of thesis

The outline of this thesis is as follows: In Chapter 2, I present the theory and design methodology of the atmospheric O_2 and CO_2 measurement system installed at HBA. In Chapter 3, I provide an assessment of the reliability of the measurement system, within the context of global atmospheric measurement goals, based on diagnostic data collected over one year of operation. In Chapter 4, I present the first year of observations at the HBA, including an assessment of the seasonal cycles of CO_2, O_2 and APO, a comparison of HBA APO against other Southern Ocean APO monitoring stations and two OCBMs. In Chapter 5, I present a revision and extension of the WAO atmospheric O_2, CO_2 and APO measurement record, including a detailed discussion of baseline extraction and curve fitting techniques, and a comparison to the original data presented by Wilson (2012). In Chapter 6, I assess the variability in the seasonal cycle and growth rates of O_2, CO_2 and APO observed at WAO and compare this to variability in climatic variables, such as temperature and precipitation, and hemispheric scale climate indices. Finally, in Chapter 7, I present the summary and conclusions from the main findings of this research, including a discussion of future work.

1.8. References

Anderson, L.A. (1995) On the hydrogen and oxygen content of marine phytoplankton. Deep Sea Research Part I: Oceanographic Research Papers 42, 1675-1680.

Arrhenius, S. (1896) On the influence of carbonic acid in the air upon the temperature of the ground. Philosophical Magazine 41, 237-276.

Bacastow, R.B. (1976) Modulation of atmospheric carbon dioxide by southern oscillation. Nature 261, 116-118.

Bacastow, R.B., Keeling, C.D., Whorf, T.P. (1985) Seasonal amplitude increase in atmospheric CO_2 concentration at Mauna Loa, Hawaii, 1959-1982. Journal of Geophysical Research-Atmospheres 90, 10529-10540.

Bakker, D.C.E., Hoppema, M., Schröder, M., Geibert, W., De Baar, H.J.W. (2008) A rapid transition from ice covered CO_2-rich waters to a biologically mediated CO_2 sink in the eastern Weddell Gyre. Biogeosciences Discussions 5, 1205-1235.

Bakker, D.C.E., Pfeil, B., Landa, C.S., Metzl, N., O'Brien, K.M., Olsen, A., Smith, K., Cosca, C., Harasawa, S., Jones, S.D., Nakaoka, S.I., Nojiri, Y., Schuster, U., Steinhoff, T., Sweeney, C., Takahashi, T., Tilbrook, B., Wada, C., Wanninkhof, R., Alin, S.R., Balestrini, C.F., Barbero, L., Bates, N.R., Bianchi, A.A., Bonou, F., Boutin, J., Bozec, Y., Burger, E.F., Cai, W.J., Castle, R.D., Chen, L., Chierici, M., Currie, K., Evans, W., Featherstone, C., Feely, R.A., Fransson, A., Goyet, C., Greenwood, N., Gregor, L., Hankin, S., Hardman-Mountford, N.J., Harlay, J., Hauck, J., Hoppema, M., Humphreys, M.P., Hunt, C.W., Huss, B., Ibánhez, J.S.P., Johannessen, T., Keeling, R., Kitidis, V., Körtzinger, A., Kozyr, A., Krasakopoulou, E., Kuwata, A., Landschützer, P., Lauvset, S.K., Lefèvre, N., Lo Monaco, C., Manke, A., Mathis, J.T., Merlivat, L., Millero, F.J., Monteiro, P.M.S., Munro, D.R., Murata, A., Newberger, T., Omar, A.M., Ono, T., Paterson, K., Pearce, D., Pierrot, D., Robbins, L.L., Saito, S., Salisbury, J., Schlitzer, R., Schneider, B., Schweitzer, R., Sieger, R., Skjelvan, I., Sullivan, K.F., Sutherland, S.C., Sutton, A.J., Tadokoro, K., Telszewski, M., Tuma, M., van Heuven, S.M.A.C., Vandemark, D., Ward, B., Watson, A.J., Xu, S. (2016) A multi-decade record of high-quality fCO_2 data in version 3 of the Surface Ocean CO_2 Atlas (SOCAT). Earth Syst. Sci. Data 8, 383-413.

Barichivich, J., Briffa, K.R., Osborn, T.J., Melvin, T.M., Caesar, J. (2012) Thermal growing season and timing of biospheric carbon uptake across the Northern Hemisphere. Global Biogeochemical Cycles 26, n/a-n/a.

Barnola, J.M., Anklin, M., Porcheron, J., Raynaud, D., Schwander, J., Stauffer, B. (1995) CO_2 evolution during the last millennium as recorded by Antarctic and Greenland ice. Tellus B 47, 264-272.

Battle, M., Mikaloff Fletcher, S., Bender, M.L., Keeling, R.F., Manning, A.C., Gruber, N., Tans, P.P., Hendricks, M.B., Ho, D.T., Simonds, C., Mika, R., Paplawsky, B. (2006) Atmospheric potential oxygen: New observations and their implications

for some atmospheric and oceanic models. Global Biogeochemical Cycles 20, doi:10.1029/2005GB002534.

Behrenfeld, M.J., Falkowski, P.G. (1997) Photosynthetic rates derived from satellite-based chlorophyll concentration. Limnology and Oceanography 42, 1-20.

Bender, M., Ellis, T., Tans, P., Francey, R., Lowe, D. (1996) Variability in the O_2/N_2 ratio of southern hemisphere air, 1991-1994: Implications for the carbon cycle. Global Biogeochemical Cycles 10, 9-21, doi:10.1029/1095GB03295.

Bender, M.L., Battle, M., Keeling, R.F. (1998) The O_2 balance of the atmosphere: A tool for studying the fate of fossil-fuel CO_2. Annu. Rev. Energy Environ. 23, 207-223.

Bender, M.L., Battle, M.O. (1999) Carbon cycle studies based on the distribution of O_2 in air. Tellus Series B-Chemical and Physical Meteorology 51, 165-169.

Berner, R.A. (1998) The Carbon Cycle and Carbon Dioxide over Phanerozoic Time: The Role of Land Plants. Philosophical Transactions of the Royal Society B: Biological Sciences 353, 75–82.

Bolin, B., Keeling, C.D. (1963) Large-scale atmospheric mixing as deduced from the seasonal and meridional variations of carbon dioxide. Journal of Geophysical Research 68, 3899-3920.

Bopp, L., Le Quéré, C., Heimann, M., Manning, A.C., Monfray, P. (2002) Climate-induced oceanic oxygen fluxes: Implications for the contemporary carbon budget. Global Biogeochemical Cycles 16, 6-1-6-13.

Broecker, W.S., Peng, T.-H. (1982) Tracers in the Sea. Lamont-Doherty Geological Observatory, Columbia University, Palisades, New York.

Broecker, W.S., Takahashi, T., Simpson, H.J., Peng, T.-H. (1979) Fate of fossil fuel carbon dioxide and the global carbon budget. Science 206, 409-418.

Butler, A.H., Thompson, D.W.J., Gurney, K.R. (2007) Observed relationships between the Southern Annular Mode and atmospheric carbon dioxide. Global Biogeochemical Cycles 21, -.

Doney, S.C., Fabry, V.J., Feely, R.A., Kleypas, J.A. (2009) Ocean Acidification: The Other CO2 Problem. Annual Review of Marine Science 1, 169-192.

Eddebbar, Y.A., Long, M.C., Resplandy, L., Rödenbeck, C., Rodgers, K.B., Manizza, M., Keeling, R.F. (2017) Impacts of ENSO on air-sea oxygen exchange: Observations and mechanisms. Global Biogeochemical Cycles 31, 901-921.

Evans, G.R., McDonagh, E.L., King, B.A., Bryden, H.L., Bakker, D.C.E., Brown, P.J., Schuster, U., Speer, K.G., van Heuven, S.M.A.C. (2017) South Atlantic interbasin

exchanges of mass, heat, salt and anthropogenic carbon. Progress in Oceanography 151, 62-82.

Forkel, M., Carvalhais, N., Rödenbeck, C., Keeling, R., Heimann, M., Thonicke, K., Zaehle, S., Reichstein, M. (2016) Enhanced seasonal CO_2 exchange caused by amplified plant productivity in northern ecosystems. Science.

Fourier, J. (1827) Mémoire Sur Les Températures Du Globe Terrestre Et Des Espaces Planétaires. Mémoires de l'Académie Royale des Sciences 7, 569-604.

Friedlingstein, P., Prentice, I.C. (2010) Carbon-climate feedbacks: a review of model and observation based estimates. Current Opinion in Environmental Sustainability 2, 251-257.

Gloor, M., Sarmiento, J.L., Gruber, N. (2010) What can be learned about carbon cycle climate feedbacks from the CO_2 airborne fraction? Atmospheric Chemistry and Physics 10, 7739-7751.

Graven, H.D., Keeling, R.F., Piper, S.C., Patra, P.K., Stephens, B.B., Wofsy, S.C., Welp, L.R., Sweeney, C., Tans, P.P., Kelley, J.J., Daube, B.C., Kort, E.A., Santoni, G.W., Bent, J.D. (2013) Enhanced Seasonal Exchange of CO_2 by Northern Ecosystems Since 1960. Science 341, 1085-1089.

Gruber, N., Gloor, M., Fan, S.-M., Sarmiento, J.L. (2001) Air-sea flux of oxygen estimated from bulk data: Implications for the marine and atmospheric oxygen cycles. Global Biogeochemical Cycles 15, 783-803.

Gruber, N., Sarmiento, J.L., Stocker, T.F. (1996) An improved method for detecting anthropogenic CO_2 in the oceans. Global Biogeochemical Cycles 10, 809-837.

Hamme, R.C., Keeling, R.F. (2008) Ocean ventilation as a driver of interannual variability in atmospheric potential oxygen. Tellus Series B-Chemical and Physical Meteorology 60, 706-717.

Hansen, J., Lacis, A., Rind, D., Russell, G., Stone, P., Fung, I., Ruedy, R., Lerner, J., (1984) Climate Sensitivity: Analysis of Feedback Mechanisms, Climate Processes and Climate Sensitivity. American Geophysical Union, pp. 130-163.

Hansen, J., Sato, M., Ruedy, R., Lacis, A., Asamoah, K., Beckford, K., Borenstein, S., Brown, E., Cairns, B., Carlson, B., Curran, B., deCastro, S., Druyan, L., Etwarrow, P., Ferede, T., Fox, M., Gaffen, D., Glascoe, J., Gordon, H., Hollandsworth, S., Jiang, X., Johnson, C., Lawrence, N., Lean, J., Lerner, J., Lo, K., Logan, J., Luckett, A., McCormick, M.P., McPeters, R., Miller, R., Minnis, P., Ramberran, I., Russell, G., Russell, P., Stone, P., Tegen, I., Thomas, S.,

Thomason, L., Thompson, A., Wilder, J., Willson, R., Zawodny, J. (1997) Forcings and chaos in interannual to decadal climate change. Journal of Geophysical Research-Atmospheres 102, 25679-25720.

Hansen, J., Sato, M., Ruedy, R., Lo, K., Lea, D.W., Medina-Elizade, M. (2006) Global temperature change. Proceedings of the National Academy of Sciences 103, 14288-14293.

Heimann, M. (1995) The global atmospheric tracer model TM2. DKRZ.

Heinze, C., Meyer, S., Goris, N., Anderson, L., Steinfeldt, R., Chang, N., Le Quéré, C., Bakker, D.C.E. (2015) The ocean carbon sink – impacts, vulnerabilities and challenges. Earth Syst. Dynam. 6, 327-358.

Houghton, R.A. (2007) Balancing the global carbon budget. Annual Review of Earth and Planetary Sciences 35, 313-347.

Imbrie, J., Boyle, E.A., Clemens, S.C., Duffy, A., Howard, W.R., Kukla, G., Kutzbach, J., Martinson, D.G., McIntyre, A., Mix, A.C., Molfino, B., Morley, J.J., Peterson, L.C., Pisias, N.G., Prell, W.L., Raymo, M.E., Shackleton, N.J., Toggweiler, J.R. (1992) On the Structure and Origin of Major Glaciation Cycles 1. Linear Responses to Milankovitch Forcing. Paleoceanography 7, 701-738.

Indermuhle, A., Stocker, T.F., Joos, F., Fischer, H., Smith, H.J., Wahlen, M., Deck, B., Mastroianni, D., Tschumi, J., Blunier, T., Meyer, R., Stauffer, B. (1999) Holocene carbon-cycle dynamics based on CO_2 trapped in ice at Taylor Dome, Antarctica. Nature 398, 121-126.

IPCC (2001) Climate Change 2001: Impacts, Adaptation and Vulnerability. Contribution of Working Group II to the Third Assessment Report of the Intergovernmental Panel on Climate Change, 2001. Cambridge University Press, Cambridge, United Kingdom and New York, NY, USA.

IPCC (2007a) Climate Change 2007: Impacts, Adaptation and Vulnerability. Contribution of Working Group II to the Fourth Assessment Report of the Intergovernmental Panel on Climate Change, 2007. Cambridge University Press, Cambridge, United Kingdom and New York, NY, USA.

IPCC (2007b) Climate Change 2007: The Physical Science Basis. Contribution of Working Group I to the Fourth Assessment Report of the Intergovernmental Panel on Climate Change. Cambridge University Press, Cambridge, United Kingdom and New York, NY, USA.

IPCC (2013) Climate Change 2013: The Physical Science Basis. Contribution of Working Group I to the Fifth Assessment Report of the Intergovernmental Panel on Climate Change Cambridge University Press, Cambridge, United Kingdom and New York, NY, USA.

IPCC (2014) Climate Change 2014: Impacts, Adaptation, and Vulnerability. Part A: Global and Sectoral Aspects. Contribution of Working Group II to the Fifth Assessment Report of the Intergovernmental Panel on Climate Change. Cambridge University Press, Cambridge, United Kingdom and New York, NY, USA. .

Ishidoya, S., Morimoto, S., Aoki, S., Taguchi, S., Goto, D., Murayama, S., Nakazawa, T. (2012) Oceanic and terrestrial biospheric CO_2 uptake estimated from atmospheric potential oxygen observed at Ny-Ålesund, Svalbard, and Syowa, Antarctica. 2012 64.

Jacob, D. (1999) Introduction to Atmospheric Chemistry. Princeton University Press.

Keeling, C.D. (1960) The concentration and isotopic abundance of carbon dioxide in the atmosphere. Tellus 12, 200-203.

Keeling, C.D., Chin, J.F.S., Whorf, T.P. (1996a) Increased activity of northern vegetation inferred from atmospheric CO_2 measurements. Nature 382, 146-149.

Keeling, R.F., (1988a) Development of an interferometric oxygen analyzer for precise measurement of the atmospheric O_2 mole fraction, Division of Applied Sciences. Harvard University, Cambridge, Massachusetts, U.S.A., p. 178.

Keeling, R.F. (1988b) Measuring correlations between atmospheric oxygen and carbon dioxide mole fractions: A preliminary study in urban air. Journal of Atmospheric Chemistry 7, 153-176.

Keeling, R.F., Manning, A.C., (2014a) 5.15 - Studies of Recent Changes in Atmospheric O2 Content, in: Turekian, H.D.H.K. (Ed.), Treatise on Geochemistry (Second Edition). Elsevier, Oxford, pp. 385-404.

Keeling, R.F., Manning, A.C., (2014b) Studies of Recent Changes in Atmospheric O_2 Content, in: Turekian, K.K. (Ed.), Treatise on Geochemistry (Second Edition). Elsevier, Oxford, pp. 385-404.

Keeling, R.F., Manning, A.C., Paplawsky, W.J., Cox, A.C., (2006) On the long-term stability of reference gases for high precision measurements of O_2/N_2 ratio, Journal of Atmospheric and Oceanic Technology.

Keeling, R.F., Najjar, R.P., Bender, M.L., Tans, P.P. (1993) What atmospheric oxygen measurements can tell us about the global carbon cycle. Global Biogeochemical Cycles 7, 37-67, doi:10.1029/1092GB02733.

Keeling, R.F., Piper, S.C., Heimann, M. (1996b) Global and hemispheric CO_2 sinks deduced from changes in atmospheric O_2 concentration. Nature 381, 218-221.

Keeling, R.F., Shertz, S.R. (1992) Seasonal and interannual variations in atmospheric oxygen and implications for the global carbon cycle. Nature 358, 723-727, doi:710.1038/358723a358720.

Knox, F., McElroy, M.B. (1984) Changes in atmospheric CO_2: Influence of the marine biota at high latitude. Journal of Geophysical Research: Atmospheres 89, 4629-4637.

Landschützer, P., Gruber, N., Haumann, A., Rödenbeck, C., Bakker, D.C.E., van Heuven, S., Hoppema, M., Metzl, N., Sweeney, C., Takahashi, T., Tilbrook, B., Wanninkof, R. (2015) The reinvigoration of the Southern Ocean carbon sink. . Science 349, 1221-1224.

Law, R.M., Matear, R.J., Francey, R.J. (2008) Comment on "Saturation of the Southern Ocean CO_2 sink due to recent climate change". Science 319, 570.

Laws, E. (2004) Export flux and stability as regulators of community composition in pelagic marine biological communities: Implications for regime shifts. Progress in Oceanography 60, 343-354.

Le Quéré, C., Raupach, M.R., Canadell, J.G., Marland, G., Bopp, L., Ciais, P., Conway, T.J., Doney, S.C., Feely, R.A., Foster, P., Friedlingstein, P., Gurney, K., Houghton, R.A., House, J.I., Huntingford, C., Levy, P.E., Lomas, M.R., Majkut, J., Metzl, N., Ometto, J.P., Peters, G.P., Prentice, I.C., Randerson, J.T., Running, S.W., Sarmiento, J.L., Schuster, U., Sitch, S., Takahashi, T., Viovy, N., van der Werf, G.R., Woodward, F.I. (2009) Trends in the sources and sinks of carbon dioxide. Nature Geoscience 2, 831-836.

Le Quéré, C., Rödenbeck, C., Buitenhuis, E.T., Conway, T.J., Langenfelds, R., Gomez, A., Labuschagne, C., Ramonet, M., Nakazawa, T., Metzl, N., Gillett, N., Heimann, M. (2007) Saturation of the Southern Ocean CO_2 sink due to recent climate change. Science 316, 1735-1738, doi:1710.1126/science.1136188.

Le Quere, C., Roedenbeck, C., Buitenhuis, E.T., Conway, T.J., Langenfelds, R., Gomez, A., Labuschagne, C., Ramonet, M., Nakazawa, T., Metzl, N., Gillett, N.P.,

Heimann, M. (2008) Response to Comments on "Saturation of the Southern Ocean CO_2 sink due to recent climate change". Science 319.

Lenton, A., Matear, R.J. (2007) Role of the Southern Annular Mode (SAM) in Southern Ocean CO2 uptake. Global Biogeochemical Cycles 21.

Lovenduski, N.S., Gruber, N., Doney, S.C. (2008) Toward a mechanistic understanding of the decadal trends in the Southern Ocean carbon sink. Global Biogeochemical Cycles 22.

Lovenduski, N.S., Gruber, N., Doney, S.C., Lima, I.D. (2007) Enhanced CO_2 outgassing in the Southern Ocean from a positive phase of the Southern Annular Mode. Global Biogeochemical Cycles 21.

Lumpkin, R., Speer, K. (2007) Global Ocean Meridional Overturning. Journal of Physical Oceanography 37, 2550-2562.

Machta, L.E., (1980) Oxygen depletion, in: Jacoby (Ed.), Carbon Dioxide Effcts Research and Assessment Program: Proceedings of the International Meeting on Stable isotopes in Tree-Ring Research. U.S. Department of Energy, pp. 125-127.

Mahowald, N.M., Rasch, P.J., Eaton, B.E., Whittlestone, S., Prinn, R.G. (1997) Transport of ^{222}radon to the remote troposphere using the Model of Atmospheric Transport and Chemistry and assimilated winds from ECMWF and the National Center for Environmental Prediction/NCAR. Journal of Geophysical Research: Atmospheres 102, 28139-28151.

Manning, A.C., (2001) Temporal variability of atmospheric oxygen from both continuous measurements and a flask sampling network: Tools for studying the global carbon cycle, Scripps Institution of Oceanography. University of California, San Diego, La Jolla, California, U.S.A., p. 202.

Manning, A.C., Keeling, R.F. (2006) Global oceanic and land biotic carbon sinks from the Scripps atmospheric oxygen flask sampling network. Tellus-B 58B, 95-116, doi:110.1111/j.1600-0889.2006.00175.x.

Marshall, J., Speer, K. (2012) Closure of the meridional overturning circulation through Southern Ocean upwelling. Nature Geoscience 5, 171.

Metzl, N., Brunet, C., Jabaud-Jan, A., Poisson, A., Schauer, B. (2006) Summer and winter air–sea CO_2 fluxes in the Southern Ocean. Deep Sea Research Part I: Oceanographic Research Papers 53, 1548-1563.

Mikaloff Fletcher, S.E., Gruber, N., Jacobson, A.R., Gloor, M., Doney, S.C., Dutkiewicz, S., Gerber, M., Follows, M., Joos, F., Lindsay, K., Menemenlis, D., Mouchet, A.,

Muller, S.A., Sarmiento, J.L. (2007) Inverse estimates of the oceanic sources and sinks of natural CO_2 and the implied oceanic carbon transport. Global Biogeochemical Cycles 21.

Milankovitch, M.R. (1941) Kanon der Erdbestrahlung. (Canon of insolation and the ice-age problem, English translation by Israel Program for Scientific Translations, Jerusalem, 1969). Royaal Serbian Academy Specialist Publication 132.

Munro, D.R., Lovenduski, N.S., Takahashi, T., Stephens, B.B., Newberger, T., Sweeney, C. (2015) Recent evidence for a strengthening CO_2 sink in the Southern Ocean from carbonate system measurements in the Drake Passage (2002–2015). Geophysical Research Letters 42, 7623-7630.

Myneni, R.B., Keeling, C.D., Tucker, C.J., Asrar, G., Nemani, R.R. (1997) Increased plant growth in the northern high latitudes from 1981 to 1991. Nature 386, 698-702.

Naegler, T., Ciais, P., Orr, J.C., Aumont, O., RÖDenbeck, C. (2007) On evaluating ocean models with atmospheric potential oxygen. Tellus B 59, 138-156.

Nemani, R.R., Keeling, C.D., Hashimoto, H., Jolly, W.M., Piper, S.C., Tucker, C.J., Myneni, R.B., Running, S.W. (2003) Climate-Driven Increases in Global Terrestrial Net Primary Production from 1982 to 1999. Science 300, 1560-1563.

Nevison, C.D., Keeling, R.F., Kahru, M., Manizza, M., Mitchell, B.G., Cassar, N. (2012) Estimating net community production in the Southern Ocean based on atmospheric potential oxygen and satellite ocean color data. Global Biogeochemical Cycles 26.

Nevison, C.D., Manizza, M., Keeling, R.F., Kahru, M., Bopp, L., Dunne, J., Tiputra, J., Ilyina, T., Mitchell, B.G. (2015) Evaluating the ocean biogeochemical components of Earth system models using atmospheric potential oxygen and ocean color data. Biogeosciences 12, 193-208.

Nevison, C.D., Manizza, M., Keeling, R.F., Stephens, B.B., Bent, J.D., Dunne, J., Ilyina, T., Long, M., Resplandy, L., Tjiputra, J., Yukimoto, S. (2016) Evaluating CMIP5 ocean biogeochemistry and Southern Ocean carbon uptake using atmospheric potential oxygen: Present-day performance and future projection. Geophysical Research Letters 43, 2077-2085.

Olbers, D., Borowski, D., Volker, C., Wolff, J. (2004) The dynamical balance, transport and circulation of the Antarctic Circumpolar Current. Antarctic Science 16, 439-470.

Pearman, G.I., Hyson, P. (1980) Activities of the global biosphere as reflected in atmospheric CO_2 records. Journal of Geophysical Research: Oceans 85, 4457-4467.

Pearman, G.I., Hyson, P. (1981) The annual variation of atmospheric CO2 concentration observed in the northern hemisphere. Journal of Geophysical Research: Oceans 86, 9839-9843.

Pepper, W. (1992) Emission scenarios for the IPCC, an update, assumptions, methodology, and results. Prepared for the Intergovernmental Panel on Climate Change, Working Group 1.

Petit, J.R., Jouzel, J., Raynaud, D., Barkov, N.I., Barnola, J.M., Basile, I., Bender, M., Chappellaz, J., Davis, M., Delaygue, G., Delmotte, M., Kotlyakov, V.M., Legrand, M., Lipenkov, V.Y., Lorius, C., Pepin, L., Ritz, C., Saltzman, E., Stievenard, M. (1999) Climate and atmospheric history of the past 420,000 years from the Vostok ice core, Antarctica. Nature 399, 429-436.

Peylin, P., Law, R.M., Gurney, K.R., Chevallier, F., Jacobson, A.R., Maki, T., Niwa, Y., Patra, P.K., Peters, W., Rayner, P.J., Rödenbeck, C., van der Laan-Luijkx, I.T., Zhang, X. (2013) Global atmospheric carbon budget: results from an ensemble of atmospheric CO₂ inversions. Biogeosciences 10, 6699-6720.

Piao, S.L., Ciais, P., Friedlingstein, P., Peylin, P., Reichstein, M., Luyssaert, S., Margolis, H., Fang, J.Y., Barr, A., Chen, A.P., Grelle, A., Hollinger, D.Y., Laurila, T., Lindroth, A., Richardson, A.D., Vesala, T. (2008) Net carbon dioxide losses of northern ecosystems in response to autumn warming. Nature 451, 49-U43.

Plattner, G.K., Joos, F., Stocker, T.F., (2002) Revision of the global carbon budget due to changing air-sea oxygen fluxes, GBC.

Randerson, J.T., Thompson, M.V., Conway, T.J., Fung, I.Y., Field, C.B. (1997) The contribution of terrestrial sources and sinks to trends in the seasonal cycle of atmospheric carbon dioxide. Global Biogeochemical Cycles 11, 535-560.

Rasch, P.J., Mahowald, N.M., Eaton, B.E. (1997) Representations of transport, convection, and the hydrologic cycle in chemical transport models: Implications for the modeling of short-lived and soluble species. Journal of Geophysical Research: Atmospheres 102, 28127-28138.

Redfield, A.C., Ketchum, B.H., Richards, F.A., (1963) The influence of organisms on the composition of sea-water, in: Hill, M.N. (Ed.), The Sea. Wiley Interscience, New York, pp. 26-77.

Revelle, R., Suess, H.E. (1957) Carbon dioxide exchange between atmosphere and ocean and the question of an increase of atmospheric CO_2 during the past decades. Tellus 9, 18-27.

Rintoul, S.R. (2011) The Southern Ocean in the Earth System.

Rödenbeck, C., Le Quéré, C., Heimann, M., Keeling, R.F. (2008) Interannual variability in oceanic biogeochemical processes inferred by inversion of atmospheric O_2/N_2 and CO_2 data. Tellus B: Chemical and Physical Meteorology 60, 685-705.

Roy, T., Rayner, P., Matear, R., Francey, R. (2003) Southern hemisphere ocean CO_2 uptake: reconciling atmospheric and oceanic estimates. Tellus Series B-Chemical and Physical Meteorology 55, 701-710.

Sabine, C.L., Feely, R.A., Gruber, N., Key, R.M., Lee, K., Bullister, J.L., Wanninkhof, R., Wong, C.S., Wallace, D.W.R., Tilbrook, B., Millero, F.J., Peng, T.-H., Kozyr, A., Ono, T., Rios, A.F. (2004) The oceanic sink for anthropogenic CO_2. Science 305, 367-371.

Sallee, J.-B., Matear, R.J., Rintoul, S.R., Lenton, A. (2012) Localized subduction of anthropogenic carbon dioxide in the Southern Hemisphere oceans. Nature Geosci 5, 579-584.

Sarmiento, J.L., Murnane, R., Le Quéré, C. (1995) Air-sea CO_2 transfer and the carbon budget of the North Atlantic. Philosophical Transactions of the Royal Society of London B 348, 211-219.

Schimel, D., Stephens, B.B., Fisher, J.B. (2015) Effect of increasing CO₂ on the terrestrial carbon cycle. Proceedings of the National Academy of Sciences 112, 436-441.

Schulze, E.D. (2006) Biological control of the terrestrial carbon sink. Biogeosciences 3, 147-166.

Severinghaus, J.P., (1995) Studies of the terrestrial O_2 and carbon cycles in sand dune gases and in Biosphere 2. Columbia University, New York, U.S.A., p. 148.

Shindell, D.T., Schmidt, G.A. (2004) Southern Hemisphere climate response to ozone changes and greenhouse gas increases. Geophysical Research Letters 31.

Siegenthaler, U., Stocker, T.F., Monnin, E., Lüthi, D., Schwander, J., Stauffer, B., Raynaud, D., Barnola, J.-M., Fischer, H., Masson-Delmotte, V., Jouzel, J. (2005) Stable Carbon Cycle Climate Relationship During the Late Pleistocene. Science 310, 1313-1317.

Siegenthaler, U., Wenk, T. (1984) Rapid atmospheric CO_2 variations and ocean circulation. Nature 308, 624-626.

Sigman, D.M., Boyle, E.A. (2000) Glacial/interglacial variations in atmospheric carbon dioxide. Nature 407, 859-869.

Six, K.D., Maier-Reimer, E. (1996) Effects of plankton dynamics on seasonal carbon fluxes in an ocean general circulation model. Global Biogeochemical Cycles 10, 559-583.

Stephens, B.B., Keeling, R.F., Heimann, M., Six, K.D., Murnane, R., Caldeira, K. (1998) Testing global ocean carbon cycle models using measurements of atmospheric O_2 and CO_2 concentration. Global Biogeochemical Cycles 12, 213-230.

Takahashi, T., Sutherland, S.C., Wanninkhof, R., Sweeney, C., Feely, R.A., Chipman, D.W., Hales, B., Friederich, G., Chavez, F., Sabine, C., Watson, A., Bakker, D.C.E., Schuster, U., Metzl, N., Yoshikawa-Inoue, H., Ishii, M., Midorikawa, T., Nojiri, Y., Kortzinger, A., Steinhoff, T., Hoppema, M., Olafsson, J., Arnarson, T.S., Tilbrook, B., Johannessen, T., Olsen, A., Bellerby, R., Wong, C.S., Delille, B., Bates, N.R., de Baar, H.J.W. (2009) Climatological mean and decadal change in surface ocean pCO_2, and net sea-air CO_2 flux over the global oceans. Deep-Sea Research Part II -Topical Studies in Oceanography 56, 554-577.

Takahashi, T., Sweeney, C., Hales, B., Chipman, D.W., Newberger, T., Goddard, J.G., Iannuzzi, R.A., Sutherland, S.C. (2012) The changing carbon cycle in the Southern Ocean. Oceanography 25, 26-37.

Taylor, K.E., Stouffer, R.J., Meehl, G.A. (2012) An Overview of CMIP5 and the Experiment Design. Bulletin of the American Meteorological Society 93, 485-498.

Thomas, R.T., Prentice, I.C., Graven, H., Ciais, P., Fisher, J.B., Hayes, D.J., Huang, M., Huntzinger, D.N., Ito, A., Jain, A., Mao, J., Michalak, A.M., Peng, S., Poulter, B., Ricciuto, D.M., Shi, X., Schwalm, C., Tian, H., Zeng, N. (2016) Increased light-use efficiency in northern terrestrial ecosystems indicated by CO_2 and greening observations. Geophysical Research Letters 43, 11,339-311,349.

Thompson, D.W.J., Solomon, S. (2002) Interpretation of Recent Southern Hemisphere Climate Change. Science 296, 895-899.

Toggweiler, J.R. (1999) Variation of atmospheric CO_2 by ventilation of the ocean's deepest water. Paleoceanography 14, 571-588.

Toggweiler, J.R., Samuels, B. (1995) Effect of drake passage on the global thermohaline circulation. Deep Sea Research Part I: Oceanographic Research Papers 42, 477-500.

Tohjima, Y., Mukai, H., Machida, T., Nojiri, Y., Gloor, M. (2005) First measurements of the latitudinal atmospheric O_2 and CO_2 distributions across the western Pacific. Geophysical Research Letters 32, 1-4.

Tohjima, Y., Mukai, H., Nojiri, Y., Yamagishi, H., Machida, T. (2008) Atmospheric O_2/N_2 measurements at two Japanese sites: estimation of global oceanic and land biotic carbon sinks and analysis of the variations in atmospheric potential oxygen (APO). Tellus Series B-Chemical and Physical Meteorology 60, 213-225.

Tyndall, J. (1864) On the Absorption and Radiation of Heat by Gaseous and Liquid Matter. Fourth Memoir. Philosophical Transactions of the Royal Society of London 154, 201-225.

Verdy, A., Dutkiewicz, S., Follows, M.J., Marshall, J., Czaja, A. (2007) Carbon dioxide and oxygen fluxes in the Southern Ocean: Mechanisms of interannual variability. Global Biogeochemical Cycles 21.

Wanninkhof, R., Asher, W.E., Ho, D.T., Sweeney, C., McGillis, W.R. (2009) Advances in Quantifying Air-Sea Gas Exchange and Environmental Forcing*. Annual Review of Marine Science 1, 213-244.

Watson, A.J., Naveira Garabato, A.C. (2006) The role of Southern Ocean mixing and upwelling in glacial-interglacial atmospheric CO_2 change. Tellus B 58, 73-87.

Wenzel, S., Cox, P.M., Eyring, V., Friedlingstein, P. (2016) Projected land photosynthesis constrained by changes in the seasonal cycle of atmospheric CO_2. Nature 538, 499-501.

Wilson, P., (2012) Insight into the Carbon Cycle from Continuous Measurements of Oxygen and Carbon Dioxide at Weybourne Atmospheric Observatory, UK, School of Environmental Sciences. Univeristy of East Anglia, Norwich, p. 155.

Zachos, J., Pagani, M., Sloan, L., Thomas, E., Billups, K. (2001) Trends, Rhythms, and Aberrations in Global Climate 65 Ma to Present. Science 292, 686-693.

Zhou, L., Tucker, C.J., Kaufmann, R.K., Slayback, D., Shabanov, N.V., Myneni, R.B. (2001) Variations in northern vegetation activity inferred from satellite data of vegetation index during 1981 to 1999. Journal of Geophysical Research: Atmospheres 106, 20069-20083.

Zickfeld, K., Fyfe, J.C., Eby, M., Weaver, A.J. (2008) Comment on "Saturation of the Southern Ocean CO_2 sink due to recent climate change". Science 319, -.

CHAPTER 2 METHODOLOGY OF ATMOSPHERIC O_2 AND CO_2 MEASUREMENTS

PART I: THEORY AND DESIGN

2.1. Introduction

2.1.1. Outline of this chapter

This chapter describes in detail the O_2 and CO_2 measurement system I built at the University of East Anglia (UEA) between 2013 and 2015 and subsequently installed at the Halley Research Station, Antarctica, at the beginning of 2016. O_2 and CO_2 measurement is achieved using a commercially available O_2 analyser, utilising lead fuel cell based measurement technology, and a CO_2 analyser employing the Non Dispersive Infrared (NDIR) absorption based technique. The use of these analysers and the gas handling procedure required to attain the precision necessary for carbon cycle research were developed by A. Manning (UEA, Norwich, U.K.) and B. Stephens (National Center for Atmospheric Research (NCAR), Colorado, USA) in the early 2000s. The blueprint for this type of measurement system has been used and developed by subsequent systems (Patecki and Manning, 2007a; Pickers, 2016; Stephens et al., 2007; Thompson, 2005; van der Laan-Luijkx, 2010; Wilson, 2012), with modifications made to suit the environment that the system was to be installed in (e.g. ship based, remote field site, local field site etc.).

The specific aim in this chapter was to build an O_2 and CO_2 measurement system that could be installed at the Halley Research Station, Antarctica (HBA), in order to fill in the South Atlantic observational O_2 "gap" highlighted in Chapter 1. Halley is ideally placed to sample air masses that have had contact with the ocean in the South Atlantic and Weddell Sea – a key region of the Southern Ocean for carbon export and exchange with the atmosphere (Bakker et al., 2008; Evans et al., 2017). By making the measurement system a continuous one, rather than discrete measurements, allows me to investigate areas of air-sea gas exchange within the region through the analysis of synoptic scale variability of atmospheric O_2 and CO_2.

Furthermore, the system needs to be a largely automated such that it can run for extended periods of time with minimal human intervention – a key requirement for installing at such a remote field station where personnel time is stretched between many different experiments.

With the above aims and constraints in mind, I have chosen to build my system following the blueprint of the most recent UEA's Carbon Related Atmospheric Measurement (CRAM) group iteration of a continuous O_2 and CO_2 field measurement system based at the Weybourne Atmospheric Observatory, Norfolk, U.K. (Wilson, 2012).

This system has been proven reliable to produce continuous O_2 and CO_2 observations for several years via a largely automated process and has proven it's skill in capturing synoptic scale O_2 and CO_2 variability that represent regional carbon cycle processes (Wilson, 2012). In this chapter, I give a thorough description of the measurement system I built and installed at HBA. The build of the system and the amount of troubleshooting required to optimise the measurement process to attain the required measurement precision and accuracy represented 1.5 years of work during this Ph.D. The major differences between the system of Wilson (2012) and that constructed here are:

1. A new position for the "fast purge" line (see later).
2. The removal of a "first stage" drying component.
3. Improved precision through analysis and modification of the "switching time" for the sample and reference lines entering the two fuel cells.

I begin this chapter by giving a brief overview of the history of O_2 measurements to inform the reader of the techniques historically and currently employed. Knowledge of the advantages and disadvantages of each technique ultimately determined why the lead fuel based O_2 measurement system outlined above had to be employed for this project. In Section 2.2, I describe the background and theory behind how atmospheric O_2 measurements are reported and maintained using the Scripps S2 O_2 scale, to which the measurement system described in this chapter is tied to. Readers interested in establishing their own O_2 measurement system are encouraged to read this section to understand how compatibility between independent O_2 measurements should be maintained. In Section 2.3, I describe the measurement system in detail, highlighting individual components and explaining the theory and purpose behind the gas handling procedure employed. In Section 2.4, I detail how the raw analyser outputs are converted into CO_2 mole fraction and $\delta(O_2/N_2)$ ratios. I then go on to detail the different levels of calibration and quality control that are used. Section 2.5 details the data acquisition and the control software, produced and developed by UEA's Electronic and Software engineers. Both of these components have been continuously developed since 2008 by the engineers in conjunction with present and past members of A. Manning's CRAM research group (Pickers, 2016; Wilson, 2012). The modifications I made to the measurement system were subsequently incorporated into this measurement system's version of the acquisition and control software by the engineers upon my request. I conclude with a brief discussion of

the impact the modifications and whether they would be suitable for systems employed by other members of the O_2 measurement community.

Readers not concerned with methodological details of the system are referred to Section 2.6 for a summary of this chapter and an approximate construction timeline that leads onto the assessment of system performance following installation at Halley presented in Chapter 3.

2.1.2. A brief history of atmospheric O_2 measurements

There are currently 26 stations monitoring atmospheric O_2 compared to 113 monitoring stations for CO_2 (A. Manning, 2014; personal communication). The lack of O_2 stations, in comparison to those for CO_2, reflects the difficulty in making atmospheric O_2 measurements. Although changes in atmospheric O_2 are of a similar absolute magnitude to those of CO_2, (the seasonal processes discussed in Chapter 1 result in a seasonal amplitude of ~20 ppm for O_2 at mid-latitudes), they must be detected against a much higher background mole fraction. For example, to measure a 0.1 ppm change of CO_2 in a background of 400 ppm requires a precision of 0.025%. For O_2 however, a 0.1 ppm change needs to be measured against a background of 209,392 ppm (Tohjima et al., 2005a); thus requiring a precision of ~0.00005%.

The first reliable atmospheric O_2 measurements were carried out by Benedict (1912), who determined that the atmospheric O_2 mole fraction is constant (209,380 ± 60 ppm) using a chemical extraction technique followed by volumetric analysis (reviewed in Manning (2001)). This work was later corroborated by Machta and Hughes (1970) who sampled clean marine background air collected in flasks during oceanographic cruises between 1967 and 1968. They obtained a value of 20.946 ± 0.006 % using a Beckman oxygen analyser that utilises the paramagnetic properties of O_2 molecules (i.e. O_2 is *attracted* to a magnetic field) (Machta and Hughes, 1970). Furthermore, Machta and Hughes (1970) noted that one would expect the atmospheric O_2 mole fraction to be decreasing due to the combustion of fossil fuels. The authors calculated an expected depletion of 0.005 percent by volume (50 ppm) of atmospheric O_2 between 1910 and 1967 but were unable to determine this due to uncertainties in their measurements (measurement error: ± 60 ppm) (Machta and Hughes, 1970). In a follow up to this paper Machta (1980a) first proposed that precise atmospheric O_2 measurements, in conjunction with atmospheric CO_2 measurements, could give insights into the state of the global carbon cycle (described in Chapter 1). Such precise measurements ($1{:}10^6$), however, were

not possible until the development of an interferometric oxygen analyser by Ralph Keeling (Keeling, 1988a). This technique involves measuring changes in the relative refractivity of dry air between 4358 and 2537 Å and obtains a precision of 0.00005% (0.1 ppm) that is only made possible by rigorous gas handling procedures (Keeling, 1988a). Keeling (1988b) used this method to demonstrate the anti-correlation of O_2 with CO_2 due to combustion processes within urban air and championed its use as a tool for studying the global carbon cycle (see Chapter 1). Subsequent to this to work, the first atmospheric O_2 flask sampling network was set up and the first estimates of the terrestrial biosphere and oceanic carbon sinks were determined (Keeling and Shertz, 1992).

Several independent techniques for measuring atmospheric O_2 to the required precision have now been established; these include the use of an isotope ratio mass spectrometry (Bender et al., 1994b), a continuous paramagnetic technique (Manning et al., 1999), a gas chromatography technique (Tohjima, 2000), a vacuum ultra violet (VUV) absorption technique (Stephens et al., 2003), and a differential measurement technique based on lead fuel cell technology (Stephens et al., 2007). However, not all of these techniques are suitable for wide-scale deployment at field stations, where the cost of the instruments, the logistical feasibility of installation and the maintenance required in keeping the instruments running all have to be considered. For example, although paramagnetic O_2 analysers are commercially available, they are very sensitive to external environmental factors (e.g. temperature, pressure and motion) and therefore require a lot of modifications and fine-tuning to attain the desired precision, making the technique both labour intensive and costly (Manning, 2001). The VUV absorption technique is completely unique in its design and construction (Stephens et al., 2003) and therefore does not make it a suitable technique to be applied at multiple field stations. The same goes for the interferometric oxygen analyser, this being a one-off construction built by Ralph Keeling during his Ph.D research (Keeling, 1988a). Mass spectrometers and gas chromatography set-ups are commercially available, but expensive and are typically installed in laboratories, owing to their size, again making them unsuitable for field stations. O_2 analysers based on lead-fuel cell technology are a more recent addition to the suite of O_2 analysis techniques. They have the advantage of being compact, commercially available, relatively cheap, and require few modifications, making them an attractive candidate for use in the field (Stephens et al., 2007).

2.2. Defining the atmospheric O_2 scale

2.2.1. $\partial(O_2/N_2)$ and "per meg"

Keeling and Shertz (1992) proposed the convention of reporting atmospheric O_2 concentrations as changes in the ratio of O_2 to N_2, $\delta(O_2/N_2)$, in dry air. This is primarily due to the fact that the O_2 mole fraction is susceptible to changes in other trace gases, such as CO_2. For example, consider a parcel of air containing 1000000 molecules. CO_2 is represented by 400 molecules, O_2 by 210000 and N_2 by 780000. The mixing ratios are therefore 400 ppm, 210000 ppm and 780000, respectively. If one then adds 10 molecules of CO_2 but keeps both O_2 and N_2 constant, the mixing ratios then become (to the nearest ppm): 400 ppm, 209997 ppm and 779992 ppm. Consequently, the O_2 and N_2 mixing ratios have decreased by 3 and 8 ppm, respectively. Hence, if one reports the $\delta(O_2/N_2)$ ratio, this problem is circumvented. N_2 makes up the majority of the composition of the atmosphere (78.084%) and can be considered as inert at the scale of interest (ppm-level). Its variability, therefore, is assumed to be negligible, (in comparison to O_2 variability). With this reasonable assumption, any changes to the O_2/N_2 ratio reflect changes in atmospheric O_2 mole fraction. Furthermore, the O_2/N_2 ratio is insensitive to changes in other atmospheric gases, unlike O_2, which may change considerably on seasonal and long term time scales (CO_2 for example). Changes in the O_2/N_2 ratio of a sample are expressed as relative deviations from a known reference gas (Equation **(2.1)**) (Keeling and Shertz, 1992):

$$\partial(O_2/N_2) = \frac{(O_2/N_2)_{sample} - (O_2/N_2)_{reference}}{(O_2/N_2)_{reference}} \qquad \textbf{(2.1)}$$

Since variations of $\delta(O_2/N_2)$ in natural air are relatively small, the ratio is multiplied by 10^6 and expressed in "per meg" units. In these units, 4.77 per meg of $\delta(O_2/N_2)$ is equivalent to the same number of molecules as 1 ppm of a trace gas (Keeling et al., 1998a).

Of the techniques mentioned, only the mass spectrometry method can measure the O_2/N_2 ratio directly. All other techniques are sensitive to the O_2 mole fraction and hence a correction must be made to account for CO_2 dilution due to changes in the CO_2 mole fraction. To do this, one must measure the CO_2 mole fraction concurrently with the O_2 mole fraction. In this case, Equation (2.2) is used to derive $\delta(O_2/N_2)$ (in per meg units):

$$\partial\,(O_2/N_2) = \frac{\partial X_{O_2} + \left(X_{CO_2} - 363.29\right).S_{O_2}}{S_{O_2}\left(1 - S_{O_2}\right)} \qquad \textbf{(2.2)}$$

Here, S_{O2} represents the standard O_2 mole fraction of air: 0.209392 (Tohjima et al., 2005a); δX_{O2} represents the measured O_2 mole fraction determined by the analyser (multiplied by 10^6), whilst X_{CO2} represents the measured CO_2 mole fraction (in ppm). Hence, a 1µmol mol^{-1} change of the O_2 mole fraction, without any concurrent change in the CO_2 mole fraction, results in a $\delta(O_2/N_2)$ ratio change of 6.04 per meg. Whereas if there *is* a concurrent change in the CO_2 mole fraction, of the same magnitude but in the opposite direction (due to terrestrial biosphere exchange for example), the $\delta(O_2/N_2)$ ratio change will be 4.77 per meg.

2.2.2. The Scripps "S2 Scale" for O_2

Since O_2 measurements are not reported as a mole fraction and are instead reported as an arbitrarily defined ratio with non SI per meg units, it is important to briefly consider: (1). How is "zero" per meg defined? And (2). How is this relative scale maintained?

O_2 measurements are always made relative to a reference gas, this is a high pressure cylinder of ambient air and, as long as it is composed of real air, the relative composition of its constituents does not matter. This is referred to as a Working Tank (WT), as this cylinder is constantly run through respective measurement systems and is against which all measurements of O_2 are made. When Ralph Keeling first started making O_2 measurements at the Scripps Institution of Oceanography (SIO) in the 1980's (Keeling, 1988a), he defined the WT O_2 concentration once a day when the span sensitivity of his interferometric analyser was calibrated against two secondary reference cylinders, known as "High Span" (HS) and "Low Span" (LS). These cylinders are initially filled to span the range of the ambient O_2 concentrations expected and referred to hence forth as Working Secondary Standards (WSSes). The initial mole fraction of these secondary cylinders (see below as to why they are referred to as "secondary") were defined by the analyser itself since it's measurement technique is based on the theoretical principles of how O_2 molecules affect the refractive index of air (see Appendix A in Keeling et al. (1998a) and also (1988a)). As a check, the reliability of the initial span

calibration of the analyser was confirmed against gravimetric standards of O_2, CO_2, N_2 and Ar (Keeling et al., 1998a).

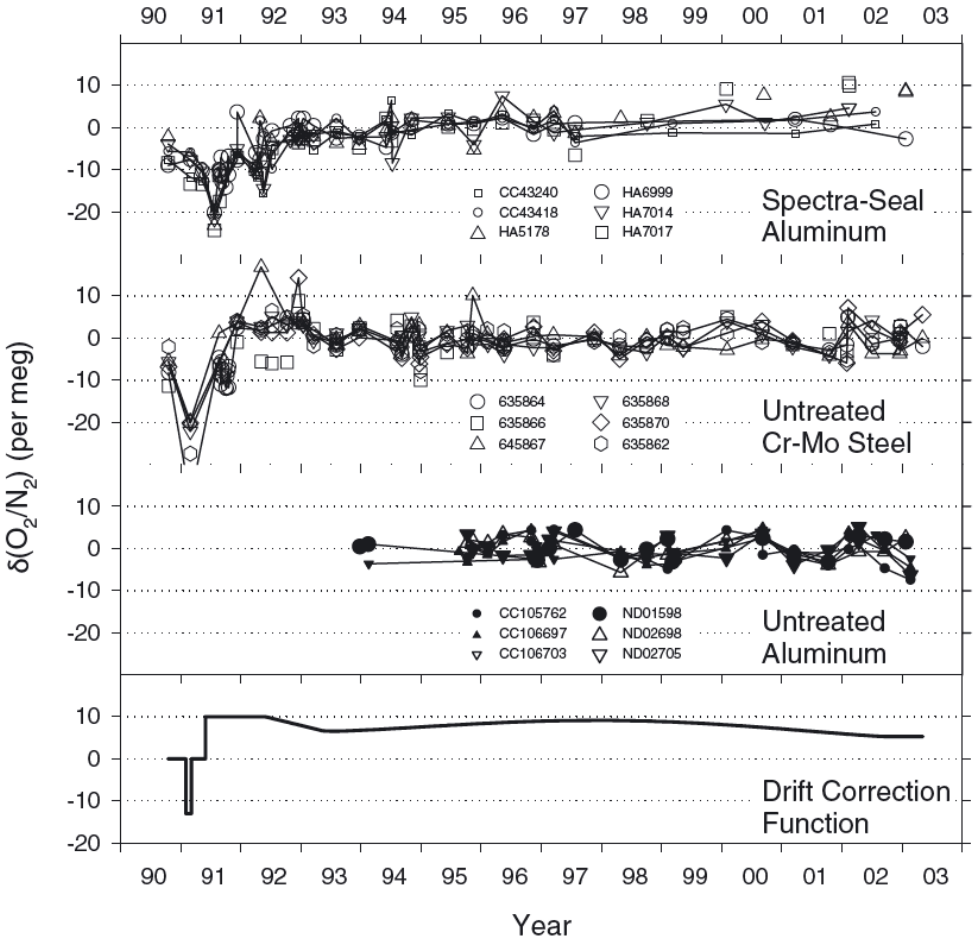

Figure 2.1. Long term stability of the $\delta(O_2/N_2)$ ratio in the 18 SIO PSSes from Keeling et al. (2007). The top three panels represent cylinders composed of a different materials. The bottom panel is the drift correction function (C_t) applied to the S1 scale to derive the S2 scale (see text). Individual symbols represent different cylinders (IDs within the figure). Measurements are presented as the difference from mean value since 1992. Step changes at the beginning of the record represent the transition from storing cylinders vertically to storing them horizontally inside a thermally insulated enclosure. For more details on the differences between individual PSSes and on the stability of the S2 scale, see Keeling et al. (2007).

The assigned concentrations of the WSSes, which are fixed, are then used to perform the daily calibration of the analyser and assign the daily WT concentration (and all subsequent WT cylinders) that sample air is measured in reference to. All three reference cylinders are then said to be on the "S1 Scale". When a WSS is about to run out, a new replacement cylinder (nextWSS) is analysed several times alongside the current WSSes and assigned a value based on the S1 scale. No two cylinders are ever

replaced at the same time and hence the S1 scale can be propagated indefinitely into the future.

However, with this system, it is impossible to determine whether one or more of the WSS cylinders are unstable, resulting in a drift of the O_2 concentration over time and therefore reducing the reliability of the S1 scale propagation (cylinder instability may be caused by a small leak or reactions on the inner surface of the cylinder for example - for a review of all potential causes of cylinder instability, see Keeling et al. (2007)). Ensuring the stability of the reference gases is crucial when using O_2 measurements to partition the land and ocean carbon sinks (see Chapter 1). A greater than 1 per meg yr^{-1} drift for example, would result in an achievable sink resolution of only 0.4 Pg C yr^{-1}, or put another way, a 20% uncertainty on a (typical) 2.0 Pg C yr^{-1} sink.

Thus, to counter this issue, SIO have 18 reference cylinders, known as Primary Secondary Standards (PSSes), composed of different materials, with different valve and regulator connections (**Figure 2.1**). The cylinders were filled at SIO between 1985 and 1994 and the WSSes are analysed against them every six months. The PSSes are assumed to be stable with respect to the WSSes. Therefore, if the O_2 concentration of the PSSes changes with time, it is assumed to reflect a drift within the WSSes and hence the S1 scale. By having a large number of PSSes, composed of different materials and with different fittings, one can reasonably assume that each PSS will not be drifting by the same amount, nor be drifting due to the same reason; if one PSS is, it will be immediately apparent.

The S1 scale can therefore be drift corrected to the S2 scale based on the PSS analyses, where S2 = S1 + C(t) and C(t) is a single drift correction function (**Figure 2.1**) (Keeling et al., 1998a; Keeling et al., 2007).

The S1 and S2 scales are arbitrarily defined to coincide on October 1990 and define zero per meg for a particular PSS (Tank HA7017) measured at that time, but filled with ambient air in La Jolla, California in September 1986 (Keeling et al., 1998a). All O_2 measurement programs around the world are thus linked to the SIO S2 scale by requesting that their own PSSes be filled by SIO and assigned concentration values using the SIO WSSes on the S1 scale, which is subsequently corrected to the S2 scale. Furthermore, all

O_2 values are reported as negative owing to the consumption of atmospheric O_2 due to the combustion of fossil fuels[2].

As can be seen in **Figure 2.1**, the SIO PSSes have been incredibly stable since the early 1990's. The large step changes at the beginning of the record are real changes in the delivered cylinder $\delta(O_2/N_2)$ owing to the discovery of thermal and gravitational effects on the O_2/N_2 ratio. Upon discovering this unwanted affect, all reference cylinders were stored horizontally in thermally insulated enclosures (for a more complete discussion, see Section 2.3 and Keeling et al. (2007)). On the corrected SIO S2 scale, the long term drift of the $\delta(O_2/N_2)$ is 0 ± 0.4 per meg yr^{-1} giving an uncertainty in O_2 based carbon sink calculations of ± 0.16 Pg C yr^{-1} (Keeling et al., 2007).

2.3. The O_2 and CO_2 measurement system and gas handling

The Halley O_2 and CO_2 measurement system (**Figure 2.2**) is based on a similar set ups first developed by A. Manning (UEA, Norfolk, UK) and B. Stephens (NCAR, Colorado, USA) and later refined by subsequent authors (Patecki and Manning, 2007a; Pickers, 2016; Stephens et al., 2007; Thompson, 2005; van der Laan-Luijkx, 2010; Wilson, 2012). In order to make very precise O_2 measurements at the level required to study the carbon cycle, one must take care to avoid certain sampling artefacts that can influence the O_2/N_2 ratio.

Firstly, fractionation of O_2 molecules relative to N_2 by diffusive separation owing to gradients in pressure, temperature and water vapour can occur. O_2, because it is the heavier molecule, preferentially accumulates in regions of higher pressure, lower temperature and higher humidity (Keeling et al., 1998a; Severinghaus et al., 1996). The influence of these effects on the O_2/N_2 ratio are not arbitrary, with variations of between 1000 to 10000 per meg (see Table 1. in Keeling et al. (1998a)). As such, the O_2 and CO_2 measurement system is designed in such a way as to minimise the effects of these phenomenon by using an extensive gas handling system that achieves: (1) very fine pressure and flow control ($\pm$ 20 mbar; $\pm$ 1 ml min^{-1}); (2) a H_2O content of < 0.5 ppm and

[2] This depletion of atmospheric O_2 does not pose a health risk to human beings see Broecker, W.S. (1970) Mans Oxygen Reserves. Science 168, 1537-1538.

(3) temperature control within the room of ± 2˚C, between calibration cylinders of ± 0.5˚C and within the analysers of ± 0.025˚C. Where gradients cannot be avoided, such as in vapour traps (see Section 2.3.2) the steady state flow achieved through (1), ensures that mass balance can be applied, such that the relative flows of O_2 and N_2 into a region equal that leaving the region, even if a concentration gradient exists (Keeling et al., 1998a).

Secondly, adsorption and subsequent desorption of molecules on the wetted materials of the system can cause fractionation of O_2 relative to N_2. Different molecules have different capacities for adsorption onto the surface of materials and the amount of adsorption typically increases with pressure (Keeling et al., 1998a). To avoid this, it is important to ensure that all inner surfaces exposed to sample or reference gas flow are well conditioned. Hence, where possible, flow and pressure are maintained throughout the system even if a particular section, the sample line for example, is not being run through the analysers. Hence a series of "purging" lines are used to achieve this (see Sections 2.3.1 and 2.3.2).

One final issue that essential to avoid is that of leaks. If the diameter of the orifice the leak is originating from is smaller than the mean free path between molecular collisions, then molecular flow will be governed by Knudsen diffusion. The velocity by which individual molecules flow out of the orifice will therefore be dependent on their molecular weight. Hence N_2 will flow out from the leak more so than O_2, again leading to fractionation (Keeling et al., 1998a).

The layout of the system is shown (**Figure 2.2**). I refer to the numbering system employed in the diagram in the following text.

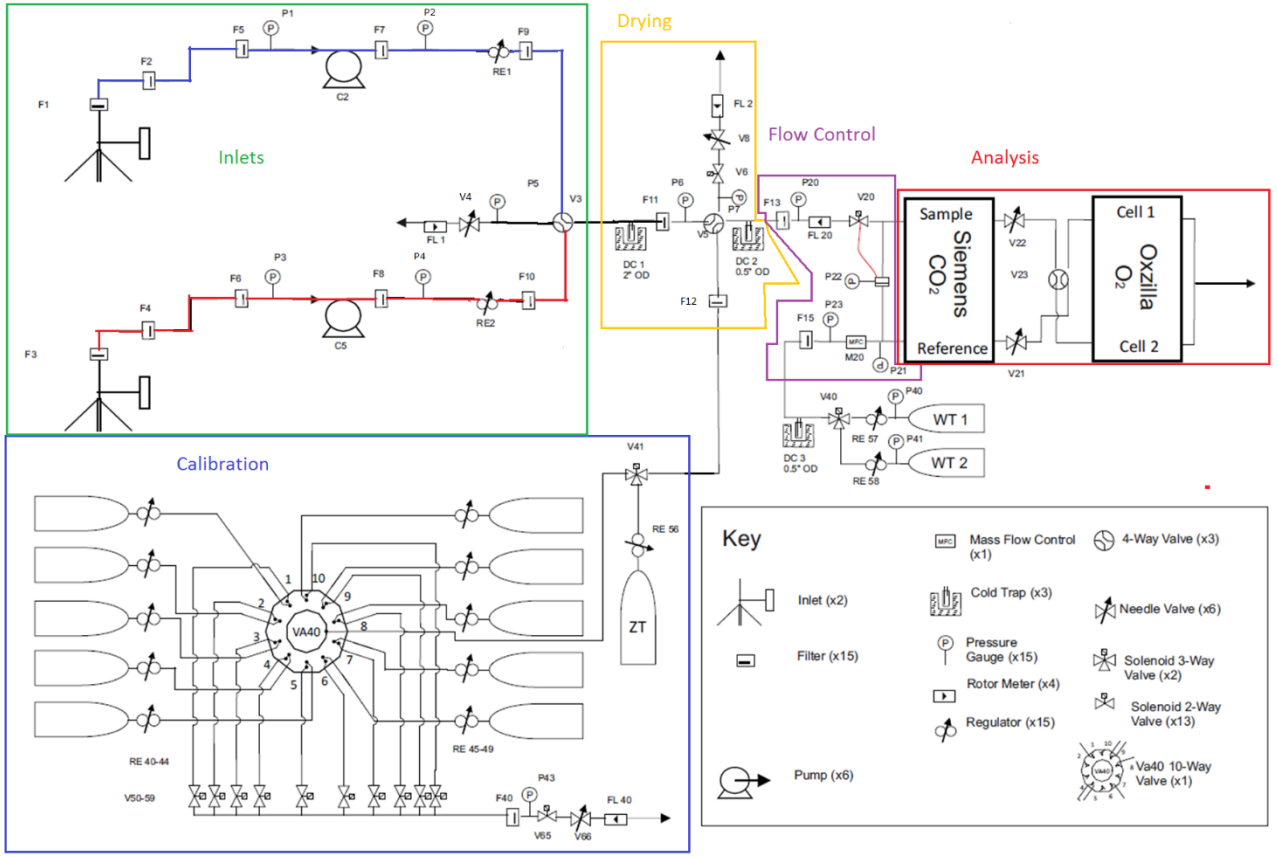

Figure 2.2. Gas handling diagram of the Halley O_2 and CO_2 measurement system. Each of the respective sections mentioned in the text are surrounded by a coloured box. Within the green "inlets" box, the red and blue lines are coloured accordingly

2.3.1. Sampling lines

Air is sampled at a height of 5m from two independent 6 mm outside diameter (OD) sample lines (termed the "red" and "blue" line) (Saint-Gobain Performance Plastics, Synflex 1300) attached to railings on the east facing side of the Clean Air Sector Laboratory roof (**Figure 2.3**A). Air is drawn into the system at a flow rate of 100 ml min^{-1} using a diaphragm pump (KNF Neuberger Inc. Type N05 on each line (C2, C5) (**Figure 2.3**B). I specifically avoid the use of elastomeric wetted materials on the pump (diaphragm and valve plates) as these have been shown to be more permeable to O_2 than

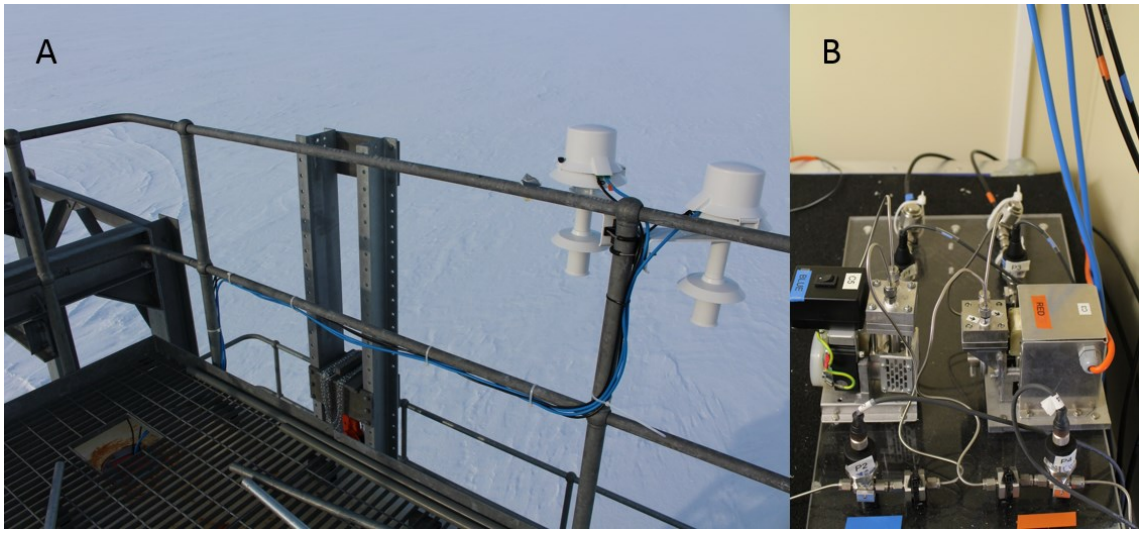

Figure 2.3. A. Location of the red (left) and blue (right) aspirated air inlets on the eastern side of the CASLab roof, approximately 5m above the ice level. Sample lines run into the building via an insulated access hole in the left of the picture. B. Sample lines run from the access hole in the roof of the measurement room to the KNF pumps (C2 and C5) via a series of filters a pressure sensors.

N_2 (Keeling et al., 1998a; Keeling et al., 2007). Instead, these components are composed of poly-chloro-tri-fluoro-ethylene (PCTFE) which has a much lower permeability for atmospheric gases (Sturm et al., 2004). At the inlet itself, I employ an aspirated radiation shield (R.M Young Company, Model 43502) (**Figure 2.3**A), the purpose of which is to minimise radiation induced thermal gradient at the inlet which has been shown to result in the fractionation of O_2 molecules relative to N_2 (Blaine et al., 2005). Each line is also fitted with a 40 micron filter (Swagelok ®, SS-4TF-40) (F1, F3) to protect the system from particulate matter, and a dielectric fitting, (Swagelok ®, .SS-4-DE-6) to protect the sensitive analysis equipment from lightning strike. A forward pressure regulator (Porter Instrument Co. Inc. Model 8286) (Re1, Re2) (**Figure 2.4**A) then steps down the pressure to ~1650 mbar on each line, which is then maintained throughout the remainder of the

system until the sample line reaches the analysers. A 4-way valve (ASCO Numatics, 3/2 series, Type 188 Micro Solenoid Valves (x2)) (V3) (**Figure 2.4**A), selects either the red or blue sample line to enter the drying stage. The remaining line is then purged to the room at a flow rate of 100 ml min^{-1} in order to maintain the conditioning of the tubing walls in the sample line and to prevent a disturbance in flow, and hence any physical gradients, downstream of V3.

The purpose of having two sampling lines is to aid in the diagnosis of issues that may arise that may influence the $\delta(O_2/N_2)$ ratio and CO_2 mole fraction - a leak for example. If only one line is employed then the change in $\delta(O_2/N_2)$ and CO_2 due to the leak may be misinterpreted as real variability in sample air. Continuously switching between two lines will prevent this misinterpretation, assuming each line will not simultaneously have the same issue in exactly the same place. During construction, this feature was invaluable for fault finding and detecting leaks.

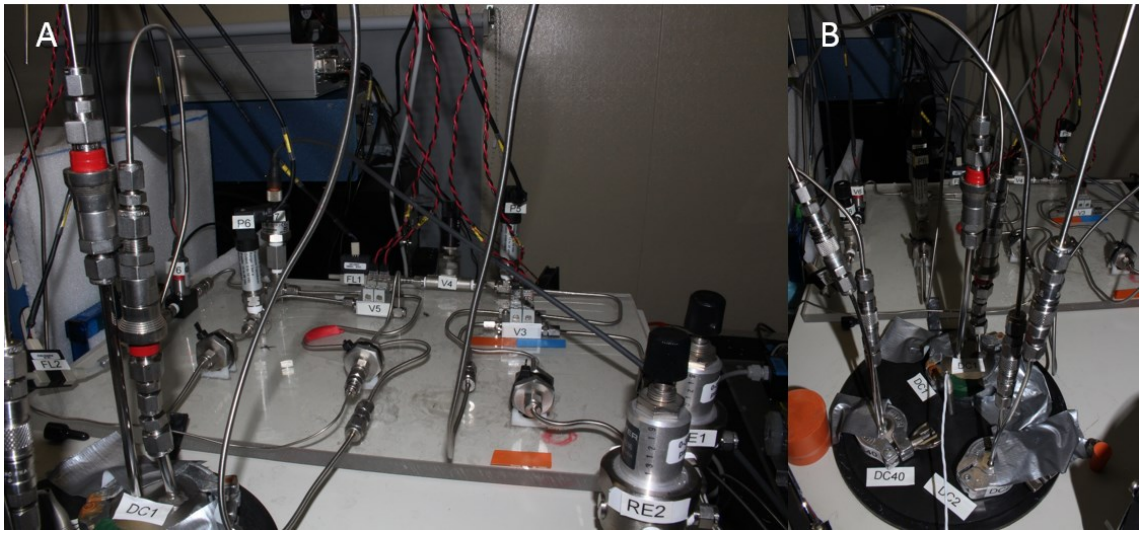

Figure 2.4. A. Gas handling set up from the blue and red line regulators (RE1 and RE2) through the line selection valve (V3) to either the line purge (P5-V4-FL1) or DC1 (see also picture B). From DC1 the sample line runs via P6 to V5 which select's either the sample line or calibration line to run to the analysers or to the slow purge (P7-V6-FL2). B. Showing the location of the three vapour traps (DC1 = 1.5" OD; DC2 and DC40 = 0.5" OD) submerged in an ethanol bath held at -90˚C. All labels in the picture correspond to the text and to that shown in **Figure 2.2**.

2.3.2. Drying

Unlike the system of Wilson (2012), I do not employ a vapour trap held at a temperature of ~1-2˚C to condense the majority of water from the air stream and therefore

extend the lifetime of a vapour trap further downstream held at -90˚C (see below). This additional drying phase was deemed unnecessary due to the low vapour content of air sampled at Halley (typically an order of magnitude dryer than that found in the UK).

The drying system consists of a vapour trap (DC1) (**Figure 2.4**B) submerged in an ethanol bath maintained at a temperature of -90˚C using a cryogenic cooler, (SP Scientific, VT490D). At this dew point temperature, one can expect a water content of 0.09 ppm (for comparison, -50˚C = 38.8 ppm H_2O). This 1.5" OD trap consists of electro-polished stainless steel, in order to reduce the capacity for monolayer adsorption of gases.

A large thermal gradient exists from -90˚C to ambient temperature at the exit of the vapour trap. At steady state, mass balance ensures the relative flows of O_2 and N_2 into and out of the trap are equal. However, when V3 switches to select a different sample line upstream of the vapour trap, a small pressure pulse is sent through the trap, disturbing the thermal gradient, resulting in O_2 fractionation and an elevated O_2/N_2 ratio at the analyser until flow returns to steady state (Severinghaus et al., 1996). To reduce the impact of this I filled with trap with 4 mm borosilicate beads that both reduce the internal volume of the trap, and increase the surface area for water vapour to condense and freeze onto (Manning, 2001). By keeping each sample line at the same flow and pressure by way of the purging line, the pressure pulse disturbing the equilibrium is also kept to a minimum. One further fail-safe I employ is to a have a "sweep out" period after a line has switched in which no measurements are recorded in order to avoid any of the above mentioned artefacts.

Following the vapour trap, a second four-way valve (V5 - as above) (**Figure 2.4**A) selects either the sample or calibration line to run through the fine pressure and flow control section of the system and subsequently onto the analysers. The line not selected for measurement is vented to the room via the "slow purge" (P7 to FL2) (**Figure 2.4**A) at a flow-rate of 100 ml min^{-1}, again to maintain conditioning of the tubing walls. The venting can also be stopped via a two-way solenoid valve (ASCO Numatics S-series) which can also be used to isolate sections of the gas handling for pressure leak checks. Immediately following V5 is a third, much smaller vapour trap 0.5" OD (**Figure 2.4**B) also held at -90˚C within the cryogenic cooler. The purpose of this trap is to ensure that both the suite of calibration cylinders and sample air pass through the analyser with the exact same water vapour content, therefore minimising any potential measurement bias.

2.3.3. Pressure and flow control.

Both the O_2 and CO_2 analysers operate in a differential mode (see Sections 2.3.5 and 2.4.1) and therefore continuously measure the sample against the WT. Although only one WT is run at a time, two WTs are always connected up to the system in order to minimise down-time between changing cylinders. The system software (see Section 2.5) continuously reads the pressure in each cylinder via a digital high pressure transmitter (WIKA, Model A-10). Once a WT is depleted (less than 5 bar[3]), three-way valve (V40 –

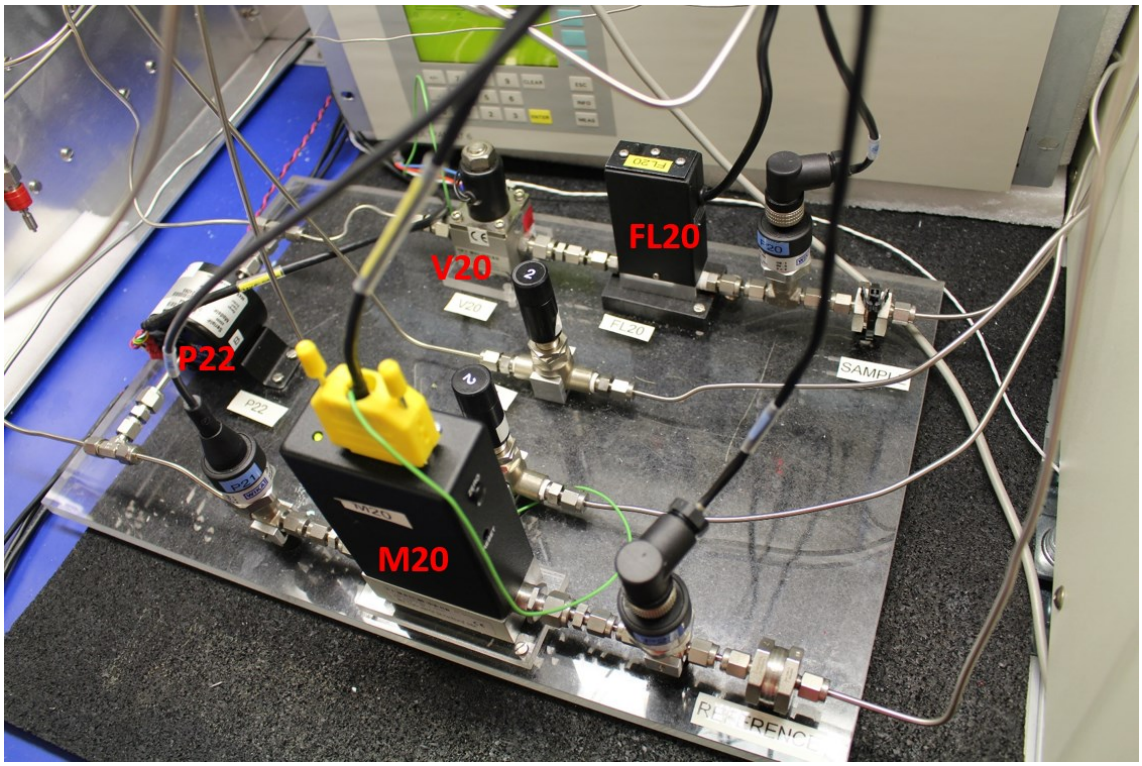

Figure 2.5. Gas handling set up for the pressure and flow control. The sample line (top of the picture) pressure and therefore flow is matched to the reference line (bottom of the picture) using a mass flow controller (M20), a differential pressure transducer (P22) and a solenoid valve (V20). The sample flow rate is monitored via FL20. Other pressure sensors (not labelled) monitor upstream and downstream pressures on the sample and reference lines.

as above) automatically switches to the full WT. Working tank air is then passed through single dedicated WT vapour trap (0.5" OD; DC40; **Figure 2.4**A), again packed with borosilicate beads and held at a temperature of -90˚C in order to ensure the water vapour content of the reference gas matches that of sample and calibration gases.

[3] 5 bar is deemed necessary to avoid preferential desorption of O_2 relative to N_2 from cylinder walls at low pressures.

The reference gas flow rate is then set to the desired 100 ml min^{-1} using a mass-flow controller (M20, MKS Instruments Inc. Type 1179A; **Figure 2.5**). The same flow rate on the sample line is then achieved through an active pressure and flow control unit consisting of: a differential pressure transducer (P22, MKS Instruments Inc. Type 223; **Figure 2.5**) connected to both lines, an electronic flow controller (MKS Instruments Inc. Type 250E) and a solenoid valve (V20, MKS Instruments Inc. Type 248A; **Figure 2.5**) on the sample line. By adjusting the valve, zero differential pressure is maintained between the sample and reference lines to within 0.001 mbar and hence the flow rate of each line is matched. As a further diagnostic, a mass flow meter (FL20, McMillan Co. Model 50D; **Figure 2.5**) is placed upstream of V20 to check the sample line flow-rate.

2.3.4. Filters

Throughout the system there are a series of 2 μm filters (Swagelok ®, SS-4FW-2) placed at locations where particulate matter could be introduced to the system and could either damage sensitive components or affect the measurements. For example, filters are placed before and after the diaphragm pumps, which have moving parts against PCTFE wetted materials. The borosilicate beads within each vapour trap can also fracture easily when they are packed into the traps, causing minute particles of glass to enter the system, hence filters are placed after each trap as well.

2.3.5. Analyser operation

Following FL20 and M20, the sample and reference lines flow into the sample and reference cells of the Siemens CO_2 analyser (**Figure 2.6**A and C). At the outlet, two metering needle valves (Brooks Instruments, model 8504) are used to match the level of restriction experienced by both the sample and reference lines (since they are of different lengths) before they reach the 4-way switching valve (V23 – as above) placed upstream of the Oxzilla O_2 analyser (**Figure 2.6**B and C). This ensures that the matched pressures at P22 result in matched flows at the analysers. This is particularly important at the inlet of the Oxzilla unit, where V23 switches the sample and reference lines every 30 seconds

so that the sample and reference lines are continuously analysed alternatively on the two individual fuel cells inside the Oxzilla unit. (See Section 2.3.5.2).

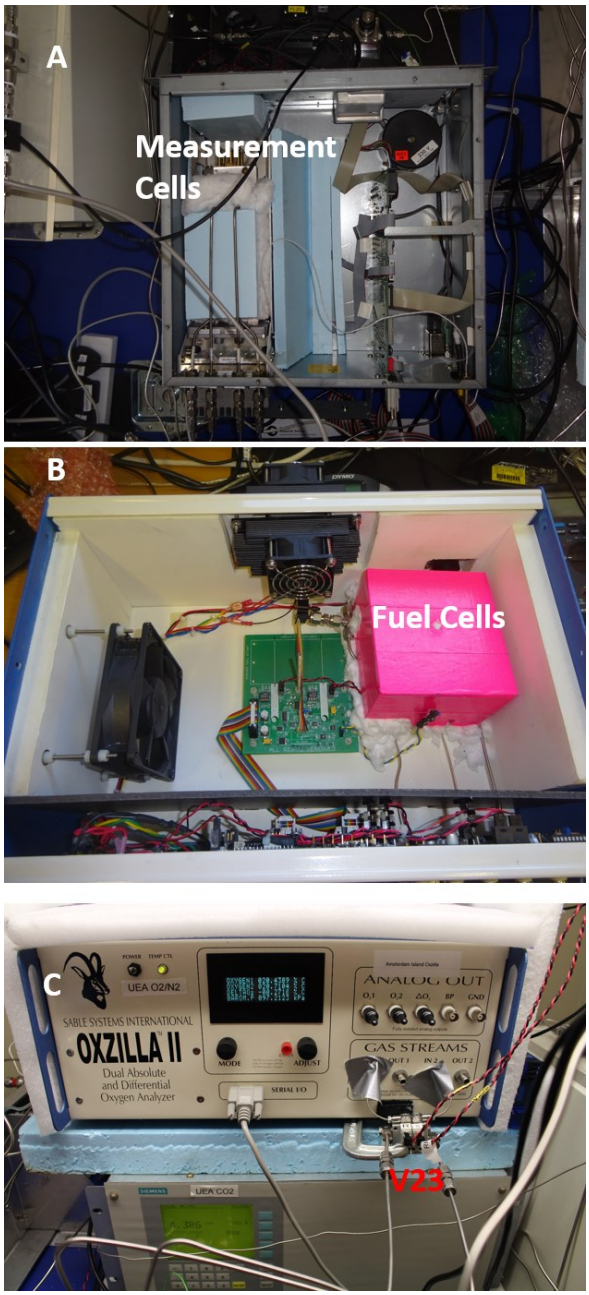

Figure 2.6. A. Internal set up of the NDIR Siemens Ultramat CO_2 Analyser with added insulation to keep the sample and reference measurement cells stable. B. Internal set up of the Sable Systems Oxzilla II analyser. The measurement fuel cells were relocated from the electronics board and housed inside a heavily insulated box to minimise small temperature and pressure variations on the cells. C. Location of V23 (switching valve) in relation to the Oxzilla inlets. The Oxzilla is located on top of the insulated Siemens CO_2 analyser.

2.3.5.1. Principles of the NDIR Siemens Ultramat CO_2 Analyser

To determine the atmospheric CO_2 mole fraction of the sample stream I use the commercially available non-dispersive infra-red (NDIR) Siemens Ultramat 6E analyser (**Figure 2.6A** and **C**). The unit consists of an infra-red (IR) source that is tuned to the absorption band for CO_2 (4.26 μm) using an optical filter. The beam is then split equally by a beam divider into a sample and reference cell. Sample air is passed through the sample cell and WT air is passed through the reference cell. The attenuation of the IR source is then measured for each cell by a detector and related to the CO_2 mole fraction using the Beer-Lambert law. By operating in differential mode, the sample stream is always measured as the difference (ΔCO_2) from the reference (WT) stream. External environmental conditions that will impact the amount of IR absorption in the cells, such as changes in temperature and pressure, will therefore impact on each cell equally. Hence, in calculating ΔCO_2, any variability driven by temperature and pressure variations will largely cancel out. The absolute value of the WT CO_2 mole fraction is determined by calibration every 47 hours (see Section 2.4.3). To further minimise the impact of external temperature variations on the response of the analyser (also known as the analyser baseline drift), I have extensively insulated the measurement cell (**Figure 2.6A**)

2.3.5.2. Principles of the Differential Lead Fuel-Cell O_2 Analyser

In this system, I use the commercially available Sable Systems International "Oxzilla II" model (*Firmware version 2.10, 2005)* (**Figure 2.6B** and **C**). The unit consists of two lead fuel-cells (Maxtec Inc. MAX-250) that alternately analyse the sample and reference gas streams, performing a differential analysis that derives the O_2 mole fraction from the difference between the signal of the sample cell and the signal of the reference cell. The fuel cells consist of a lead anode, a gold cathode and a weakly acidic electrolyte solution, which is isolated from the air stream by a semi-permeable Teflon membrane attached to the gold cathode. O_2 molecules from the air stream diffuse across the membrane and react electrochemically at the cathode, simultaneous oxidation occurs at the lead anode, liberating electrons and completing the circuit. The resulting change in the potential across the cell is measured and is proportional to the rate at which O_2 diffuses across the membrane and is therefore proportional to the partial pressure of O_2 in the air stream. This voltage (approximately $1/100^{th}$ of a volt) is then amplified by precision, low-noise circuitry within the unit.

The reactions at the anode, cathode and net reaction taking place within the fuel cells are shown in Equations **(2.3)**, **(2.4)** and **(2.5**):

$$Cathode: O_2 + 4H^+ + 4e^- \rightarrow H_2O \quad \textbf{(2.3)}$$

$$Anode: 2Pb \rightarrow 2Pb^{2+} + 4e^- \quad \textbf{(2.4)}$$

$$Net\ Reaction: 2Pb + O_2 + 4H^+ \rightarrow 2Pb^{2+} + 2H_2O \quad \textbf{(2.5)}$$

Since the output from the fuel cells is proportional to the partial pressure of O_2, any change in atmospheric pressure will cause the fuel cell output to drift. The Oxzilla II unit therefore measures the pressure of the air stream as it leaves the fuel cell and corrects this to standard barometric pressure (1013 kPa) using Equation **(2.6)**:

$$S_t = S_m \times \frac{1013}{P} \quad \textbf{(2.6)}$$

Whereby S_m is the measured fuel-cell signal output, P is the measured pressure in the outlet air stream and S_t is the corrected fuel cell signal.

In order to make the unit suitable for high precision measurements a few modifications have to be made. Firstly, all internal plastic tubing has to be replaced with 1/8" O.D. stainless steel tubing (**Figure 2.6B**) because O_2 molecules diffuse too easily through plastic (Keeling et al., 1998a). Secondly, in order to minimise the pressure difference between the two cells, the two outlet lines are combined into one with the Oxzilla internal pressure sensor repositioned to measure the pressure in this line, rather than ambient pressure. Finally, since the fuel cell response is temperature dependent, the internal temperature of the unit is monitored by the Oxzilla and maintained at a constant 32˚C using an internal fan to evenly distribute the heat within the unit. Even with this internal temperature control, I have found it necessary to insulate the fuel cells further, using glass wool, in order to protect them from tiny temperature and pressure variations induced by the internal heater and fan variability (**Figure 2.6B**).

2.4. Deriving O_2 and CO_2 mole fractions and calibration

2.4.1. From delta values to per meg and ppm

As mentioned, the Oxzilla unit derives the sample air O_2 mole fraction differentially, by continuously measuring the difference between the sample and

reference cells (ΔO_2). By doing this, any long-term drift induced by variations in external temperature and pressure affect both sample and reference lines simultaneously. To reduce short-term drift induced by individual cell noise, the sample and reference cell are switched every 60 seconds[4] using an upstream four-way valve (V23, as above). The difference of the difference between the cells in then taken, referred to as the "*double delta*" ($\Delta\Delta O_2$). This concept is displayed in **Figure 2.7**.

Here, a jog (J) is defined as three switches of V23. Such that:

$$J_1\Delta O_{2_a} = Sample_{cell\,1} - WT_{cell\,2} \quad \textbf{(2.7)}$$

$$J_1\Delta O_{2_b} = WT_{cell\,1} - Sample_{cell\,2} \quad \textbf{(2.8)}$$

$$J_1\Delta O_{2_c} = Sample_{cell\,1} - WT_{cell\,2} \quad \textbf{(2.9)}$$

"Sample" and "WT" are given in O_2 % units. The diffusivity of the fuel-cell membrane results in a characteristic response time for the sensors, hence, the first 30 seconds of measurement are discarded and the average of the data points in the remaining 30 seconds is used to determine the cell O_2% before the next switch (black boxes denoted by the letters "a", "b" and "c" in **Figure 2.7**).

The $\Delta\Delta O_2$ value is then derived such that the average of the preceding cell difference and the succeeding cell difference, is subtracted from the cell difference at the time at which the $\Delta(\Delta)$ is to be calculated – the "centre" value (b), as shown in Figure 1.4 and Equation (2.10) where:

$$J_1\Delta\Delta O_2 = \left(\frac{\bar{a} + \bar{c}}{2}\right) - \bar{b} \quad \textbf{(2.10)}$$

[4] The switching period has been optimised to 30s using Allan deviation analysis, see section 2.4.2.

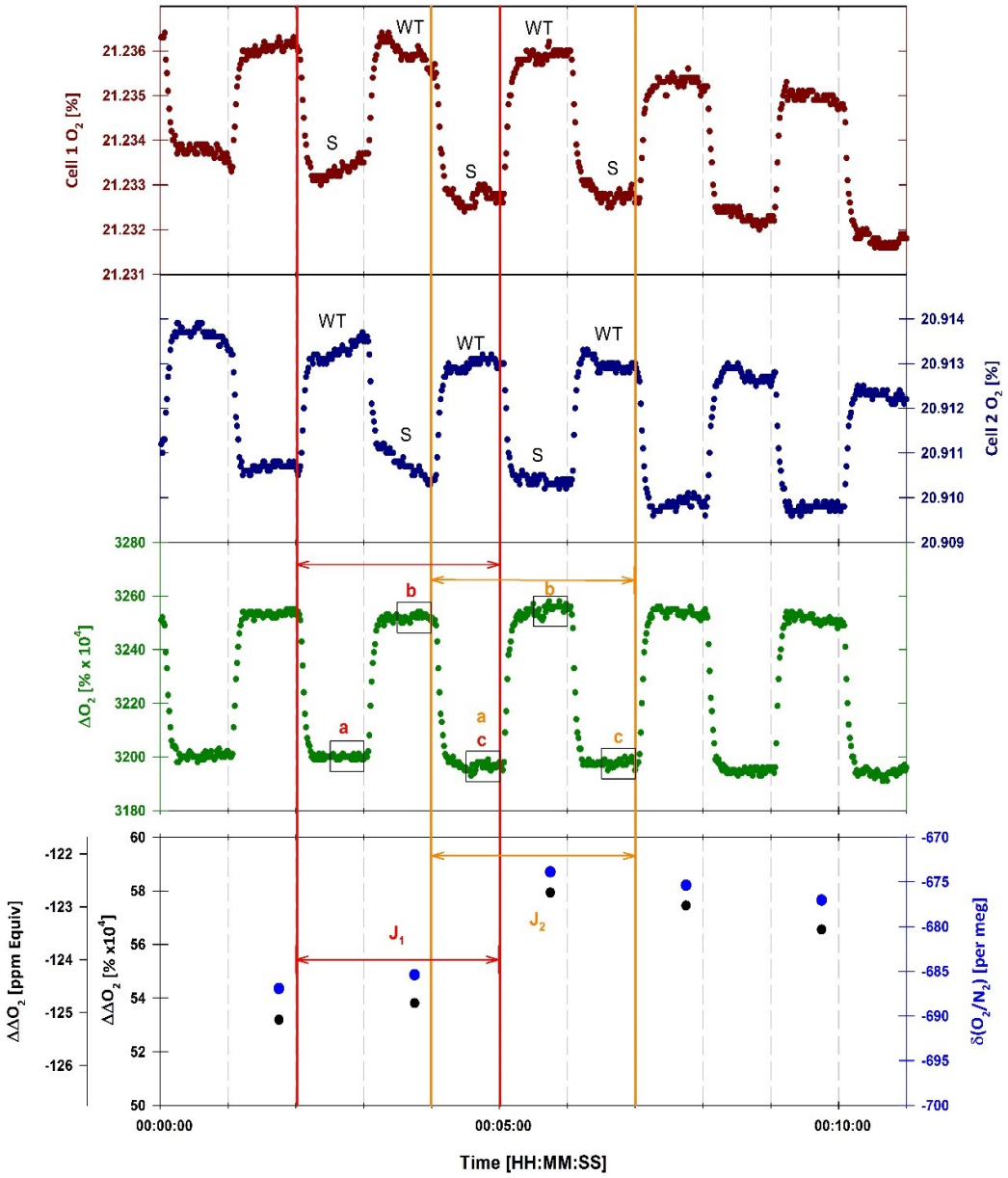

Figure 2.7. Typical repsonse of the Oxzilla during each jog, defined by the red (J_1) and orange (J_2) vertical lines, where sample (S) and reference (WT) gas are switched between cell 1 (red points) and cell 2 (upper dark blue points). The difference between each cell, ΔO_2, (green points) is taken and each jog is made up of three switches of V23, comprised of a,b and c, where the average of the last 30 seconds of measurment (black boxes) is used in the calcuation of the difference of the difference ($\Delta\Delta O_2$), as shown by Equation (2.10) in the text. The $\Delta\Delta O_2$ (black points) values are then converted to $\Delta\Delta O_2$ in ppm equivalents (ppm Equiv) (also black points) using a calibration run **Figure 2.8**), before being converted into $\delta(O_2/N_2)$ value (lower blue points) in per meg using the CO_2 mixing ratio at the point of measurment.

The second jog (J_2) then takes the preceding jog's "c" value as it's "a" value in the calculation of the next $\Delta\Delta O_2$ value with new "b" and "c" terms. By calculating $\Delta\Delta O_2$ in this manner, each data point retains enough of a relationship with the preceding data point, whilst still maintaining its independence to capture real, short term variability.

The $\Delta\Delta O_2$ % value is then converted to an O_2 value with units that are *equivalent* to parts per million (ppmEquiv) by running a calibration. Three or four cylinders, known as "Working Secondary Standards" (WSSes) with declared O_2 and CO_2 values are run on the system and a calibration curve is determined. For O_2, a simple linear relationship is determined between $\Delta\Delta O_2$ [%] and O_2 [ppmEquiv] and the equation of the line used to convert all subsequent $\Delta\Delta O_2$ values to ppmEquiv, until the next calibration is run.

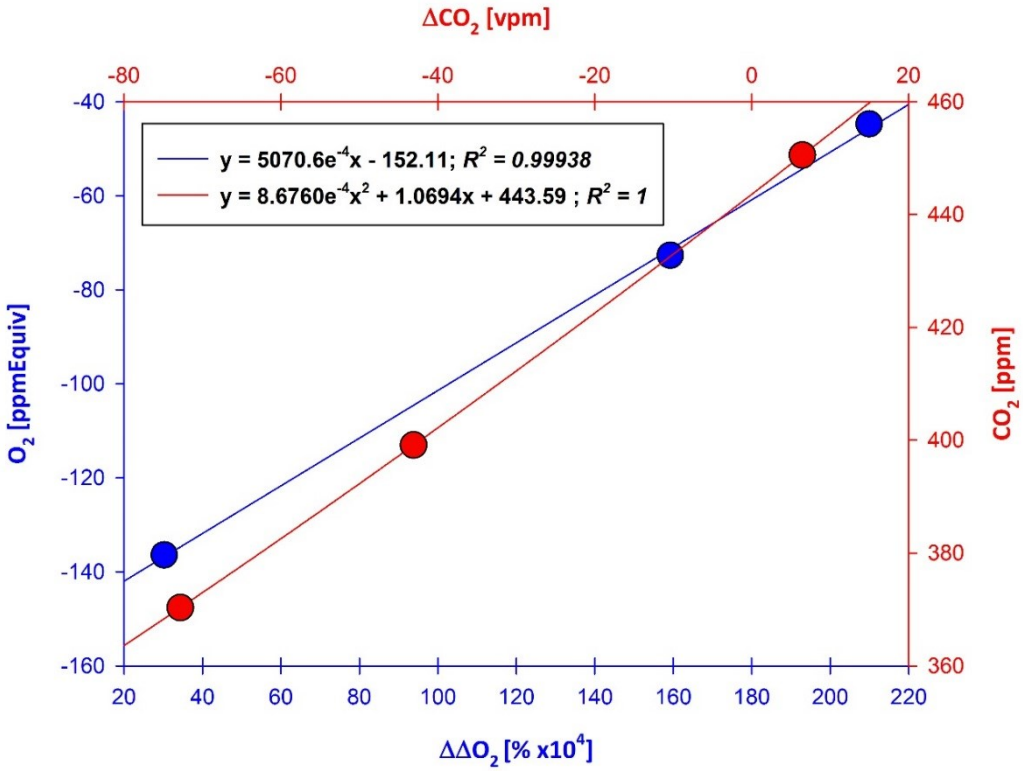

Figure 2.8. One calibration run for three WSSes showing the O_2 calibration (blue) and CO_2 calibration (red). The equation used to convert all raw sample values until the next calibration is also shown, along with the "goodness of fit" parameter of that particular calibration (R^2).

Finally, to derive the $\delta(O_2/N_2)$ value with units of per meg, the mole fraction of CO_2 is needed at the time of measurement. One then uses Equation (2.2).

For CO_2, the derivation of real mole fraction values is simpler. Rather than switching sample and reference lines every minute, the sample line is constantly measured against the WT and its difference, ΔCO_2 [vpm], is determined. The overall averaging period is 3 minutes, as for the O_2 jogs, with the "next" jog taking the last minute of the previous jog into the averaging calculation. Although the WT CO_2 mole fraction is not known before it is used as a reference gas on the system, its value is determined during

each calibration run and recalculated every four hours between calibrations using a subsequent calibration cylinder in order to account for analyser drift (known as the Zero Tank (ZT) – see section 2.4.4.1).

2.4.2. Improvements in short-term atmospheric O_2 measurement precision

Within fuel cell based O_2 measurement systems, short-term drift induced by individual cell noise is reduced by switching the sample and reference cell. This switching time has been typically set to between 60 and 120 seconds by the measurement community (Patecki and Manning, 2007b; Popa, 2008; Stephens et al., 2007; Thompson, 2005; Wilson, 2012). Since an individual measurement is determined from the average difference determined over three switches (after accounting for a 30s fuel cell sweep out time), the total averaging time is 90 seconds for 60 second switching. This 90 second average will therefore encompasses three things: ambient variability in the O_2 mole fraction, individual fuel cell noise and fuel cell drift due to variability in ambient temperature and pressure. An analysis of the Allan deviation can reliably inform on the optimum averaging time based on the trade-off between reducing noise and in reducing long term drift in the fuel cell. Hence, by running cylinder air of a fixed O_2 mole fraction through the fuel cells, without switching, one can determine the optimum averaging time. The results of this analysis are shown in **Figure 2.9**, whilst the improvements in the precision, as determined by the 1σ standard deviation of an individual $\delta(O_2/N_2)$ measurement, is shown in **Table 2.1**.

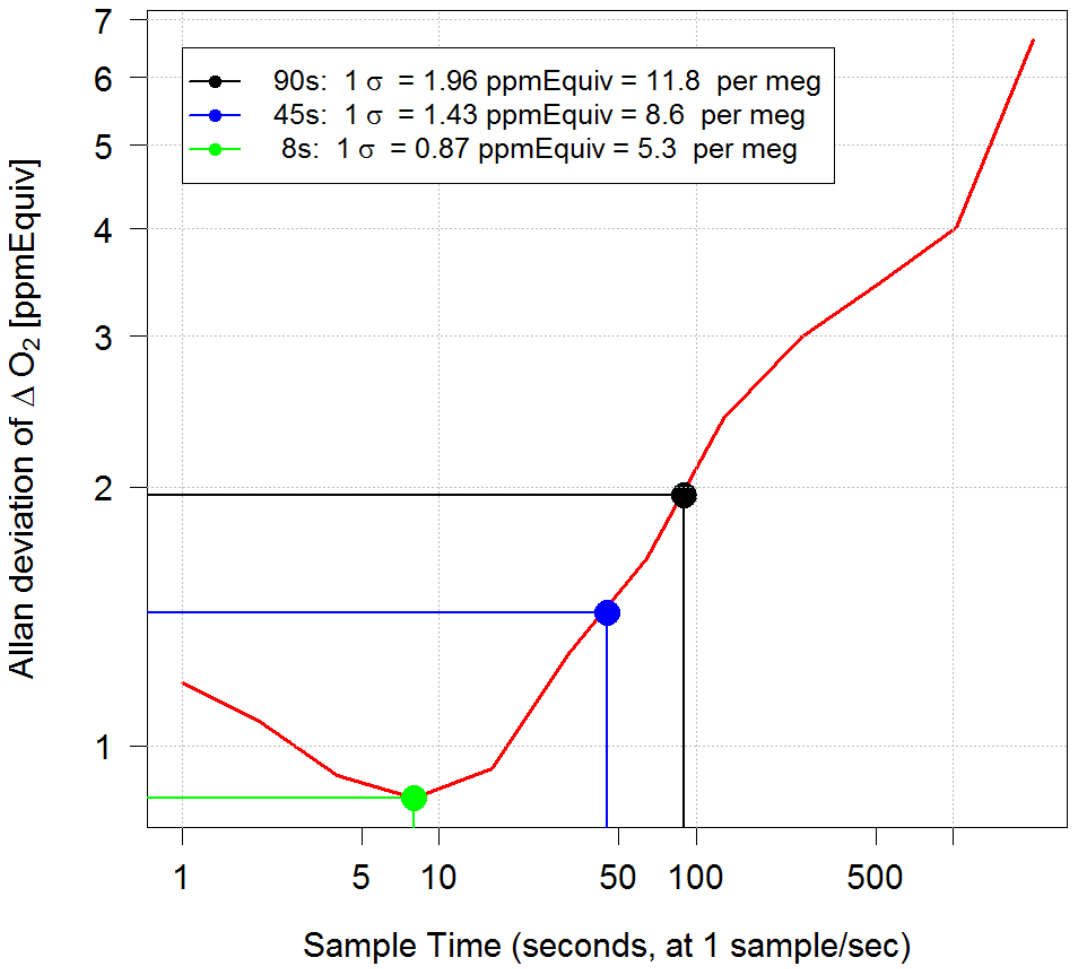

Figure 2.9. Allan deviation plot showing the optimum averaging time of the fuel cell output (green dot) based on the trade-off between reducing noise and in reducing long term drift in the fuel cell. The Allan deviation for a typical switching time (1 minute) used by colleagues is shown by the black dot. A 1 minute switching time results in three 30 second jogs which are then averaged (90 seconds). The blue dot represents the Allan deviation of the switching time used here (30 seconds; resulting in 45 seconds of averaging time). Whilst there is an improvement, the switching time cannot be reduced further due to the response time of the fuel cells (15 seconds) and in the software's ability to control valve switching in multiples of 30 seconds.

The optimum averaging time was found to be 8 seconds. This represents a ~ 2 fold improvement in the precision of $\Delta\Delta O_2$ compared to the current averaging time determined from 1 minute switching (90s). However, the optimum averaging time would require sample and reference cells to be switched every 2.7 seconds, which is well below the response time for the Maxtex © 250 fuel cell of 15 seconds. The switching frequency would therefore have to be at least ~ 18 seconds. Moreover, the current version of the software would only allow a switching frequency in multiples of 30 seconds (in order to

remain in sync with the computer clock). Consequently, using the current fuel cells and software, the optimum averaging can only be 45 seconds based on three 30s switches. Nevertheless, this still represents a 1.4 fold improvement in the precision of the $\Delta\Delta O_2$ measurement.

Future improvements in the software's ability to control the switching time could significantly improve the precision with the current fuel cell design. There is, however, a more expensive fuel cell, the Maxtec 240 ESF, which has a response time of 5 seconds, which could bring about further improvements in the measurement precision of $\Delta\Delta O_2$.

Table 2.1. Improvement in the 1σ standard deviation of an individual Target Tank and Zero Tank run from 60 second switching with 30 seconds of sweep out, to 30 second switching with 15 seconds of sweep out.

Cylinder	**Switching time : sweep-out time (s)**		**# of runs**
	60:30 1σ (per meg)	30:15 1σ (per meg)	
Target Tank	± 3.8 (n=7)	± 3.0 (n=13)	26
Zero Tank	± 3.6 (n=6)	± 2.9 (n=11)	44

2.4.3. Calibration

There are several levels of "calibration" designed to determine the span sensitivity of the analysers, account for analyser drift, characterise the performance of the system from a day to day basis and determine the long-term inter-compatibility precision and accuracy goals with similar measurement systems around the globe (See Chapter 3, Section 3.1.1).

2.4.3.1. Calibration gas handling

All of the calibration cylinders are stored horizontally in a thermally insulated enclosure, known as the "blue box" (**Figure 2.10**). Storing cylinders in such a way is crucial for achieving accurate O_2 measurements. Firstly, as already highlighted, thermal gradients cause the preferential accumulation of O_2 with respect to N_2 within the colder region due to its larger relative molecular mass, resulting in fractionation. In order to prevent this occurring within calibration cylinders, the blue box is well insulated and its temperature monitored in all corners of the enclosure. With this set up, it is possible to

achieve a thermal gradient of <1˚C m $^{-1}$. Secondly, gravimetric fractionation can occur, by up to 17 per meg per meter height, if cylinders are stored upright (Keeling et al., 2007). Storing cylinders horizontally and hence drawing gas from the relative mid–point of the cylinders (rather than the top), circumvents this problem.

To reduce the need to open the blue box, the cylinder regulators (RE40-49) are fixed to a manifold outside of the enclosure and are connected to the cylinders via 1/16”

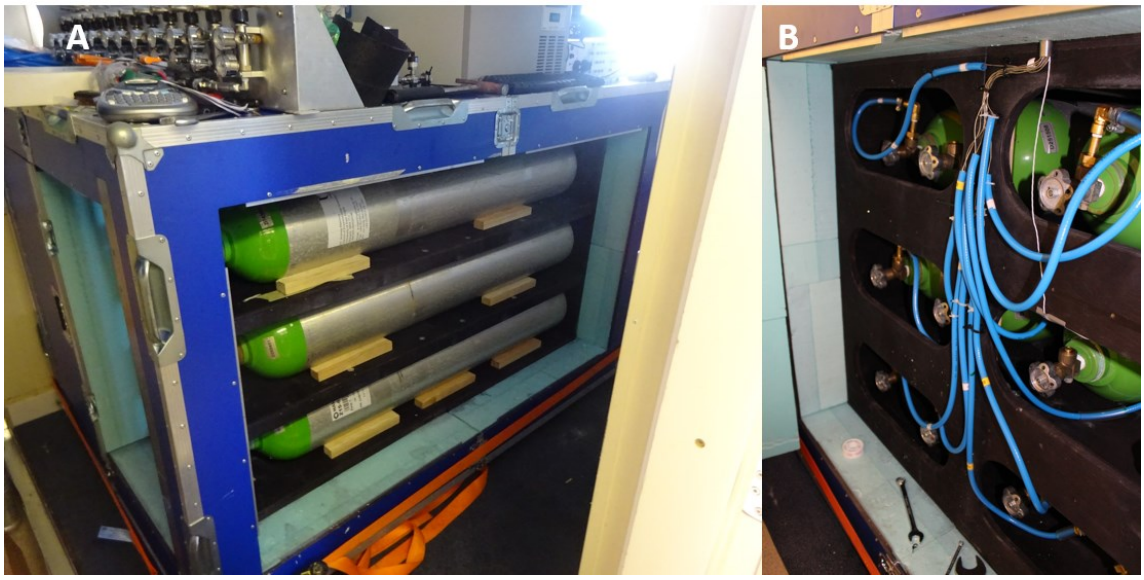

Figure 2.10. A. Horizontal storage of all cylinders, used in the calibration and quality control of the measurement system, inside the thermally insulated “blue box”. Unlike other measurement system employing the use of a cylinder storage box, the confinements of the CASLab room meant it had to be designed such that cylinders could be loaded from the side panel, rather than the front. The regulator manifold can be seen in the upper left of the picture. B. Cylinder head valve access door at the front of the blue box. 1/16” nickel tubing runs from the cylinder to the regulator manifold, located above, inside the protective blue sheath.

nickel tubing. Nickel is preferred over stainless steel as tubing material in this instance, due to these lines being at cylinder pressure (~ 200 bar). At these pressures, adsorption of gas molecules into the inner walls becomes an issue and hence the sweep out time required to flush stale air out of the tubing becomes longer. At the molecular level, nickel is much smoother than stainless steel, hence the capacity for adsorption, and sweep out time, is greatly reduced. This helps to conserve the reference gases and therefore increase their lifetime.

From the regulator, all calibration cylinders apart from the WT and Zero Tank (ZT) (Section 2.4.4.1) are connected to a multi-port valve (Valco Instruments Co Inc., SF – 10 port flow through) (Va40). Through this valve, each cylinder has its own outlet, via a two way valve (V50-59; as above), connected in parallel to a common “fast purge” line,

consisting of a two-way valve (Parker, Series 9 solenoid valve) (V65), a needle valve (V66; as above) and a mass flow meter (Honeywell, AWM3300V) (FL40).

Before cylinder air is sent to the analysers, the cylinder line is opened to the fast purge via one of V50-59 and then opened to the room via V65 and purged at a flow rate of 500 ml min^{-1} for ~10 minutes in order to sweep out the high pressure lines. Va40 then selects the required cylinder to send into the system via V5. At first, the cylinder is sent through the "slow" purge at a flow rate of 100 ml min^{-1}, before V5 is switched and the cylinder sent to the analysers. Again, the purpose of the slow purge is to maintain the conditioning of the inner walls of the reference line and prevent a pressure spike through the system on switching V5.

The above feature is in contrast to the system of Wilson (2012). Wilson (2012) has the fast purge line connected in parallel to the slow purge, by a way of a tee junction downstream of V5. The drawback of this set up is that the tubing walls between the Valco valve and V5 are subject to varying flow rates (100 ml min^{-1} and 500 ml min^{-1}). This may impact the conditioning of the walls which could therefore lead to adsorption and subsequent desorption of $O_2$and N_2, resulting in fractionation. By separating the fast purge line entirely from the rest of the system, this risk is entirely mitigated.

2.4.4. Working Secondary Standards

Firstly, as mentioned, WSSes are used to characterise the response of the analysers. The Oxzilla II fuel cell analyser has a highly linear response and so a minimum of two calibration cylinders are needed to determine the calibration curve of the form $y = a + bx$. The Siemens NDIR analyser, on the other hand, is non-linear and hence a minimum of three cylinders are needed to determine the calibration curve, following that of a quadratic of the form $y = a + bx + cx^2$. In order to improve the "goodness of fit" of the calibration curves (the R^2 value), I add one more WSS, bringing the total to four.

Two of the four WSSes were taken from a now discontinued O_2 and CO_2 measurement system that was based in Mace Head, Ireland and were therefore only 50% consumed. The remaining two WSSes were filled using ambient dry air to 200 bar at the cylinder filling facility (CFF) by Phil Wilson at UEA in August-September 2015. This facility allows the mole fraction of each species to be altered using molecular sieves and concentrated "spikes" of pure gas in order to have standards with CO_2 mole fractions and $\delta(O_2/N_2)$ ratios that span the range expected in ambient air. Unfortunately, at the time of filling, there were issues with drying of the outside air stream within the CFF set up. This

resulted in variable amounts of the water mole fraction inside the cylinders. This was quantified using a dew point meter (**Table 2.2**). I then analysed the four WSSes (in addition to two Target Tanks; see Section 2.4.4.2) on the UEA's Carbon Related Atmospheric Measurement laboratory (CRAM Lab) Vacuum Ultra Violet (VUV) O_2 (Stephens et al., 2003) and NDIR CO_2 system against a suite of PSSes in order to determine their declared $\delta(O_2/N_2)$ ratio and CO_2 mole fraction to be used in the calibration of the system. The results of this analysis are shown in **Table 2.2**. Furthermore, the CRAM lab CO_2 PSSes were filled and analysed at The National Oceanic and Atmospheric Administration (NOAA) central calibration laboratory and mole fractions determined on the WMO X2007 scale. This scale spans the range of 250-520 ppm and is maintained by a suite of 15 high pressure cylinders of ambient air, with the CO_2 mole fraction changed for each cylinder. A further 20 cylinders are used to analyse the original 15 against in order to determine if an individual cylinder is drifting (in much the same way SIO do for O_2 (Section 2.2.2) (Tans and Zellweger, 2014). The O_2 PSSes were filled and analysed at SIO and their mole fractions declared on the SIO S2 scale for O_2. In this way, my own measurement system is linked to an internal CRAM Lab CO_2 and O_2 scale, which is then linked to the primary WMO X2007 and SIO S2 for CO_2 and O_2, respectively. This allows my measurements to be "compatible" (see definition in Chapter 3, Section 3.1.1) with all other measurement systems on these scales. However, this "link" still needs be quantified, such that CRAM Lab is "comparable" (see definition in Chapter 3, Section 3.1.1) to other laboratories on the same scale. This is done using inter-comparison cylinders with known atmospheric gas mole fractions. The internal compatibility between the CRAM Lab scale and my own measurement system scale is subsequently determined using the Target Tank analyses (see section 2.4.4.2) and ideally, through reanalysis of the WSSes at the end of their lifetime.

The four WSSes are analysed on the system every 47 hours and the new calibration curve for O_2 and CO_2 used for all subsequent data points until the next calibration run. The WSS run is timed such that it is not a multiple of 24 hours to avoid calibrations being determined at precisely the same time of day when external environmental conditions may be similar.

Table 2.2. CO_2 mole fractions and $\delta(O_2/N_2)$ ratios of the calibration cylinders (WSSes) and Target Tanks (TT) used on the Halley measurement system, defined using the CRAM Lab VUV O_2 and Siemens NDIR CO_2 measurement system. Dew points were determined using a Vaisala dew point meter. The number of runs refers to the amount of times each cylinder was analysed on the CRAM lab system and therefore the number of measurements used to calculate a mean defined value.

Cylinder ID	Purpose	Pressure (psi)	$\delta(O_2/N_2)$ (per meg)	σ (per meg)	n runs	CO_2 (ppm)	σ (ppm)	n runs	Dew point H_2O (ppm)
D273561	WSS1	2690	-762.87	0.55	9	412.697	0.007	7	9.3
D743657	WSS2	2670	-548.61	0.34	1	399.763	0.004	8	6.5
D743659	WSS3	1250	-857.25	0.63	9	409.306	0.006	6	-
D801293	WSS4	1500	-647.49	0.41	8	388.292	0.004	7	0.4
D743652	TT1	2600	-596.47	0.78	6	394.690	0.007	4	15.4
D089506	TT2	2550	-595.11	0.66	6	402.780	0.007	4	8.0

When a new WSS cylinder is needed, termed "nextWSS", it is analysed against the original WSSes several times and given declared values based on the original WSS scale. The replacement of WSSes are staggered such that only one WSS is ever replaced at once. Thus, the nextWSSes remains on the original HBA scale and so this independent station scale can be propagated into the future.

2.4.4.1. Zero tank

As mentioned previously, a fifth calibration cylinder, termed the Zero Tank (ZT), is run every four hours between calibrations. The purpose of the ZT is to correct for any baseline drift in the CO_2 analyser, which, due to its operation principle, is very sensitive to changes in ambient temperature. The correction is applied to the "a" term (the intercept) in the CO_2 calibration curve since it is the most sensitive term in this equation to baseline drift. The ZT itself does not contain "zero" CO_2, rather, it contains an ambient CO_2 mole fraction within the range of the calibration WSSes. This makes the ZT much more suitable to be used in the correction of the calibration curve a-term.

Immediately following a WSS calibration, the ZT is run and it is assigned a CO_2 mole fraction (ZT_a). Here, I make the reasonable assumption that no analyser drift has occurred between the end of the WSS run and the ZT run. Four hours later, the ZT is run again and a new CO_2 mole fraction determined (ZT_b). The difference between ZT_a and ZT_b is then used as the correctional factor for the a-term in the quadratic equation, therefore adjusting the calibration curve used in the determination of subsequent sample air CO_2 mole fractions and thus accounting for any drift in the baseline response of the CO_2 analyser. On the next ZT run, the CO_2 mole fraction for the cylinder is once again determined (ZT_c), however, rather than taking the difference to the previous run (ZT_c -

ZT_b), the difference is taken to the first run (ZT_c - ZT_a). This is because in the previous a-term correction, the drift between ZT_a and ZT_b has already been accounted for. In other words, if no drift had occurred between ZT_b and ZT_c, then the difference between ZT_c and ZT_a will be zero, because the initial drift between ZT_b and ZT_a has already been accounted for.

The ZT is not used for any correction to the O_2 calibration curve. The operational principle of the Oxzilla II means that it is not susceptible to baseline drift in the way the CO_2 analyser is. However, the $\delta(O_2/N_2)$ is still reported and can therefore be used as a diagnostic to assess the state of the system. For example, an anomalous ZT $\delta(O_2/N_2)$ may indicate a malfunction in the system (e.g. a leak) or a drifting ZT cylinder.

The ZT is stored inside the blue box, but instead of being connected to Va40, it is connected via a three-way valve (V41, as above) to the reference line that joins the system at V5. Since the ZT is run so frequently, it does not need to be "fast purged" to clear stale air as much as the WSSes or Target Tank (see section 2.4.4.2). Instead, it is sent through the slow purge for ~4 minutes before V5 and the ZT is run through the analysers.

2.4.4.2. Target Tank

The Target Tank (TT) is a cylinder of air, with a known $\delta(O_2/N_2)$ ratio and CO_2 mole fraction that I determined on the CRAM Lab measurement system before installation on the HBA system (**Table 2.2**). It is run every 10 hours and is used as a quality control check on the performance of the system. It is important to note that it is not used in the calibration of the system. Within the system software (see Section 2.5) acceptable deviations from the declared values are set. If the TT results fall outside of this range, then the run is flagged. If no explanation can be found for the anomalous results, such as a spike in the analyser response, then a question is placed over the validity of the previous calibration and sample air data may need to be discarded.

The results of the TT runs also serve as a measure of the internal reproducibility and compatibility (definitions given in Chapter 3) of the overall system and helps to quantify any offsets the HBA scale may have from the CRAM Lab scale. Although it would be more favourable to run the TT through the same gas handling procedure as outside air (through the pump and drying sections), this is not possible with the current gas handling set up. Instead, the TT is run through the same route as the WSS gas handling.

2.5. Data acquisition, control software and automation

The measurement system is designed in such a way such that sample air measurements, analyser calibration and quality control can all be carried out autonomously with minimal human intervention. This is one of the key requirements for installing on a remote Antarctic base where personnel time in split between many different scientific experiments. To achieve this, I have inherited sophisticated control software that integrates with each of the system components, described above, through an electronics control box (**Figure 2.11**). This bespoke control and data acquisition system has been developed by the UEA's Research Computing Services software engineer, Alex Etchells, the UEA's Electrical Engineering team, Nick Griffin and Dave Blomfield, in conjunction with current and previous CRAM research group members over

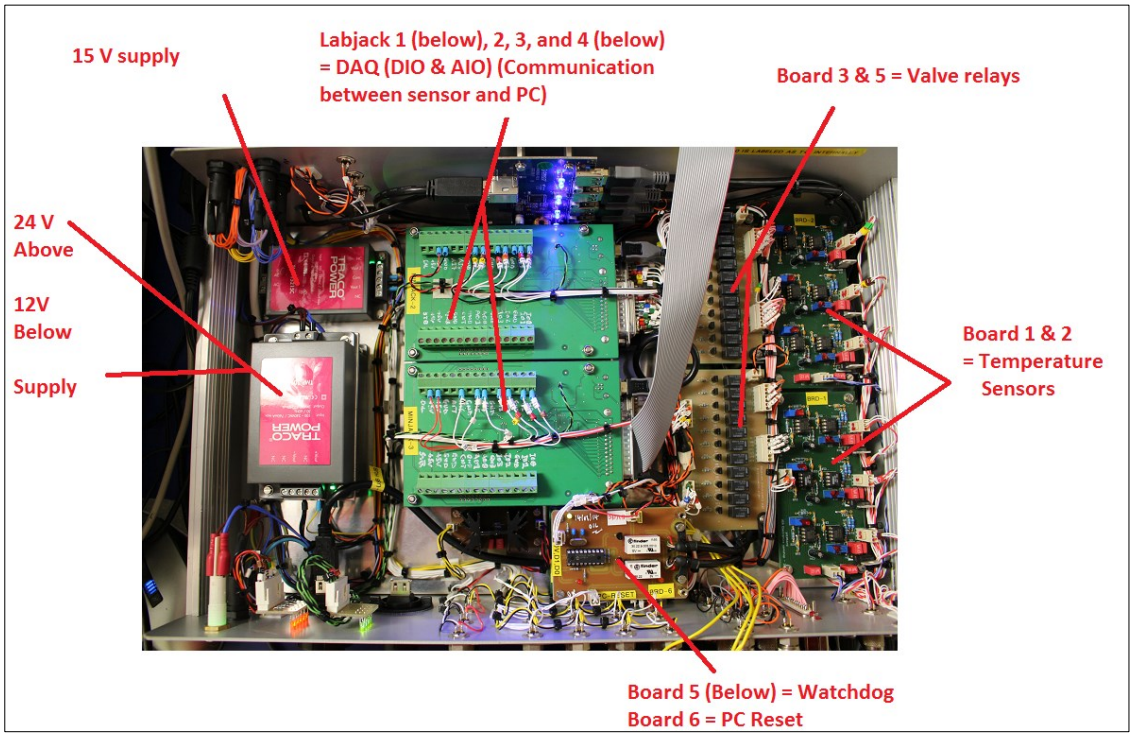

Figure 2.11. Overview of the main components within the electronics control box, designed and built by Nick Griffin of the UEA Environmental Sciences Electrical Engineering Workshop. The "watchdog" on board 5 detects if the computer software has malfunctioned and therefore sends a command via the PC Reset board for the computer to automatically reboot. All other components are self-explanatory or explained in the text.

a 10 year period. The first iteration of this setup was installed on the Weybourne Atmospheric Observatory (WAO) O_2 and CO_2 measurement system (Wilson, 2012). Since then, the software and electronics has been continuously upgraded and improved

as the automation technique becomes more refined and encounters more unique field station specific issues. The most recent iteration of the software was utilised on the Hamburg Sud Ship O_2 and CO_2 measurement system (Pickers, 2016).

All pressures sensors (15), flow meters/controllers (5), temperature sensors (6) and control valves (19) are powered via an electronics control box (custom built by Nick Griffin; **Figure 2.11**). Diagnostic data from each of these components are collected via four USB DAQ (Universal Serial Bus Data Acquisition) U12 series Labjacks which are then passed to the control computer (Shuttle XH61V Intel System, Ambros Direct UK Ltd) via a USB connection. All of the diagnostic data is recorded via the bespoke control software, written by Alex Etchells in C#, and written to diagnostic files every 30 seconds. The software, also known as "Baloo" (to distinguish it from similar data acquisition systems within the CRAM Lab group), provides an interactive user interface to allow real time monitoring of all diagnostic data and allows remote manipulation of individual valves (**Figure 2.12**) via a relay board, installed within the electronics box.

In order for Baloo to run the O_2 and CO_2 measurement system without human intervention, several Macros are written that are called at user defined intervals (for example, running a Zero Tank, every 4 hours). The commands within the macros open, close and switch valves when required to send cylinder air or sample air to measurement. Through the macros, the user has complete control over the timing between individual commands to allow for the correct amount of purging on calibration and TT cylinders and to allow the correct amount of sweep-out time within the analysers before measurement data is recorded. Furthermore, various quality control thresholds can be set by the user, such as acceptable TT deviations and acceptable calibration analyser response function coefficients - which allows poor calibrations to be rejected automatically or enables the user to enter information into a quality control file that ranks the validity of the data. Various diagnostics thresholds are also definable to allow for further quick determination of various issues; a drop in the current to the aspirated air inlet fans, for example, indicating a faulty fan, or a drop in the pressure of P6 (**Figure 2.12**) indicating the blocking of the vapour trap with ice. For those interested in the operating procedure of the measurement system, please refer to the user-friendly "Baloo Manual" in the

Appendix A. I wrote this for the technicians tasked with maintaining my system at the Halley Research Station.

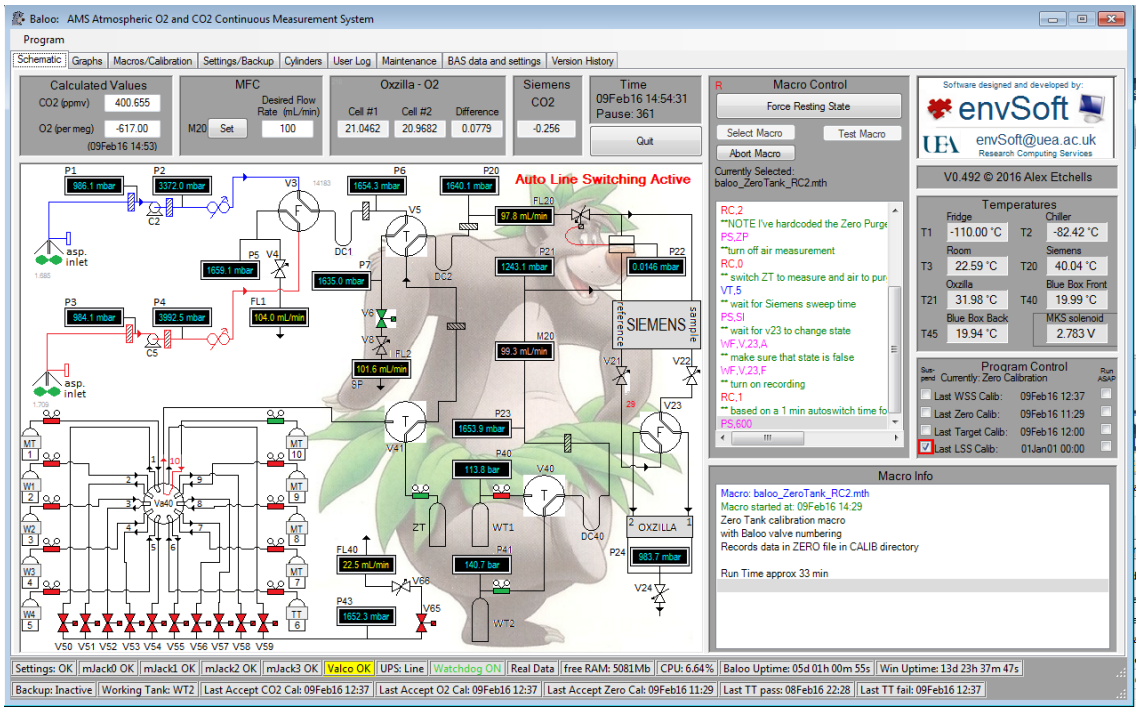

Figure 2.12. The main "Schematic" tab within the Baloo software responsible for the control, automation and data acquisition of the HBA O_2 and CO_2 measurement system. All valves are clickable such that a user can override the macro control in order to identify potential issues within the system. Pressure sensors, flow meters and temperature sensors all display live read outs. Other tabs within the software allow the user to (1) see a live plot of the previous hours analyser, flow and temperature data (Graphs), (2) display diagnostics of the most recent calibration and quality control checks and determine the order and run time of individual macros (Macros/Calibration), (3) input sensor calibration information and determine back up directories (Settings/Backup), (4) upload information of the CO_2 mole fraction and $\delta(O_2/N_2)$ ratio of calibration cylinders (Cylinders), (5) enter information into a logbook to record system maintenance and potential issues relating to the quality of the data (User Log), (6) Display information relating to general maintenance tasks and the dates at which they should be carried out by (Maintenance), and finally (10), which is unique to the HBA measurement system, a live read out of all meteorological data and other trace gases recorded by a suite of analysers housed within the CASLab (BAS data and settings). The software was written in C# by Alex Etchells of the UEA Research Computing Services department.

2.6. Summary and conclusions

In this chapter, I began by outlining the history and theory of making atmospheric O_2 measurements. This knowledge then fed into the choice of the system design required for *in situ* continuous atmospheric O_2 and CO_2 measurements at a remote field station such as Halley Research Station. I explained in detail the gas handling procedure, sample gas drying, analyser operation, and calibration procedures and data acquisition. The initial build and testing of the system occurred between January 2014 and August 2015 at UEA. The system was tested using air sampled from the roof of the School of Environmental

Sciences at UEA between March and August 2015. However, since calibration standards were not available at the time, calibrations were run infrequently (once every 2 to 3 weeks). Consequently, although this period was invaluable in overcoming "teething" problems, particularly with the software and electronics control system, I have not included it here in this thesis. Instead, I have presented an assessment of system performance in the following Chapter 3.

The period of testing did prove that the system fulfilled the objectives laid out in the introduction of this chapter, that is, to have a fully automated, continuous atmospheric O_2 and CO_2 measurement system that could be installed at the Halley Research Station in order to fill in the observational O_2 "gap" in the South Atlantic sector of the Southern Ocean. The next step is to determine whether the system meets comparability, compatibility and reproducibility goals, set out by the World Meteorological Organisation's (WMO) Global Atmospheric Watch (GAW) programme, which determine whether the measurements can be deemed useful for regional to global carbon cycle analyses. This will be the focus of the next chapter.

The modifications I have implemented in this build compared to the system of Wilson (2012) do represent improvements in system design that other members of the O_2 measurement community may want to consider.

Firstly, the separation of the "fast purge" line, that is required to remove stale air from the cylinder lines, from the "slow purge" line. This modification allows the line from the Valco valve to V5 to only receive air flowing at 100 ml min^{-1}, therefore maintaining the conditioning of the tubing walls that minimises differential adsorption and subsequent desorption of O_2 and N_2, which may lead to fractionation effects. However, I was not able to quantify the potential improvement this modification may have had on the reproducibility of a target gas owing to time constraints. To do this, one would have to run a target gas through the system and make repeated measurements of the $\delta(O_2/N_2)$ ratio at predefined intervals over the period of a week or longer. The system could then be modified back to the original set up of Wilson (2012) for the fast purge and the analysis run again. The difference between the results, if there are any, would then quantify the effect this improvement may have had on the internal reproducibility of the system.

Secondly, I removed the first stage drying component from my system compared to that of Wilson (2012). This was achievable due to the low water vapour content of air sampled at the Halley Research Station. Implementation of this modification by others

therefore depends on the ambient water vapour content at their chosen measurement site. This should be considered however, as there is the potential to reduce the cost and reduce the complexity of the system, removing components which otherwise could contribute to leaks due to the additional number of fittings required. On the other hand, the lifetime of the vapour trap submersed in the cryogenic cooler (typically 1 month, before it needs to be replaced at Halley) could be extended by having a first stage drying component. For the Halley system, I would recommend chemical drying, such as the use of magnesium perchlorate, over the more traditional water vapour condensation technique employed by Wilson (2012). This is simply because the air sampled at Halley is already below the dew point that can be achieved from such a condensation based drying set up.

Finally, and perhaps most importantly, I have demonstrated the impact that a faster sample and reference fuel cell switching time has on improving the precision, by up to a factor of 1.4 in this case. The ideal averaging time was found to be 8 seconds, which would require switching sample and reference lines every 2.6 seconds. Owing to the current fuel cells response time (Maxtec MAX-250; 15 seconds) and the constraints imparted by the software control, this was simply not possible. A switching time of 30 seconds was instead implemented allowing a reduction of the averaging time from 90 seconds to 45 seconds which lead to the 1.4 fold improvement in precision. However, the more expensive Maxtec 240 ESF fuel cell has a response time of 5 seconds. Using this, one could then switch the sample and reference lines every 7.6 seconds (if software control constraints were also overcome), allowing the ideal averaging time of 8 seconds to be reached which would results in 2.2 fold improvement in precision. Future O_2 measurement system builds should therefore consider this if they are to use the fuel cell measurement technique.

In the following chapter, I present an analysis of the measurement system diagnostics; a crucial inquiry if the system is to comply with WMO/GAW standards which are set so as to ensure the recording of observations that can be used reliably in the scientific investigation of greenhouse gas emissions and sinks.

2.7. References

Bakker, D.C.E., Hoppema, M., Schröder, M., Geibert, W., De Baar, H.J.W. (2008) A rapid transition from ice covered CO_2-rich waters to a biologically mediated CO_2 sink in the eastern Weddell Gyre. Biogeosciences Discussions 5, 1205-1235.

Bender, M.L., Tans, P.P., Ellis, J.T., Orchardo, J., Habfast, K. (1994) A high precision isotope ratio mass spectrometry method for measuring the O_2/N_2 ratio of air. Geochimica et Cosmochimica Acta 58, 4751-4758.

Benedict, F.G. (1912) The composition of the atmosphere with special reference to its oxygen content. Carnegie Institution of Washington.

Blaine, T.W., Keeling, R.F., Paplawsky, W.J. (2005) An improved inlet for precisely measuring the atmospheric Ar/N_2 ratio. Atmos. Chem. Phys. Discuss. 5, 11899-11910.

Broecker, W.S. (1970) Mans Oxygen Reserves. Science 168, 1537-1538.

Evans, G.R., McDonagh, E.L., King, B.A., Bryden, H.L., Bakker, D.C.E., Brown, P.J., Schuster, U., Speer, K.G., van Heuven, S.M.A.C. (2017) South Atlantic interbasin exchanges of mass, heat, salt and anthropogenic carbon. Progress in Oceanography 151, 62-82.

Keeling, R.F., (1988a) Development of an interferometric oxygen analyzer for precise measurement of the atmospheric O_2 mole fraction, Division of Applied Sciences. Harvard University, Cambridge, Massachusetts, U.S.A., p. 178.

Keeling, R.F. (1988b) Measuring correlations between atmospheric oxygen and carbon dioxide mole fractions: A preliminary study in urban air. Journal of Atmospheric Chemistry 7, 153-176.

Keeling, R.F., Manning, A.C., McEvoy, E.M., Shertz, S.R. (1998) Methods for measuring changes in atmospheric O_2 concentration and their applications in southern hemisphere air. Journal of Geophysical Research-Atmospheres 103, 3381-3397.

Keeling, R.F., Manning, A.C., Paplawsky, W.J., Cox, A.C. (2007) On the long-term stability of reference gases for atmospheric O_2/N_2 measurements. Tellus Series B-Chemical and Physical Meteorology 59, 3-14, doi:10.1111/j.1600-0889.2006.00228.x.

Keeling, R.F., Shertz, S.R. (1992) Seasonal and interannual variations in atmospheric oxygen and implications for the global carbon cycle. Nature 358, 723-727, doi:710.1038/358723a358720.

Machta, L., (1980) Oxygen depletion, in: Jacoby, G.C. (Ed.), Proceedings of the International Meeting on Stable Isotopes in Tree Ring Research, pp. 125-127.

Machta, L., Hughes, E. (1970) Atmospheric oxygen in 1967 to 1970. Science 168, 1582-1584.

Manning, A.C., (2001) Temporal variability of atmospheric oxygen from both continuous measurements and a flask sampling network: Tools for studying the global carbon cycle, Scripps Institution of Oceanography. University of California, San Diego, La Jolla, California, U.S.A., p. 202.

Manning, A.C., Keeling, R.F., Severinghaus, J.P. (1999) Precise atmospheric oxygen measurements with a paramagnetic oxygen analyzer. Global Biogeochemical Cycles 13, 1107-1115.

Patecki, M., Manning, A.C., (2007a) First results from shipboard atmospheric O_2 and CO_2 measurements over the North Atlantic Ocean, Oceans 2007 - Europe. doi: 10.1109/OCEANSE.2007.4302351, IEEE, Aberdeen, Scotland, UK.

Patecki, M., Manning, A.C., (2007b) First results from shipboard atmospheric O_2 and CO_2 measurements over the North Atlantic Ocean, Oceans 07. IEEE, Aberdeen, pp. 1-6, doi: 10.1109/OCEANSE.2007.4302351.

Pickers, P.A., (2016) New applications of continuous atmospheric O_2 measurements: meridional transects across the Atlantic Ocean, and improved quantification of fossil fuel-derived CO_2, School of Environmental Sciences. University of East anglia Norwich p. 291.

Popa, E.M., (2008) Contunuous tall tower multispecies measurements in Europe for quantifying and understanding land-atmosphere carbon exchange.

Severinghaus, J.P., Bender, M.L., Keeling, R.F., Broecker, W.S. (1996) Fractionation of soil gases by diffusion of water vapor, gravitational settling, and thermal diffusion. Geochimica et Cosmochimica Acta 60, 1005-1018.

Stephens, B.B., Bakwin, P.S., Tans, P.P., Teclaw, R.M., Baumann, D.D. (2007) Application of a differential fuel-cell analyzer for measuring atmospheric oxygen variations. Journal of Atmospheric and Oceanic Technology 24, 82-94, doi:10.1175/JTECH1959.1171.

Stephens, B.B., Keeling, R.F., Paplawsky, W.J. (2003) Shipboard measurements of atmospheric oxygen using a vacuum-ultraviolet absorption technique. Tellus Series B-Chemical and Physical Meteorology 55, 857-878.

Sturm, P., Leuenberger, M., Sirignano, C., Neubert, R.E.M., Meijer, H.A.J., Langenfelds, R., Brand, W.A., Tohjima, Y. (2004) Permeation of atmospheric gases through polymer O-rings used in flasks for air sampling. Journal of Geophysical Research-Atmospheres 109.

Tans, P.P., Zellweger, C., (2014) Report of the Seventeeth WMO/IAEA Meeting on Carbon Dioxide, Other Greenhouse Gases, and Related Measurement Techniques (GGMT-2013), in: Tans, P.P., Zellweger, C. (Eds.), Beijing, China, pp. available at http://www.wmo.int/pages/prog/arep/gaw/gaw-reports.html.

Thompson, R.L., (2005) Variations in Atmospheric O_2 and CO_2 in the Southern Ocean Region from Continuous Ship-based Measurements. Victoria University of Wellington, Wellington, p. 184.

Tohjima, Y. (2000) Method for measuring changes in the atmospheric O_2/N_2 ratio by a gas chromatograph equipped with a thermal conductivity detector. Journal of Geophysical Research-Atmospheres 105, 14575-14584.

Tohjima, Y., Machida, T., Watai, T., Akama, I., Amari, T., Moriwaki, Y. (2005) Preparation of gravimetric standards for measurements of atmospheric oxygen and reevaluation of atmospheric oxygen concentration. Journal of Geophysical Research D: Atmospheres 110, 1-11.

van der Laan-Luijkx, I.T., (2010) Atmospheric oxygen and the global carbon cycle: Observations from the new F3 North Sea platform monitoring station and 6 additional locations in Europe and Siberia, Centre for Isotope Research. University of Groningen, Groningen, The Netherlands.

Wilson, P., (2012) Insight into the Carbon Cycle from Continuous Measurements of Oxygen and Carbon Dioxide at Weybourne Atmospheric Observatory, UK, School of Environmental Sciences. Univeristy of East Anglia, Norwich, p. 155.

CHAPTER 3 METHODOLOGY OF ATMOSPHERIC O_2 AND CO_2 MEASUREMENTS PART II: INSTALLATION AND SYSTEM PERFORMANCE

3.1. Introduction

In this chapter, I present an analysis of the O_2 and CO_2 measurement system diagnostics collected over the operating lifetime of the system following it's installation at the Halley Research Station, Antarctica. This is a crucial inquiry if the system is to comply with the World Meteorological Organisation's (WMO) Global Atmospheric Watch (GAW) standards which are set so as to ensure the recording of observations that can be used reliably in the scientific investigation of natural and anthropogenic greenhouse gas sources and sinks (Section 3.1.1).

Following the initial period of testing at UEA during the summer of 2015, the system was dismantled and shipped to Halley, arriving at the Brunt Ice Shelf in December 2015. I then installed the system, with the assistance of Alex Etchells, in January 2016. Sample air measurement data collection began in February. I then handed over the system to the responsible technicians at Halley at the beginning of March. Unfortunately, due to an unprecedented closure of the Halley research station in 2017, the system had to be shut down in January 2017.

I will begin by outlining the WMO/GAW measurement guidelines and discuss why these guidelines have been set in order for the measurements to be used as a tool for answering the research questions outlined in Chapter 1 of this thesis. I will then briefly discuss the installation of the O_2 and CO_2 measurement system at the Halley Research Station, Antarctica (HBA) (Section 3.2). In Section 3.3, I discuss the major reasons for loss of data during measurement period. Section 3.4 consists of an assessment of the system performance based on diagnostic data collected during the measurement period and frames this in the context of the WMO/GAW guidelines for comparability, compatibility and reproducibility of measurements. Finally, in Section 3.5, I briefly discuss and summarise the results from Section 3.4. Readers not interested in the technical details of the measurement system performance are encouraged to read Section 3.5 in order to appreciate the reliability of the system and therefore providing confidence in the validity of the data presented in Chapter 4 and its scientific interpretation.

3.1.1. WMO/GAW guidelines: Comparability, compatibility and reproducibility

The GAW programme of the WMO is the primary global body responsible for the development and implementation of integrated greenhouse gas observations. These

observations are specifically required in order to answer the call set out in Article 7 of the Conference of Parties (COP21) Paris Agreement signed in December 2015 that specifically asks for: "strengthening scientific knowledge on climate, including research, systematic observation of the climate system and early warning systems, in a manner that informs climate services and supports decision-making". Achieving such a goal requires global atmospheric measurements to be both comparable and compatible.

"Comparable" simply means that the results of measurements made independently can be compared. This requires the results to be on the same scale. For CO_2 measurements, this is currently the WMO CO_2 X2007 scale maintained by the central calibration laboratory (CCL) at the United States (U.S.) National Oceanic and Atmospheric Administration Earth System Research Laboratory (NOAA/ESRL). For $\delta(O_2/N_2)$ measurements, there is no universally accepted scale and, as such, no CCL responsible for its maintenance. However, many laboratories within the O_2 community report their measurements on the SIO S2 scale. Both CO_2 and $\delta(O_2/N_2)$ are declared on their respective scales, defined above, for my calibration standards (as documented in Chapter 2, Section 2.4.4)

"Compatibility" means that independent measurements are compatible within a specified numeric value, such that : "the absolute value of the difference between any pair of measured values from two different measurement results is within a chosen value which does not have to be the same as the total combined uncertainty" (Tans and Zellweger, 2016). Which, stated more simply, means that different laboratories measuring the same quantity (400 ppm of CO_2, for example) must agree within a specified value. This can also be defined as the accuracy of a measurement. This value is chosen based on the precision and accuracy required to achieve the scientific goals behind the purpose of the measurement (see below). Furthermore, the WMO/GAW guidelines also define an extended compatibility goal for each species which is less stringent. This is defined because the highest precision and accuracy may not be required to achieve the scientific goals of a particular study, in studies where there are large local fluxes for example. Moreover, compatibility can be considered on two different, but connected levels. Firstly, external compatibility, between individual laboratories, can only be determined by the use of what are known as inter-comparison cylinders: cylinders of air with mole fractions declared by the respective CCL. Secondly, internal compatibility, within a laboratory and between the laboratory and its field stations, can be determined by the use of a Target Tank (TT). This is often referred to as the "internal reproducibility" goal and, although

not strictly defined, should be approximately half of the compatibility goal (Tans and Zellweger, 2016). This measure encompasses imprecision due to the analyser, the gas handling and the transfer of the calibration scale from the "home" laboratory standards (in this case, the University of East Anglia's (UEA) Carbon Related Atmospheric Measurement Laboratory (CRAM Lab) primaries) to the working secondary standards (WSSes). The compatibility and reproducibility goals for CO_2 and $\delta(O_2/N_2)$ are shown in **Table 3.1**.

The choice of these goals represents the precision required to detect small but significant trends and gradients in greenhouse gases across the globe. For example, the decline in the efficiency of the Southern Ocean CO_2 sink of 0.08 Pg C yr^{-1} $decade^{-1}$ proposed by Le Quéré et al. (2007), represents a decline in the amount of the atmospheric CO_2 mole fraction taken up by the Southern Ocean of 0.04 ppm $yr^{-1}decade^{-1}$. Hence a compatibility goal of ± 0.05 ppm is appropriate for CO_2 measurements in the southern hemisphere. The example just given indicates we should still be striving to improve this compatibility goal; although many measurement stations do meet this requirement, many still do not.

O_2 fluxes are typically much larger than those for CO_2 (Chapter 1) and therefore a goal of ± 2 per meg (± 0.4 ppm Equiv) is adopted (Tans and Zellweger, 2016). However, this goal can only be currently achieved by large laboratory based $\delta(O_2/N_2)$ measurement systems such as those employing the interferometry (Keeling, 1988a) and vacuum ultra violet (VUV) (Stephens et al., 2003) techniques. Field based measurement systems using the fuel cell technique, like that employed here, can typically achieve a precision of ± 5 to ± 10 per meg.(Kozlova and Manning, 2009; Pickers, 2016; Stephens et al., 2007; Wilson, 2012).

Table 3.1. Compatibility and internal reproducibility goals as set by the WMO/GAW programme (see text for definitions). For $\delta(O_2/N_2)$, the goals defined inside the brackets refer to the currently accepted compatibility and reproducibility goals within the O_2 measurement community.

Species	Compatibility goal	Extended Compatibility goal	Internal reproducibility goal
CO_2	±0.1 ppm (NH) ±0.05 ppm (SH)	± 0.2 ppm	± 0.05 ppm (NH) ± 0.025 ppm (SH)
$\delta(O_2/N_2)$	±2 per meg (± 5 per meg)	± 10 per meg	±1 per meg (± 2.5 per meg)

The following assessment of the system performance relates to the internal reproducibility goals for CO_2 and $\delta(O_2/N_2)$. For the southern hemisphere, these are ±

0.025 ppm and ± 1 per meg, respectively. However, with respect to $\delta(O_2/N_2)$, since current international comparisons show that the compatibility between independent laboratories is not better than ± 5 per meg, I have adopted the internal reproducibility goal of ± 2.5 per meg for my measurement system.

3.2. Installation and integration with the Halley science infrastructure

The measurement system, along with myself and Alex Etchells, arrived at Halley, via ship, at the end of December 2015. It took approximately one month to complete the installation, with sample air data collection beginning in February.

One of the major issues at the beginning of the installation, was the regulation of the temperature within the small room that housed my equipment at the Clean Air Sector Laboratory CASLab (**Figure 3.1**A). The lack of ventilation in the room, coupled with the large heat output of the instrumentation, resulted in an initial room temperature of ~ 35˚C. This particularly affected two resettable fuses within the electronics control box connected to the aspirators inside the inlets (Chapter 2, Section 2.5 and 2.3.1 respectively). Since the ambient temperature was close to their triggering temperature (normally achieved through an overload of current) they repeatedly cut out when what would otherwise be an acceptable amount of current was applied. To circumvent this, we replaced the fuses with non-resettable higher current rating fuses.

The main issue from the large heat output, however, was the resulting temperature gradient within the room, which at times was up to 5˚C/m. This would have undoubtedly affected the temperature gradient inside the blue box and by extension the calibration cylinders, despite the insulation. A series of small fans were therefore placed at strategic points around the room to circulate the air. This, in addition to ensuring the door connecting to the main room (with active temperature control) was always left open, brought the ambient room temperature down to ~23˚C with a temperature gradient of no more than 2˚C/m.

Power outages, mainly temporary (minutes), can be common at HBA. To try and mitigate this, the analysers, control computer, vapour trap, electronics box, diaphragm pumps, Valco valve and MKS controller (Chapter 2) were connected to a PowerGem Pro (British Power Conversion Company) 1000 W uninterruptible power supply (UPS), which can run the entire system for approximately 30 minutes without mains power.

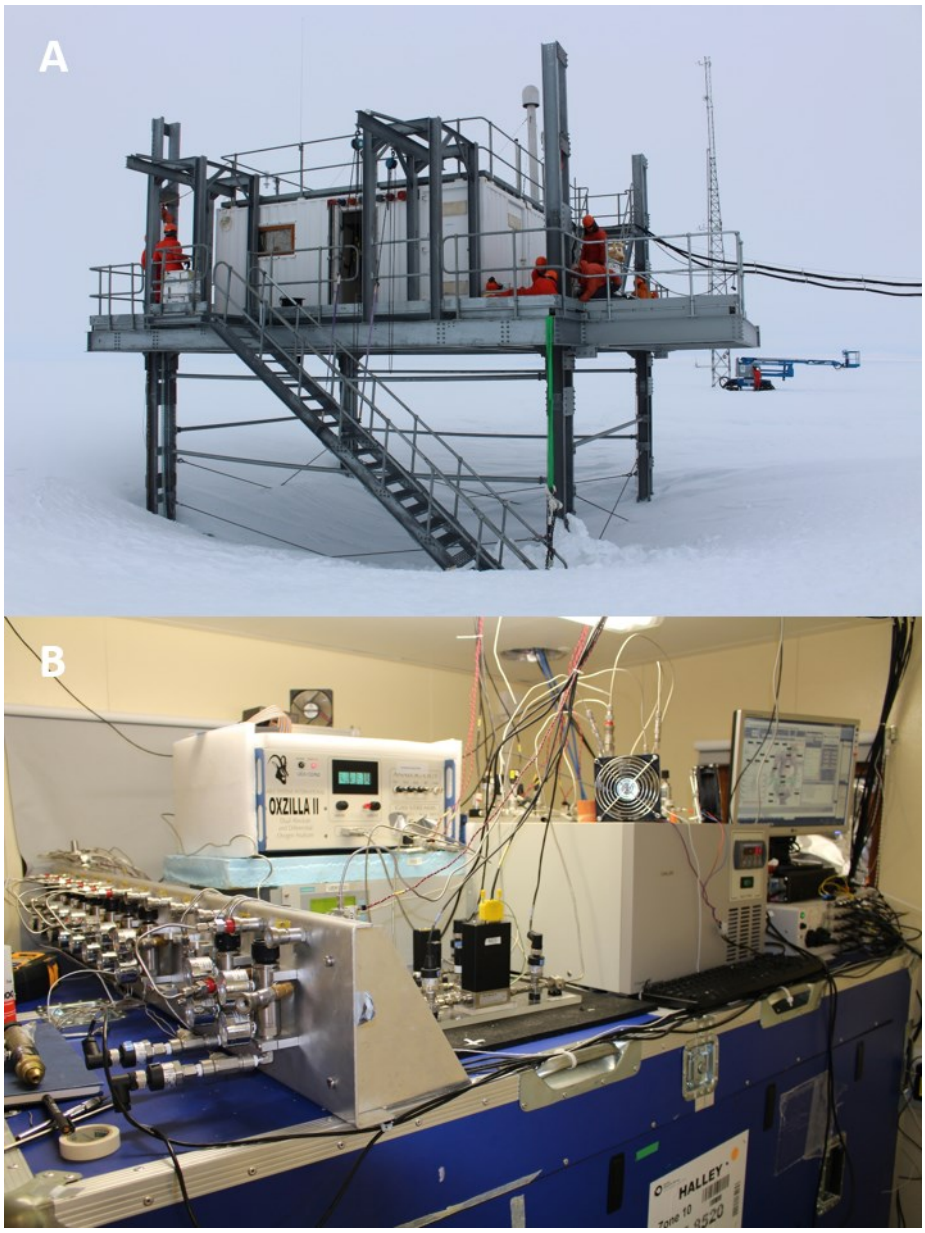

Figure 3.1. A. The Clean Air Sector Laboratory (CASLab) at the Halley Research Station Antarctica. The photo looks towards the south east. Sample inlets are located on the roof of the building. B. The small room housing the O_2 and CO_2 measurements system.

All scientific experiments at the HBA are monitored by an in house Nagios Warning System (Nagios Enterprises Ltd). At the request of the Principal Investigator, various automated checks can be performed on the experiments control computer to determine any faults or major issues. If an error does occur, a warning is flashed onto the communal monitors on the station so the responsible persons are notified and can respond. The automated checks performed that I implemented on my system with the help of Alex Etchells and the local HBA Data Manager included (refer to Chapter 2 for the background on the technical aspects of the system mentioned here):

1. A drop in the current being received at the aspirated air inlets; indicating that the aspirators were drawing against a restriction, which usually indicated the inlets were becoming blocked with rime; a type of ice that forms under freezing fog conditions.
2. A sustained drop in pressure on P6, indicating that the cold trap was blocking.
3. A change in the Working Tank (WT), indicating that a new cylinder could be installed inside the blue box.

Moreover, further checks were performed on crucial aspects of the system set up, which include:

1. The Valco valve, which, if at fault could lead to the depletion of valuable calibration gases.
2. The Labjack status, which perform the data acquisition.
3. Whether the software was running in "auto-run" mode, indicating that the system was recording data, or whether it was in "resting state", indicating that data was not being recorded. This is important because, depending on a particular error, the system could put itself into resting state to maintain calibration and reference gases if there was a reasonable reason not to record data. Resting state could be reached automatically, by a fault for example, or by human intervention when maintenance is being performed on the system. If the user forgot to restart auto-run, then this check would catch that fault.

3.3. Quality control and data loss

As was discussed in Chapter 2, Section 2.5, the measurement system records a wealth of diagnostic data that aid in data quality control. I use this information, coupled with user observations, to populate a flag file which subsequently excludes measurement data from the time periods recorded. Fortunately, the success of the installation meant these excluded periods were kept to a minimum, but I will briefly discuss the most prominent reasons for flagging certain periods of measurement data.

Firstly, within the "Macros/Calibration" tab of the software, I can define acceptable bounds for the analyser response terms of the respective CO_2 and $\delta(O_2/N_2)$

calibration curves (see Chapter 2, section 2.3.5). To determine these at HBA, I examined the mean, the 1σ standard deviation and the range of each parameter for every calibration that ran up until the point I had to leave the base. Unfortunately, the choice of bounds were too tight and resulted in four calibrations not being accepted between 26th March and 01st April 2016 resulting in uncalibrated data. This data is recoverable and requires reprocessing the calibration data. At the time of writing, software is being developed to facilitate this reprocessing. However, it is currently not at an advanced enough stage to reprocess my own data for inclusion in this thesis.

The only other major reason for flagging data was after a prolonged power down (i.e. longer than the ~30 minutes that the UPS battery can maintain power to the system). The system is designed to restart automatically once power resumes and begin recording immediately. However, a number of factors mean that the data is unlikely to be useable in the case. These include, but are not limited to, the following: partial blocking of the cryogenic vapour trap due to melting and refreezing of water within the trap; lack of flow through the Oxzilla fuel cells (which can take upwards of 24 hours to stabilise once flow has been re-established) and finally, it may have been too long since a calibration. This could be due to the ZT (a partial calibration) (i.e. not run in the last 3 hours, which would only impact CO_2) or it could be due to a full calibration (greater than 47 hours), in which case the $\delta(O_2/N_2)$ data will be suspect too. Two major power downs occurred on the 30th May and the 8th October 2016.

With human error, suspect data based on system diagnostics and leaks detected (during February, whilst I was still working on the system), the total number of days flagged = 39.9 days which represents a 11.3% data loss (with respect to the total number of days the system was running, rather than the number of data points lost).

3.4. System Performance at Halley

3.4.1. Calibration parameters

The operating principle of the Siemens NDIR CO_2 analyser is such that the analyser response is non-linear with respect to the variability in the CO_2 mole fraction. The analyser has an in built internal correction for this non-linearity, however, this is not suffice for the typical precision required by the atmospheric CO_2 measurement community. Hence, to calibrate the CO_2 analyser, a non-linear response function of the form $y= a+bx+cx^2$ is used, whereby the non-linearity coefficient "c" characterises the

non-linearity that has not already being corrected for. The Oxzilla O_2 fuel cell analyser, on the other hand, has a highly linear response function of the form y= a+bx. The CO_2 analyser reports the difference in volume parts per million (vpm) of the sample cell CO_2 from the reference cell CO_2, whilst the O_2 analyser reports the double delta difference ($\Delta\Delta O_2$) in % units (Chapter 2, Section 2.4). The calibration parameters for O_2 and CO_2 are therefore reported in ppm vpm^{-2} for the CO_2 analyser non-linearity response coefficient (c), ppm vpm^{-1} for the CO_2 analyser sensitivity coefficient (b) and ppmEquiv $\%^{-1}$ for the O_2 analyser sensitivity coefficient, respectively.

If any of the calibration coefficient terms drift over time, it could firstly be an indication of drift in the sensitivity of the analyser, which may become more or less sensitive at a particular mole fraction over time, impacting both the precision and the accuracy. By calibrating frequently, the accuracy of the measurement should not be impacted by this potential deterioration or improvement of the analysers' sensitivity. However, a deterioration in the precision cannot be corrected for. Secondly, the coefficients may drift as a result of a calibration scale drift caused by internal drift within one or more of the calibration cylinders. This can only be fully determined after reanalysis of the calibration cylinders towards the end of their lifetime, which, at the time of writing, is not possible to determine. Consequently, it is not possible to separate analyser sensitivity drift from calibration drift in the analysis of the calibration coefficients. However, I am able to determine what the maximum drift could be in terms of the combined measure of the analyser response and the calibration scale drift.

In order to be directly comparable to the WMO/GAW internal reproducibility goals, it is necessary to convert these units into ppm and ppmEquiv. To do this, one needs to multiply each term by a constant analyser response at an ambient mole fraction. For CO_2, this was determined by the analyser response on WSS2 (~400 ppm = 1.24 vpm) and for O_2, the response on WSS4 (~ -650 per meg = -0.00103 %), using an arbitrarily defined WT concentration (and hence ΔCO_2 and $\Delta\Delta O_2$).

Figure 3.2 depicts the variability in the non-linearity (CO_2) and sensitivity (CO_2 and O_2) coefficients over the full period of operation and compares these metrics against the laboratory temperature. Firstly, the drift in the non-linearity of the CO_2 response is approximately -0.0007 ppm yr^{-1} and most of this appears to have occurred from the WT change in May through to the WT change in November. By calculating cylinder depletion dates for each WSS, one can determine the maximum amount of drift expected over the lifetime of the WSS. D743659 (WSS3) has the shortest lifetime of ~2 years. This would

equate to a minimum drift of -0.0014 ppm. However, if all of the standards were prepared from 50L cylinders and filled to 180 bar, such as D743657, then the maximum lifetime would be ~5 years, resulting in a maximum drift of -0.0035 ppm. This is almost an order of magnitude smaller than the internal reproducibility goal for CO_2 and is therefore

insignificant. Secondly, the variability in the of the CO_2 non-linearity response coefficient increases between the months of April and September/October in line with the variability in the lab temperature. The impact of the improvement of the stability of the lab temperature between November and January on the CO_2 non-linearity response

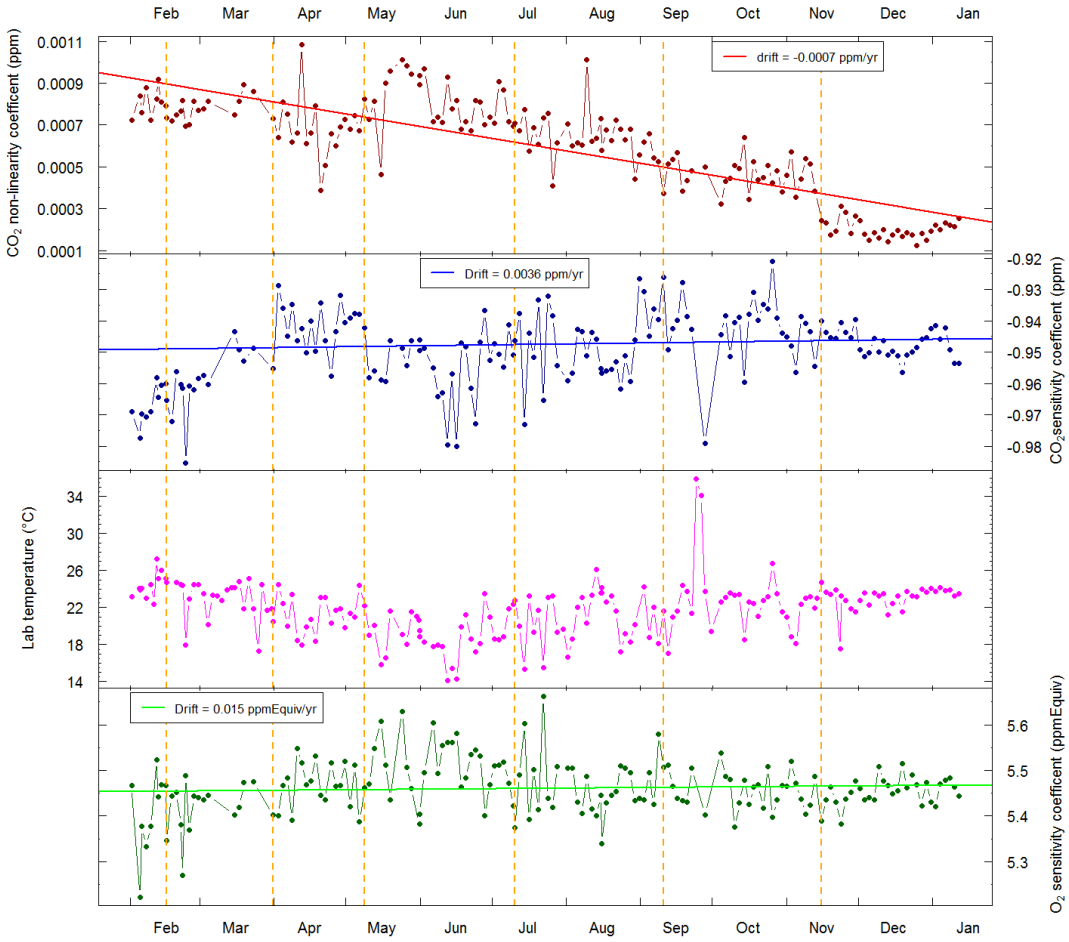

Figure 3.2. Drift and variability of the calibration coefficients for CO_2 (top two panels) and O_2 (bottom panel) over the measurement period shown alongside the lab temperature at the time of calibration (bottom middle panel). Each measure is redefined at every calibration and connecting lines are drawn between calibrations to highlight the direction and magnitude of the change. Each of the coefficients have been converted into meaningful units in order to be directly comparable to the internal reproducibility goal (ppm for CO_2 and ppmEquiv for O_2; see text for details). Dashed vertical lines in all panels represent WT changes. Top panel: the CO_2 non-linearity coefficient or the c-term in the analyser response function (ppm; dark red points). The trend in the drift (ppm yr^{-1}; red line) was determined using all data points over the measurement period. Top middle panel: the CO_2 sensitivity coefficient or the b-term in the analyser response function (ppm; dark blue points). The trend in the drift (ppm yr^{-1}; blue line) was determined using data points from the beginning of April onwards. Prior to this date, the data are unfairly biased by a clear upwards drift that is not sustained after this date. Bottom middle panel: the lab temperature at the time of calibration (˚C; pink points). Bottom panel: the O_2 sensitivity coefficient or the b-term in the analyser response function (ppmEquiv; dark green points). The trend in the drift (ppmEquiv yr^{-1}; green line) was determined using all data points over the measurement period.

coefficient is particularly evident. The same is true for the sensitivity coefficient of the CO_2 analyser and, to a lesser extent, the O_2 analyser.

Neither of the analysers show a sensitivity trend that is significant with respect to the internal reproducibility goal, meaning the analysers are not becoming more or less sensitive over the measurement period. However, the variability in the sensitivity does appear to be impacted by the stability of the lab temperature. For CO_2, the largest jump in sensitivity (~0.04 ppm) is seen towards the end of September when the lab temperature changes by approximately 10˚C between calibrations. This was due to the door being closed between the room housing my measurement system and the rest of the laboratory, isolating the system from any active temperature control within lab. Although the jump in sensitivity is larger than the internal reproducibility goal, the data will have been flagged during this time and therefore not used in analysis. Overall, the 1σ standard deviation of the CO_2 sensitivity is equal to ± 0.011 ppm, which is below the internal reproducibility goal. However, it is worth noting the improvement in this value when the lab temperature stability improved from the beginning of November to ± 0.005 ppm.

Finally, the stability of the sensitivity of the O_2 analyser does deteriorate when the lab temperature is not stable, but not to the same extent as the sensitivity in CO_2. This is likely because the Oxzilla unit employs an active temperature control, whereas the Siemens unit does not. Nevertheless, active temperature control within the unit will be improved when the lab temperature is stable. Again, this is shown in the improvement in the 1σ standard deviation of the O_2 sensitivity coefficient between the full year (± 0.06 ppmEquiv (0.3 per meg)) and when the lab temperature stability improves (0.03 ppmEquiv (0.2 per meg)).

3.4.2. Stability of WT concentrations

The "a" term in the analyser response functions represents the WT concentration and is similarly redefined for O_2 and CO_2 every 47 hours during a calibration (for CO_2, it is further redefined every 4 hours by running the ZT in between calibrations, see below). The stability of the WT concentration therefore provides another measure of system

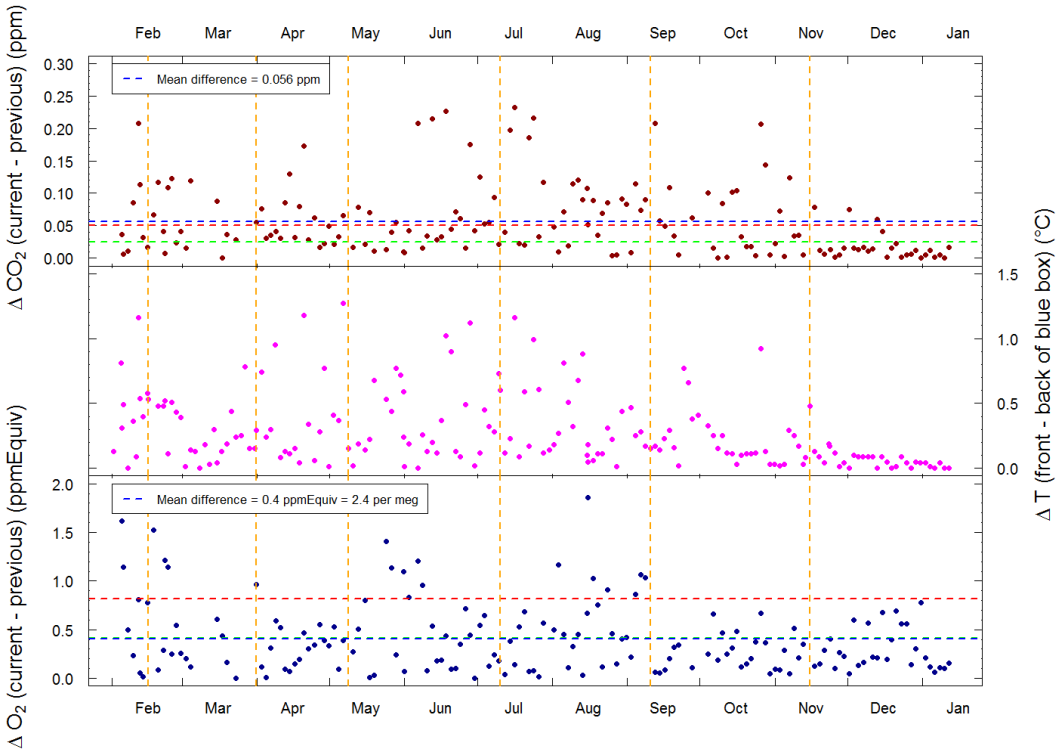

Figure 3.3. The absolute difference between the current and the previous WT mole fraction between calibrations for CO_2 (top panel; dark red points) and O_2 (bottom panel; dark blue points) compared against the difference in the internal temperature between the front and the back the blue box, i.e. across the length of the cylinders (~2m) at the time of calibration (middle panel (pink points). Orange vertical dashed lines represent WT changes. In the top panel, the red and green dashed lines represent the southern hemisphere compatibility (± 0.05 ppm) and internal reproducibility (± 0.025 ppm) goals for CO_2, whilst the blue dashed line represents the mean WT difference between all successive calibrations. In the bottom panel the red and green dashed lines represent the accepted compatibility (± 5.0 per meg) and internal reproducibility (± 2.5 per meg) goals for O_2 in ppmEquiv. Again, the blue dashed line represents the mean WT difference between all successive calibrations.

performance. For O_2, the absolute difference between successive calibrations indicates whether the calibration cycle is being run frequently enough to not be affected by either the drift in the analyser response or by variations in external environmental conditions (which may impact individual cylinders, in addition to the analyser response itself, despite measures used in the construction of the blue box to minimise this). For CO_2, the absolute difference between calibrations does not matter, since the WT is redefined every time the

ZT is run (every 4 hours). However, the results will indicate how necessary it is to redefine the baseline between calibrations.

The difference between the current and previous WT concentration for all calibrations during the measurement period are shown for both CO_2 and O_2 in **Figure 3.3**. The mean absolute WT difference between calibrations for CO_2 is 0.056 ± 0.056 ppm. This is above the internal reproducibility goal of ± 0.025 ppm for systems measuring southern hemisphere air and an order of magnitude worse than the stability displayed by Kozlova and Manning (2009) (~ ± 0.005 ppm). However, Kozlova and Manning (2009) had much better temperature control within their measurement lab (± 1˚C) and calibrated twice as frequently (every 26 hours) (A. Manning, personal communication, 2017). This confirms the need to run the ZT in order to correct for baseline drift between calibrations. For O_2, the mean WT difference between calibrations is 0.4 ± 0.4 ppmEquiv (2.4 ± 2.4 per meg), which is just below the internal reproducibility goal accepted by the O_2 community of ± 2.5 per meg, but above the ultimate internal reproducibility required by the scientific needs defined by the WMO/GAW guidelines of ± 1 per meg. As was highlighted before, individual WTs appear to display different levels of variability between calibrations. In particular, the last two WT changes show a distinct improvement in both the mean and 1σ standard deviation, whilst for CO_2, the final WT displays a vastly improved mean and standard deviation (see **Table 3.2**). There could be two possible explanations for this. Firstly, some of the WT connections may not have been as leak tight as others. Although absolute care is taken to ensure the individual WTs are leak tight before they are run on the system by undertaking a pressure leak test, imperceptible leaks at the cylinder head cannot be ruled out. The second, what I believe to be the more likely explanation, again invokes the temperature stability of the lab which, as already highlighted, improves dramatically around October/November. This likely coincides with a change in the active temperature control within the lab. The lab has two modes for its internal temperature control: “winter” and “summer” mode. The switch to “summer” mode likely happened around October/November (although the responsible technicians are unable to confirm this).

Furthermore, if one ignores the variability of the first few data points in February when the system was still undergoing partial testing and "teething" problems were still being addressed, then one can discern an overall increase in the WT difference in both CO_2 and O_2 that closely follows the increase in the temperature gradient within the blue box during the winter months, when the temperature control in the lab becomes poor. The poor temperature control will directly impact the sensitivity of the CO_2 analyser, as already mentioned. However, it is the temperature gradient across the calibration and WT cylinders that will impact the O_2.

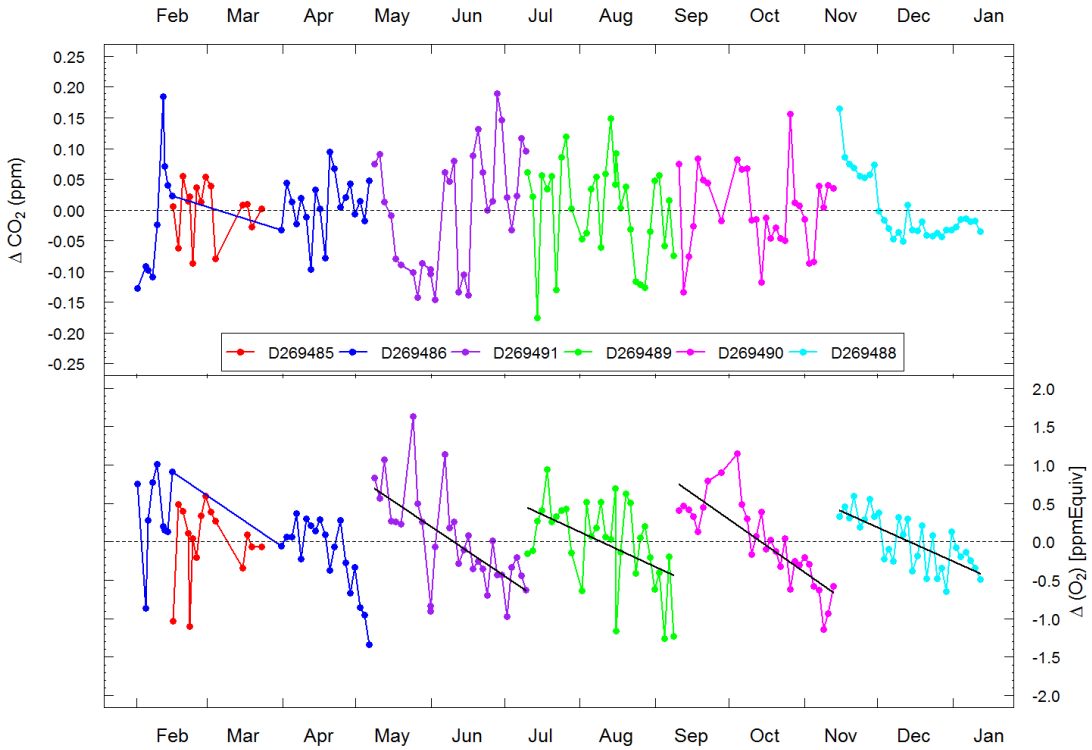

Figure 3.4. Stability of the CO_2 mole fraction (ppm; top panel) and O_2 mole fraction (ppmEquiv; bottom panel) within each WT used over the measurement period. For each WT, the data, determined after every calibration, are shown as the difference from the mean mole fraction determined over the lifetime of the WT. All WTs are run continuously from a starting pressure of ~180 bar to a finishing pressure of 5 bar, except WTs D269485 and D269486, which were utilised during testing and therefore not run sequentially. The trend in the O_2 depletion, typically ~ -6.6 per meg/WT, is shown as a black line for the final four WTs.

Figure 3.4 depicts the difference of the WT mole fraction, defined during a calibration, from the mean mole fraction determined from all calibrations on that particular WT. As shown in the bottom panel of **Figure 3.4**, the O_2 mole fraction becomes progressively depleted as the cylinder air is consumed. This composition change as the pressure in a cylinder decreases was first noted by Keeling et al. (1998a) and has been

subsequently observed by Manning (2001), Keeling et al. (2007), Kozlova and Manning (2009), (Wilson, 2012) and Pickers (2016). This effect is most likely caused by the preferential desorption of N_2 relative to O_2 from the interior walls of the cylinders as the pressure decreases, owing to the difference in their molecular mass (Keeling et al., 1998a; Kozlova and Manning, 2009). Excluding the first two WT cylinders (which were not run sequentially to depletion), the mean depletion observed in the O_2 mole fraction is -1.1 ppmEquiv (-6.6 per meg) over the lifetime a cylinder. This is five times smaller than that found by Kozlova and Manning (2009) and much smaller than that found by Pickers (2016), which could be as much as -54 per meg over the lifetime of a cylinder. However, it is similar to that found by Manning (2001) and only slightly larger than that found by Keeling et al. (1998a) (-5 per meg). The larger O_2 depletion observed by Pickers (2016) and Kozlova and Manning (2009) can be explained by their respective cylinder depletion rates. Kozlova and Manning (2009) used a higher flow rate (150 ml min-1) through their system, resulting in a higher cylinder depletion rate. Pickers (2016), on the other hand used the same flow rate as used on my system (100 mL min-1), but used smaller WT cylinders (10L) at a higher pressure (300 bar). The relative depletion rate (per unit volume of air) was therefore much higher than observed on my own system.

The WT CO_2 data show very poor precision and stability over the lifetime of the WT (**Figure 3.4**) reinforcing the need to run a ZT frequently between calibrations. It is interesting to note that the mean difference increases above ± 0.05 ppm for cylinders D269491 and D269489 between May and September, before improving for the final two WT (**Table 3.2**). Again, this pertains to the argument outlined above between as to whether WTs were leak tight or whether the stability of the lab temperature is having an impact. To further reinforce the argument that the primary driver of this decrease in WT CO_2 stability, and in the response of the CO_2 analyser as a whole, is due to temperature, I have presented the coefficient of determination (R^2) of the calibration curve fit for each individual calibration against time for both analysers alongside the lab temperature (**Figure 3.5**). Firstly, the O_2 R^2 does not show any improvement throughout the measurement period. This highlights two things; firstly, if individual WTs had leaks compared to others, then there would be a clear change between WTs in the O_2 R^2. This is not the case. Secondly, the O_2 analyser, as already mentioned, has active temperature control and so is less affected by temperature variability than the CO_2 analyser would be (which does not have active temperature control).

The CO_2 R^2, on the other hand, does show deterioration throughout the winter months when the lab temperature stability decreases. Although the second to last WT does show improved stability compared to the others, this stability does not improve exactly when the WT changes, instead, it becomes progressively better throughout September and October as the temperature stability of the lab improves.

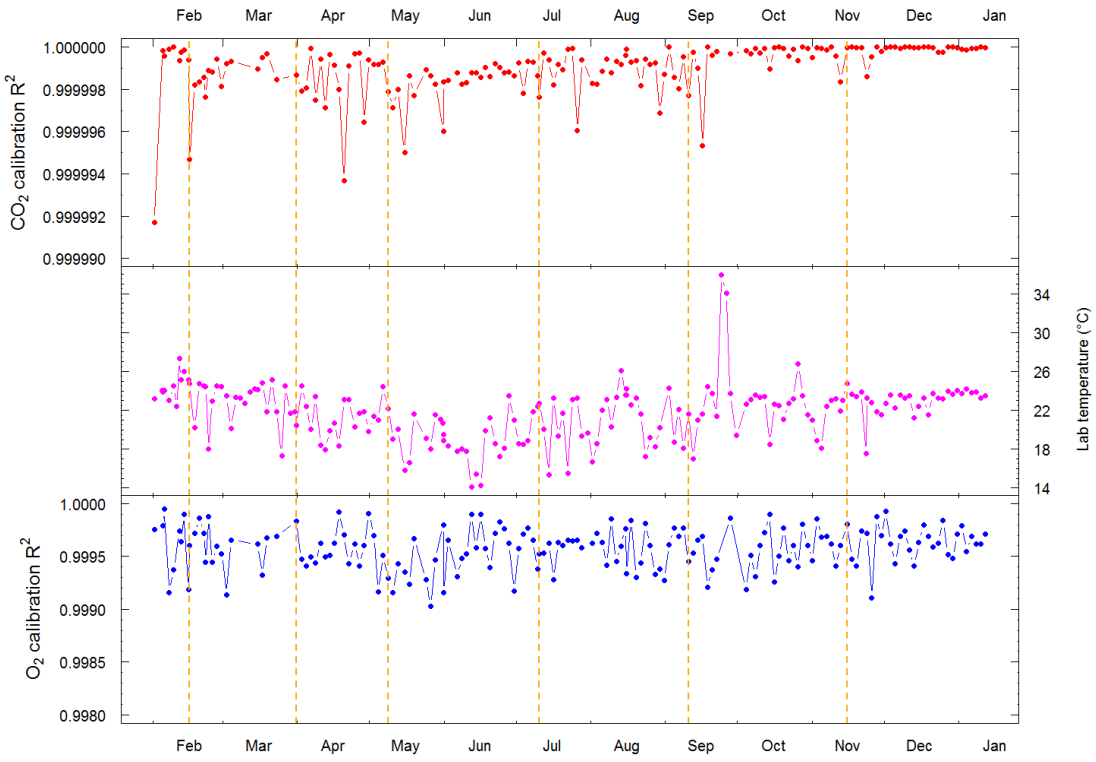

Figure 3.5. Quality of the calibration curve fit over the measurement period, as depicted by the coefficient of determination (R^2), for CO_2 (top panel; red points) and O_2 (bottom panel; blue points) in comparison with the lab temperature (middle panel; pink points) at the time of calibration. In each panel, the data points are connected by straight lines to make the difference between calibrations more apparent. Orange vertical dashed lines represent WT changes.

3.4.3. Zero Tank correction

As was discussed in Chapter 2 Section 2.4.4.1, the Zero Tank (ZT) is run between respective calibrations in order to correct for baseline drift in the CO_2 analyser response, which, as highlighted above, is mainly caused by laboratory temperature variations. In order to achieve the internal reproducibility goal, the difference between individual ZT

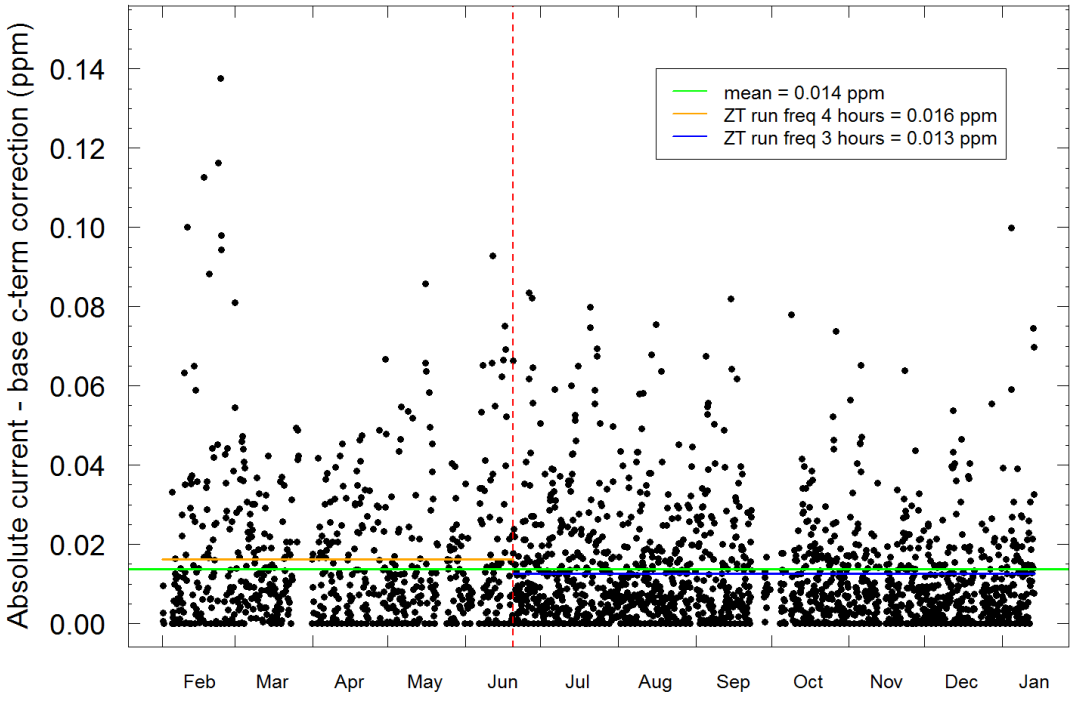

Figure 3.6. The absolute CO_2 difference (ppm) between consecutive ZT runs which equals the magnitude of the correction applied to the "a" term in the CO_2 calibration curve every 4 hours and therefore represents a measure of the baseline drift in the analyser response. The vertical red dashed line represents when the run frequency of the ZT was increased from every 4 to every 3 hours in attempt to minimise the impact of baseline drift on sample air measurements. The solid green line represents the mean absolute baseline correction applied between ZT runs over the full measurement period (0.014 ppm; percentage of data points > 0.025 ppm = 7.6%). The solid orange line represents the mean absolute correction applied prior to the ZT run frequency change (0.016 ppm; 9.7 % > 0.025 ppm), whilst the solid blue line represents the mean absolute correction applied after to the ZT run frequency change (0.013 ppm; 6.6 % > 0.025 ppm).

runs should be no more than ± 0.025 ppm. **Figure 3.6** shows the absolute difference between a ZT run and the "base" run, that is to say, the ZT run immediately following a calibration, which represents the maximum difference between ZT runs, since after each run, the "a" term in the quadratic calibration curve is corrected. These results clearly justify the need for running the ZT in between calibrations in order to correct for baseline drift, as the difference between ZT runs can be greater than 0.025 ppm (7.6% of the data). However, over the full measurement period, the mean correction applied to the baseline is 0.014 ppm, which achieves the internal reproducibility goal. In June, I decided to increase the ZT run frequency from 4 hours to 3 hours in attempt to reduce the correction applied to the baseline, largely in response to an assessment of temperature variability within the lab, which could be up to 5 ˚C between calibrations (47 hours) during the winter months (dotted red line in **Figure 3.6**). The mean absolute difference between ZT runs prior to the frequency change was 0.016 ppm and the proportion of the data above

0.025 ppm was 9.7%. Whereas after the change, the mean correction was reduced to 0.013 ppm (6.6 % > 0.025ppm). Using a two tailed t-test assuming unequal variances, this change was found to be significant at the 95% confidence level ($p < 0.05$).

In addition to being used as a CO_2 calibration cylinder, the ZT can also serve as an additional assessment of system performance, much like the TT, since the measured

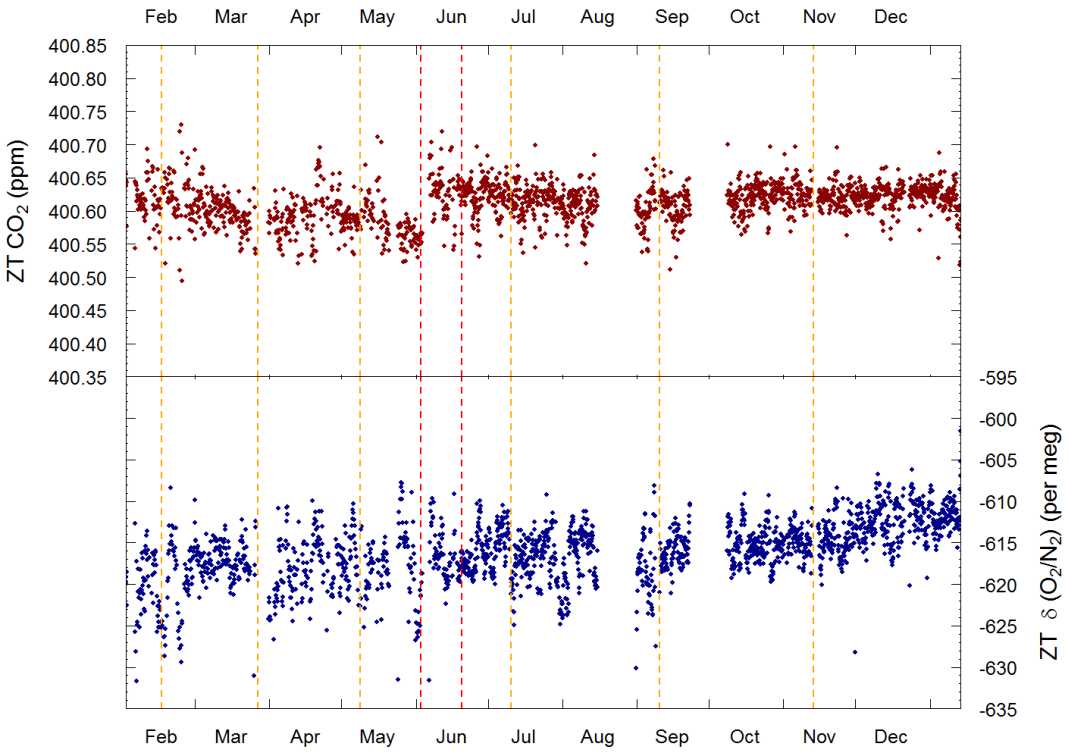

Figure 3.7. Stability of the ZT CO_2 mole fraction (ppm; top panel; dark red points) and $\delta(O_2/N_2)$ ratio (per meg; bottom panel; dark blue points) over the full measurement period. Orange vertical dashed lines represent WT changes. The first red vertical dashed line represents a > 1 day power failure at the lab. The second red vertical dashed line represents when the run frequency of the ZT was increased from every 4 hours to every 3 hours. There are several gaps in the data. The first, at the end of March, is due to the fact that the bounds on the acceptable calibration parameters set in the software were too stringent (Section 3.3). This resulted in calibrations not being accepted for several days until it was caught. Consequently, the CO_2 and $\delta(O_2/N_2)$ values are offset by ~ 2 ppm and 50 per meg, respectively and so are not included. It will be possible to recover these values by post processing the data, but this had not been done at the time of writing. The gaps in late August and late September were when cylinders were being moved to different positions within the blue box so that a cylinder designated to be the next ZT could be used as a WT instead, prolonging the lifetime of available reference gas due to ship resupply restrictions. The ZT and TT therefore had to be disconnected and reconnected and leak checked and were therefore not in use during these periods. In order to still make a ZT correction during these periods, the next TT (TT2) was used as a ZT instead and since the absolute concentrations in this cylinder are different to the initial ZT, therefore these results are not shown.

CO_2 and $\delta(O_2/N_2)$ are declared each time the ZT is run. This aids in the identification of potential issues on the system. The CO_2 mole fraction and $\delta(O_2/N_2)$ ratio for the ZT

cylinder are shown in **Figure 3.7**. There are several interesting features in this dataset that relate system performance and highlight several issues that were undetected at the time of data collection. Firstly, the CO_2 data show a clear step change following a power failure at the end of May. Prior to this this point, there appears to be a downward drift of ~ - 0.1 ppm between February and May and there is a considerable amount of noise. After the step change, the CO_2 mole fraction stabilises and the noise reduces. However, 20 days after the step change, the ZT run frequency was increased from 4 to 3 hours (see above) in an attempt to reduce the magnitude of the baseline correction in between ZT runs. Unfortunately, due to the proximity of these two changes, it is difficult to attribute which caused the reduction in the noise. On the other hand, the step change can clearly be attributed to the change at the power down. A reasonable explanation for the step change due to the power down has yet to be found.

3.4.4. Target Tank Results

As was discussed in Chapter 2 Section 2.4.4.2, the Target Tank (TT) serves the purpose of a quality control check on the measurement system. However, with the current gas handling procedure, it is not possible to run the TT through the inlets, diaphragm pumps and the first stage of the drying system (DC1) and therefore does not perform a full quality control on the entire system. Future improvements to the design of the system may include this feature. Instead, it does provide a quality control check on the calibration gas handling, pressure and flow control and analyser response.

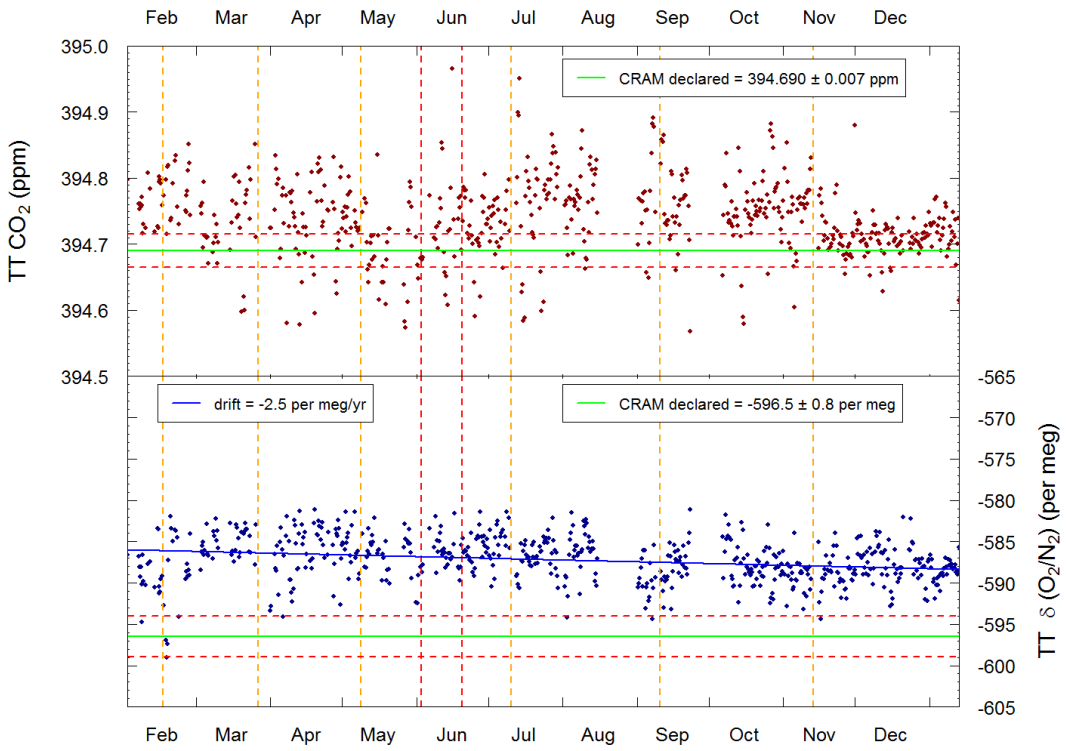

Figure 3.8. Stability of the TT (D743652) CO_2 mole fraction (ppm; top panel; dark red points) and $\delta(O_2/N_2)$ ratio (per meg; bottom panel; dark blue points) over the full measurement period. Orange vertical dashed lines represent WT changes. The first red vertical dashed line represents a > 1 day power failure at the lab. The second red vertical dashed line represents when the run frequency of the ZT was increased from every 4 hours to every 3 hours. Green horizontal line represent the CRAM lab declared value, whilst red dashed lines represent the ± the internal reproducibility goals for CO_2 (± 0.025 ppm) and $\delta(O_2/N_2)$ (± 2.5 per meg). The blue vertical line in the bottom panel represents the drift in the $\delta(O_2/N_2)$ observed over the analysis period. See Figure 3.7 For an explanation behind the gaps in the data.

Before installation, two TTs were filled and analysed for their CO_2 mole fraction and $\delta(O_2/N_2)$ ratio in the CRAM lab before being shipped to HBA. During the measurement period, only one of these was used as the designated TT (D743652) and run every 9 hours. However, towards the end of the installation period in February I ran the second TT (TT2) (D089506) through the measurement system several times as an additional, independent check on the first TT results. Furthermore, during August and late September/early October, cylinders positions were reshuffled within the blue box which meant the TT2 had to be run as a ZT, allowing further analyses on this cylinder.

The results of the first TT analyses are shown in **Figure 3.8**. There are several features of interest. Firstly, the variability in the CO_2 data is incredibly poor, with a 1σ standard deviation for all measurements of ± 0.044 ppm, above the internal reproducibility goal. Furthermore, the mean difference form the declared CRAM lab value is 0.049 ± 0.057 ppm, which is only marginally within the southern hemisphere

compatibility goal. Moreover, there again appears to be a deterioration in the variability of the results during the winter months, when lab temperature control was poor followed by an improvement the following summer, when temperature control improved. In contrast to the ZT results, there is no step change after the power down in early June, yet there is a clear step change after the final WT change. Finally, the change is towards the declared value for the cylinder. On first appearances, this suggests the final WT was more leak tight than the previous, and by extension, all others. Although this cannot be entirely ruled out, closer inspection of the data reveals that the data immediately following the change are not significantly different to those before. Instead, during the first quarter of the WT lifetime, there is a steady drift down towards the declared value, that is more in line with the improvement in the variability in the sensitivity of the analyser as a result of the improvement in the lab temperature control.

The O_2 results are significantly better than the CO_2 results. The 1σ standard deviation of all runs is 2.2 ± 1.7 per meg which is below the accepted achievable internal reproducibility goal (but above the WMO scientific goal). In contrast to CO_2, there are no step changes in the O_2 value, nor are there any improvements in the variability of the data either between WTs, or when the temperature control has improved. This further reinforces the lab temperature variability explanation invoked to explain the CO_2 data. A leak would significantly impact the O_2 data, more so than the CO_2 data, and in Figure 3.8 this is not seen, whilst the active temperature control inside the Oxzilla unit means it is not as susceptible to lab temperature variability as the CO_2 analyser. Secondly, and perhaps more significantly, there is a drift of -2.2 per meg per year. There are three possible explanations for this: (1) a drift in the one or more of the calibration cylinders, (2) a drift in the analyser response and (3), a drift within the TT cylinder itself. In the analysis in Section 3.4.1, it was shown that there is no significant drift in the sensitivity term of the O_2 analyser, which likely indicates that neither the calibration scale, nor the analyser response is drifting (unless they were both equally drifting in opposite directions, which, although possible, would be highly unlikely). Instead the evidence points to an internal drift within the cylinder. This could be caused by preferential desorption of N_2 relative to O_2. This may be compounded by the fact that this cylinder is relatively wet (15.4 ppm H_2O; (Chapter 2, **Table 2.2**) which may encourage surface reactions. The high water content of the cylinder could also be invoked to explain the large offset from the declared value (9.3 ± 2.8 per meg). Unfortunately, at the time that this cylinder was filled

in the CFF, there were known issues with the drying set up for incoming air. Time-constraints meant that another cylinder couldn't be filled to replace this one.

The evidence outlined above leads me to conclude that the poor TT results on cylinder D743652 for CO_2 and $\delta(O_2/N_2)$, for different reasons, are largely unique to this particular cylinder, and perhaps the individual gas handling line between the cylinder and the common outlet on the Valco valve, rather than issues with the entire system. The CO_2 results do however indicate issues with the lab temperature control. One final line of evidence that indicates the issues are unique to cylinder D743652 are the results of the TT2 cylinder (D089506)**.** Although there are fewer runs than on D743652, the measurement results are well within the compatibility goal (mean difference from declared = 0.020 ± 0.014) and in the internal reproducibility goal (0.017 ± 0.014 for CO_2 and 2.5 ± 2.2 for $\delta(O_2/N_2)$).

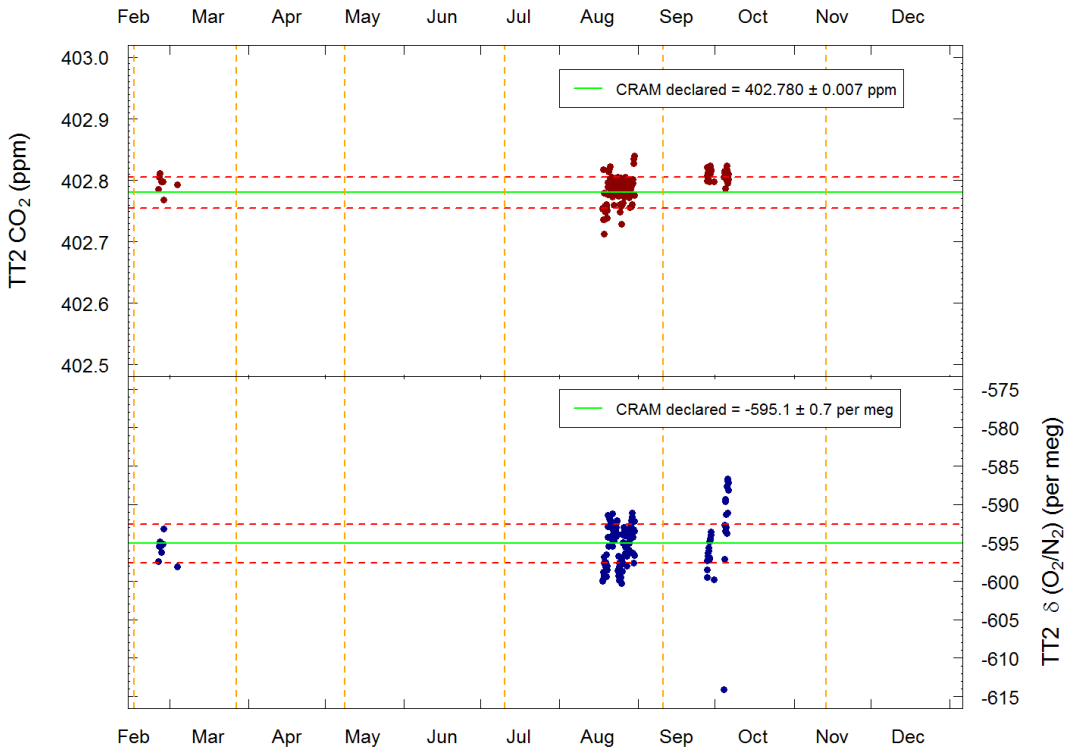

Figure 3.9. As in Figure 3.8, but for the second TT cylinder (D089506). This cylinder was run through the system as a ZT in August and September/October (see Figure 3.7 for an explanation) and therefore did not adhere to the same protocols as the initial TT in Figure 3.8.

3.4.5. Internal reproducibility from ambient air measurements

Finally, the ultimate internal reproducibility of the system can only be determined from air measurements that have been run through all parts of the system, unlike the TT

However, this measure also encompasses real atmospheric variability in O_2 and CO_2. In an attempt to circumvent this I examined a period during sample collection when ambient variability was particularly low. I chose ~ 4 days of data towards the end of May: CO_2 = ~ 400; O_2 = ~ -580 per meg; wind speed between ~ 5 and 10 ms^{-1}. Based on this analysis the internal reproducibility for $\delta(O_2/N_2)$ was ± 6.1 per meg and CO_2 was ± 0.007 ppm (**Table 3.4**). Ultimately, this is the precision I can assign to ambient air measurements for the measurement system, as all components of the system are tested, unlike the TT measurements, which do not pass through the pumps or the drying system.

Table 3.2. Individual WT statistics on all calibration parameters discusses thus far in the text. The first three columns following the cylinder ID refer to the 1σ standard deviation of the non-linearity (CO_2 c-term) and linearity (b-term) coefficients of all calibrations using that particular WT cylinder. The next four columns refer to the mean and 1σ standard deviation of the current WT concentration minus the previous concentration defined during the previous calibration and so gives a measure of the stability of the WT over its lifetime. The final two columns refer firstly to the O_2 depletion rate over the lifetime of the cylinder and secondly to the total number of calibrations recorded on each WT.

Cylinder	**σ CO_2 c term x10 $^{-5}$ [ppm]**	**σ CO_2 b term x10 $^{-3}$ [ppm]**	**σ O_2 b term [ppmEquiv]**	**Mean CO_2 cur-prev [ppm]**	**σ CO_2 diff [ppm]**	**Mean O_2 cur-prev [ppmEquiv] ([per meg])**	**σ O_2 diff [ppmEquiv] ([per meg])**	**O_2 depletion/cylinder [ppmEquiv] (per meg)**	**n**
D269485	3.7	8.1	56	0.058	0.044	0.49 (3.0)	0.47 (2.8)	0.20 (1.2)	15
D269486	8.6	11	68	0.058	0.049	0.43 (2.6)	0.38 (2.3)	-0.60 (-3.6)	28
D269491	8.1	8.3	61	0.065	0.064	0.47 (2.8)	0.40 (2.4)	-1.2 (-7.2)	30
D269489	7.1	8.8	66	0.082	0.062	0.52 (3.1)	0.43 (2.6)	-0.89 (-5.4)	31
D269490	5.0	9.0	40	0.059	0.059	0.26 (1.6)	0.18 (1.1)	-1.31 (7.9)	29
D269488	2.9	3.5	29	0.017	0.021	0.29 (1.8)	0.22 (1.3)	-0.89 (5.4)	30
All WTs	**5.9**	**8.1**	**53**	**0.057**	**0.050**	**0.41 (2.5)**	**0.35 (2.1)**	**-1.1 (6.6) excluding first two WTs**	**120**

Table 3.3. Target Tank results for cylinders D743652 (main TT) and D089506 (TT2). The Internal reproducibility and compatibility goals as set by the WMO/GAW guidelines are shown, respectively. Each TT run is declared as the mean and 1σ standard deviation of 13 one minute data points from the analysers. Hence the fourth column represents the mean of the declared 1σ standard deviation of all runs on the TT. The fifth column, on the other hand, represents the 1σ standard deviation of all of the declared values on the TT. Finally, the seventh column represents the mean difference of all individual runs from the declared value determined at the CRAM Lab.

TT ID	Species	Reproducibility			Compatibility		
		Goal	Mean 1σ of all individual runs	1σ of all runs	Goal	Mean difference form declared CRAM value.	n
D743652	CO_2 (ppm)	± 0.025	0.014 ± 0.017	0.044 ± 0.037	± 0.050	0.049 ± 0.057	627
	O_2 (per meg)	± 1.0 (± 2.5)	5.6 ± 1.9	2.2 ± 1.7	± 2.0 (± 5.0)	9.3 ± 2.8	
D089506	CO_2 (ppm)	± 0.025	0.017 ± 0.029	0.017 ± 0.014	± 0.050	0.020 ± 0.014	306
	O_2 (per meg)	± 1.0 (± 2.5)	5.8 ± 1.7	2.5 ± 2.2	± 2.0 (± 5.0)	2.5 ± 2.2	

Table 3.4. Summary of the compatibility and reproducibility of the HBA O_2 and CO_2 measurement system as depicted by analyses of the TT (D743652) (third, fourth and seventh columns, which are the same as the fourth, fifth and sixth columns in (**Table 3.3**) and by analysis of the 1σ standard deviation of successive pairs of measurements from sample air when ambient conditions were relatively stable (fifth column). This represents 4 days of sample air data (n=6182) towards the end of May 2016: CO_2 = 400.001 ± 0.108; O_2 = -579.8 ± 11.1 per meg with wind speed between ~ 5 and 10 ms^{-1}). The air line data reproducibility gives the best measure of the precision attainted on sample data points.

Species	Reproducibility				Compatibility	
	Goal	Target Tank		Air lines	Goal	Mean difference form declared CRAM value.
		Mean 1σ of all individual runs (n=627)	1σ of all runs n=(627)	Mean SD of successive pairs of measurements (n= 6182)		
CO_2 (ppm)	± 0.025	0.014 ± 0.017	0.044 ± 0.037	± 0.007	± 0.050	0.049 ± 0.057
O_2 (per meg)	± 1.0 (± 2.5)	5.6 ± 1.9	2.2 ± 1.7	± 6.1	± 2.0 (± 5.0)	9.3 ± 2.8

3.5. Summary and conclusions

The O_2 and CO_2 measurement system installed at HBA performed well for a period of ~11 months with minimal downtime. The compatibility and internal reproducibility of the system was determined by frequent (every 11 hours) analysis of a Target Tank (TT; D743652). For O_2, the 1σ standard deviation of all runs (n=632) was ± 2.2 per meg, which represents the repeatability of a measurement and is within the accepted internal reproducibility goal as determined by the O_2 community, but not within the WMO goal. Conversely, the mean (n=632) 1σ standard deviation of an individual run (n=13) was ± 5.6 per meg, which represents the reproducibility of the system. Although this is outside of the internal reproducibility goal, it is comparable to other fuel cell measurement systems (Kozlova and Manning, 2009; Pickers, 2016; Stephens et al., 2007; Wilson, 2012). Unfortunately, however, this TT shows a 9.3 ± 2.8 per meg offset from the CRAM Lab declared value. This is not within the WMO or the accepted O_2 community compatibility goal. However, this particular cylinder is known to be wet (~15 ppm H_2O) which could explain this offset through surface reactions on the cylinder walls. Moreover, when a second TT cylinder was run (TT2; D089506) on the system, the mean offset was 2.5 ± 2.2 per meg, well within the above mentioned goals and so likely indicates the compatibility issues arising from the TT analysis on cylinder D743652 are unique to that particular cylinder, rather than the system. Furthermore, a downward drift of 2.2 per meg per year is observed over the lifetime of the cylinder and could also be related to the above, in addition to preferential desorption of N_2 relative to O_2 as discussed.

For CO_2, the repeatability of measurements on the TT was ± 0.044 ppm, whereas the internal reproducibility over an individual run was ± 0.014 ppm, which is within the internal reproducibility goal. Furthermore, the mean difference from the declared CRAM Lab value is 0.049 ± 0.057 ppm, which is only marginally within the southern hemisphere compatibility goal. **Figure 3.8** shows that for the majority of the measurement period this measurement was positively offset.

The disappointing CO_2 results were shown to be related to a deterioration in the stability of the laboratory temperature over the winter months. In particular, the sensitivity of the CO_2 analyser improved from the beginning of November when the laboratory temperature became much more stable (**Figure 3.2**). This was reflected in the stability of WT mole fractions, which are redefined every calibration: the largest variability is

observed from May to September when the temperature control was poor (**Figure 3.3**). This was further reflected in the "goodness of fit" parameter (R^2) for the CO_2 calibrations (**Figure 3.5**). An attempt was made to account for the poor temperature control by increasing the ZT run frequency and this decreased the percentage of ZT runs that were > 0.025 ppm from the previous run from 9.75 to 6.6%, a significant ($p < 0.05$) improvement (**Figure 3.6**)

The above analysis of the system clearly shows that the data collected can be utilised for scientific analysis, with an ambient uncertainty on the measurements of ± 6.1 per meg for O_2 and ± 0.007 ppm for CO_2. However, there are clearly some improvements which can be made, particularly with regards to laboratory temperature control. The requirement for excellent laboratory temperature control is one of the drawbacks of using the Siemens Ultramat NDIR CO_2 analyser. More stable CO_2 analysers that are not as sensitive to external temperature variations do exist, such as those produced by Picarro or Los Gatos Research (LGR). However they require much higher sample flow rates than that used here (typically 400 ml min^{-1}) and use vacuum pumps to draw air through. With the requirement to measure O_2 and CO_2 simultaneously, to account for CO_2 dilution effects on the O_2 mole fraction, a flow rate of 400 ml min^{-1} would be too high to determine an accurate response from the O_2 analyser's fuel cells, whilst a vacuum system would not allow for precise pressure and flow control. Higher flow rate O_2 measurement systems are currently being trialled for eddy flux measurement campaigns within forest ecosystems (P.Pickers *personal communication,* 2017). However, much larger O_2 and CO_2 fluxes are expected in such a region and so measurement precision does not have to be as stringent as is necessary for Southern Ocean carbon cycle research. As such, the technique would not be appropriate here

3.6. References

Bergamaschi, P., Lowe, D.C., Manning, M.R., Moss, R., Bromley, T., Clarkson, T.S. (2001) Transects of atmospheric CO, CH_4, and their isotopic composition across the Pacific: Shipboard measurements and validation of inverse models. Journal of Geophysical Research-Atmospheres 106, 7993-8011.

Keeling, R.F., (1988) Development of an interferometric oxygen analyzer for precise measurement of the atmospheric O_2 mole fraction, Division of Applied Sciences. Harvard University, Cambridge, Massachusetts, U.S.A., p. 178.

Keeling, R.F., Manning, A.C., McEvoy, E.M., Shertz, S.R. (1998) Methods for measuring changes in atmospheric O_2 concentration and their applications in southern hemisphere air. Journal of Geophysical Research-Atmospheres 103, 3381-3397.

Keeling, R.F., Manning, A.C., Paplawsky, W.J., Cox, A.C. (2007) On the long-term stability of reference gases for atmospheric O_2/N_2 measurements. Tellus Series B-Chemical and Physical Meteorology 59, 3-14, doi:10.1111/j.1600-0889.2006.00228.x.

Kozlova, E.A., Manning, A.C. (2009) Methodology and calibration for continuous measurements of biogeochemical trace gas and O_2 concentrations from a 300-m tall tower in central Siberia. Atmospheric Measurement Techniques 2, 205-220.

Le Quéré, C., Rödenbeck, C., Buitenhuis, E.T., Conway, T.J., Langenfelds, R., Gomez, A., Labuschagne, C., Ramonet, M., Nakazawa, T., Metzl, N., Gillett, N., Heimann, M. (2007) Saturation of the Southern Ocean CO_2 sink due to recent climate change. Science 316, 1735-1738, doi:1710.1126/science.1136188.

Pickers, P.A., (2016) New applications of continuous atmospheric O_2 measurements: meridional transects across the Atlantic Ocean, and improved quantification of fossil fuel-derived CO_2, School of Environmental Sciences. University of East anglia Norwich p. 291.

Stephens, B.B., Bakwin, P.S., Tans, P.P., Teclaw, R.M., Baumann, D.D. (2007) Application of a differential fuel-cell analyzer for measuring atmospheric oxygen variations. Journal of Atmospheric and Oceanic Technology 24, 82-94, doi:10.1175/JTECH1959.1171.

Stephens, B.B., Keeling, R.F., Paplawsky, W.J. (2003) Shipboard measurements of atmospheric oxygen using a vacuum-ultraviolet absorption technique. Tellus Series B-Chemical and Physical Meteorology 55, 857-878.

Tans, P.P., Zellweger, C., (2016) Report of the Eighteenth WMO/IAEA Meeting on Carbon Dioxide, Other Greenhouse Gases, and Related Measurement Techniques (GGMT-2015), in: Tans, P.P., Zellweger, C. (Eds.), San Diego, USA, pp. available at http://www.wmo.int/pages/prog/arep/gaw/gaw-reports.html.

Wilson, P., (2012) Insight into the Carbon Cycle from Continuous Measurements of Oxygen and Carbon Dioxide at Weybourne Atmospheric Observatory, UK, School of Environmental Sciences. Univeristy of East Anglia, Norwich, p. 155.

CHAPTER 4 ATMOSPHERIC O_2, CO_2 AND APO MEASUREMENTS AT THE HALLEY RESEARCH STATION, ANTARCTICA

4.1. Introduction

The over-arching aim of this thesis was investigate the processes that control the variability of atmospheric CO_2, $\delta(O_2/N_2)$ and APO on different spatial and temporal scales at two contrasting coastal locations. Here, I ask, to what extent do carbon cycle processes in the South Atlantic sector of the Southern Ocean control the variability of atmospheric CO_2, $\delta(O_2/N_2)$ and APO observations at the Halley Research Station, Antarctica? In order to achieve this, I have established a new, *in situ,* continuous atmospheric CO_2 and O_2 measurement system at the station. The design and evaluation of this system was addressed in Chapters 2 and 3, respectively. This chapter primarily presents the analysis of those observations in order to answer the question defined above.

The Southern Ocean carbon cycle, in its natural state, is characterised by a balance between physical and biogeochemical processes: Firstly, the upwelling of deep water rich in dissolved inorganic carbon (DIC), to the south of the Antarctic Circumpolar Current (ACC), constitutes a significant source of CO_2 to the atmosphere (Mikaloff Fletcher et al., 2007; Rintoul, 2011; Takahashi et al., 2012). Secondly, nutrients brought to the surface by this upwelling stimulate biological production that results in a low partial pressure of dissolved CO_2 (pCO_2) within the surface ocean (Takahashi et al., 2012). If the partial pressure of CO_2 in the overlying atmosphere is greater than the surface ocean pCO_2, then there will be a flux of CO_2 from the atmosphere to the ocean according to Henry's Law. This dissolved CO_2 then rapidly dissociates into bicarbonate and carbonate ions. Finally, north of the ACC, surface waters are subducted into the ocean interior, sequestering carbon (Mikaloff Fletcher et al., 2007; Rintoul, 2011; Takahashi et al., 2012). It is the formation of these water masses, known as sub-Antarctic Mode Water and Antarctic Intermediate Water, that are thought to currently account for the uptake and storage of anthropogenic CO_2 within the Southern Ocean (0.42 ± 0.2 Pg C yr^{-1} (Sabine et al., 2004). Physical changes within the ocean due to climate change, such as changes in surface currents and the mixed layer depth, may well effect this subduction processes (Sallee et al., 2012). Although biological productivity does not constitute a sink for anthropogenic CO_2 itself (due to the limitation of other nutrients), the process is indirectly involved in the uptake of anthropogenic CO_2 by the Southern Ocean by creating low pCO_2 surface waters (Takahashi et al., 2012). Moreover, the export of carbon from the surface layer via the biological pump is key to the carbon balance of the ocean (maintaining a

gradient in DIC from the surface (low) to the deep (high)) and future climatic changes on ocean biology and circulation may affect this (Houghton, 2007; Riebesell et al., 2009)

Monitoring of these physical and biogeochemical processes is an inherently difficult task given the scarcity of observations in this region (Bakker et al., 2016) and thus is the source of much scientific debate (e.g. Landschützer et al., 2015; Law et al., 2008; Le Quéré et al., 2007; Le Quere et al., 2008; Metzl et al., 2006; Munro et al., 2015; Roy et al., 2003; Zickfeld et al., 2008). This uncertainty in the evolution of the Southern Ocean carbon sink demonstrates an imperative to use continuous, *in situ* observations to observe and quantify biogeochemical processes that influence CO_2 exchange between the Southern Ocean and the atmosphere.

The Clean Air Sector Laboratory (CASLab) (Jones et al., 2008) at the Halley Research Station, Antarctica (HBA: 75°35′S, 26°34′W) provides the ideal location to monitor these Southern Ocean carbon cycle processes. Atmospheric circulatory patterns within the region (see later) dictate that the station is situated in the outflow of the South Atlantic sector of the Southern Ocean, including the Weddell Sea. Locally, these regions exhibit complicated carbon dynamics driven by the interplay of local atmospheric, cryospheric and oceanic features and processes (Bakker et al., 2008; Brown et al., 2015). Consequently, the region is key to understanding the carbon cycle of the Southern Ocean (Evans et al., 2017; Sallee et al., 2012).

Although atmospheric CO_2 measurements are made at the CASLab (both low temporal resolution in collaboration with the National Oceanic and Atmospheric Administration (NOAA) Earth System Research Laboratory (ESRL) Global Monitoring Division (GMD) flask sampling network, and high resolution by the British Antarctic Survey (BAS)), a number of biogeochemical factors combine to dampen and delay the atmospheric signal of air-sea CO_2 exchange (Broecker and Peng, 1982b). Over a full seasonal cycle, the thermal and biological drivers of air-sea CO_2 exchange act in opposite directions, resulting in a small net air-sea flux of CO_2 that is difficult to detect. Secondly, CO_2 exchange is dampened by the buffering effects of carbonate chemistry in sea-water. This results in equilibration timescale between ocean and atmosphere of approximately 6 months (Broecker and Peng, 1982b). Moreover, the seasonal cycle of atmospheric CO_2 in the southern hemisphere represents the combined influence of southern hemisphere terrestrial and oceanic fluxes, in addition to northern hemisphere terrestrial fluxes that are delayed by approximately 6 months due interhemispheric transport, such that they are in phase with, and so reinforce, the southern hemisphere terrestrial fluxes (Heimann et al.,

1989; Nevison et al., 2008b; Stephens et al., 2013). It is therefore difficult to draw conclusions about ocean carbon processes from atmospheric measurements of CO_2 alone.

Atmospheric inversion schemes are one method of untangling these processes. Atmospheric inversion modelling, with respect to CO_2, attempts to optimise *a priori* fluxes of CO_2 (from measurements and/or inventories of carbon from the ocean, land and fossil fuel emissions) to actual measurements in time and space of atmospheric CO_2, via a numerical atmospheric transport model (Ciais et al., 2010). In doing this, the *a priori* fluxes, which will likely have been arrived at via interpolation of measurements that are sparse in both space and time, are optimised to match the atmospheric CO_2 observations, such that a new, potentially more reliable set of fluxes is arrived at. The relative influence of each flux on atmospheric CO_2 at a particular location can then be assessed.

One such inversion scheme is the CarbonTracker ensemble data assimilation system developed by NOAA/ESRL (Peters et al., 2005). It was first used to estimate fluxes between the terrestrial biosphere and the atmosphere in North America (Peters et al., 2007) and then subsequently developed to estimate European terrestrial fluxes (Peters et al., 2010). More recently it has been used to untangle biosphere and ocean carbon flux impacts on the atmospheric CO_2 seasonal cycle (Stephens et al., 2013). The most recent development of the modelling system, CarbonTracker Europe 2016 (CTE2016), is presented in van der Laan-Luijkx et al. (2017). To date and to my knowledge, only one such application of CTE2016 has been used: within the Global Carbon Project's annual carbon budget to estimate global fluxes of CO_2 in conjunction with a suite of other atmospheric inversion schemes (Le Quéré et al., 2016).

Consequently, before examining the new atmospheric data from the recently installed atmospheric O_2 and CO_2 measurement system, I have decided to investigate the current HBA CO_2 record from flask observations using CTE2016. The first objective of this chapter was to determine which carbon cycle processes control the variability in the seasonality of atmospheric CO_2 from flask observations collected at HBA using the CTE2016 model.

Air-sea O_2 fluxes are driven by the same carbon cycle processes that drive CO_2 exchange, but some of the fluxes act in the opposite direction, such that the drivers of air-sea O_2 exchange reinforce one another over the seasonal cycle (Keeling, 1988b; Keeling et al., 1993; Keeling and Shertz, 1992). Moreover, the equilibration time of air-sea exchange for O_2 is an order of magnitude faster than for CO_2 since there is no O_2 equivalent of the carbonate chemistry of sea water (Broecker and Peng, 1974). These

effects result in atmospheric O_2 variations that can be 20 times larger than CO_2, making it much easier to identify ocean carbon cycle processes (Keeling and Shertz, 1992).

Measurements of the atmospheric $\delta(O_2/N_2)$ ratio began in the vicinity of the

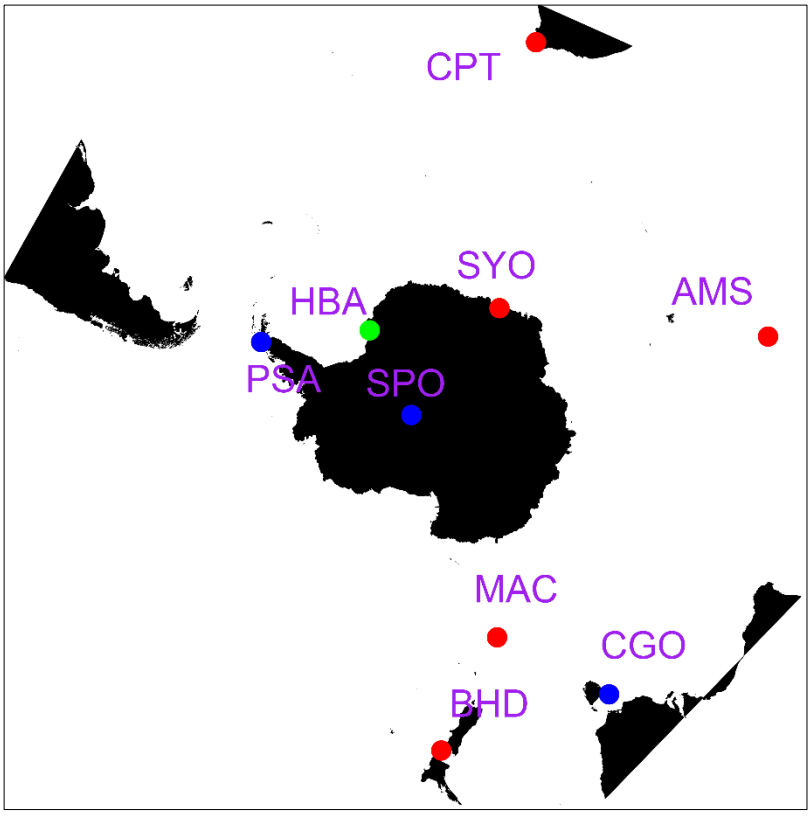

Figure 4.1. Location of historical and current O_2 monitoring stations part of either the SIO or PU flask sampling network within the vicinity of the Southern Ocean. The location of the new continuous *in situ* atmospheric O_2 and CO_2 measurement system installed as part of this thesis research at the Halley Research Station (HBA) is shown by the green dot. Other stations considered in this chapter that are a part of the SIO network are shown by blue dots: PSA = Palmer Station, Antarctica, SPO = South Pole Observatory; CGO = Cape Grim Observatory. The remaining stations, shown by the red dots, are either part of the discontinued PU flask sampling network (CPT = Cape Point, South Africa, AMS = Amsterdam Island, MAC = Macquarie Island). The remaining two stations, Syowa (SYO) maintained by the Japanese Meteorological Agency, and Baring Head (BHD), maintained by the National Institute of Water and Atmospheric Research, New Zealand, represent the only two continues *in situ* atmospheric O_2 and CO_2 measurement systems in the region.

Southern Ocean in 1991 as part of both the Scripps Institution of Oceanography (SIO) and Princeton University (PU) O_2 flask sampling networks (Bender et al., 1996; Bender et al., 1998; Keeling and Shertz, 1992; Manning, 2001). Historically, there have been a total of eight O_2 monitoring stations within the region (**Figure 4.1**). Unfortunately, many of the Princeton stations are now discontinued and only those that are part of the SIO

network have data that are both quality controlled and publicly available. Furthermore, the current network of O_2 monitoring stations result in an O_2 observational gap in the South Atlantic sector of the Southern Ocean, whilst only two of the stations in **Figure 4.1** represent continuous *in situ* measurements (SYO and BHD). Consequently, one of the main objectives of this thesis was address this gap by establishing a continuous *in situ* atmospheric O_2 measurement system. Continuous observations have an advantage over discrete flask observations in that they allow investigation of atmospheric CO_2, O_2 and APO variability on synoptic timescales. The second objective of this chapter, therefore, was to investigate synoptic scale variability and determine to what extent the variability observed in O_2, CO_2, and APO can be attributed to local to regional scale carbon cycle processes.

Long term atmospheric O_2 observations allow one to investigate the seasonality and inter-annual variability of carbon cycle processes. The seasonal carbon cycle dynamics in the upper portions of the Southern Ocean largely account for the atmospheric $\delta(O_2/N_2)$ seasonal cycle observed at the monitoring stations displayed in **Figure 4.1** (Bender et al., 1996; Keeling et al., 1993; Keeling and Shertz, 1992). Briefly, increased insolation and stratification of the upper ocean in the southern hemisphere spring and summer stimulates biological productivity. The predominance of photosynthesis over respiration results in O_2 supersaturation in the surface layer that drives a net flux of O_2 to the atmosphere. A fraction of this "new" production sinks below the mixed layer where it becomes respired at depth, resulting in O_2 under-saturation. In the autumn and winter, as the surface layer cools and the thermocline breaks down, the under-saturated waters are mixed to the surface where they drive an O_2 demand from the atmosphere.

Recognition of these processes in atmospheric $\delta(O_2/N_2)$ observations lead to the formal definition of atmospheric "oceanic oxygen" (Keeling et al., 1998b) or Atmospheric Potential Oxygen (APO $\sim O_2 + 1.1CO_2$ (Stephens et al., 1998)), an atmospheric tracer that is conservative with respect to terrestrial biosphere O_2 and CO_2 exchange processes. This subsequently stimulated the interrogation of global ocean circulation and biogeochemistry models (OCBMs) by mixing modelled ocean CO_2, O_2 and N_2 fluxes within an atmospheric transport model (ATM) to generate an APO field that could be compared with APO measurements (Battle et al., 2006; García and Keeling, 2001; Gruber et al., 2001; Manizza et al., 2012; Naegler et al., 2007; Nevison et al., 2012; Nevison et al., 2005; Nevison et al., 2015; Nevison et al., 2016; Rödenbeck et al., 2008; Stephens et al., 1998). The majority of this work focused on the models ability to recreate

the observed annual mean interhemispheric APO gradient and the mean climatological seasonal cycle. However, very few of these studies had a specific focus on APO observations and modelling efforts within the Southern Ocean region (Nevison et al., 2012; Nevison et al., 2005; Nevison et al., 2016).

Surprisingly, none of the above mentioned research considered the site to site differences in the APO seasonal cycle in depth, focusing instead on model performance. Differences in the observed APO seasonal cycle between Southern Ocean monitoring stations can potentially elucidate the spatial and temporal variability of carbon cycle processes between different regions of the ocean following integration with atmospheric transport. Consequently, the third objective of this chapter was to investigate the seasonal cycle in APO observed at HBA from the installed measurement system and compare it to the observed seasonal cycle at three other APO monitoring stations whose data were publically available: SPO, PSA and CGO. I will ascertain whether these comparisons indicate anything about the spatial and temporal variability of carbon cycle processes that have, until now, been overlooked.

Furthermore, the most recent Southern Ocean APO model-observation comparison study (Nevison et al., 2016) tested eight OCBMs that participated in Phase 5 of the Coupled Model Inter comparison Project (CMIP5) (Taylor et al., 2012) against the SIO O_2 network of Palmer Station, Antarctica (PSA), South Pole Observatory (SPO) and Cape Grim Observatory (CGO) (see Section 4.2.6) (**Figure 4.1**). However, owing to vertical mixing uncertainties within the ATM (Naegler et al., 2007), Nevison et al. (2016) chose to focus their evaluation of the models against SPO observations only, which, owing to its location on the central Antarctic Plateau, means it is least sensitive to the vertical transport uncertainties discussed by Naegler et al. (2007). Of the eight models, only two performed well with respect to recreating both the phasing and seasonal cycle of APO observed at SPO. These were the NOAA Geophysical Fluid Dynamics Laboratory's (GFDL) Modular Ocean Model (Griffies et al., 2000) coupled to the TOPAZ biogeochemistry model (Dunne et al., 2013), often referred to as "ESM2G"; and, the current version of the NCAR Community Earth System Model (Long et al., 2013), which consists of version 2 of the POP physical oceanography model (Smith et al., 2010) coupled to the Biogeochemical Elemental cycling module of Doney et al. (1996), often simply referred to as "CESM". Both of these models have also performed well at other northern and southern hemisphere stations (Nevison et al., 2015). Consequently, the final objective of this chapter was, building upon the work of Nevison et al., (2016), to select

the two best performing Southern Ocean models with respect to APO, ESM2G and CESM, and test them against all available Southern Ocean APO monitoring stations (HBA, PSA, SPO and CGO). In doing this, I hope to answer the following question: do HBA APO measurements highlight deficiencies or strengths in the models that are otherwise overlooked with fewer stations to compare against?

4.1.1. Aims and objectives of this chapter

The primary aim of this chapter was to determine the extent with which carbon cycle processes in the South Atlantic sector of the Southern Ocean control the variability of atmospheric CO_2, $\delta(O_2/N_2)$ and APO observations at the Halley Research Station, Antarctica.

This will be achieved through the following objectives:

1. Determine what carbon cycle processes control the seasonality of atmospheric CO_2 from flask observations collected at the Halley Research Station using the CTE2016 atmospheric inversion scheme.
2. Investigate synoptic scale variability and determine to what extent the variability can be explained by local to regional carbon cycle processes.
3. Compare the seasonal cycle of APO observed at HBA to that observed at other Southern Ocean stations and assess what can be learned about the spatial and temporal variability of carbon cycle processes within the Southern Ocean region.
4. Do HBA APO observations highlight deficiencies or strengths in OCBMs that are otherwise overlooked with fewer stations to compare against?

This analysis will represent the first time that the CTE2016 model has been used to investigate the processes that control the variability of the seasonal cycle of atmospheric CO_2. It also represents the first time that the CarbonTracker modelling environment has been used to examine carbon cycle processes at a coastal Antarctic Station.

Moreover, the HBA O_2 and CO_2 measurement system is the first of its kind in the South Atlantic sector of the Southern Ocean. It is the second coastal continuous measurement system in the region (a similar system exists at Syowa station (Ishidoya et al., 2012)) and the third in total (a continuous system runs on the research ship the Laurence M. Gould which supplies PSA, but the data has yet to be published). As such,

the measurement system represents a considerable contribution to the atmospheric $\delta(O_2/N_2)$, CO_2 and APO observation record in the Southern Ocean and Antarctica.

4.1.2. Outline of this chapter

In this chapter I will present the first year of continuous, *in situ*, atmospheric $\delta(O_2/N_2)$, CO_2 and APO measurements from the successful installation of the O_2 and CO_2 measurement system within the CASLab at the Halley Research Station. Readers interested in the details of the system itself are referred back to Chapters 2 and 3. I will begin by giving a brief overview of the measurement location before describing a thorough filtering analysis of the data to remove local pollution from the station. I then describe the model set up for the analyses outlined in Objectives 1 and 4.

The results section first considers the drivers of variability in the NOAA flask observations of CO_2 using output from CTE2016. I then present the first year of atmospheric $\delta(O_2/N_2)$, CO_2 and APO observations from the measurement system presented in this thesis. I consider synoptic variability first before examining the seasonal cycles of the species. Finally, I compare the APO seasonal cycle at HBA to other Antarctic APO stations before using the data to examine two OCBMs coupled to an ATM.

4.2. Background and methodology

4.2.1. Site location and history.

The Halley Research Station (HBA: 75°35′S, 26°34′W) is a coastal Antarctic scientific research station established by the British Antarctic Survey in 1956 and has been used to facilitate scientific research in the polar region ever since. Sitting 30 m above sea level on the floating Brunt Ice Shelf, the station is located approximately 15km from Weddell Sea (**Error! Reference source not found.**). It is manned year-round by a team of support staff and scientists responsible for maintaining a suite of scientific equipment that's primary goal is to contribute to global atmospheric and space weather observations. The station is inaccessible by ship between March and December due to the prevalence of sea ice in the region and by plane between April and October due to poor winter weather and 24-hour darkness (May-July).

The main station (**Error! Reference source not found.**C) is aligned approximately North-South and is surrounded by an approximately 5km oval shaped perimeter. The Clean Air Sector laboratory (CASLab) is approximately 1km south east

of the main station in a designated "clean air sector" where vehicles are not authorised and access to the lab is by ski or by foot. Power is provided by cable from the main station so that no generators are required at the lab itself. The predominant wind directions are from the east or the west (**Figure** 4.2). As such, and with the above measures in place, pollution from the station is kept to a minimum (Jones et al., 2008).

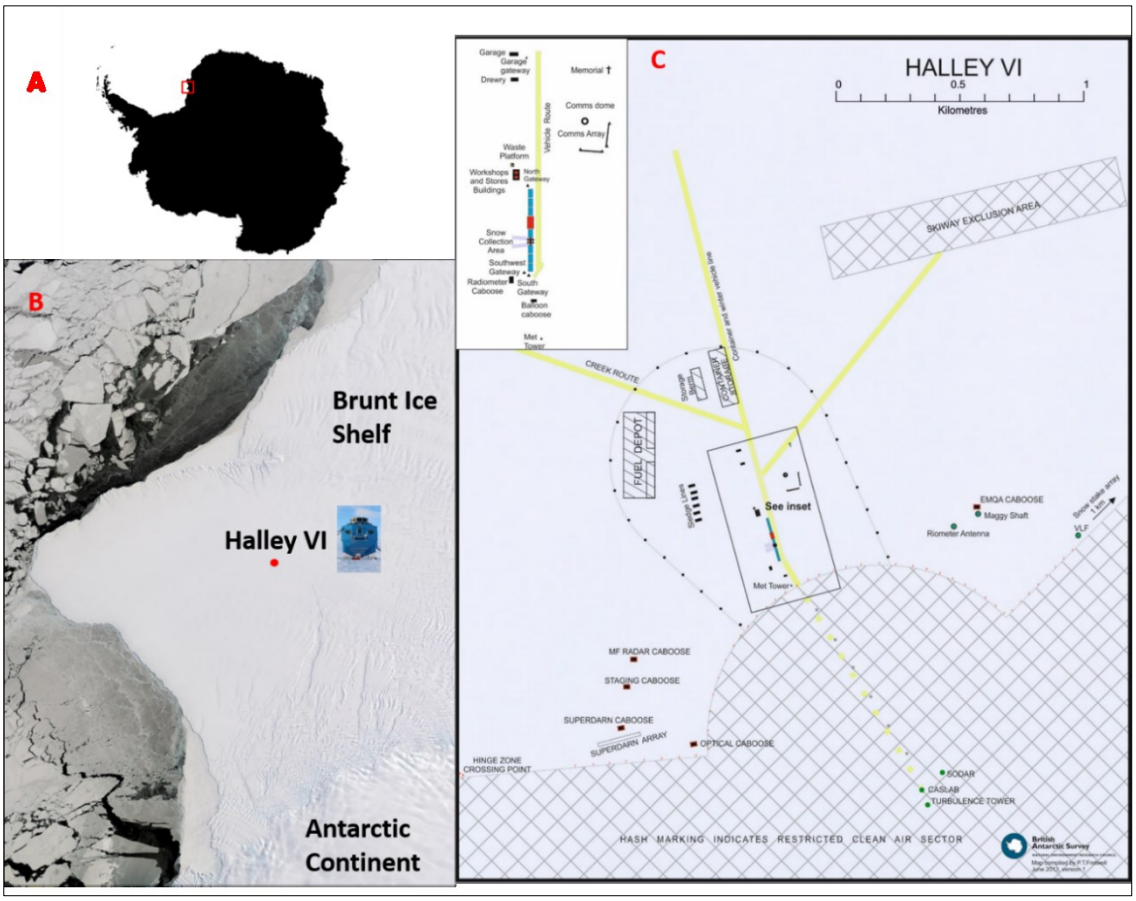

The lab is constructed from three shipping containers suspended from four vertical steel girders approximately 3m above the snow level and was first established at the Halley V research station in 2003. It subsequently closed in 2008 and was re-established at the new Halley VI research station in 2012, approximately 20km to the south east of Halley V.

Multiple atmospheric species are measured via a suite of analysers housed in the main room of the lab. Each analyser samples air from the main trace gas inlet stack (100 mm internal diameter) from a ventilated air flow of ~ 5000 L/min. Aerosols are sampled from a separate chimney stack (200 mm ID) from a ventilated air flow of ~240 L/min.

The majority of research campaigns conducted at the CASLab have been concerned with understanding reactive polar tropospheric chemistry. This includes understanding ozone depletion events (Jones et al., 2013), aerosol production in the sea ice zone (Roscoe et al., 2015) and wider scale snow-atmosphere interactions (Jones et al., 2008). Furthermore, the station is part of the World Meteorological Organisation (WMO) Global Atmospheric Watch (GAW) programme and submits continuous, *in-situ,* carbon monoxide (CO) and ozone (O_3) data as part of its commitment to this. Finally, in addition to the continuous data the station records, HBA has also been part of NOAA/ESRL/GMD Carbon Cycle Greenhouse Gas (CCGG) cooperative air sampling network since 1983, providing weekly samples on a suite of climatically relevant trace gases, including CO_2.

4.2.2. Air mass origin at Halley.

Wind direction and wind speed were recorded at the main station approximately 8m above the snow surface from the meteorological observation tower (**Error! Reference source not found.**C). The wind rose in **Figure 4.2**A demonstrates the most prominent wind origin observed at HBA during 2016 was from the ENE and that this is also associated with the highest wind speeds (>12 ms^{-1}). **Figure 4.2** also demonstrates that a significant proportion of the winds derived from the WSW, where air is likely to have recently being in contact with a year-round open water in the polynya named Precious Bay (Jones et al., 2008). The mean wind speed during this period was 6.5 ms^{-1}.

To determine typical air mass origins of air sampled at HBA I have performed a cluster analysis of seven day length back trajectories. These were generated by releasing a particle every 3 hours within a modelled meteorological field and following its path for seven days., using the HYSPLIT_4 (HYbrid Single-Particle Lagrangian Integrated Trajectory) model (Version 4) (Draxler and Hess, 1998). The Hysplit model uses previously gridded meteorological data from the Global NOAA-NCEP/NCAR reanalysis[5] to determine simple particle trajectories, run either forward or backward, from a particular starting location and time.

A total of four trajectory clusters were determined using an angle distance matrix that determines whether individual trajectories are similar or not based on their angle from the starting location rather than their Euclidean distance (Carslaw and Ropkins, 2012). The angle based approach to determining trajectory clusters is thought to be better at

[5] http://www.cpc.ncep.noaa.gov/products/wesley/reanalysis.html

capturing atmospheric circulatory features (Polar lows, for example) than the Euclidean distance approach (Carslaw and Ropkins, 2012) and I therefore deemed this a more appropriate methodology for determining typical air mass origins over wide areas of the Southern Ocean and Antarctica.

The clustering was performed using the trajClust function that is part of the openAir package implemented in the R programming language (Carslaw and Ropkins, 2012) and further mathematical details of the computation can be found in the openAir reference manual (Carslaw and Ropkins, 2012).This analysis shows that for 61% of the time HBA receives air that has been in contact with the South Atlantic sector of the

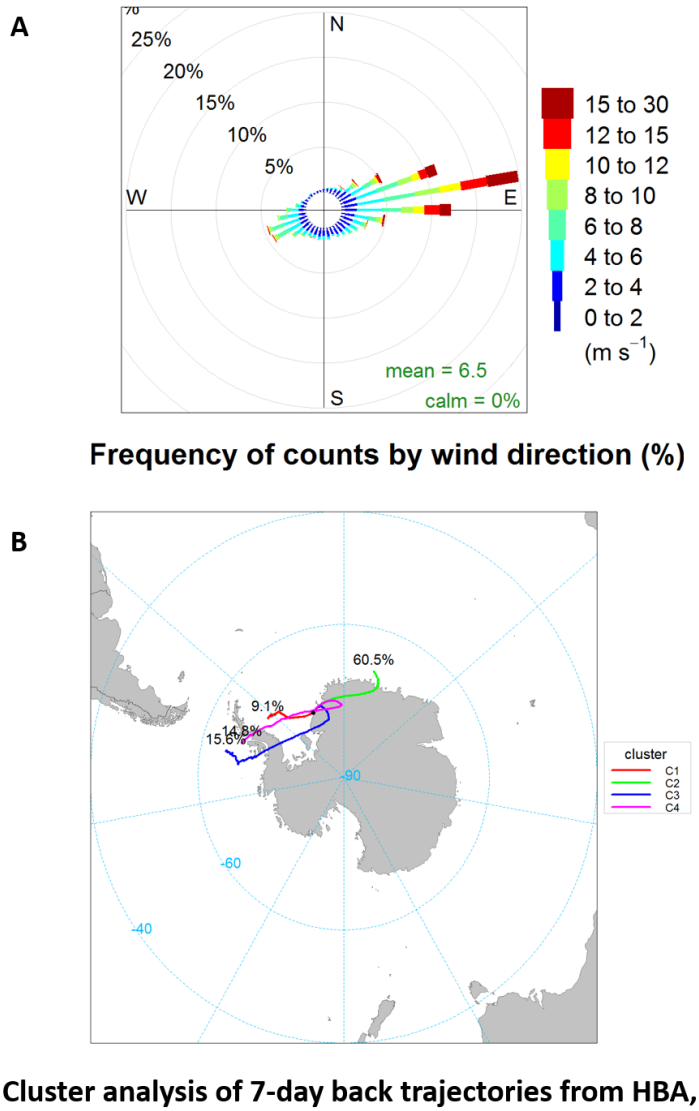

Figure 4.2.A Wind rose depicting the wind direction and wind speed observed at HBA during the measurement period (February 2016-January 2017). B. cluster analysis of 7-day backwards trajectories starting from HBA every 3 hours for the year of 2016. Trajectories were computed using the Hysplit Model and the cluster analysis was performed using the "openair" data analysis package implemented in the R Programming language (specific details are given in Section 4.2.2). The percentage of trajectories that were associated with each cluster (depicted by the coloured lines) are shown next to each of the respective trajectory cluster lines.

Southern Ocean and the Weddell Sea. Air deriving from the east can also originally be from the west, close to the Antarctic Peninsula, after spending time on the continual plateau.

A clustering trajectory analysis was also performed on the three other Southern Ocean APO monitoring stations discussed in this Chapter (Section 4.2.6).

4.2.3. Installation

Installation of the atmospheric O_2 and CO_2 measurement system began at the beginning of January 2016. The system was installed in a small room, adjacent to the main ventilated room of the lab. Due to the requirements of the low flow rate and the need to avoid tee junctions in the sample line (See Chapter 2 Section 2.3), two separate dedicated aspirated air inlets were installed on the east facing rail (the most prominent wind direction (**Figure 4.2**)) of the CASlab roof, approximately 2 meters from the main sample stack. More detail regarding the specifics of the installation can be found in Chapter 3, section 3.2.

During the testing period it was noted that room air could accidently be sampled from the inlets. This occurred when wind speeds were low (< 2 ms^{-1}), originating from the west and when the external laboratory door or one of the internal windows were open. A log of when people were working in the lab was therefore taken and consulted during the data filtering process (Section 4.2.4). Additionally, when wind speeds were very high (>15 ms^{-1}) the suspended laboratory could be felt to be shaking or oscillating. This appeared to correlate with an increase in the noise in the measurements, particularly in the response of the Siemens analyser in CO_2 (**Figure 1.2**, Appendix B).

Sample air data collection began in February 2016. CO_2 and $\delta(O_2/N_2)$ measurements were collected at 1 minute intervals. However, this was subsequently averaged up to 10 minute means, primarily to facilitate merging with both meteorological and diagnostic data.

4.2.4. Data filtering.

As was first discussed in Chapter 3 Section 3.3, suspect data based on system diagnostics and leaks detected (during February, whilst I was still working on the system), the total number of days flagged = 39.9 days which represents a 11.3% data loss (with respect to the total number of days the system was running, rather than the number of data points lost).

4.2.4.1. Contamination from the station

Despite the measures taken to minimise pollution at the laboratory sample inlets outlined above, sometimes the prevailing wind direction and wind speed make it unavoidable. For example, with a north-westerly wind, the lab is directly downstream of the main station (**Error! Reference source not found.**C). It was noted at the time of installation that even if the wind direction was such that the lab was not downstream of the station (i.e. clean air, deriving from the south, east or west.), yet the wind speed was low, that pollution from both the station and vehicle movements could still be transported to the lab. Furthermore, during the time of installation and in the following summer

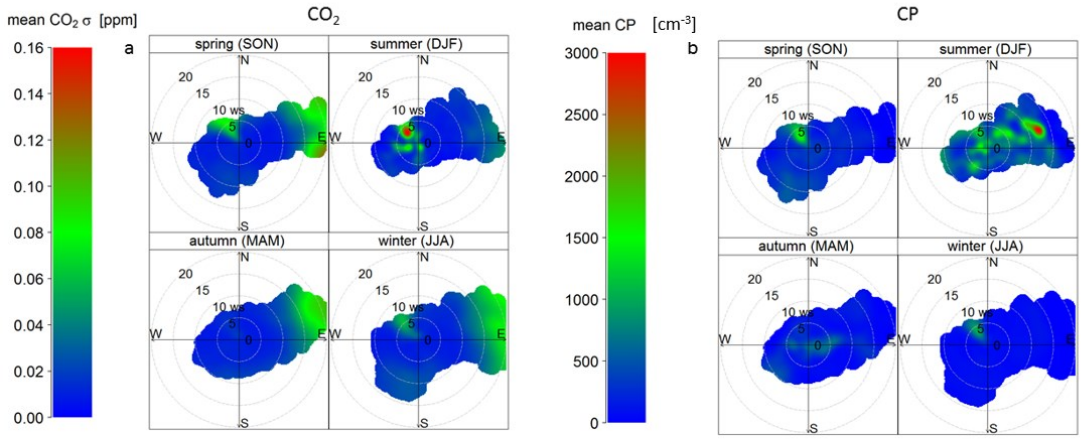

Figure 4.3. Bivariate polar plots depicting how (a) the standard deviation of a 10 minute mean of CO_2 mole fraction and (b) the concentration of aerosols (condensation particulates; CP) vary with wind direction and wind speed in each season of the year. The plot was constructed using the "polarPlot" function within the openair package in R (Carslaw and Ropkins, 2012). More detail on its construction can be found in Carslaw et al. (2006) and Carslaw and Ropkins (2012; Sallee et al., 2012). Briefly, however, wind speed and wind direction are partitioned into bins (1ms^{-1} and 10 degrees, respectively) and the mean of the third variable (in this case the 1σ standard deviation of CO_2 and aerosol concentration) for each bin is calculated. A Generalised Additive Model (GAM) (Wood, 2006) is then used to describe how a variable varies with wind speed and wind direction.

season (December 2016 - February 2017), the main station was being relocated to the east (the prevailing wind direction) due to a crack in the ice shelf[6]. Consequently, more pollution was observed than would otherwise be likely in a typical summer season and

[6] https://www.bas.ac.uk/media-post/relocation-of-halley-research-station/

was derived from wind directions that are typically considered clean. This made it difficult to apply a simple meteorological filter to the data.

To circumvent this, I performed an analysis of the standard deviation of 10 minute means (10 data points) of the CO_2 mole fraction and of the mean aerosol concentration determined from the condensation particle counter (CPC) installed within the CASLab. Since clean background mole fractions are very stable at HBA, the standard deviation represents a good measure of short term variability. If the standard deviation is high, then CO_2 mole fractions will be changing rapidly during the 10 minute recording interval and will therefore likely represent a short-term pollution event form the station. Aerosol particles on the other hand, vary naturally in coastal Antarctica and typically derive from the sea-ice zone from various sources of marine origin (Roscoe et al., 2015; Weller et al., 2015). However, they are also produced as a product of combustion and concentrations are typically high in polluted areas (Kulmala et al., 2005). Due to the seasonal cycle in the natural precursors to aerosols in coastal Antarctica (Roscoe et al., 2015), the threshold for polluted values varies throughout the year. For example, at the Neumayer Antarctic research station, polluted air is defined when aerosol concentrations are >2500 cm^{-3} during summer, >800 cm^{-3} during spring/autumn and >400 cm^{-3} during winter (Weller et al., 2007).

The results of this analysis are shown in **Figure 4.3** which represent bivariate polar plots that depict how a particular variable varies with wind speed and wind direction (Carslaw et al., 2006) (details of the plots construction are given in the figure caption). **Figure 4.3**a shows that the highest CO_2 standard deviations, and therefore the highest CO_2 mole fraction variability, originate from the NWN in the direction of the station during spring, summer and winter. This is corroborated by the mean aerosol concentration depicted in **Figure 4.3**b. **Figure 4.3**b also demonstrates that high aerosol concentrations are observed from almost all directions and wind speeds during the summer (note the spread of green in the "summer" panel in **Figure 4.3**b). This is likely to be a combination of natural sources (Roscoe et al., 2015) and station pollution. The same panel in **Figure 4.3**a, shows that the CO_2 standard deviation can be high, depicting pollution when the laboratory is not downstream of the station but when wind speeds are low (<5 ms^{-1}) as was described earlier from manual observations during the installation period. **Figure 4.3**a also demonstrates how CO_2 variability increases with increasing wind speed. It was observed at the time that this is likely due to the lab oscillating in the wind, and therefore

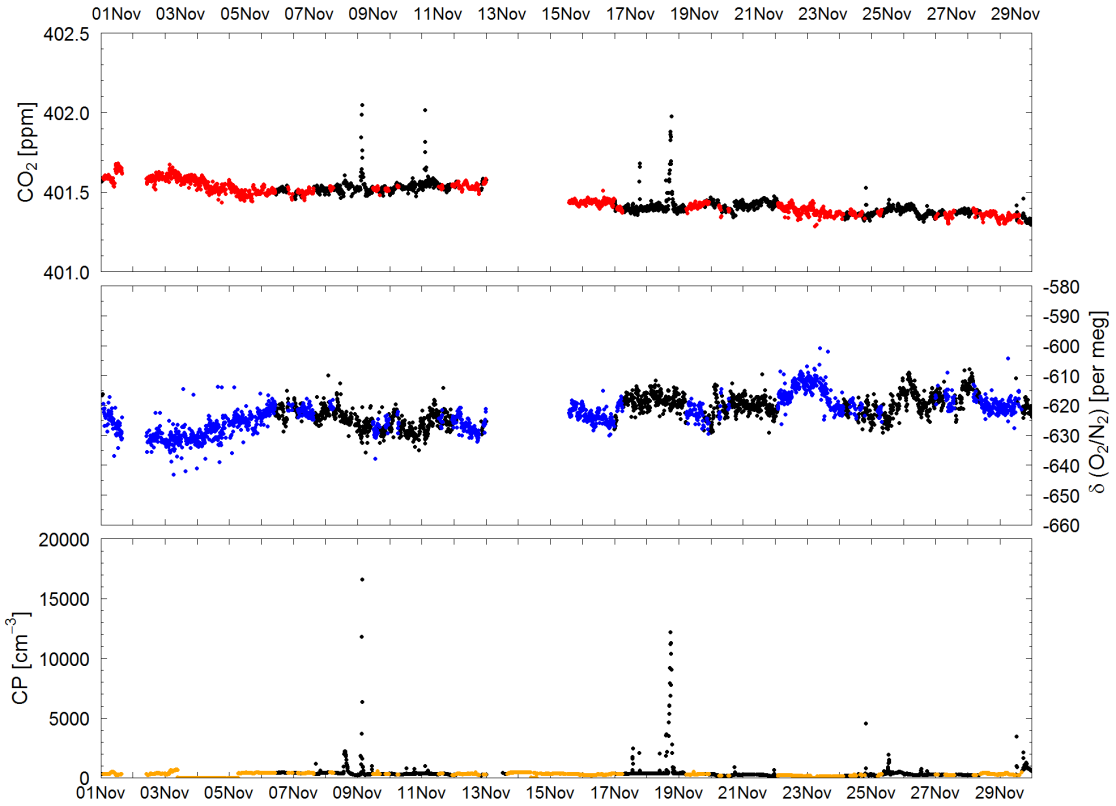

Figure 4.4. Example of the skill of the filtering process described in the text for the month of November, 2016. Day of the month is shown on the x-axis. Black points in all panels show the data that has been discarded. Top panel = CO_2 (red points). Middle panel = $\delta(O_2/N_2)$ (blue points). Bottom panel = aerosol concentration (or condensation particulates (CP) (orange). CO_2 and $\delta(O_2/N_2)$ axes are not scaled on a mole per mole basis as is often shown. Data are from the month of November 2016.

impacting the stability of the laser in the measurement cell as mentioned previously (Appendix B **Figure 1.2**).

Following this analysis, I have decided to exclude data using the following criteria: when winds were derived from 290-360° and/or when wind speeds were < 5 ms^{-1} and/or when aerosol concentration were >2500 cm^{-3} during summer, >800 cm^{-3} during spring/autumn and >400 cm^{-3} during winter, adopting the method of filtering applied at Neumayer research station (Weller et al., 2007). A demonstration of the skill of the filtering technique to remove pollution events, yet still retain a large amount of data is shown in **Figure 4.4**.

4.2.5. Curve fitting routines: "CCGCRV" and "HPspline"

There are three curve fitting routines that are typically used by the greenhouse gas community in order to decompose a time-series into its respective seasonal, trend and residual components. These are: "CCGCRV", "HPspline" and "STL". For a fuller

discussion as to the mechanisms behind each routine see Pickers and Manning (2015). However, I will briefly outline the concept behind each method here. However "STL" will not be discussed further due to its inability to deal with gaps in the data (see Pickers and Manning (2015)).

CCGCRV is a curve fitting routine developed by Thoning et al. (1989) and is used extensively by the CCG/ESRL research group at NOAA. The routine fits a polynomial equation plus a harmonic function to the time series (Equation **(4.1)**):

$$C(t) = a_0 + a_1 t + a_2 t^2 + \cdots + a_{(n-1)} t^{(n-1)} + \sum_{k=1}^{h} m_k [\sin(2\pi k t + \varphi_k)] \quad \textbf{(4.1)}$$

Where t is time in years, n is the number of polynomial terms, a_0, $a_1 \ldots a_{(n-1)}$ are coefficients of the fit, h represents the number of harmonics in the function, and m_k and φ_k define the magnitude and phase of each sinusoidal component, respectively (Pickers and Manning, 2015). The residuals of the *C (t)* are then transferred from the time domain into the frequency domain using a Fast Fourier Transform (FFT), upon which a digital low pass filter is applied (Equation **(4.2)**) In doing this, regular variations within the time series, such as the seasonal cycle, can be identified since they vary with a defined frequency :

$$H(f) = e^{\left[-\ln(2).\left(\frac{f}{f_c}\right)^6\right]} \quad \textbf{(4.2)}$$

Where f_c is the cut-off frequency of a low pass filter expressed in cycles yr^{-1}(Pickers and Manning, 2015). The low pass filter has a short term and a long term cut off value. The short term value corresponds to short term variations in the data, such as the seasonal cycle, and is typically set at 80 days (Thoning et al., 1989). The long term cut off value corresponds to longer term variations in the overall trend seen in the data, such as inter-annual variability and is typically set at 667 days (Thoning et al., 1989). Once the filter has been applied and the respective components extracted, the residuals are transformed back into the time domain. The long term trend component of the time series is then derived by summing the polynomial plus the long term data from the filter and the seasonal component is extracted by summing the polynomial component and the short

term data from the filter, and finally subtracting the long term trend from it. The version used in this analysis was written by Paul Krummel (CSIRO) and is implemented using the IDL programming language.

HPspline is a routine derived from the Fortran program "Stationfit" developed by Bacastow et al. (1985). It also fits the sum of a polynomial equation plus a harmonic function to the data, but instead of using a FFT to extract the respective components, a stiff cubic spline *R(t)* (Reinsch, 1967) is used to fit the data. The long term trend *E (t)* is determined by the polynomial fit and is firstly removed from the data (Equation **(4.3)**):

$$E(t) = a_0 + a_1 t + a_2 t^2 + \cdots + a_{(n-1)} t^{(n-1)} \quad \textbf{(4.3)}$$

Values are as above in Equation (4.1) (Pickers and Manning, 2015). The harmonic function *S (t)* is then fit to the data (Equation **(4.4)**):

$$S(t) = \sum_{k=1}^{h} [x_k \sin(2\pi kt) + y_k \cos(2\pi kt)] \quad \textbf{(4.4)}$$

Where *S (t)* the seasonal variation represented by a harmonic function; *h*, is the number of harmonics; *t* is the time in years, 2πk is the angular frequency, and x_k and y_k define the magnitude of the sinusoidal and cosine components of the curve (Pickers and Manning, 2015). The function (1 + *γt*) *S(t)* is fit to the seasonal component, where *γt* is a time dependent gain factor, whilst the residuals of *S (t)* are fit to the cubic spline. The cubic spline fit is then subtracted from the data and the residuals fit to the harmonic function. The final two steps are repeated in an iterative process until convergence is achieved and the overall curve fit to the data, *P (t),* is represented by Equation **(4.5)** (Keeling et al., 1989):

$$P(t) = E(t) + (1 + \gamma t)S(t) + R(t) \quad \textbf{(4.5)}$$

4.2.5.1. Choice of routines

The choice of curve fitting routine used to extract seasonal and long term trends from an atmospheric dataset depends both on the data and the questions being asked of it (Pickers and Manning, 2015). With regards to the HBA $\delta(O_2/N_2)$, CO_2 and APO data, the

purpose of the extraction is to estimate the seasonal cycle in each species from only one year of data. Consequently, I chose to use the HPspline curve fitting routine due to its inflexibility in the curve fit, thus making it more insensitive to outliers that might be expected in such a short data set. However, for this curve fitting routine to be successful, more than one year of data is required. To address this, I repeated the data for 2016 both forwards (2017) and backwards (2015) with estimated growth and depletion rates (see Section 4.2.5.2) for CO_2 and $\delta(O_2/N_2)$ respectively (Appendix B **Figure 1.3**). I use a 3rd order polynomial plus the sum of the four harmonics to fit each of the data series

Conversely, in the analysis of the variability in the atmospheric CO_2 seasonal cycle observed at HBA from NOAA flask sample measurements I opted to use CCGCRV. A fuller discussion behind this choice is discussed in the Results section. However, briefly, CCGCRV is known to capture real variations on the seasonal cycle of atmospheric species better than HPspline, since the curve fit derived via HPspline is relatively stiff (Pickers and Manning, 2015).

4.2.5.2. Extraction of seasonal cycles

To estimate the growth rate in CO_2, I compared my continuous data to the NOAA flask data for the previous year at Halley (**Figure 4.5**). The continuous data was first averaged to daily means – to be comparable with the flask data, and then the mean difference between each corresponding point in the year was taken. This approach makes the following assumptions: (1). the flask data and my continuous data are on the on the same CO_2 scale, which they are (NOAA 2007x); (2). NOAA flask data and my continuous data agree to within ± 0.05 ppm to be within the WMO compatibility goals for the southern hemisphere. Unfortunately, this assumption cannot be validated until the NOAA flask data for 2016 has been analysed (which, at the timing of writing, had not). However, ± 0.05 ppm represents < 2% of the current CO_2 growth rate (2-3 ppm yr^{-1}) and so will not impact the results significantly. Finally, (3). The mean growth rate over 2015 and 2016 is

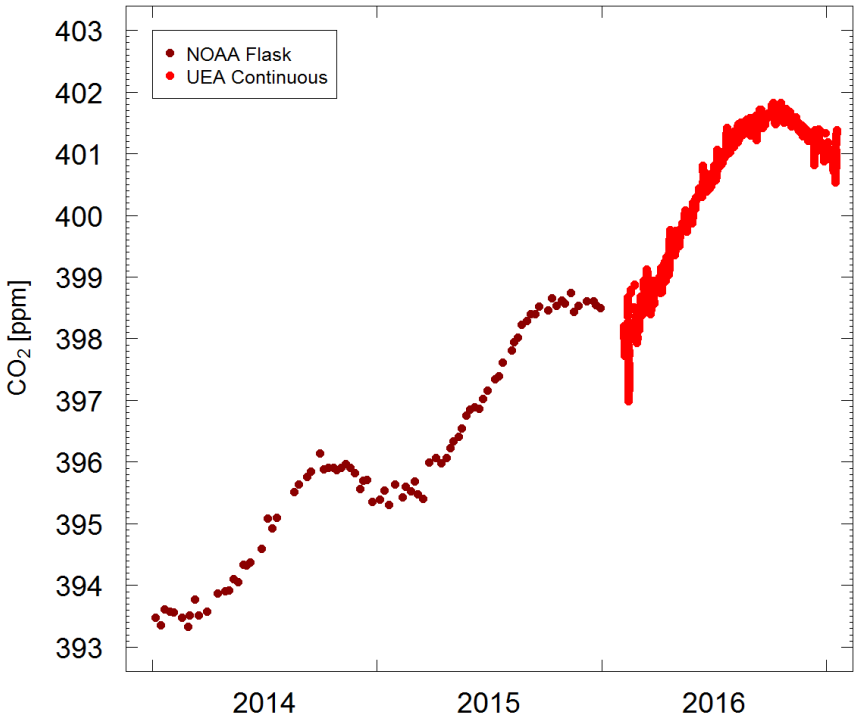

Figure 4.5. The atmospheric CO_2 mole fraction from NOAA flask samples collected at HBA in 2014 and 2015 (dark red points) compared to the continuous data observed in 2016 from the measurement system installed as a part of the research presented here (red points). The continuous data were averaged to daily means and the difference between the corresponding day in the 2015 flask data was taken and the mean of all differences used to estimate the growth rate applied in the construction of data for the curve fitting routine described in the text.

maintained between 2016 and 2017. In reality, inter-annual variability in the CO_2 growth rate is significant (Le Quéré et al., 2016).

Using the method outlined above resulted in a mean growth rate of 3.27 ppm yr^{-1} ± 0.46 ppm. This is a high growth rate compared to the typical global mean (2.24 ± 0.48 ppm yr^{-1}; 2006-2016[7]) However, it has been noted that due to the recent strong El Niño, the growth rate observed between 2015 and 2016 is the largest on record (Betts et al., 2016). Whilst NOAA note high 2015 and 2016 growth rates and comment that this may continue in 2017[8].

The small amplitude of the CO_2 seasonal cycle in the southern hemisphere (Stephens et al., 2013) makes it sensitive to the to the assumed growth rate, since the magnitude of the growth rate is greater than the amplitude. Consequently, in order to test the sensitivity of the CO_2 seasonal cycle to the assumed growth rate, I have applied two extra growth rates at using the 1σ standard deviation of the mean: 3.73 and 2.81 ppm yr^{-1}.

[7] https://www.esrl.noaa.gov/gmd/ccgg/trends/gr

[8] http://www.noaa.gov/news/carbon-dioxide-levels-rose-at-record-pace-for-2nd-straight-year

The lower limit in particular is more comparable to the mean NOAA growth rate for the past decade and might therefore be more applicable.

The $\delta(O_2/N_2)$ amplitude, on the other hand, is much less sensitive to the growth (or depletion) rate estimate than that for CO_2. Typical Southern Ocean based monitoring stations observe seasonal $\delta(O_2/N_2)$ amplitudes of 70 to 90 per meg (Battle et al., 2006) and is therefore much larger than typical global growth rate for $\delta(O_2/N_2)$ (-19 per meg yr^{-1}; SIO website[9]).

$\delta(O_2/N_2)$ flask samples have been collected at HBA since 2014 by Harro Mejer's group at the University of Groningen. However, at the time of writing, these samples had not been analysed. Once these data are available it will provide a good estimation of the growth rate of $\delta(O_2/N_2)$ at Halley over recent years and also provide a good comparison exercise between the continuous and flask sampling system. For the meantime, to estimate the growth rate, I took the mean difference between the 2016 HBA continuous data and the 2015 flask data for PSA. Again, this requires a few assumptions: firstly, that they're both on the same $\delta(O_2/N_2)$ scale, which they are: SIO S2 O_2 scale. The largest assumption is that the $\delta(O_2/N_2)$ growth rate at PSA is representative of the Southern Ocean and therefore of the data at HBA. Given the well mixed nature Southern Ocean air this assumption is reasonable. On the other hand, one of the goals of establishing new observations in the region is to test this assumption. The final assumption, as it was for CO_2, is that the $\delta(O_2/N_2)$ growth rate is constant between 2015, 2016 and 2017. Using this method, the assumed growth rate for $\delta(O_2/N_2)$ used at HBA is -21.4 per meg. This estimate appears to be reasonable, given the typical global growth rate is -19 per meg yr^{-1} (see above).

The replicated data and the results of the curve fit are shown in **Figure 1.3**, Appendix B, the standard deviation of the residuals: $CO_2 = \pm 0.13$ ppm, $\delta(O_2/N_2) = \pm 5.4$ per meg and APO = ± 5.2 per meg.

4.2.6. SIO O_2 and NOAA CO_2 flask data.

The SIO O_2 flask data were obtained from SIO O_2 website[5] and cover the period 2000 to 2015 for the following stations: Palmer Station, Antarctica (PSA, 64°46′S, 64°05′W), South Pole Observatory (SPO, 89°58′S, 24°48′W) and Cape Grim Observatory (CGO, 40°42′S, 144°41′E).The samples are collected at approximately monthly intervals.

[9] http://scrippso2.ucsd.edu

The NOAA flask data were obtained from the ObsPack GLOBALVIEWplus v2.1 package (ObsPack, 2016). The flask samples were collected approximately twice per week by BAS staff at HBA.

Seasonal cycles were extracted from the data using the curve fitting routines described in Section 4.2.5, the particular choice of which is discussed in the results discussion (Section 4.3).

4.2.7. Modelling tools

4.2.7.1. CarbonTracker Europe 2016

CarbonTracker is an ensemble data assimilation system that estimates surface CO_2 fluxes by assimilating global atmospheric observations of CO_2 mole fractions. Originally developed by the National Oceanic and Atmospheric Administration's (NOAA) Earth System Research Laboratory (ESRL) (Peters et al., 2007; Peters et al., 2005), the model has been adapted for European carbon cycle research purposes (Peters et al., 2010) and has subsequently developed independently of the original NOAA/ESRL version (van der Laan-Luijkx et al., 2017). In this study, I use the most recent release of the European version of the model, CarbonTracker Europe 2016 (CTE2016, (Peters et al., 2010; van der Laan-Luijkx et al., 2017)) which provide optimised surface fluxes for the 2001-2015 period. The optimized fluxes are subsequently run in forward mode to obtain simulated CO_2 mole fractions, including the individual contributions of the biosphere and ocean fluxes as well as the emissions from fossil fuel combustion and biomass burning.

CarbonTracker uses prior estimates of surface CO_2 fluxes which are transported by the TM5 transport model (Krol et al., 2005) forced with ERA-interim meteorology from the European Centre for Medium-Range Weather Forecasting (ECMWF). The surface fluxes for the net biosphere and ocean exchange are optimized using an Ensemble Kalman smoother using atmospheric CO_2 mole fraction observations. The result is a modelled CO_2 flux (F) at a given location in time (x,y,t) given by Equation **(4.6)**:

$$F(x,y,t) = \lambda_r.\, F_{bio}(x,y,t) + \lambda_r.\, F_{oce}(x,y,t) + F_{fossil}(x,y,t) + F_{fire}(x,y,t) \quad \textbf{(4.6)}$$

The prior terrestrial biosphere (F_{bio}) and ocean (F_{oce}) fluxes are derived from the respective ocean and biosphere models, and are scaled by an optimised scaling factor (λ_r), whilst the emissions from fossil fuel (F_{fossil}) combustion and the biomass burning (F_{fire})

are kept constant. The prior fluxes for each module are obtained from the following: ocean fluxes are derived from the ocean inversion of Jacobson et al. (2007); The biosphere and biomass burning fluxes are derived from the SiBCASA-GFED4 model (van der Velde et al., 2014) and the fossil fuel emissions are derived from the EDGAR4.2 Database (2011) with sector specific and time-profiles derived by the Institute for Energy Economics and the Rational Use of Energy (IER) from the University of Stuttgart and constructed for the CARBONES project[10]. The fossil fuel emissions are additionally scaled with different regional annual trends for each continent to global totals as used in the annual global carbon budget produced by the Global Carbon Project (GCP) (Le Quéré et al., 2016; van der Laan-Luijkx et al., 2017). The observations used in CTE2016 are from the ObsPack GLOBALVIEWplus v2.1 package (ObsPack, 2016). The model was run by Ingrid van der Laan-Luijkx in 2016. The total model plus individual component fluxes were subsequently sampled at HBA on the same weekly time frequency as the NOAA flask observations by Ingrid and provided to me.

4.2.7.2. Ocean biogeochemistry models

I have chosen two OCBMs that participated in phase 5 of the Coupled Model Inter-comparison Project (CMIP5) (Taylor et al., 2012) and that are known to perform well in the Southern Ocean (Nevison et al., 2016). I refer to these as MOM4 and CESM. MOM4 is version 4 (the most recent) of the NOAA Geophysical Fluid Dynamics Laboratory's Modular Ocean Model (Griffies et al., 2000) coupled to the TOPAZ biogeochemistry model (Dunne et al., 2013). In the Introduction to this chapter, I have reoffered to this model as ESM2G, however, in keeping with the naming convention of the model output provided to me (see below) I refer to it as MOM4. Whilst CESM is the current version of the NCAR Community Earth System Model (Long et al., 2013), which consists of version 2 of the POP physical oceanography model (Smith et al., 2010) coupled to the Biogeochemical Elemental cycling module of Doney et al. (1996).

Air-sea fluxes of N_2, O_2 and CO_2 from each of these models were then fed into the TM3 atmospheric transport model (Heimann, 2003). Heat fluxes were used to calculate the air-sea N_2 fluxes (mol m^{-2} s^{-1}) based on Equation **(4.7)**:

$$N_2Flux = Q.\left(\frac{dS}{dT}\right)_{N_2}/C_p \qquad \textbf{(4.7)}$$

[10] http://www.carbones.eu/

Whereby Q is the heat flux (J m^{-2} s^{-1}), dS/dT is the temperature derivative of the N_2 solubility coefficient (mol m^{-3} K^{-1}) and C_p is the heat capacity of water (J m^{-3} K^{-1}).

TM3 has 3.8° latitude by 5° longitude resolution with 19 resolved vertical levels. TM3 is a three dimensional Eulerian model driven by offline National Centres for Environmental Prediction (NCEP) reanalysis winds (Kalnay et al., 1996). NCEP data have 6 hourly time resolution that are interpolated onto the 40-minute TM3 resolution.

In addition to the ocean fluxes, gridded monthly estimates with 1° by 1° resolution of fossil fuel emissions are fed into TM3 from the Carbon Dioxide Information Analysis Center (CDIAC) (Boden, 2009).

This analysis is similar to that of Nevison et al. (2016), except a different ATM is used, I focus on only two of the OCGM models that perform well in the Southern Ocean and finally, and perhaps most importantly, I have added HBA into the analysis, whose air mass footprint represents a sector of the Southern Ocean not covered by the other SIO stations **Figure 4.2B** (also see **Figure 4.16** later)

The model was run from 1991-2005 by Sara Mikaloff Fletcher in 2013. From her, I obtained the following output at HBA and the other Southern Ocean stations considered at a 40-minute values time resolution, in units of mol mol^{-1}: Ocean O_2, N_2 and CO_2 and fossil fuel CO_2. I have converted these into APO values in per meg using the equations below (see Appendix of A Rödenbeck et al. (2008) for derivation) and assuming background mole fractions observed at SPO at the beginning of the model run Equation **(4.8)**:

$$APO\ (per\ meg) = \left(\frac{ocean_{O_2} - 0.3 \times ff_{CO_2} + 1.1 \times ocean_{CO_2}}{S_{O_2}} - \frac{ocean_{N_2}}{S_{N_2}}\right) \times 10^6 \quad \textbf{(4.8)}$$

Here, *ocean O_2, CO_2 and N_2* represent the ocean fluxes of these species, SO_2 and SN_2 are the observed dry air atmospheric mole fractions of O_2 and N_2, respectively, and $ffCO_2$ represents fossil fuel emission fluxes.

Finally, I fit a curve consisting of a 3rd order polynomial plus the sum of the 4 harmonics to each of the component fluxes and the resulting CO_2, O_2 and APO mole

fractions using the HPspline curve fitting routine (Section 4.2.5) in order to extract a mean climatological seasonal cycle to compare to observations.

4.3. Results and discussion

4.3.1. Seasonal CO_2 variability at Halley (2001-2015): a modelling analysis

In the following section, I will use a global CO_2 data assimilation model (CarbonTracker Europe 2016 (CTE2016) (Peters et al., 2010; van der Laan-Luijkx et al., 2017) (Section 4.2.7.1)) to investigate the following question: Which carbon cycle processes control the seasonal variability in CO_2 observed at HBA and to what extent?

4.3.1.1. Model-observation comparison

I applied the CCGCRV curve fitting routine to the NOAA flask observations and to the CTE2016 output, using long and short term cut off values of 1500 and 150, respectively. The de-trended CTE2016 curve fit, along with the de-trended flask observations are shown in **Figure 4.6**. To evaluate the model performance I have examined two metrics, following Nevison et al. (2008a). Firstly, the correlation coefficient, R, between the model and the observations represents the agreement in phasing and shape of the two datasets. A perfect agreement would result in R = 1, whilst the significance of the agreement is determined by a two-tailed t-test assuming unequal variances. Secondly, the ratio of the 1σ standard deviation of the model and observations: $\sigma_{model}/\sigma_{obs}$ is a measure of the agreement in the amplitude between the two datasets, whereby a value > 1 represents a model overestimate of the amplitude and value < 1 represents an underestimate. Whether the model amplitude is significantly different ($p < 0.05$) from the observed amplitude is determined by performing an F-test on the hypothesis that the $\sigma^2_{model} = \sigma^2_{obs}$ (see Nevison et al. (2008b) and references therein).

Overall, the CTE2016 model performs very well at recreating the observed variability in the seasonal cycle at HBA between 2001 and 2015 (R = 0.95, $p < 0.001$, n = 5464; **Figure 4.6A**), with a mean model-observation residual of 0.14 ± 0.17 ppm. This is to be expected, since the model is optimised to the observations (van der Laan-Luijkx et al., 2017). The mean model seasonal cycle for 2001-2015 (**Figure 4.6B**) is earlier in phase by almost one month and the amplitude is overestimated ($\sigma_{model}/\sigma_{obs}$ = 1.22). However, the model-observation differences are within the year to year variability

observed both in the model and observations (as depicted by the 1σ standard deviation of the monthly means used to compute the seasonal cycle). Moreover, the F-test stipulates that the $\sigma^2_{model}/\sigma^2_{obs}$ ratios must be < 0.53 or > 3.78 for the model and observation amplitude to be significantly different from each other. In this instance, $\sigma^2_{model}/\sigma^2_{obs}$ = 1.42 and so is not significantly different ($p < 0.05$). The skill of the CTE2016 model at recreating the observed variability in the seasonal cycle therefore allows further investigation of the individual model components.

The CTE2016 model estimated contributions to the seasonal cycle are shown in **Figure 4.6C** and again in **Figure 4.7**. The terrestrial biosphere component shows the strongest agreement with the total modelled cycle ($R = 0.95$, $p < 0.001$; $\sigma_{bio}/\sigma_{model} = 1.08$) with a concomitant peak in late austral winter (August), but with a trough in late austral summer/autumn (March-April) that lags the total modelled cycle by approximately one month. The one month phase lag is maintained at the upward and downward zero crossing days (UZC, DZC, respectively). The ocean contribution, on the other hand, leads the terrestrial biosphere contribution by approximately 5 months, depicting a broad peak in autumn (March-June; maximum in June) and a broad trough in spring/early summer (October-December; minimum in October). The amplitude of the ocean contribution is approximately a third of that for the terrestrial biosphere. The fossil fuel contribution shows a broad peak from autumn, throughout the winter and with a maximum in early spring (September-October) and a well-defined minima in late summer (February). In contrast, the biomass burning contribution depicts a more symmetrical cycle, with a well-defined trough in activity in winter (July-August) and a peak in late spring/summer (November).

Interestingly, the combined contribution of the fossil fuel and biomass burning component is such that they largely cancel each other out between autumn and winter, with a resultant peak in late spring and trough in summer that has an amplitude approximately 60% of that for the ocean (**Figure 4.7B**). Consequently, the sum of the fossil fuel and biomass burning contributions modifies the ocean contribution such that the combined trough (dark blue line, **Figure 4.7C**) lags the ocean only contribution by approximately three months and modifies the trough to be much broader. However, due to the cancelling out of both the biomass burning and fossil contribution in autumn-winter, the combined peak is at the same time as the ocean only peak and the combined contribution is only a slight modification of the late summer, early autumn peak in ocean contribution. As a result, the modelled CO_2 seasonal cycle at HBA appears to be largely

controlled by the terrestrial biosphere, particularly the amplitude. However, the timing of the UZC and DZC of the modelled CO_2 seasonal cycle, although primarily determined by the phase (timing of UZC and DZC) of the terrestrial biosphere fluxes, appears to be modulated somewhat by the magnitude of the late summer-early autumn ocean outgassing (terminating at the DZC) and the combined influence of ocean CO_2 uptake

and the decrease in biomass burning and fossil emissions in the late spring-early summer (UZC).

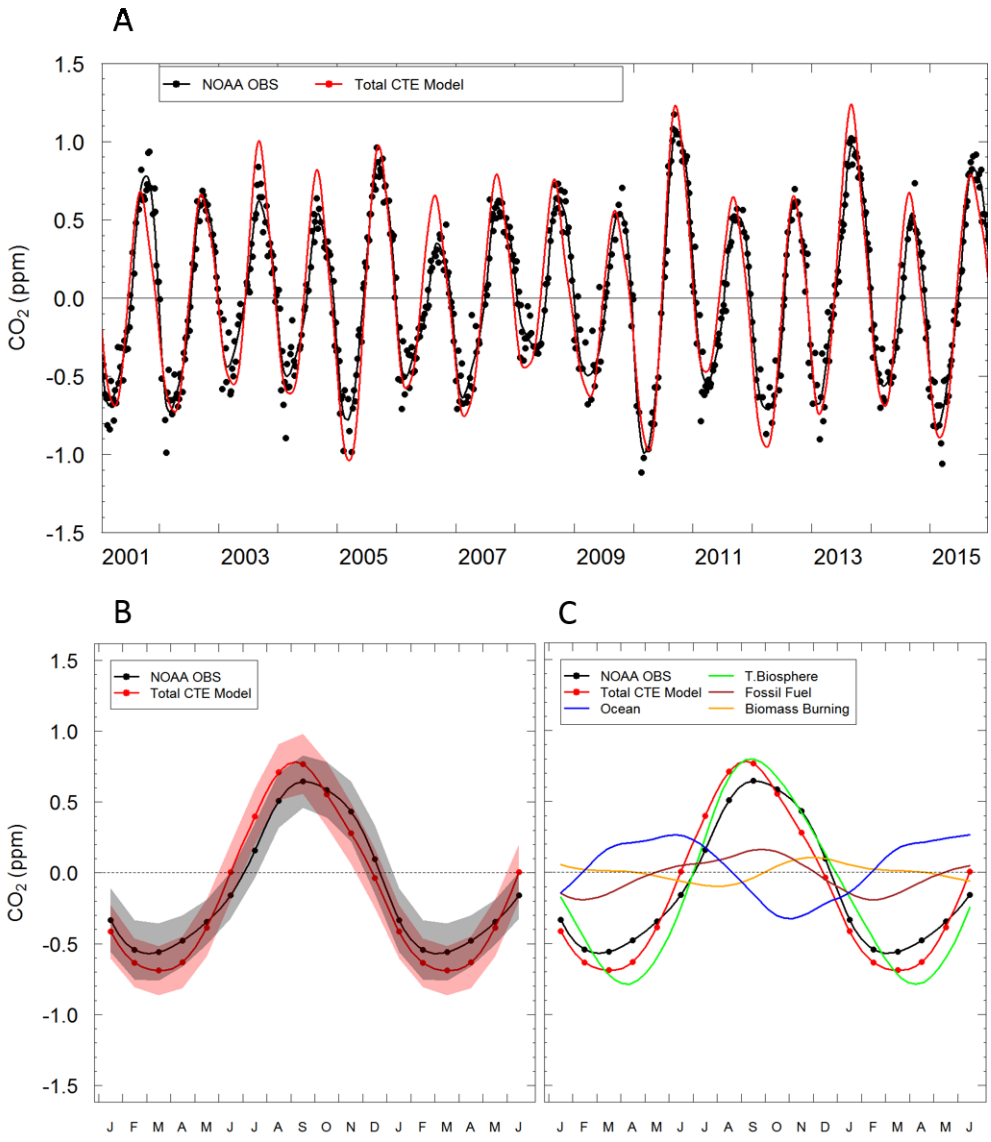

Figure 4.6. A: De-trended NOAA flask observations (NOAA OBS) of CO_2 at HBA (black points), de-trended curve fit to the NOAA observations (black line) and de-trended curve fit to modelled CO_2 from CTE2016 (red line). The x-axis represents the year of the observation B: climatological mean seasonal cycle determined from the curve fit to NOAA flask observations (black points and line) and the curve fit to the CTE2016 model (red points and line), shading represents 1σ of the monthly mean of all years and hence represents real year to year variability. The x-axis represents the first letter of individual months and the first 6 months are repeated to aid visual interpretation of the cycles. C: as in B. but with the individual flux contributions (in ppm units) to the modelled atmospheric CO_2 seasonal cycle at HBA: Ocean (blue line), terrestrial biosphere (green line), fossil fuel emissions (brown line) and biomass burning (orange line). In A, Band C all seasonal cycles were extracted from a CCGRV curve fit to either the real or modelled data using the fitting parameters outlined in the text.

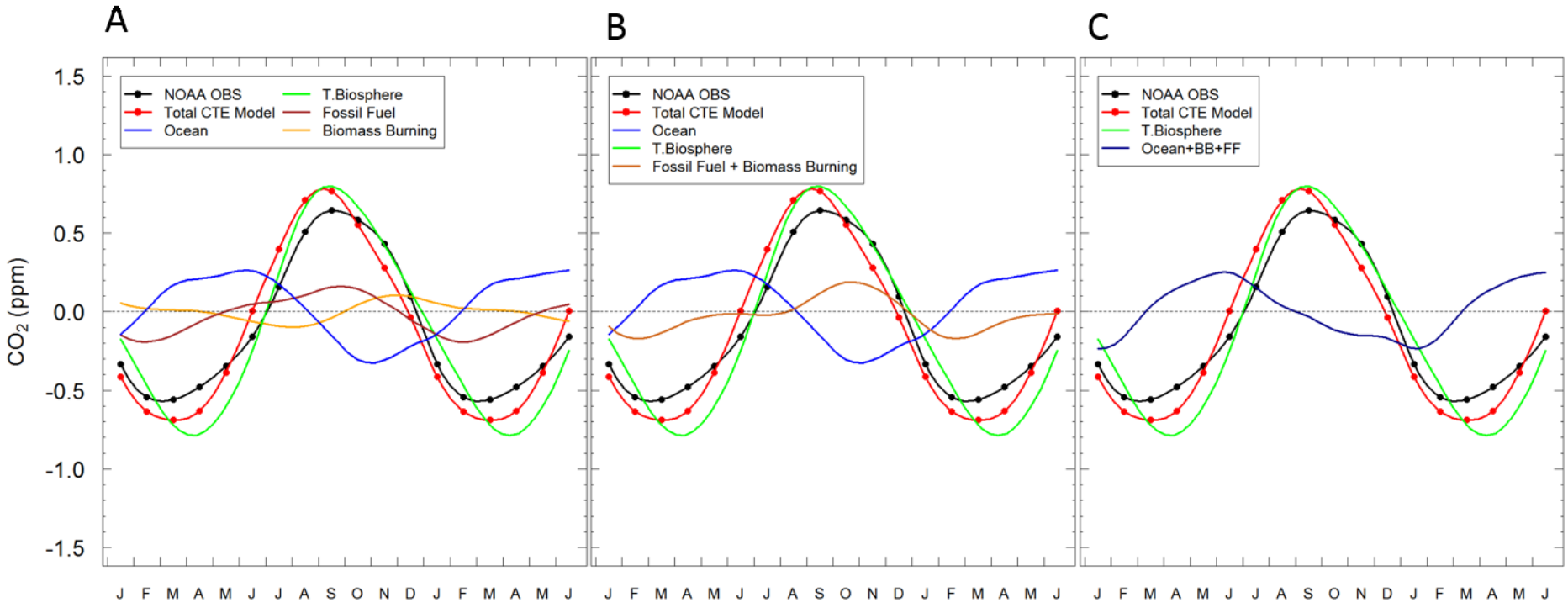

Figure 4.7. Individual CO_2 flux breakdown from the CTE2016 model. (A): same as **Figure 4.6C**. (B): as for (A) but with the fossil fuel and biomass burning seasonal fluxes combined additively to form one seasonal curve (light brown line). (C): as for (B) but with the ocean, fossil fuel and biomass burning seasonal fluxes combined additivity to form one seasonal curve (dark blue line).

4.3.1.2. Linear regression of component seasonal cycle and total modelled CO_2 cycle metrics

Based on the above interpretation of the mean modelled seasonal cycle I have constructed a hypothesis for the variability in the CO_2 seasonal cycle at HBA in the 2001-2015 period: The variability in the amplitude and phase is largely determined by variability in terrestrial biosphere fluxes, which itself is slightly modulated by variability in ocean CO_2 fluxes and, to a lesser extent, seasonal variability in biomass burning and fossil fuel emissions. To test this hypothesis, I have performed a simple linear regression of the following seasonal cycle metrics of the total modelled seasonal cycle against those for each individual component: the inter-annual variability in the amplitude and the timing of the UZC and DZC. In doing a linear regression, caution must be taken with the results due to the sample size (n=15), since each metric can only be determined once per year. Nevertheless, the significance of the regression between individual variables can still be determined and the strength of their relationship assessed. Here, I use the Mann-Kendall test for significance since the data are not normally distributed. The following results only depict the relationships, the strength of which is expressed as the value "*Tau*" which is analogous to the Pearson's "R" value (Meals, 2011), that were significant at the $p < 0.1$ level and hence representing a 90% probability that the relationship is not down to chance.

Figure 4.8 depicts the strongest predictors of the model CO_2 peak to peak amplitude. Overall, the peak to peak amplitude in the terrestrial biosphere CO_2 mole fractions shows the strongest relationship with the total model CO_2 peak to peak amplitude (*Tau* = 0.52, $p < 0.01$; **Figure 4.8C**). This confirms the prior hypothesis that the terrestrial biosphere has the strongest influence on the inter-annual variability of the CO_2 seasonal cycle at HBA. This is in agreement with similar studies from other southern hemisphere CO_2 monitoring stations (Heimann et al., 1989; Pearman and Hyson, 1980; Stephens et al., 2013). Furthermore, the timing of the DZC for the ocean CO_2 seasonal cycle is also weakly correlated with the total model peak to peak amplitude (*Tau* = 0.35, $p < 0.1$; **Figure 4.8A**). This relationship becomes stronger (*Tau* = 0.43) and more significant ($p < 0.05$) when the ocean seasonal cycle is combined additively with the seasonal cycle in fossil fuel emissions (FF) and biomass burning (BB) (**Figure 4.8B**). The

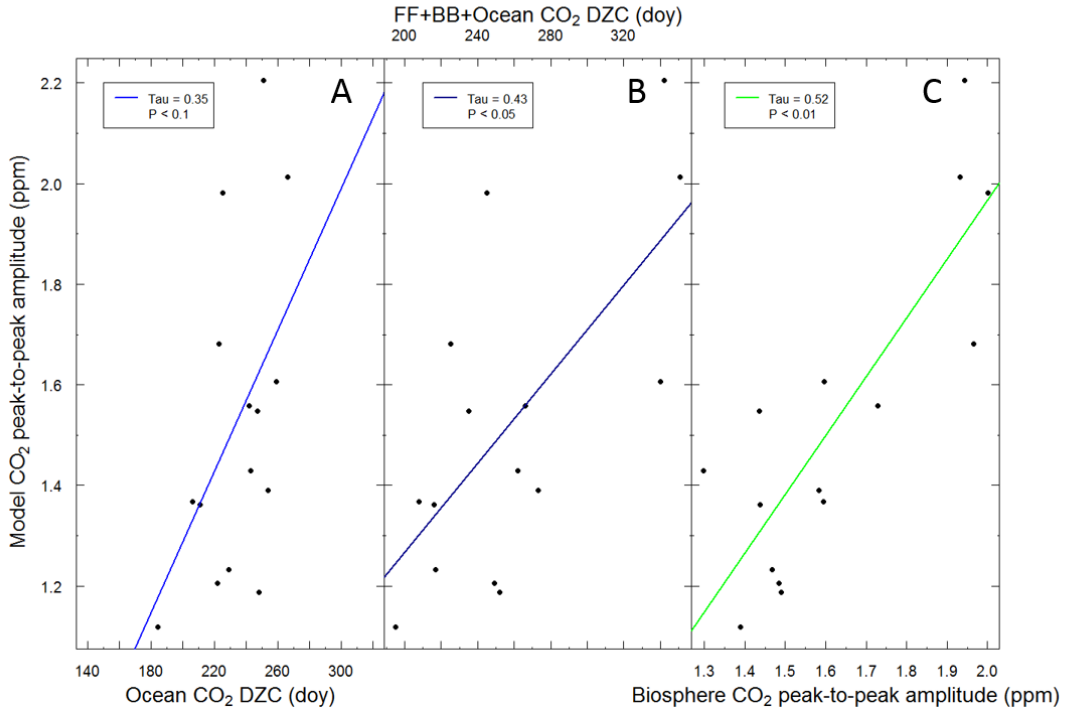

Figure 4.8. Linear regression of the model CO_2 peak-to-peak seasonal amplitude against: (A) the ocean CO_2 downwards zero crossing day (DZC) (blue line),(B) the fossil fuel plus biomass burning plus ocean (FF+BB+Ocean CO_2) DZC (dark blue line) and (C) the terrestrial biosphere CO_2 peak-to-peak seasonal amplitude (green line). The zero crossing days are expressed as the Julian day of the year.

mean DZC for the ocean CO_2 and the FF+BB+Ocean seasonal cycles occur approximately 1 month before the mean peak in the total modelled CO_2 seasonal cycle. The proximity of the two seasonal events appears to be key; an earlier (later) termination of the net ocean CO_2 outgassing period, would lead to a smaller (larger) overall seasonal atmospheric CO_2 amplitude for that year. Since the DZC in the individual fossil fuel and biomass burning emissions seasonality show no relationship with the total model CO_2 amplitude, the timing of the ocean DZC appears to be the main driver in this weak relationship. However, since the combined FF+BB+Ocean DZC shows both a stronger and more significant relationship with the modelled CO_2 amplitude, their significance in modulating the ocean influence on the overall atmospheric CO_2 amplitude cannot understated.

Figure 4.9 depicts the strongest and most significant predictors of the total model CO_2 UZC. As with the previous analysis of the total model amplitude, the strongest and most significant relationship exists between the terrestrial biosphere UZC and the model UZC day (*Tau* = 0.60, $p < 0.01$; **Figure 4.9A**). Again, this implies that the terrestrial

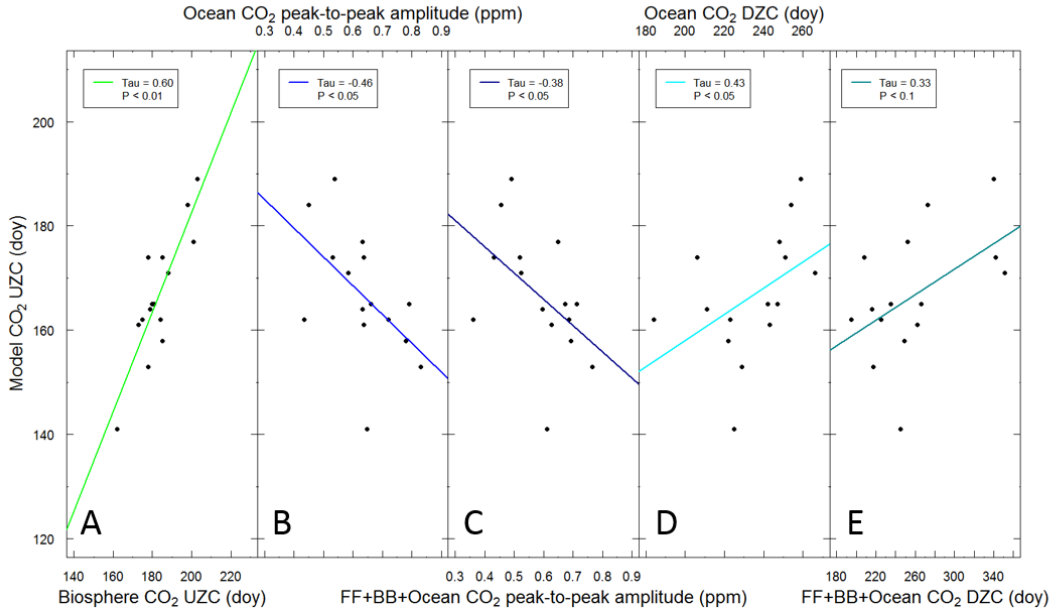

Figure 4.9. Linear regression of the model CO_2 upwards zero crossing day (UZC) against: the (A) terrestrial biosphere CO_2 UZC (green line), (B) the ocean CO_2 peak to peak amplitude (blue line), (C) the fossil fuel plus biomass burning plus ocean CO_2 peak to peak amplitude (dark blue line), (D) the ocean CO_2 downwards zero crossing day (DZC) (turquoise line) and (E) the FF+BB+Ocean CO_2 DZC (dark turquoise line). The zero crossing days are expressed as the Julian day of the year.

biosphere can explain most of the variability in the phasing of the CO_2 seasonal cycle. However, as was found with the amplitude, both the ocean (**Figure 4.9D**) and FF+BB+Ocean (**Figure 4.9E**) DZC show a weak positive relationship with the total modelled UZC. The reasoning behind this will be similar to that outlined in the analysis of the modelled amplitude, whereby the proximity in the timing of the respective events can largely explain their relationship: with an earlier (later) termination of the net ocean CO_2 outgassing period, would lead to an earlier (later) onset of the total atmospheric CO_2 UZC for that year.

What is perhaps the most interesting result of this analysis is that there appears to be a weak but significant inverse relationship between the magnitude of the ocean peak to peak amplitude and the timing of the total model UZC for CO_2 (Tau = -0.46, $p < 0.05$; **Figure 4.9B**) (whilst a similar relationship is observed when the FF+BB+Ocean amplitude is considered; 'Tau = -0.38, $p < 0.05$, **Figure 4.9C**). Again, this will be down to the timing of the two events: A larger amplitude is suggestive, although not always, of a larger peak in the ocean CO_2 seasonal cycle that is approximately synchronous with the timing of the mean total model UZC. Again, this makes sense: if the seasonal ocean

outgassing is particularly large in one year, then the UZC in the atmospheric CO_2 day will be brought forward simply because more CO_2 is entering the atmosphere.

4.3.1.3. Conclusion

In conclusion, this brief analysis has shown that the seasonal cycle in terrestrial biosphere CO_2 has the strongest most significant relationship with the total modelled atmospheric CO_2 seasonal cycle observed at HBA in CTE2016. However, I was unable to split the terrestrial biosphere influence into its northern and southern hemisphere components. It is likely that the northern hemisphere component will be of a similar magnitude and in phase with the southern hemisphere component due to the approximately 6 month timescale required for inter-hemispheric mixing (Stephens et al., 2013). A further run of CTE2016 would need to be done to confirm this.

Although the ocean influence on the total modelled CO_2 seasonal cycle appears to be small, the magnitude and timing of the flux do exhibit a weak relationship with the atmospheric seasonal cycle. Since CTE2016 CO_2 fluxes are ultimately optimized to the observations, this suggests a more prominent role for the terrestrial biosphere at high southern hemisphere latitudes than has previously been considered and more modulating role for the ocean CO_2 contribution to the seasonal cycle.

However, a certain amount of caution must be applied when interpreting the relationships described above due to uncertainties that are inherent within the CTE2016 model which I will now discuss. Firstly, optimization of fluxes in the vicinity of Antarctica will be less well constrained than those in regions with a more dense coverage of atmospheric CO_2 monitoring stations. Moreover, fluxes are only optimized relative to atmospheric observations that are within a 5 week transport window (van der Laan-Luijkx et al., 2017). These two factors will likely increase the uncertainty associated with fluxes in this region. No attempt has been made here to quantify this uncertainty. In future work, it would be prudent to calculate the uncertainty on the fluxes in a densely populated region of atmospheric observations, Europe for example, and compare to those derived for Antarctic regions.

Furthermore, the uncertainty associated with the *a priori* fluxes also need to be considered. The ocean fluxes, for example, are derived from a joint atmosphere-ocean inversion system (Jacobson et al., 2007). Thus, the *a priori* fluxes will also be subject to uncertainty associated with sparse data coverage of both atmospheric and oceanic observations in the region (e.g. Bakker et al., 2016). The inclusion or omission of a

particular monitoring station within atmospheric inversions has been shown to alter the results and hence conclusions about ocean fluxes within the Southern Ocean region (Law et al., 2008). Quantifying these errors must be the primary focus of future analyses if the oceanic and terrestrial controls on the variability of atmospheric CO_2 are to be more robustly assessed.

Finally, the choice of curve fitting routine and its parametrisation will inevitably lead to a bias in this analysis, as has been discussed in Section 4.3.4. With respect to determining which carbon cycle process controls the variability of the atmospheric CO_2 seasonal cycle, the amount of variability assigned to (i). The total seasonal cycle and (ii). The individual component seasonal cycles, when applying the curve fitting routine underpins the entire analysis. For example, would the variability seen within the atmospheric CO_2 observation record be better characterised by assigning less flexibility to the seasonal cycle and more to the long-term growth rate? In which case the explanation for the variability seen could be better described by global scale carbon cycle variability. Conversely, could the variability within the seasonal cycle be explained by variability at the regional level, by atmospheric transport variability for example? The choice of curve fitting routine and is subsequent parameterisation determine what level of variability is being characterised.

In terms of determining whether the inter-annual variability in the growth rate is appropriate, comparison with universally accepted global growth rate variability, such as that derived by Thoning et al. (1989), seems appropriate and this would be a the logical next step in this analysis to address this issue. Determining whether a single flask observation has been influenced by atmospheric transport variability is more difficult to determine. However, continuous observations, where synoptic scale variability can be more readily assessed would circumvent this. This is only possible form 2011 onwards however at HBA (when a continuous Picarro CO_2 measurement system was installed).

Finally, to further test the strength of the relationships between the respective fluxes and the total atmospheric CO_2 seasonal cycle, more data would be required. This is possible with HBA flask record, as one could extend further back from 2000 to the beginning of the record in 1986. This would increase the number of sample points from 15 to 29.

The final question in this analysis would be to ask what could be causing the inter-annual variability in the seasonal fluxes from the terrestrial biosphere and ocean. This is likely to be driven by large scale climatic phenomena, such El Nino (McPhaden et al.,

2006) and the Southern Annular Mode (Lovenduski et al., 2007). However, this is beyond the scope of the analysis presented in this thesis and will instead form the foundation of future work with the CTE2016 model between Ingrid van der Laan-Luijkx and myself.

4.3.2. First year of observations from the Halley O_2 and CO_2 measurement system

The first year of atmospheric $\delta(O_2/N_2)$, CO_2 and APO observations following the successful installation of the measurement system at the Halley Research Station are shown in **Figure 4.10**.

Firstly, synoptic scale variability is observed across all three species. In particular, note the relatively large event at the beginning of the record in February whereby a decrease and subsequent increase in CO_2 is mirrored by an increase and subsequent decrease in both $\delta(O_2/N_2)$ and APO. By using a combination of air mass back trajectory,

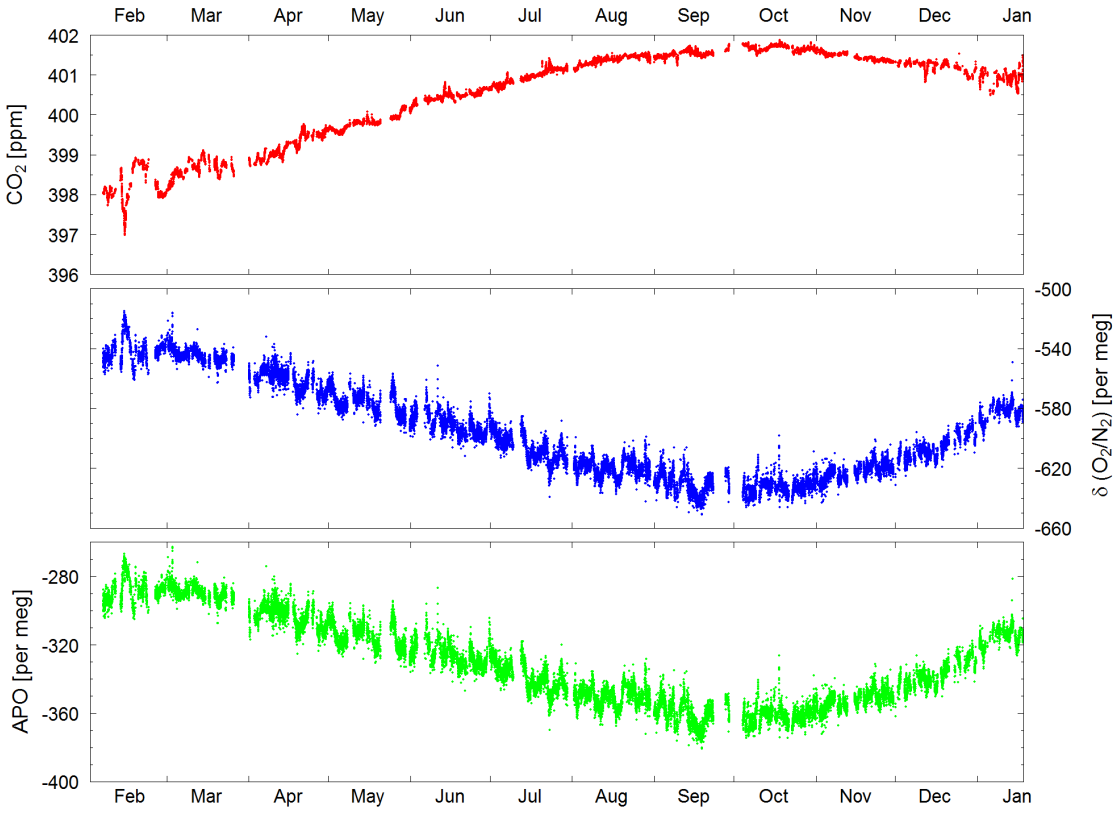

Figure 4.10. The first year of atmospheric CO_2 (red points, top panel), $\delta(O_2/N_2)$ (blue points, middle panel) and APO (green points, bottom panel) observations from the Halley Research Station, Antarctica. Data collection began in February 2016 and stopped in January 2017 due to the unprecedented closure of the station. Gaps in the data in March are due to a calibration malfunction resulting in uncalibrated data and these are therefore not shown. The gaps in September/October were due to power outages.

satellite primary productivity and sea-ice data, this feature could be explained by air deriving from the marine boundary layer over a productive region in the South Atlantic (see Appendix B for further analysis). Unfortunately, synoptic events of this magnitude were rare in the data record and so I was not able address the second objective of this chapter. The event seen occurred in the short summer months (January-February). Continuous CO_2 observation from a separate analyser installed in the CASLab since 2011 show an increase in the magnitude of the synoptic scale events during the summer months. Perhaps if the data record had been extended longer in this analysis (a second summer) more events may have been discovered. Moreover, synoptic scale carbon cycle events in the winter will be difficult to detect because of the large distances between the station and the open ocean due to sea-ice coverage. Any signals, will likely be diluted by atmospheric mixing resulting a small signal seen. Those events seen a rarely more than 2σ of the curve fit, and are close to the measurement uncertainty ± 7 per meg. An analysis of these events will be addressed in later work. However, the reader is referred to the Appendix B for an analysis of the event discussed.

Secondly, it is difficult to reliably interpret the growth rate of each of the species from one year of data since it is concealed somewhat by the signal of the seasonal cycle. However, the increasing trend in the CO_2 mole fraction due to fossil fuel emissions, cement production and land use change is evident in the CO_2 data and represents an approximate increase of 3 ppm yr^{-1}. For $\delta(O_2/N_2)$ and APO a decrease of approximately 20 per meg and 10 per meg, respectively, which agrees with has recently been observed from global SIO flask measurements[11] and is again driven by the above mentioned anthropogenic activities (Keeling and Shertz, 1992).

The CO_2 growth rate observed at HBA is larger than the mean global growth rate observed from the NOAA flask sampling network for the 2006-2016 period (2.24 ± 0.48 ppm yr^{-1})[12]. However, a strong El Niño was recorded throughout 2015 and 2016 (Varotsos et al., 2016), which will act to increase the global CO_2 growth rate due to the response of the terrestrial carbon cycle to globally warmer and drier conditions (Friedlingstein and Prentice, 2010; Jones et al., 2001). The growth rate observed between 2015 and 2016 is the largest on record (Betts et al., 2016), whilst NOAA note high 2015 and 2016 growth

[11] http://scrippso2.ucsd.edu/ accessed

[12] https://www.esrl.noaa.gov/gmd/ccgg/trends/gr.html accessed

rates and comment that this may continue in 2017[13]. The elevated CO_2 growth rate observed at HBA with respect to the previous decade, therefore, supports these predictions.

4.3.3. Seasonal cycles of CO_2, $\delta(O_2/N_2)$ and APO at the Halley Research Station

Figure 4.11 shows the mean seasonal cycles at HBA for CO_2, $\delta(O_2/N_2)$ and APO for 2016. The CO_2 seasonal cycle has an amplitude of 1.71 ± 0.13 ppm with a late winter

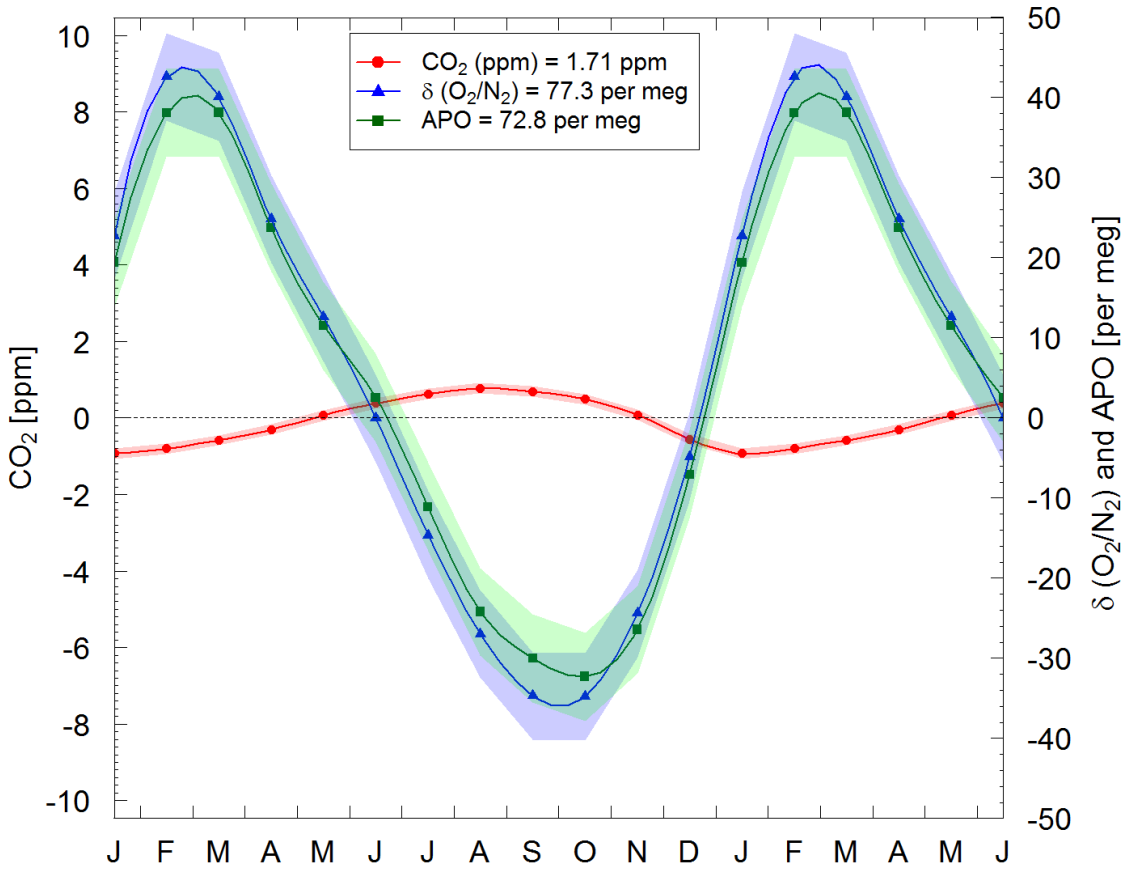

Figure 4.11. The seasonal cycle of atmospheric CO_2 (red points and lines, left y-axis), $\delta(O_2/N_2)$ (blue triangles and lines, right y-axis) and APO (green squares and lines, right y-axis) as determined from the HPspline curve fit (see Section 4.2.5). The peak to trough seasonal amplitude for each species are shown in the key. Y-axes are scaled such that CO_2, $\delta(O_2/N_2)$ and APO are visually comparable on a mole per mole basis. The x-axis represents the first letter of individual months and the first 6 months are repeated to aid visual interpretation of the cycles. Individual points represent the monthly mean values of the curve fit. Lines represent a subsequent spline fit to the monthly data. Shaded error bands represent the 1σ standard deviation of the residuals of the curve fit and so represents closeness of the fit to the measured data, rather than month to month variability as is often shown (it would be inappropriate to show such error bands for one year of data). Error bands shown are as follows: CO_2 = ± 0.13 ppm, $\delta(O_2/N_2)$ = ± 5.4 per meg and APO = ± 5.2 per meg.

[13] http://www.noaa.gov/news/carbon-dioxide-levels-rose-at-record-pace-for-2nd-straight-year

maximum in August and a mid-summer minimum in January. The cycle is much smaller than that found in the northern hemisphere (compare to the mean CO_2 seasonal cycle observed at the Weybourne Atmospheric Observatory (WAO), U.K in Chapter 5 ~ 15 ppm) and this primarily reflects the hemispheric difference in the distribution of the terrestrial biosphere. At extratropical latitudes, the northern hemisphere is dominated by land whereas the southern hemisphere is dominated by ocean. Consequently, the seasonal CO_2 exchange between the atmosphere and terrestrial biosphere, driven by photosynthesis and respiration, in the southern hemisphere is comparatively small to that for the northern hemisphere (Pearman and Hyson, 1986). Moreover, this hemispheric contrast in the magnitude of seasonal terrestrial biosphere fluxes, in combination with interhemispheric mixing, results in the northern hemisphere fluxes being delayed by 6 months such that they are in phase and so reinforce the southern hemisphere terrestrial fluxes (Heimann et al., 1989; Nevison et al., 2008b; Stephens et al., 2013).

Stephens et al. (2013), in their analysis of CO_2 seasonality recorded at Baring Head, New Zealand, decomposed the atmospheric signal into its respective flux components using CarbonTracker/TM3 model output (Peters et al., 2007). Although the total modelled CO_2 output was leading in phase by approximately 1 month than the observations, but comparable in amplitude, it was found that the signal was primarily composed of a northern and southern hemisphere terrestrial influence that were in phase with a maximum in late winter (August-September) and a minimum in autumn (March-April). Whereas the southern hemisphere ocean component lead the terrestrial components by approximately 5 months and was comparable in magnitude. In Section 4.3.1, I discuss the competing source influences on the HBA CO_2 seasonal cycle further using the most recent CarbonTracker Europe/TM5 output (Krol et al., 2005; Peters et al., 2010; van der Laan-Luijkx et al., 2017)

The $\delta(O_2/N_2)$ and APO seasonal cycles have an amplitude of 77.3 ± 5.4 and 72.8 ± 5.2 per meg, respectively, with a late summer maximum in February-March and an early spring minimum in September-October. Whilst the seasonal cycle of $\delta(O_2/N_2)$ at HBA will be influenced by both seasonal atmosphere-terrestrial biosphere and atmosphere-ocean O_2 exchange, the APO seasonal cycle will only be influenced by ocean exchange (Stephens et al., 1998). The similarity between the $\delta(O_2/N_2)$ and APO cycles demonstrate that the majority of the $\delta(O_2/N_2)$ seasonal cycle at HBA is driven by ocean processes (91.3%) as was first confirmed by $\delta(O_2/N_2)$ at high latitude southern hemisphere flask sampling stations in the 1990s (Bender et al., 1996; Keeling et al., 1993;

Keeling and Shertz, 1992). This contrasts greatly with that found for northern hemisphere stations. For example, in Chapter 5 of this thesis I demonstrate that the seasonal cycle of $\delta(O_2/N_2)$ observed WAO has only an approximately 40% influence from ocean processes. Consequently, in this chapter, the remainder of the discussion will focus on the atmospheric CO_2 and APO seasonal cycles at HBA and across the Southern Ocean.

Before discussing the HBA and Southern Ocean APO seasonality in more detail, I will discuss the likelihood that the APO seasonal cycle determined at HBA for 2016 is representative of the climatological mean. To do this I will examine NOAA CO_2 flask data for HBA that have been collected at the station since 1986 and compare to my continuous CO_2 data for 2016. For convenience, I refer to these two datasets in the following section as the NOAA flask data and the UEA continuous data.

4.3.4. Comparison of flask (2000-2015) and continuous (2016) CO_2 measurements

4.3.4.1. The CO_2 seasonal cycle from flask measurements at Halley 2000-2015

Figure 4.12 shows the seasonal cycle of CO_2 at HBA from the UEA continuous data compared to the mean seasonal cycle derived from NOAA flask data for the 2000-2015 period. The NOAA flask data were treated with the same curve fitting routine (HPspline) and curve fitting parameters (the sum of a 3rd order polynomial and four harmonics) as the UEA continuous data. This is to ensure direct comparability and to minimise seasonal variability on the climatological mean seasonal cycle. The difference in the shape, phase and amplitude between the two seasonal cycles is distinct and significant as there is very little overlap between the error bands. The 2000-2015 mean NOAA flask data CO_2 seasonal cycle is 33% smaller in amplitude and 1-2 months lagging in phase compared to the UEA continuous data.

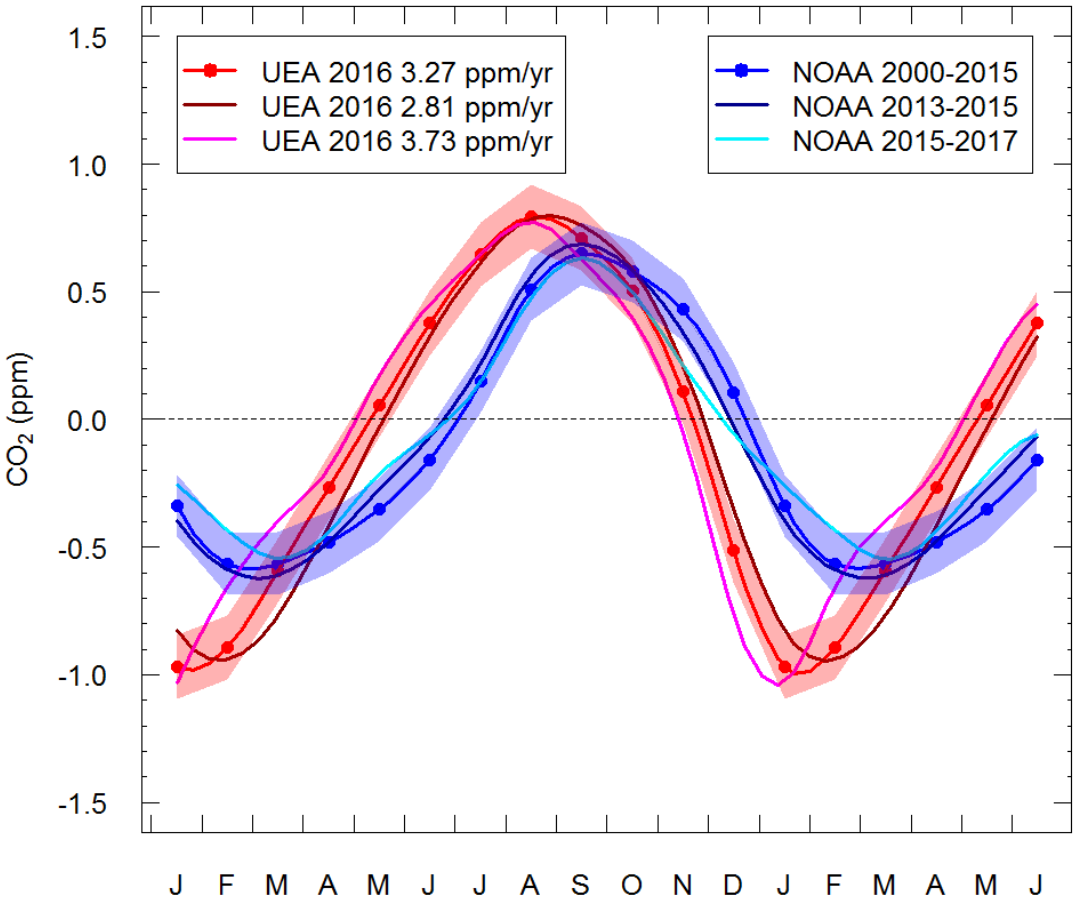

Figure 4.12. Seasonal cycle of CO_2 at HBA observed from the measurements presented in this thesis (red points and lines labelled UEA) compared to the mean CO_2 seasonal cycle observed at HBA from NOAA flask observations collected twice weekly between 2000 and 2015 (blue points and line). The x-axis represents the first letter of individual months and the first 6 months are repeated to aid visual interpretation of the cycles. Individual points represent the monthly mean values of the curve fit. Lines represent a subsequent spline fit to the monthly data. Shaded error bands represent the 1σ standard deviation of the residuals of the curve fit (UEA continuous = ± 0.13 ppm; NOAA flask = ± 0.12 ppm) and therefore represent the closeness of the fit to the measured data, rather than month to month variability as is often shown. Also shown are the seasonal cycles derived from the measurements when different growth rates are applied when recreating the data for the curve fitting routine (See Section 4.2.5.2). The original growth rate (3.27 ppm yr^{-1}) was arrived at by subtracting the measured data in 2016 from the flask data observed in 2015. The additional growth rates represent ± 1σ of that value: 2.81 ppm yr^{-1} (maroon line) and 3.73 ppm yr^{-1} (magenta line). The dark blue line represents the mean CO_2 seasonal cycle derived from the flask observations from the most recent three years of flask data (2015-2017). The turquoise line represents the seasonal cycle derived from the curve fit to the data when the 2015 flask observations are repeated forward with the same assumed growth rate as was made for the original continuous observations (3.21 ppm yr^{-1}).

4.3.4.2. Investigating bias in the derivation of the mean CO_2 seasonal cycle from continuous data

As highlighted in Section 4.2.5.2, the HBA UEA continuous CO_2 seasonal cycle is likely to be sensitive to the assumed growth rate applied to the replicated data. The results of the sensitivity analysis are depicted in **Figure 4.12**. The higher growth rate (pink line) results in a marginally larger amplitude and shifts the phase earlier by approximately 1 week. Whereas the lower growth rate (dark red line) results in a marginally smaller amplitude and shifts the phase later by approximately 1 week. Both additional curve fits lie within the error bands of the original curve fit, for the most part, and neither significantly reconcile the 2016 seasonal cycle with the 2000-2015 mean from the flasks. Although the slightly lower growth rate shifts both the phase and amplitude in the right direction, the magnitude of the growth rate required to reconcile the cycles completely would be unrealistically low based on recent global growth rate trends (Le Quéré et al., 2016).

A further of source bias could be the choice of the time period used. Since the curve fitting routine is relatively stiff (Pickers and Manning, 2015), trends and variability in the seasonal cycle over the time period may not be apparent. This is particularly pertinent given the observed phase shift and amplitude increase observed in the CO_2 seasonal cycle observed in the northern hemisphere over recent decades (Graven et al., 2013; Piao et al., 2008). Given that the southern hemisphere CO_2 seasonal cycle has a significant northern hemisphere component (Stephens et al., 2013), and that climatic trends may have impacted the southern terrestrial biosphere in the same way they have in the northern hemisphere, it is not unreasonable to consider that the seasonal cycle at HBA may have changed over the 2000-2015 period and that the climatological mean cycle won't reflect this. The seasonal cycle determined by the UEA continuous data for 2016 may not then appear to be anomalous.

To investigate this, I firstly applied the curve fitting routine to the most recent three years of flask data (2012-2015; dark blue line **Figure 4.12**). Secondly, I created a three year data set for the 2015-2017 period by replicating 2015 forwards in time, applying the same growth rate assumptions I applied to the continuous data so as to be directly comparable (turquoise line, **Figure 4.12**). Neither of the new curve fit seasonal cycles are significantly different from the climatological mean cycle and therefore still suggest that 2016 is indeed anomalous.

The final source of bias in this comparison comes not from the extraction of the seasonal cycle in the 2016 UEA continuous data, but from the NOAA flask data. The HPspline curve fitting routine was chosen to extract the seasonal cycle of the NOAA flask data in order to be consistent and comparable with the method applied to the continuous data. However, in this case, it may be unreasonable to make such a choice. Southern hemisphere CO_2 seasonal cycles are incredibly variable from year to year due to the impact of the multiple processes acting on the seasonal cycle (e.g. the interplay between ocean fluxes, terrestrial fluxes from both hemispheres and inter-hemispheric mixing) (Stephens et al., 2013). This variability will not be captured by the inflexibility of the HPspline curve fitting routine. A more appropriate curve fitting routine would therefore be the more flexible CCGCRV routine (Pickers and Manning, 2015; Thoning et al., 1989)

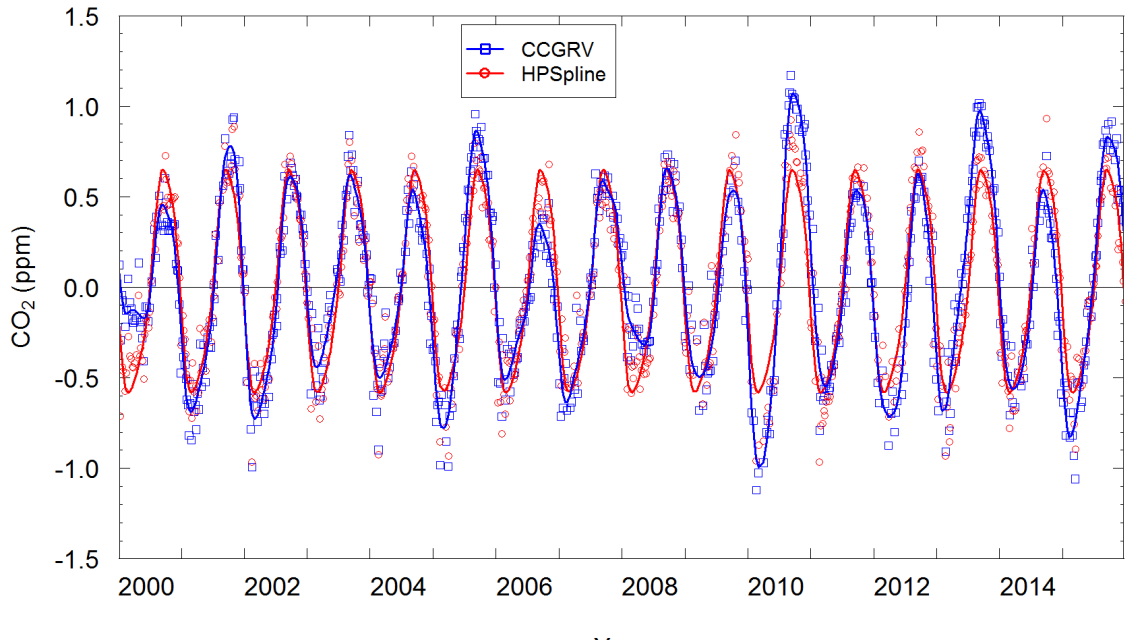

Figure 4.13. De-trended NOAA flask observations (squares and circles) collected at HBA between 2000 and 2015, as calculated by the two curve fitting routines: CCGRV (blue squares and lines) and HPspline (red circles and lines). Lines represent the de-trended curve fit to the data. The x-axis represents the year the flask sample was collected (typically twice per week).

After some experimentation, I decided to apply a short term cut off value of 150 and a long term cut off value 1500 days within the CCGCRV routine (Section 4.2.5). This allows enough variability in the seasonal cycle without it being too affected by what might be outliers. The long term cut off value was chosen as the ideal value found by Pickers and Manning (2015) on artificial data and represents a long term inter-annual smoothing of ~ 4 years. However, when examining different short and long term cut off values it is

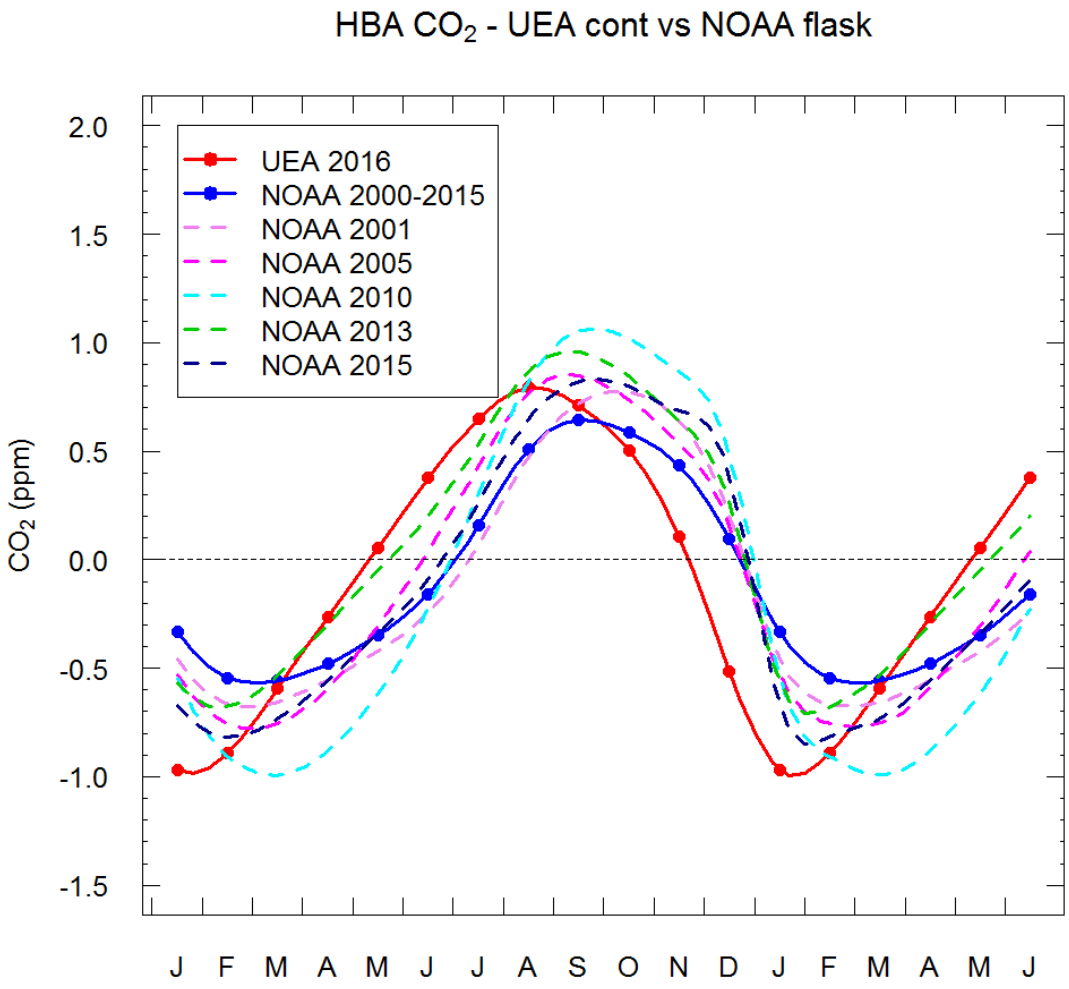

Figure 4.14. Seasonal cycle of CO_2 at HBA observed from the measurements presented in this thesis (red points and lines labelled UEA) compared to the mean CO_2 seasonal cycle observed at HBA from NOAA flask observations collected twice weekly between 2000 and 2015 (blue points and line) but derived from the CCGRV curve fitting routine, rather than HPspline (as in **Figure 4.12**). The x-axis represents the first letter of individual months and the first 6 months are repeated to aid visual interpretation of the cycles. Individual points represent the monthly mean values of the curve fit. Lines represent a subsequent spline fit to the monthly data. Individual years that were most similar to the UEA 2016 continuous year are displayed by dashed lines and are shown in the key.

difficult to determine how much variability should be due to inter-annual variability in the seasonal cycle, its phase, shape and amplitude for example, and how much should be due to inter-annual variability in the growth rate. Ultimately, these features of an atmospheric time series are inextricably linked and the investigator can choose how much variability is assigned to one, potentially at the expense of the other. This will inevitably introduce a bias in the analysis that is often overlooked by many users of curve fitting routines.

Figure 4.13 shows the individually de-trended NOAA flask data and the resulting curve fit using the HPspline and CCGCRV routines. CCGCRV captures much more of the inter-annual variability in the shape, phase and amplitude of the seasonal cycle than does HPspline. The 1σ standard deviation of the CCGCRV curve fit are ± 0.11 ppm compared to ± 0.12 ppm for HPspline. I have therefore compared the UEA continuous seasonal cycle observed in 2016 to the seasonal cycle of the NOAA flask data using the CCGCRV output (**Figure 4.14**). Interestingly, the mean seasonal cycle from CCGCRV is exactly the same as that for HPspline (not directly shown, but compare the blue lines and points in **Figure 4.12** and in **Figure 4.14**). This agreement gives confidence in both of the routines at determining a climatological mean seasonal cycle over many years. Furthermore, I have picked out the five most comparable NOAA flask sample years to the UEA continuous 2016 year (**Figure 4.14**). From this analysis, the amplitude observed in the continuous data in 2016 is not entirely unprecedented. Moreover, there is a large amount of variability in the summer minimum, autumn zero crossing and winter maximum that cannot conclusively rule out that the UEA continuous 2016 year is unique. On the other hand, the spring zero crossing is very clearly distinct from the other years highlighted in the NOAA data and therefore suggests that the UEA 2016 year is unique in its earlier phasing.

4.3.4.3. Conclusion

This comparison of NOAA flask measurements of the CO_2 seasonal cycle for the 2000-2015 period and the UEA continuous CO_2 data for 2016 have shown: (1) In terms of the seasonal peak to peak amplitude and the autumn zero crossing day, 2016 is comparable to other years in the 2000-2015 period, yet it is still not a typical year in comparison to the mean. (2) The spring zero crossing day does appear to be anomalous. There could be two possible reasons for the anomalous spring zero crossing observed in the 2016 seasonal cycle. Firstly, January (2017) and February (2016) are the weakest months in terms of data coverage from the measurement system, due to decommissioning and installation, respectively. Secondly, 2015 and 2016 observed a moderate to strong El Niño event (Betts et al., 2016; Varotsos et al., 2016). It is likely that this impacted on the seasonal cycle of CO_2 observed at HBA. This may also explain the discrepancy between

the mean seasonal cycle observed by the NOAA flask observations for 2000-2015 and the continuous 2016 seasonal cycle.

To investigate this further, one could extend the NOAA flask record back to include all observations since 1986. This would then include the large El Niño event observed in 1998. One could then ascertain the influence this had on the seasonal cycle of CO_2 observed at HBA in that year and compare it the one observed here. This will be addressed in follow on work to this thesis.

Moreover, as discussed and demonstrated, both the choice of curve fitting routine and the selection of short and long term cut off values will impact the derivation of a seasonal cycle from atmospheric data. To further confirm the above findings, a sensitivity analysis would be required. This would involve using different curve fitting routines and the use of a range of values for the short and long term cut off values described above.

The importance of this approach when drawing conclusions from atmospheric data, such as that proposed here, has been underlined by Pickers and Manning (2015).

4.3.5. Atmospheric Potential Oxygen in the Southern Ocean

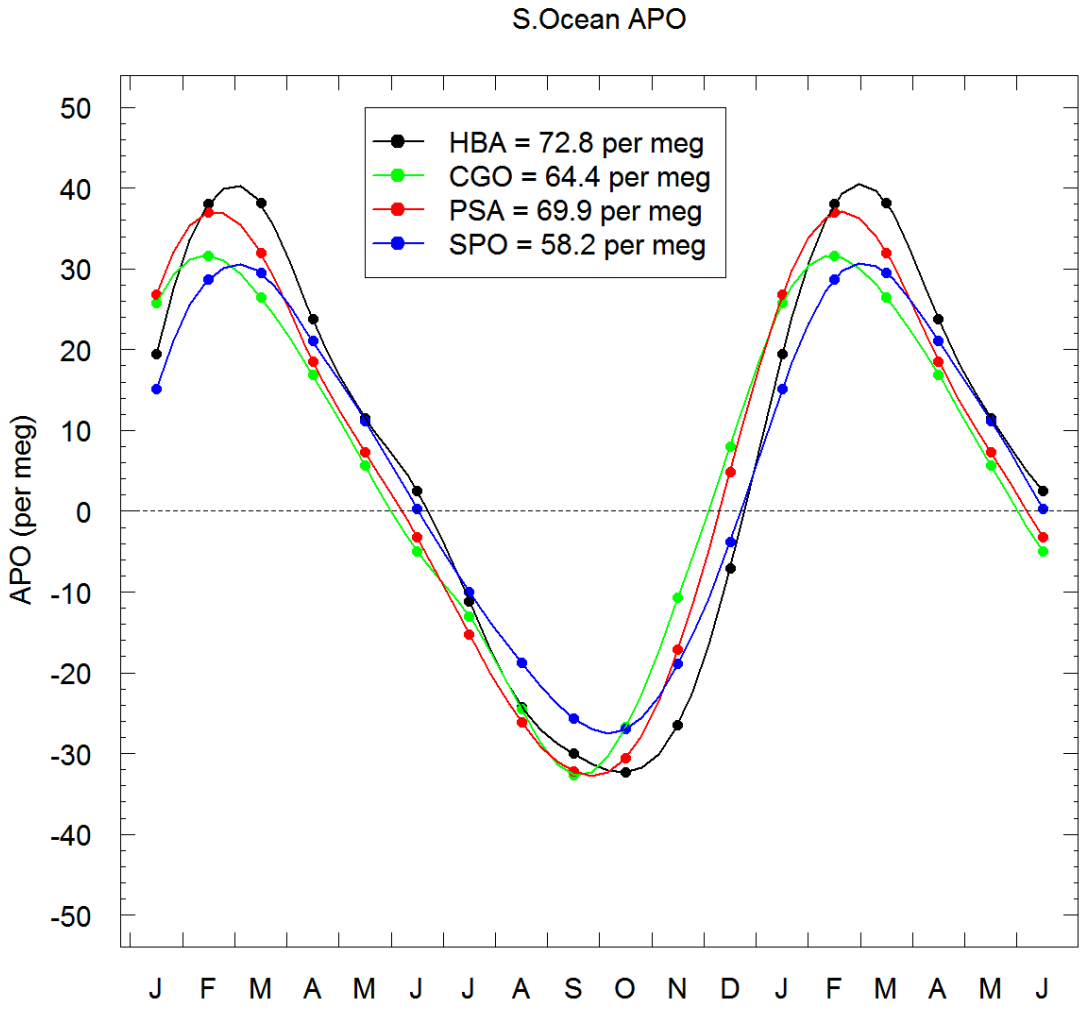

Figure 4.15. The seasonal cycle of APO observed at HBA during 2016 from the measurement system presented in this thesis (black points and lines) compared to the mean climatological seasonal cycle of APO determined from flask observations, collected at approximately weekly intervals over the 2000-2015 period, from three other Southern Ocean APO monitoring stations that are a part of the SIO flask sampling network: CGO (green points and lines), PSA (red points and lines) and SPO (blue points and lines). The x-axis represents the first letter of individual months and the first 6 months are repeated to aid visual interpretation of the cycles. Individual points represent the monthly mean values of the curve fit. Lines represent a subsequent spline fit to the monthly data. Again, to aid visual interpretation error bands are shown in the subsequent **Figure 4.17**.

In this section, I take the seasonal cycle of APO determined at HBA for 2016 and compare it to the mean climatological seasonal cycle from three other Southern Ocean

APO monitoring stations from SIO O_2 flask sampling network: Cape Grim Observatory (CGO), Palmer Station (PSA) and South Pole Observatory (SPO) (Section 4.2.6) (**Figure 4.15**). A curve consisting of a 3rd order polynomial plus the sum of four harmonics were fit to data at each station collected between 2000-2015 and the seasonal cycle extracted (Section 4.2.5).

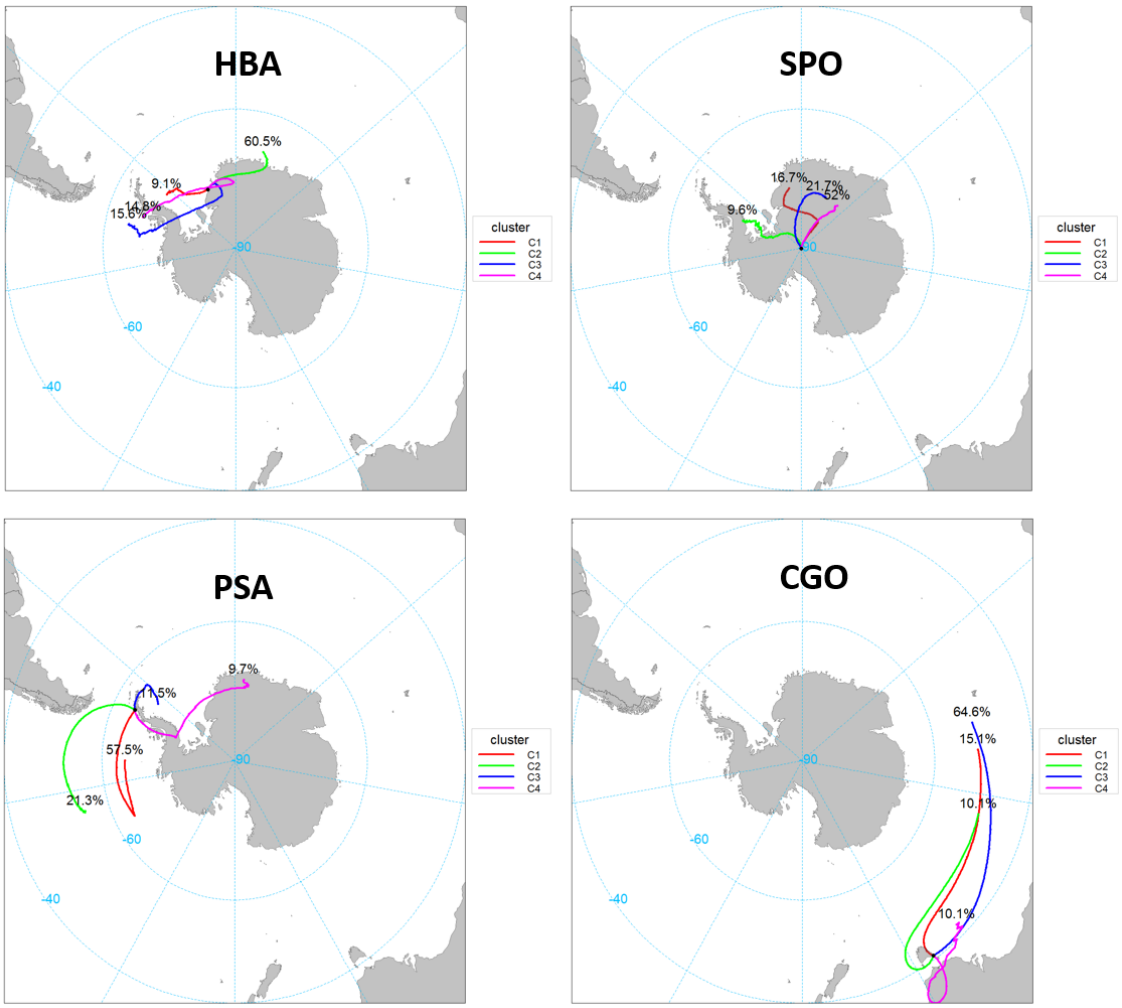

Figure 4.16. Cluster analysis of 7-day backwards trajectories starting every 3 hours for the year of 2016 for each of the stations discussed in this analysis (HBA, PSA, SPO and CGO). Trajectories were computed using Hysplit Model (Section 4.2.2). The cluster analysis was performed using the openair function trajClust (Section 4.2.2). The percentage of trajectories that were associated with each cluster (depicted by the coloured lines) are shown next to each to the respective trajectory cluster lines.

Additionally, I have performed a cluster analysis of 7 day back trajectories for each station as outlined in Section 4.2.2. The overall contribution of each trajectory cluster for this particular year (2016) is displayed as a percentage and therefore gives an indication of the typical air mass history for air sampled at each station. In doing this, I

am making the assumption that year 2016 is representative of the typical atmospheric circulation experienced at each station for the period 2000-2015. Although this will not strictly be true, year to year variations in atmospheric circulation won't differ too greatly from the typical synoptic climatology for the region (Simmonds et al., 2003). The reasoning behind only choosing the year 2016 are two-fold: Firstly, I am assuming the seasonal cycle observed at HBA in 2016 is representative of the climatological mean for the period 2000-2015 in comparison to other stations. Secondly, the computational time required to run multiple back trajectories, over a 15 year period, at multiple stations and perform a cluster analysis was deemed too great for the scope of the analysis. The results of the cluster analysis are shown in **Figure 4.16**.

When interpreting the seasonality of APO at HBA in the context of other Southern Ocean stations it is important to firstly consider the main assumption, before ascribing differences wholly due to heterogeneity in spatial and temporal carbon cycle features. I am assuming that the seasonal cycle determined from one year of data in 2016 at HBA is, as already mentioned, representative of the climatological mean seasonal cycle. The analysis of the CO_2 seasonal cycle at HBA in Section 4.3.4 clearly shows that this is unlikely to be the case and that 2016 may be unduly influenced by the large El Niño event (Betts et al., 2016; Varotsos et al., 2016) . The only possible way to circumvent this bias is to collect multiple years of data and redo the following analysis. Clearly, this is not possible within the time frame of this Ph.D. research.

4.3.6. Seasonality of APO at Halley and other Southern Ocean stations

The seasonal cycle of APO for each station are shown again in **Figure 4.17** but now with each in direct comparison with HBA. All four stations broadly reflect the seasonality of carbon cycle processes within the Southern Ocean (Bender et al., 1996; Keeling et al., 1993; Keeling and Shertz, 1992). As insolation increases in the early spring (October), the mixed layer depth shoals as a thermocline develops between the surface and deeper waters. Phytoplankton within the mixed layer are therefore brought closer to the surface where the increasing insolation levels stimulates photosynthesis leading to the production of O_2 and the consumption of CO_2 within the euphotic zone. The surface ocean eventually becomes supersaturated with O_2 (November-December), and that, in combination with the decreased solubility due to increased water temperature and the

shoaling of the mixed layer, drives a flux of O_2 from the ocean to the atmosphere. The

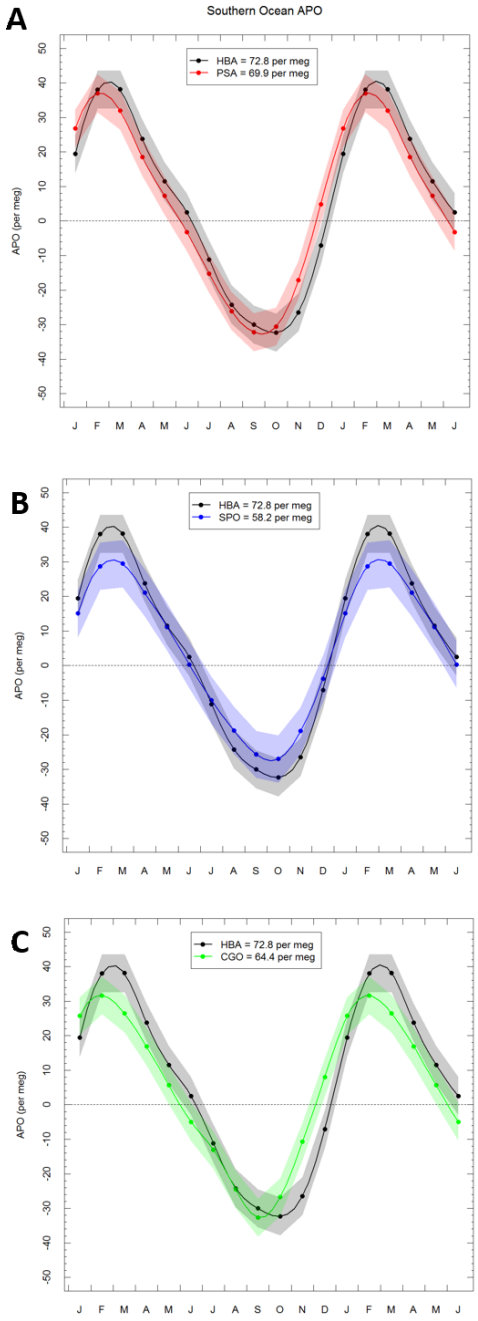

Figure 4.17. The seasonal cycle of APO observed at HBA (black points and lines) compared to other Southern Ocean APO monitoring stations: (A) PSA (red points and lines), (B) SPO (blue lines and lines) and CGO (green points and lines. The peak to peak amplitude of the seasonal cycles are displayed in the respective plot keys. The x-axis represents the first letter of individual months and the first 6 months are repeated to aid visual interpretation of the cycles. Individual points represent the monthly mean values of the curve fit. Lines represent a subsequent spline fit to the monthly data. Shaded error bands represent the 1σ standard deviation of the residuals of the curve fit and therefore represent the closeness of the fit to the measured data, rather than month to month variability as is often shown.

fraction of organic matter produced that is not immediately respired in the surface layer, sinks beneath the mixed layer, and becomes respired at depth, leading to O_2 under saturation. As insolation levels decrease and surface waters become cooler, the seasonal thermocline breaks down, the mixed layer deepens and these O_2 under saturated waters are brought to the surface driving a net flux of O_2 from the atmosphere to the ocean (June-July). The flux then peaks and begins to reverse in early spring as the cycle begins again.

All stations broadly show a similar shape and pattern of the seasonal cycle, there are, however, subtle differences between the stations in terms of their phase and amplitude, displayed in **Figure 4.15**, **Figure 4.17** and **Figure 4.19** which I will now discuss.

4.3.6.1. Amplitude

SPO has the smallest amplitude of all the stations considered (58 ± 13 per meg). This likely reflects the stations proximity to the above mentioned processes that control the seasonal cycle in APO. CGO, HBA and PSA are all coastal locations that sample air within the marine boundary layer. SPO, however, lies approximately 1500 km from the coast, an altitude of ~2800m above sea level. As such, air sampled at this altitude will be above the marine boundary layer and surface fluxes will be diluted by vertical mixing within the free troposphere. The amplitude of the seasonal cycle will therefore be reduced compared to that for surface stations (Bent, 2014).

HBA, on the other hand, exhibits the largest amplitude (73 ± 11 per meg) and therefore suggest that the site is either influenced by large local seasonal oceanic O_2 fluxes, from the Weddell Sea for example, or similarly, samples air deriving from a larger region that exhibits large seasonal fluxes, such as the South Atlantic sector of the Southern Ocean. **Figure 4.18** exhibits the areas of upwelling (Morrison, 2015) and of export production (Nevison et al., 2012) in the Southern Ocean and shows the South Atlantic sector to be particularly pervasive in both processes, compared to the other areas of the Southern Ocean and thereby supporting the above assertion. Furthermore, in terms of the amplitude of the seasonal cycle, HBA is most similar to PSA (magnitude = 70 ± 11 per meg). This likely reflects a similar latitudinal sampling location, whereby both stations

sample air masses deriving from the Southern Ocean 60-75˚S latitude band, a substantial region of both productivity and upwelling (**Figure 4.18**).

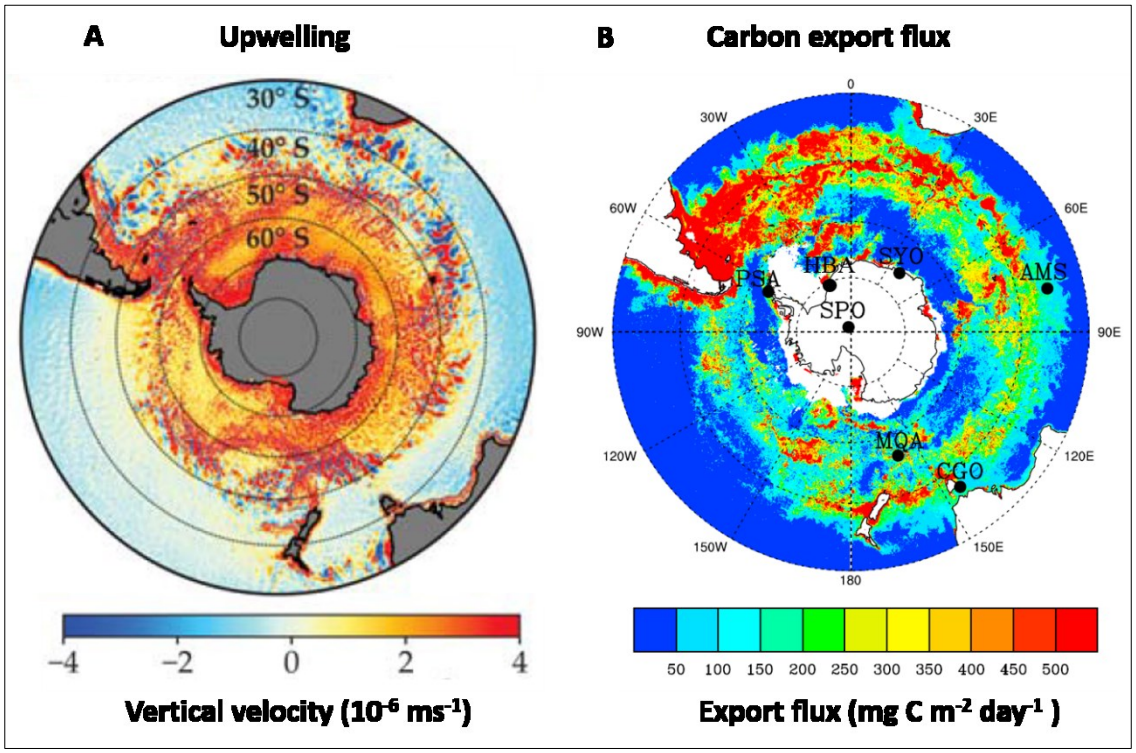

Figure 4.18. (A) Upwelling within the Southern Ocean as depicted by the vertical velocity of water (key; 10^{-6} ms^{-1}). The plot is a product of a model simulation of pre-industrial upwelling (Griffies et al., 2015)and has been adapted from (Morrison, 2015). (B) Carbon export flux within the Southern Ocean (mg C m^{-2} day^{-1}). Export production was calculated as a function Net Primary Productivity, which was subsequently derived from chlorophyll-a concentrations from satellite ocean colour data (for details on the data transformations see Nevison et al. (2012; Sallee et al., 2012), from which this plot was adapted from). Locations of Southern Ocean monitoring stations discussed in this analysis and others introduced in **Figure 4.1** are also shown.

However, all of the amplitudes stated for each station have a relatively large uncertainty (approximately ± 11 per meg). As such, only HBA and SPO could be considered as significantly different from each other. This would therefore imply that the carbon cycle processes captured in the APO seasonal cycles are representative of basin scale processes, rather than that at the regional level. This uncertainty is derived from the quality of the curve fit to the data and is of a similar magnitude to the measurement uncertainty on the data. Improvements in the measurement uncertainty and in the quality

of the curve it would be required to ascertain whether the regional influences discussed above are significant.

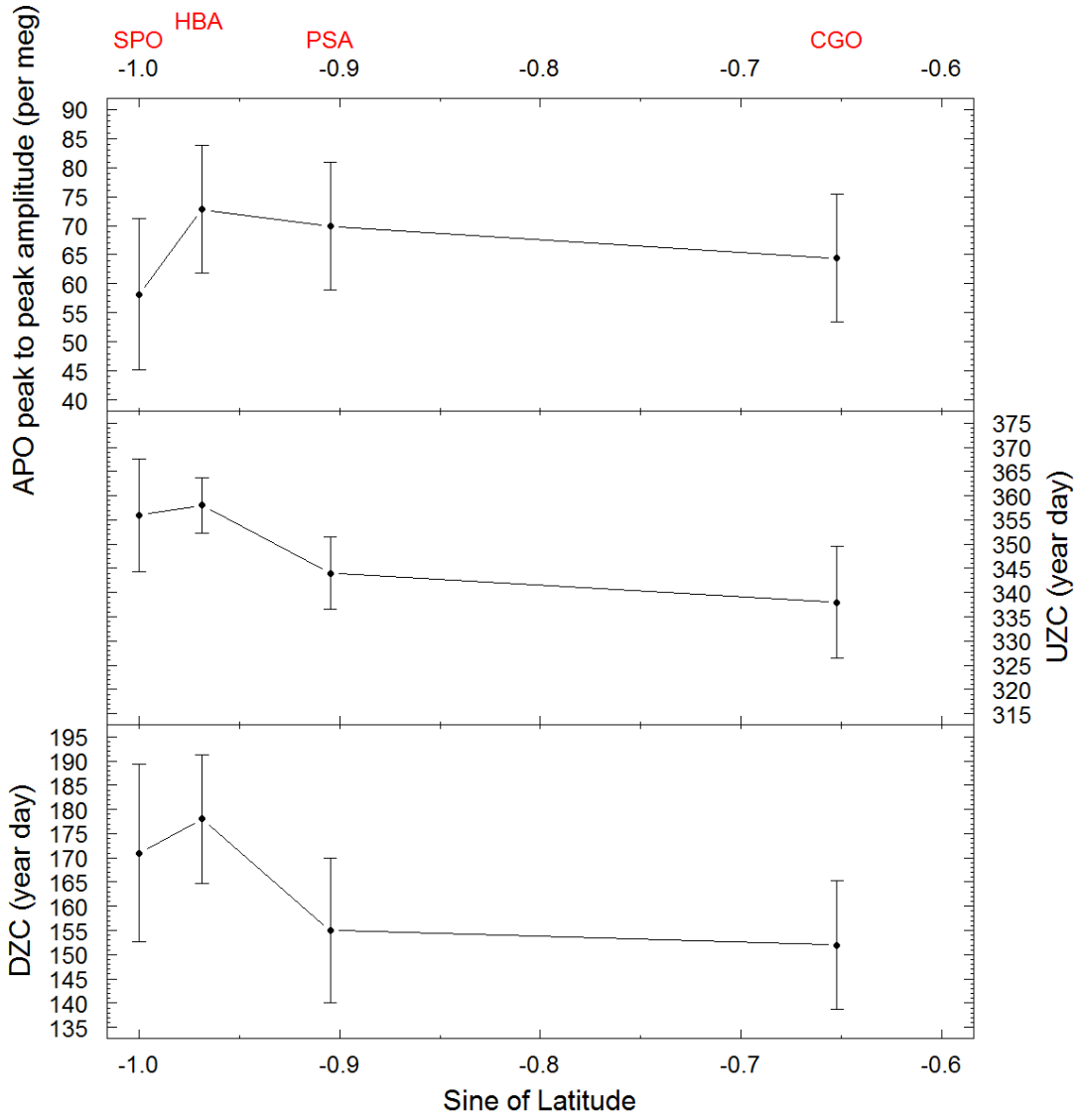

Figure 4.19. Seasonal cycle metrics of APO observed at Southern Ocean stations. Top panel: peak to peak amplitude (per meg) of the cycle. Middle panel: Timing of the upwards zero crossing (UZC). Bottom panel: Timing of the downward zero crossing (as above). The x axis represents the sine of the latitude.

Finally, by excluding SPO, there is a subtle yet clear latitudinal gradient in the amplitude of the APO seasonal cycle as one moves north from HBA (75˚S) towards CGO (40˚S) of -2.4 per meg/10˚ latitude (**Figure 4.19**). This could imply that the magnitude of seasonal O_2 exchange is largest at the southern boundary of the Southern Ocean, where it meets Antarctica, and that the magnitude of the seasonal fluxes decreases at lower latitudes in the Southern Ocean. However, each station will likely be subject to local influences that then biases this interpretation. Each station cannot be representative of the entire latitude band it sits within in the Southern Ocean. Moreover, the uncertainty in the

amplitudes, described above, indicate that the magnitude of the trend seen is below the measurement detection limits. Again, improvements in the measurement uncertainty and the quality of the curve fit to the data would be needed to ascertain whether this trend is significant. Interestingly, unpublished data from a continuous atmospheric O_2 and CO_2 measurement system on-board the Laurence M. Gould Research ship, which continuously sails between South America and PSA, displays a seasonal amplitude gradient of ~ -20 per meg /10˚ latitude (B. Stephens, *personal communication*). The latitude range that this was measured over (55-65˚S) was much smaller than that considered here however. The decrease in the amplitude with decreasing latitude could be entirely down to this latitude band. Taking this 20 per meg decrease over the latitude band considered in this analysis (40-75˚S) results in a decrease of 5.7 per meg/10˚ latitude, and therefore suggests that the analysis presented here underestimates the gradient.

4.3.6.2. Phase

Whilst the seasonal cycle of APO at HBA is most similar to PSA in terms of its amplitude, interestingly, this is not the case for the phase. The DZC for HBA is on day 178 ± 13 days, whilst for PSA it is on day 155 ± 15 days. The UZC for HBA is on day 358 ± 6 days, whilst for PSA the UZC is on day 344 ± 7 days. The UZC between the two stations could therefore be significantly different. Moreover, there could be a significant difference between the UZC of HBA and CGO, with the CGO UZC occurring on day 338 ± 8 days.

HBA is most similar to the SPO with respect to its phasing (**Figure 4.19**) (SPO UZC = 356 ± 12 days; DZC = 171 ± 18 days), although the phase of the SPO seasonal cycle is more variable than that of all stations considered in this study. The spring time peak occurs at the same time (within a week) at both stations in late February. Moreover, the upward and downward zero crossing for each station occur within a few days of each other, as does the trough. In interpreting this, it is important to consider the typical air mass origins shown in **Figure 4.16**. Interestingly, SPO samples similar air masses to HBA, within the longitudinal sector 50˚W to 50˚E. Therefore, whilst the magnitude of the fluxes that drive the amplitude of the seasonal cycle are attenuated somewhat at SPO compared to HBA due to vertical mixing, the phasing appears to be very similar and could reflect a similar air mass history. With that, it can be said the SPO could represent the surface fluxes observed at HBA that are vertically mixed over a height of 2800m. The difference between the seasonal amplitude of APO observed at HBA and SPO could

therefore represent an important test for a particular ATMs ability to correctly represent the amount of vertical mixing observed in the atmosphere. This conclusion is, however, influenced by the choice of air mass back trajectory analysis and in the short time frame

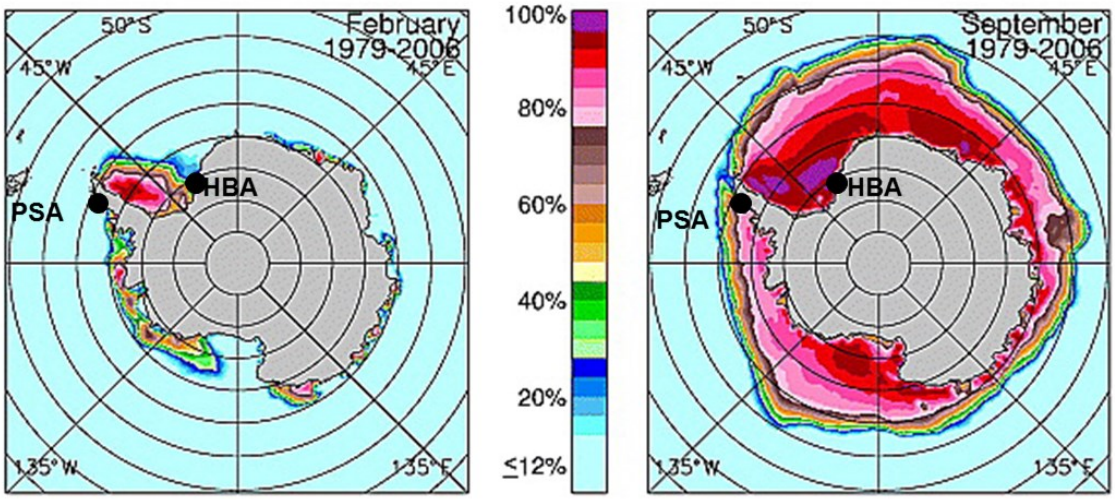

Figure 4.20. 28 year average minimum (February; left plot) and maximum (September; right plot) sea ice extent (expressed as a percentage) in the Southern Ocean. The location of HBA and PSA are also shown by the black points. Adapted from (Cavalieri and Parkinson, 2008).

that the cluster analysis of trajectories were performed (1 year). To confirm whether the SPO and HBA do have similar air mass histories, there are several sensitivity analyses that would need to be done. Firstly, a different choice of wind fields could be chosen, and secondly, a different transport or dispersion model could be used, the STILT (Lin et al., 2003) or NAME (Fleming et al., 2012) models for example. Finally, the cluster analysis would need to be performed on multiple years of back trajectories to have a more reliable sample size.

The difference in the phasing observed between HBA and PSA is on the order of 2 to 3 weeks (**Figure 4.19**). The timing of the increase and decrease cannot be due to the latitudinal difference between either the location of the station and the location history of air masses sampled because (1). There is no significant difference in insolation levels (or day length) received at different latitudes south of 66.5˚S throughout the course of a year and (2). Despite the ~25˚ latitude difference between PSA and CGO, the phasing of their seasonal cycles are within days of one another.

Instead, I propose that the difference in phasing at HBA (and subsequently SPO, see above) and both PSA and CGO is due to a combination of air mass history and sea-

ice coverage. The climatology of Antarctic sea ice concentration determined over the 1979-2006 period is shown in **Figure 4.20**. HBA samples air deriving from the South Atlantic and the Weddell Sea (**Figure 4.16**) between 60˚S and 80˚S, which for the majority of the year, is covered in sea ice. In contrast, PSA samples air that derives from the South Pacific between 55˚S and 65˚, which is almost ice free year around, except for a few pockets close to the Antarctic coastline in winter (**Figure 4.20**). CGO, on the other hand, samples air from ~50˚S in the Southern Indian Ocean sector. It is not inconceivable therefore, that the delay in phasing of 2 to 3 weeks observed at HBA (and SPO) compared to PSA (and CGO) is therefore due to the presence of sea-ice over areas of the ocean that air masses that arrive at HBA likely equilibrate with. A recent study by Rutgers van der Loeff et al., (2014) based on radon-222 profiles estimated that air-sea gas exchange is reduced by at least an order of magnitude in areas covered by sea ice compared to open water and so this could be a plausible explanation for the phasing difference seen.

However, these conclusions could again be biased by both the choice of curve fitting routine, as discussed in previously, or by the derivation of a station's air mass history as discussed above.

4.3.6.3. Evaluating ocean models with Southern Ocean APO observations

In this section, I will evaluate the skill of two ocean circulation plus biogeochemistry models (OCBMs) introduced in Section 4.2.7.2 (referred to here as MOM4 and CESM), coupled to an atmospheric transport model (TM3), at recreating the observed seasonal cycle in APO at HBA and at the other Southern Ocean stations discussed thus far. In doing this, I will assess whether HBA APO observations highlight deficiencies or strengths in OCBMs that may otherwise be overlooked with fewer stations to compare against.

Before discussing the results of this analysis it is important to firstly discuss the major caveat in a modelled APO seasonal cycle. Due to vertical mixing uncertainties in the transport model, surface fluxes may be either mixed vertically too vigorously, or, conversely, not vertically mixed enough, essentially trapping the fluxes near the surface. Consequently, when fluxes are sampled at a particular station location and a seasonal cycle is determined and compared to the observed, then a false positive may occur. That is, if the modelled ocean fluxes are in reality too small, yet vertical mixing within the transport model is too weak, then the modelled seasonal cycle will appear to be correct with respect to the observations. Conversely, if modelled ocean fluxes are too large, but

vertical mixing in the transport model is overly vigorous, then the seasonal cycle may again appear correct (Naegler et al., 2007). This makes it difficult to assess the quality of one OCBM using only one ATM across different stations because, in reality, the amount of vertical mixing in the atmosphere at different areas of the globe will be different. However, considering only one station, with one transport model, but two OCBMs, does allow an assessment of the OCBM, since the ocean fluxes will be equally biased by the level of vertical mixing.

4.3.6.3.1. Model-observation comparison

Figure 4.21 depicts how each model performs with respect to the observed APO seasonal cycle at HBA. MOM4+TM3 underestimates the late summer (February-March) peak by ~14 per meg, whereas it overestimates the early spring (September-October) minimum by ~ 5 per meg. The modelled cycle is broadly in phase with the observed, except at the UZC in early summer (November-December) where it leads the observations by ~3 weeks. Conversely, the CESM+TM3 cycle is consistently leading the observations by ~ 3 weeks. The summer peak (February) is only slightly overestimated (~3 per meg) whilst the winter minimum (September) overestimation is marginally more substantial (~8 per meg).

Also shown in **Figure 4.21** are the individual contributions to the APO seasonal cycle from the respective fluxes. Before interpreting this further it is important to note two points: firstly, the sign of the ocean N_2 cycle is misleading. The seasonality of ocean N_2 is approximated by the seasonal heat flux (Equation (4.7)). However, positive fluxes (i.e. from ocean to atmosphere) would act to dampen the atmospheric $\delta(O_2/N_2)$ ratio (and hence APO) seasonal cycle. In summer therefore, when heat fluxes and by extension N_2 fluxes from the ocean are positive, then the impact on the APO seasonal cycle will be negative.

Secondly, in this simulation, fossil fuel CO_2 ($ffCO_2$) is not prescribed any seasonality (unlike the CTE2016 simulation in Section 4.2.7.1) and therefore has no contribution to the modelled APO seasonal cycle. Given the small magnitude of the seasonality of fossil fuel emissions in the southern hemisphere (~0.4 ppm – see CTE2016 results in Section 4.3.1), the impact on the APO seasonal cycle would be negligible (~0.6 per meg amplitude) which is similar to that found by Nevison et al. (2008b).

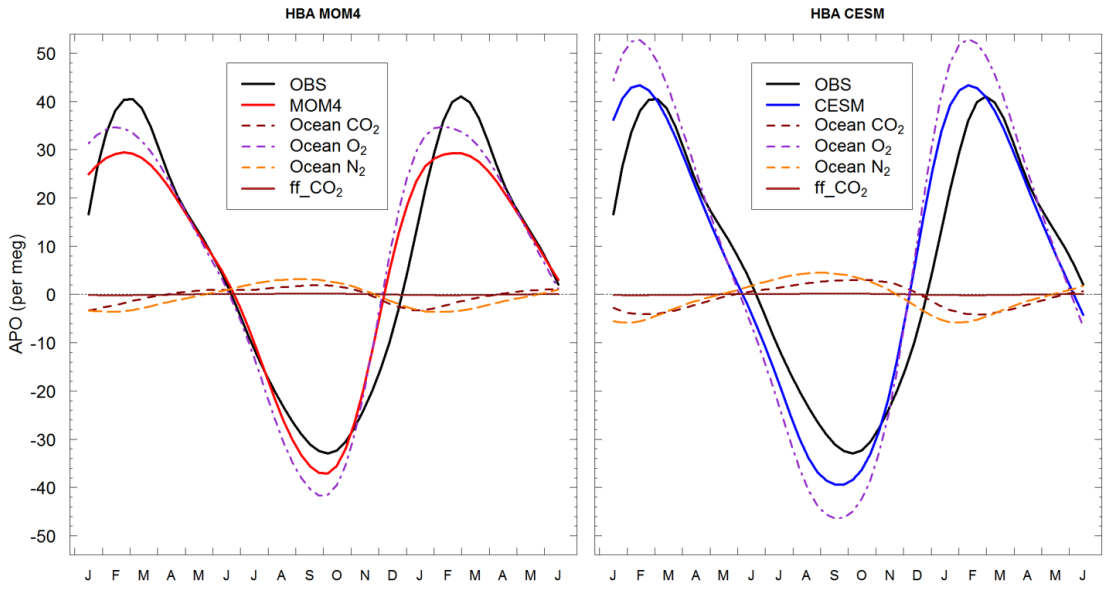

Figure 4.21. The seasonal cycle of APO (in per meg) at HBA from the MOM4 (left plot, red line) and CESM (right plot, blue line) model runs compared to the observations (OBS, black line). The individual contributions of ocean CO_2 (maroon dashed line), ocean O_2 (purple dashed line), ocean N_2 (orange dashed line) and fossil fuel CO_2 ($ffCO_2$, solid brown line) fluxes to the APO seasonal cycle are shown in per meg units. The x-axis represents the first letter of individual months and the first 6 months are repeated to aid visual interpretation of the cycles. Individual points represent the monthly mean values of the HPspline curve fit to the modelled data. Lines represent a subsequent spline fit to the monthly data. The mean seasonal cycle of all stations is shown by the solid black curve.

Plotting the individual flux contributions to the APO seasonal cycle allows one to determine which of the fluxes are driving the model differences. Firstly, although the N_2 fluxes (and hence heat fluxes) are larger in CESM+TM3 than they are in MOM4+TM3, the magnitude of the difference (2-3 per meg) it is not enough to account for the difference in amplitude in the modelled APO seasonal cycle. The heat fluxes also agree in terms of their phase and this cannot therefore be invoked to explain phasing differences.

Similarly, although the phasing and shape of the CO_2 fluxes are markedly different, the absolute difference between the two models is of the order of 1-2 per meg. Again, this is not enough to account for the magnitude of the overall difference between the modelled seasonal cycles.

The most considerable difference between the models is seen in the magnitude of the O_2 fluxes in the summer, with CESM+TM3 displaying a ~20 per meg difference to MOM4+TM3. The CESM+TM3 O_2 fluxes are still larger than MOM4+TM3 at the winter minimum, but less so (by ~5 per meg).

By examining the ratio of the amplitude of the N_2 fluxes (heat driven) between the two models (N_2 CESM+TM3: N_2 MOM4+TM3) to that for the O_2 fluxes (O_2

CESM+TM3: O_2 MOM4+TM3), one can determine whether the difference between the modelled O_2 fluxes are entirely down to the heat the fluxes alone. N_2 CESM+ TM3: N_2 MOM4+TM3 = 1.47, whilst O_2 CESM+TM3: O_2 MOM4+TM3= 1.32, therefore the difference in the O_2 flux observed in the models cannot be entirely down to differences in the representation of the heat (and therefore solubility) driven fluxes.

The difference in the magnitude of the O_2 flux between the two models and the observations in summer therefore could be a combination of the following: (1) Biological activity (or rather, net ecosystem production), whereby MOM4 underestimates the magnitude and/or extent of the summertime phytoplankton bloom and/or the amount of repsiration in the surface layer, export out of the surface layer and repiration at depth. Unfortuntely, it is not possible to separte these processes in this analysis since the total O_2 flux will be an integration of all four processes (2) Physical mixing, whereby the mixed layer depth in MOM4 is too deep in the spring and summer, suppressing O_2 saturation in the surface layer due to less phytoplankton being brought to the crtical depth for light availbility. Furthermore, if the mixed layer depth is too deep in the previous winter, then the mixed layer will become too undersaturated with respect to O_2, which would then not allow enough supersaturation the following spring and summer to drive a large enough O_2 flux to the atmosphere.

However, it is not prudent to fully evaluate different OCBMs over the Southern Ocean using only one station that will inevitably be biased by local features within the footprint of each station. Whilst indivdual stations provide important regional tests for OBCMs, a more complete evalution of each model's performance in the Southern Ocean can be determined by comparison to the other three stations higlighted in this study.

Figure 4.22 shows each of the modelled APO seasonal cycles and their indivdual flux components for each station. Taylor diagrams (Taylor, 2001) are useful visual tools for evaluating model performance against observations (e.g. Nevison et al., 2008b) and this is displayed for both models across all stations in **Figure 4.23**. Comparison of the obsevred and the modelled 1σ standard deviation of a seasoanl cycle is a measure of its amplitude with the observation normalized to 1. Whereas the correlation coefficient reflects agreements in phasing, whereby total agreement would result in R=1.

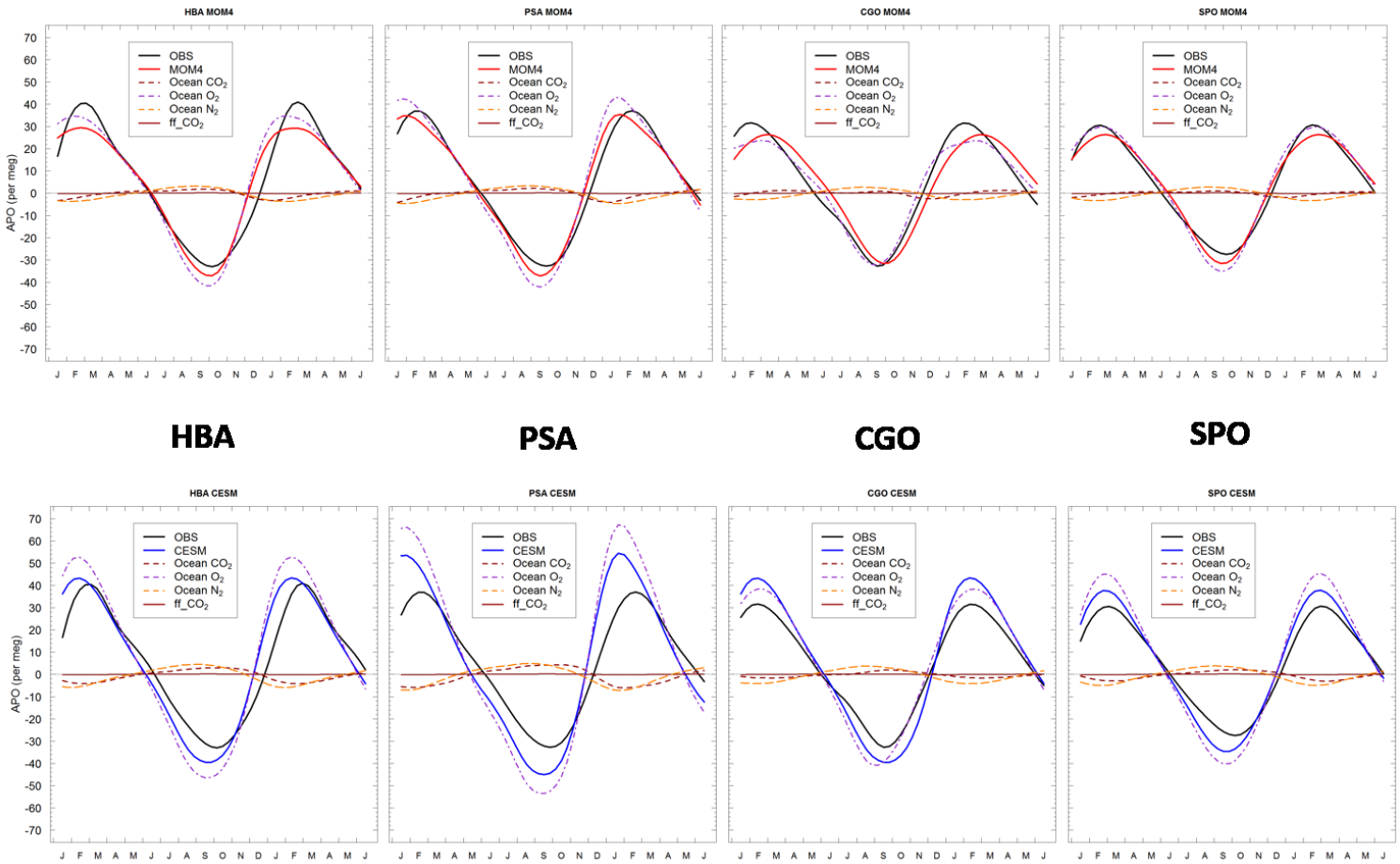

Figure 4.22. As in **Figure 4.21** but for all stations considered in this analysis: HBA, PSA, CGO and SPO.

CESM+TM3 overestimates the amplitude at all stations, particularly at PSA and SPO. Whilst MOM4+TM3 performs better, reproducing the amplitude well at PSA and SPO, it slightly underestimates it at HBA, and even more so at CGO. Overall, MOM4+TM3 performs best at reproducing the APO amplitude observed at the stations considered. In terms of the phasing, MOM4+TM3 is the most consistent across stations, achieving R values between 0.96-0.99. CESM+TM3, on the other hand, displays the best phasing agreement seen across all stations and models at CGO and SPO, yet performs the worst at HBA and PSA.

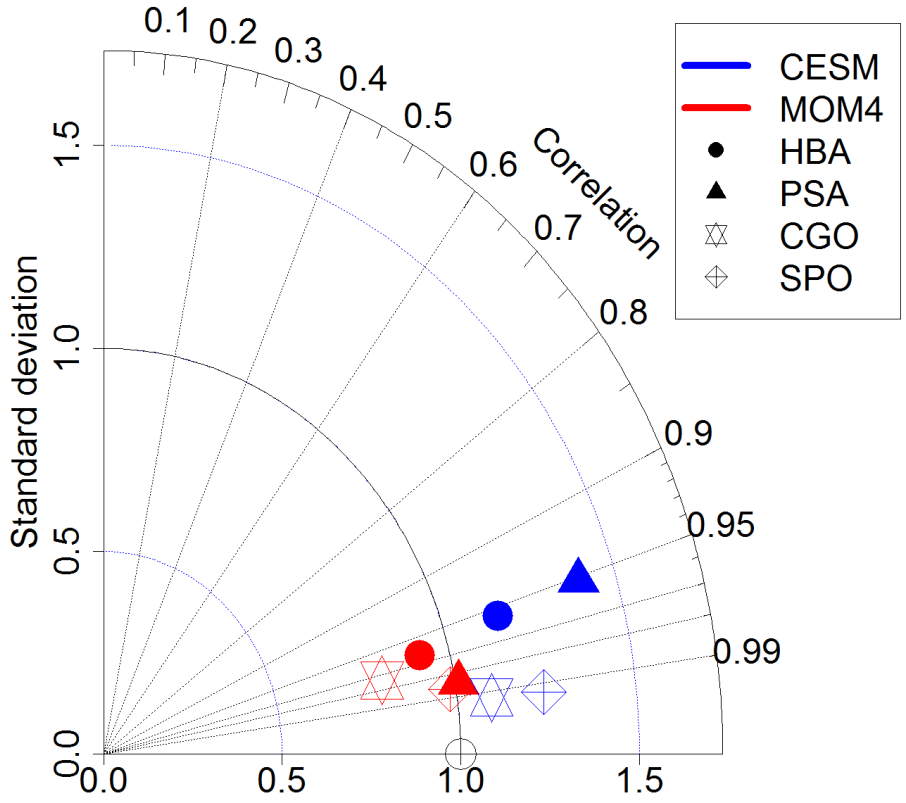

Figure 4.23. Taylor diagram evaluating model performance at each of the four Southern Ocean APO stations considered in this analysis. The radial axis (running between the x and y axes) represents the 1σ standard deviation of the modelled seasonal cycle and therefore represents a measure of the seasonal cycle amplitude; the 1σ standard deviation of the observed seasonal cycle is normalised to 1 in this case such that if the modelled amplitude agrees completely with the observed then the point should lie on the 1.0 radial curve. The angle theta from the x-axis represents the arccosine of the correlation coefficient R between the model and observed cycle which therefore represents the agreement in the phasing and shape of the cycle (Taylor, 2001). CESM is represented by the blue symbols and MOM4 by the red symbols. Individual symbols represent the respective stations as shown in the key.

Generally, CESM+TM3 appears to be overestimating the APO fluxes and, in terms of phasing, performs least well at the two coastal Antarctic stations. This could suggest that CESM+TM3 may struggle with local fluxes.

An assesment of present day performance of the CMIP5 models against observations of biological productivity in the Southern Ocean (*in situ* or satellite estimates) are limited, with many studies choosing to focus either globally and on future projections in the context of the carbon sink (e.g. Anav et al., 2013; Bopp et al., 2013). A local assesment within the Ross Sea, which, in many regards is similar to the Weddell Sea, does exisit however (Rickard and Behrens, 2016). In this study Rickard and Behren (2016) found that CESM slightly overestimates cholorphyll concentrations whilst MOM4 displays a slight underestimation between November-March with respect to satellite SeaWiFS data. Furthermore, compared to all other models, MOM4 actually peformed the best, whislt CESM was one of the worst in terms of cholophyll concentraiton. Moreover, on all of the metrics considered in the study, including nutrients, sea ice extent and depth of the seasonal thermocline, MOM4 was one of the best perfomring models, whereas CESM was again in the mid range of overall model performance (Rickard and Behrens, 2016).

With respecct to the MLD, both models display a shallow bias compared to obsevrations (**Figure 4.24**) (Huang et al., 2014; Sallée et al., 2013). That is to say, the MLD is not deep enough in winter and yet too shallow during summer. This would act to dampen air-sea fluxes during winter but increase them during summer, which in turn implies, that if a model does well at recreating the observed seasonal cycle, then the biological component of the O_2 flux could be underestimated in summer and overestimated in the winter and/or vertical mixing in the ocean circulation model is too large. This demonstrates the false positive arrived at due to in correct vertical mixing in atmopsheric transport models also applies to vertical mixing within ocean models.

Nevertheless, differences in the representation of the MLD could be invoked to explain the different model performance across the Southern Ocean. The MLD in MOM4 is more shallow than CESM in summer, yet deeper in winter (**Figure 4.24**). This implies that although the biological component is correct in winter for MOM4, it is too small in summer. Whilst in CESM, the biology must be overestimated in summer (to drive an O_2 flux greater than that seen by the observations), whislt in winter the shallow MLD implies again the biology is overestimated in the surface layer (i.e. too much repsiration) in order to overetsimate the fluxes seen. This is in agreement to what was found in terms of the

cholorphyll abundance in the Ross Sea, whereby CESM overestimates the chlorophyll concentration but MOM4 underestimates it (Rickard and Behrens, 2016). Finally, it is interesting to note in **Figure 4.24**B that MOM4 shows a very deep mixed layer depth in September (late winter/early spring) in the vicinity of the Weddell gyre, potentially entraining waters that are too deep and therefore too depleted with respect to O_2 compared to observations.

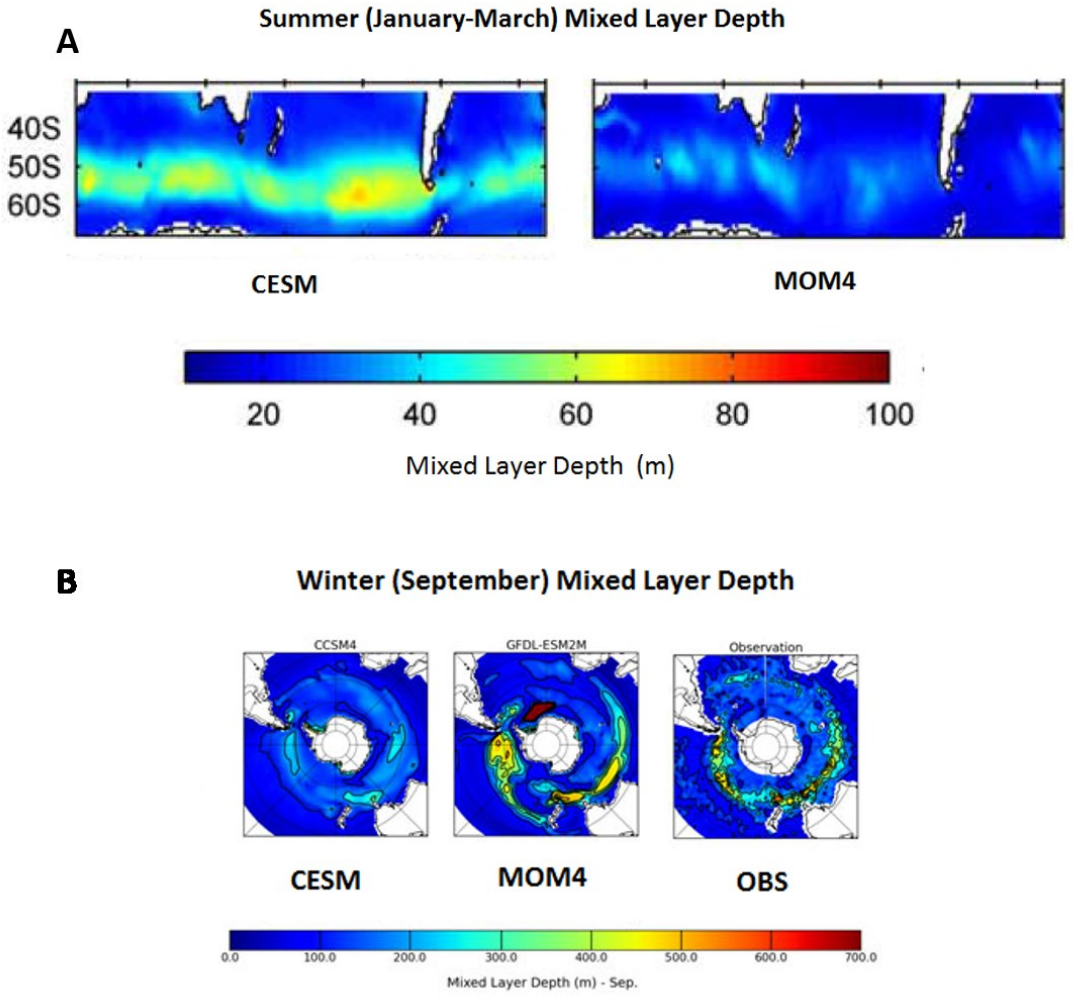

Figure 4.24. (A): Summer (January-March) mixed layer depth (MLD) (m) observed in the CESM and MOM4 models in the Southern Ocean (adapted from (Huang et al., 2014)). (B). Winter mixed layer depth observed in the CESM and MOM4 models compared to observations (OBS) from Argo float profiles (adapted from (Sallée et al., 2013). Note the different scale bar ranges in (A) and (B).

Clearly, untangling the different processes that drive the differences in the models' ability to reproduce observed APO seasonl cycles in the Southern Ocean is a difficult process. A more thorough evaluation of the models and there mechanics is beyond the scope of this project. However, from what has been discussed thus far, it

would be valuable to perform further runs with the two models discussed where the MLD is kept constant, hence allowing only the biological component to drive variability. The MLD itself is a result of interacting features within the model such as wind stress and ocean physics which all have to be considered. Moreover, to test MOM4 and CESM further in terms of their representation of ocean biology and vertical mixing, one could compare measured dissoled O_2 profiles with that produced by the models. Finally, I have not discussed the differeing characterisations of sea ice within the two models which will also impact air-sea gas exchange of the O_2 CO_2 and N_2.

4.3.6.3.2. Conclusion

This brief analysis has evaluated two OBGCM, coupled to an ATM, at reproducing the observed APO seasonal cycle at HBA and at other Southern Ocean stations in order to ascertain which model may more reliable at estimating the seasonal CO_2 seasonal cycle. Such an analysis is possible because the ocean processes that drive the seasonality in ocean CO_2 drive opposite but larger fluxes in O_2.

Overall MOM4 performed the best in terms of reproducing the observed APO seasonal cycle at all of the Southern Ocean station. CESM generally overestimated the seasonal fluxes. Based on this, MOM4 appears to be a more reliable model at reproducing seasonal CO_2 fluxes in the Southern Ocean. Nevertheless, this analysis has highlighted the importance of intermodal and interstation station differences. CESM performed better in terms of its phasing at both SPO and CGO than MOM4, but worse at HBA and PSA, potentially reflecting a deficiency in reproducing local fluxes whilst still performing well overall across the Southern Ocean Whereas MOM4, underestimated the summer peak at HBA compared to CESM. Further modelling runs are necessary to gain a more mechanistic understanding of the processes controlling the APO seasonal cycle and by extension the ocean CO_2 seasonal cycle.

4.4. Summary and conclusions

The primary focus of this chapter was to determine the extent with which carbon cycle processes in the South Atlantic sector of the Southern Ocean control the variability of atmospheric CO_2, $\delta(O_2/N_2)$ and APO observations at the Halley Research Station, Antarctica.

I began by investigating the variability in the CO_2 seasonal cycle, as depicted by NOAA flask observations, for the 2000-2015 period using the latest output from the

CarbonTracker Europe 2016 data assimilation model (van der Laan-Luijkx et al., 2017) (**Figure 4.7**). The purpose of this analysis was to ascertain which of the terrestrial biosphere, ocean, fossil fuel and biomass burning CO_2 fluxes exerted the strongest influence on the phase, shape and amplitude observed.

The analysis suggested that the modelled CO_2 seasonal cycle at HBA appears to be largely controlled by the terrestrial biosphere, particularly the amplitude (**Figure 4.8**). However, the timing of the upwards and downwards zero crossing days (UZC, DZC, respectively) of the modelled CO_2 seasonal cycle, although primarily determined by the phase (timing of UZC and DZC) of the terrestrial biosphere fluxes, appears to be modulated somewhat by (1) the magnitude of the late summer-early autumn ocean outgassing and (2) the combined influence of ocean CO_2 uptake and the decrease in biomass burning plus fossil emissions in the late spring-early summer (UZC) (**Figure 4.9**). This suggests a more prominent role for the terrestrial biosphere at high southern hemisphere latitudes than has previously been considered and more of a modulating role for the ocean CO_2 contribution to the seasonal cycle.

However, this analysis is likely to be biased by uncertainties inherent within the CTE2016 mode1. The sparse data coverage within the Southern Ocean, both atmospheric and oceanic, will impact both the *a priori* and *a posteriori* fluxes. The *a priori* ocean fluxes are the result of a joint atmosphere – ocean inversion (Jacobson et al., 2007), whereas the *a posteriori* fluxes are only optimized relative to atmospheric observations that are within a 5 week transport window. Larger uncertainties on the fluxes within the Southern Ocean will therefore exist compared to regions with a more dense data coverage. No attempt was made to quantify these uncertainties and should therefore be the focus of future work. The robustness of the fluxes should be examined by inclusion or omission of data sources within the Southern Ocean as has been done by Law et al. (2008). The magnitude of these uncertainties could then be compared to those found in more densely populated atmosphere and ocean observation regions, such as the North Atlantic Ocean and Europe.

Furthermore, I highlighted how the choice of curve fitting routine and its parametrisation used in this analysis will also influence the results. Although much consideration was given to the choice of curve fitting routine and the selection of the parametrisation values, it would be advisable to carry out a sensitivity analysis using a range of parametrisation values and by selection of a different curve fitting routine, as was demonstrated by Pickers and Manning (2015).

The second objective of this chapter was to investigate the cause of synoptic scale variability in atmospheric CO_2, $\delta(O_2/N_2)$ and APO observations from the recently installed measurement system at HBA. The first 11 months of the observation record were presented (**Figure 4.10**). Potential events were identified as those that were more than 2σ from the curve fit to the data. Although one event was identified at the beginning of the record, the remainder of the record was not forthcoming with events and so this analysis was abandoned. The atmospheric record is lacking in summer time data due to the nature of the installation and the subsequent shutdown of the station. It may not be surprising that the winter record did not exhibit events of the magnitude observed in February. This may be due to the increased distance from the ocean that HBA is due to the winter sea ice extent.

The first event (in February) was examined in Appendix A. The preliminary analysis suggests that the large deviation seen in APO (positive) and CO_2 (negative) could be associated with air masses originating in the South Atlantic in a region of productivity. The analysis did not investigate this further. In future work, I would suggest that satellite productivity data could be examined and a net O_2 flux to the atmosphere could be derived based on the O_2:C exchange ratio for phytoplankton. This flux could then be fed into a transport model with air subsequently sampled at HBA, to investigate whether a similar deviation in the atmospheric observations is seen.

The third objective of this chapter was to examine the seasonality of APO observed at HBA and compare to the APO seasonal cycle observed at other stations. I began the analysis by presenting the seasonal cycle of CO_2, $\delta(O_2/N_2)$ and APO.

The CO_2 seasonal cycle has an amplitude of 1.71 ± 0.13 ppm with a late winter maximum in August and a mid-summer minimum in January. I then investigated the likelihood that the seasonal cycle from the measurements presented here for 2016 represents the mean climatological seasonal cycle of CO_2 observed at HBA from NOAA flask observations collected at the station for the 2000-2015 period (**Figure 4.14**). Firstly, in terms of the seasonal peak to peak amplitude and the autumn zero crossing day, 2016 is comparable to other years in the 2000-2015 period, yet it is still not a typical year in comparison to the mean. Secondly, the spring zero crossing day appears to be anomalous. These differences could potentially be explained by the poor data coverage in January 2017 and February 2016 due to decommissioning and installation of the measurement system, respectively. Moreover, the differences may also be explained by the moderate to strong El Niño event that occurred in 2016 (Betts et al., 2016). To confirm this, the

analysis record (2000-2015) needs to be extended back to include the large 1998 El Niño. This is the only event in the record that is comparable in magnitude to that observed in 2016 and may help to confirm the assertion made above.

The $\delta(O_2/N_2)$ and APO seasonal cycles have an amplitude of 77 ± 11 and 73 ± 11 per meg, respectively, with a late summer maximum in February-March and an early spring minimum in September-October (**Figure 4.11**). Whilst the seasonal cycle of $\delta(O_2/N_2)$ at HBA will be influenced by both seasonal atmosphere-terrestrial biosphere and atmosphere-ocean O_2 exchange, the APO seasonal cycle will only be influenced by ocean exchange. The similarity between the $\delta(O_2/N_2)$ and APO cycles demonstrate that the majority of the $\delta(O_2/N_2)$ seasonal cycle at HBA is driven by ocean processes (91.3%).

The seasonal cycle of APO observed at HBA was compared to three other Southern Ocean APO monitoring stations (PSA, SPO and CGO) (**Figure 4.17** and **Figure 4.19**). HBA exhibited the largest amplitude (73 ± 11 per meg). I speculated that this suggests that the site is either influenced by large local seasonal oceanic O_2 fluxes, from the Weddell Sea for example, or similarly, samples air deriving from a larger region that exhibits large seasonal fluxes, such as the South Atlantic sector of the Southern Ocean (**Figure 4.18**). However, the HBA mean overlaps with the errors associated with the means of the other stations, with the exception of SPO. The absolute differences in the amplitude observed at HBA, CGO and PSA are therefore not significant. In contrast to the above, this suggests a basin wide carbon cycle influence on all stations.

Moreover, by excluding SPO, there is a subtle yet clear latitudinal gradient in the amplitude of the APO seasonal cycle as one moves north from HBA (75˚S) towards CGO (40˚S) of -2.4 per meg/10˚ latitude (**Figure 4.19**). Again, the trend is within the uncertainty defined on the amplitude for each stations. However, if these uncertainties were reduced, this could imply that the magnitude of seasonal O_2 exchange is largest at the southern boundary of the Southern Ocean, where it meets Antarctica, and that the magnitude of the seasonal fluxes decreases at lower latitudes in the Southern Ocean. Support for this theory is given by results from a continuous measurement system that sails repeatedly across the Drakes Passage and displays a seasonal amplitude gradient of ~ -20 per meg/10˚ latitude over the 55-65 ˚S latitude range (B. Stephens, *personal communication*). Averaging this over the latitude range presented here would result in -5.7 per meg/10˚ latitude gradient.

Whilst the seasonal cycle of APO at HBA is most similar to PSA in terms of its amplitude, this is not the case for the phase. HBA is instead most similar to the SPO with

respect to its phasing (**Figure 4.19**). The phasing likely reflects a similar air mass history (**Figure 4.16**). With that, I postulated that SPO could represent the surface fluxes observed at HBA that are vertically mixed over the altitude difference between the two stations. The difference between the seasonal amplitude of APO observed at HBA and SPO could therefore represent an important test for a particular ATMs ability to correctly represent the amount of vertical mixing observed in the atmosphere.

Furthermore, I proposed that the difference in phasing at HBA (and subsequently SPO) and both PSA and CGO is due to a combination of air mass history and sea-ice coverage. The delay in phasing of 2 to 3 weeks observed at HBA (and SPO) compared to PSA (and CGO) is therefore due to the presence of sea-ice over areas of the ocean that air masses that arrive at HBA likely equilibrate with (**Figure 4.20**).

The conclusions made in this section are limited somewhat by the uncertainties in the analysis. Firstly, although I have discussed possible reasons behind the differences in the seasonal cycles of APO observed between the different stations, the seasonal cycles are not significantly different from each other (with the exception of HBA and SPO). Improvements in the measurement uncertainty and in the quality of the curve it would be required to ascertain whether the regional influences discussed above are significant.

Finally, I evaluated the performance of two ocean circulation plus biogeochemistry models (MOM4 and CESM) at reproducing the seasonal cycle of APO; firstly at HBA (**Figure 4.21**), and then subsequently at the other Southern Ocean APO stations (**Figure 4.22**), following the mixing of ocean CO_2, O_2 and N_2 fluxes within an atmospheric transport model (TM3).

At HBA, a significant difference in the magnitude of the O_2 flux between the two models and the observations in summer was observed. I first determined that this difference was not driven by differences in the representation of heat and therefore solubility driven fluxes within the models. I then postulated that the difference could be due to a combination of the following: (1) net ecosystem production; whereby MOM4 underestimates, with repect to CESM, the magnitude and/or extent of the summertime phytoplankton bloom and/or the amount of repsiration in the surface layer, export out of the surface layer and repiration at depth. (2) Physical mixing, whereby the MLD in MOM4, with respect to CESM, is too deep in the spring and summer, suppressing O_2 saturation in the surface layer due to less phytoplankton being brought to the crtical depth for light availbility. Furthermore, if the MLD is too deep in the previous winter, then the mixed layer will become too undersaturated with respect to O_2, which would then not

allow enough supersaturation the following spring and summer to drive a large enough O_2 flux to the atmosphere.

Overall MOM4 performed the better in terms of reproducing the observed APO seasonal cycle at all of the Southern Ocean station (**Figure 4.23**). CESM, on the other hand, generally overestimated the seasonal fluxes. Moreover, this analysis has highlighted the importance of inter-model and inter-station differences. For example, CESM performed better in terms of its phasing at both SPO and CGO than MOM4, but worse at HBA and PSA, potentially reflecting a deficiency in reproducing local fluxes, whilst still performing well overall across the Southern Ocean. Whereas MOM4 underestimated the summer peak at observed at HBA compared to CESM, but not at others.

Finally, the differences between the models in terms of the representation of the seasonal MLD and productivity was also briefly discussed, potentially explaining some of the discrepancies seen. However, further modelling runs are necessary to gain a more mechanistic understanding of the processes controlling the APO seasonal cycle. For example, to examine the suggested heterogeneity in the characterisation of the O_2 flux across the Southern Ocean, it would be prudent to compare modelled and observed dissolved O_2 profiles within the separate ocean basins that make up the Southern Ocean.

This research has demonstrated the insight that atmospheric CO_2, $\delta(O_2/N_2)$ and APO measurements can have on both the spatial and temporal variability of carbon cycle processes in the Southern Ocean. The addition of HBA as on O_2 monitoring station has proved valuable in untangling regional differences in carbon cycle processes across the Southern Ocean. However, improvements in measurement uncertainty and in the quality of the curve fit are needed to confirm these assertions. The addition of HBA into APO model-observation comparison studies has further highlighted potential regional heterogeneity in the characterisation of carbon cycle processes within the two models.

4.5. References

Anav, A., Friedlingstein, P., Kidston, M., Bopp, L., Ciais, P., Cox, P., Jones, C., Jung, M., Myneni, R., Zhu, Z. (2013) Evaluating the Land and Ocean Components of the Global Carbon Cycle in the CMIP5 Earth System Models. Journal of Climate 26, 6801-6843.

Bacastow, R.B., Keeling, C.D., Whorf, T.P. (1985) Seasonal amplitude increase in atmospheric CO_2 concentration at Mauna Loa, Hawaii, 1959-1982. Journal of Geophysical Research-Atmospheres 90, 10529-10540.

Bakker, D.C.E., Hoppema, M., Schröder, M., Geibert, W., De Baar, H.J.W. (2008) A rapid transition from ice covered CO_2-rich waters to a biologically mediated CO_2 sink in the eastern Weddell Gyre. Biogeosciences Discussions 5, 1205-1235.

Bakker, D.C.E., Pfeil, B., Landa, C.S., Metzl, N., O'Brien, K.M., Olsen, A., Smith, K., Cosca, C., Harasawa, S., Jones, S.D., Nakaoka, S.I., Nojiri, Y., Schuster, U., Steinhoff, T., Sweeney, C., Takahashi, T., Tilbrook, B., Wada, C., Wanninkhof, R., Alin, S.R., Balestrini, C.F., Barbero, L., Bates, N.R., Bianchi, A.A., Bonou, F., Boutin, J., Bozec, Y., Burger, E.F., Cai, W.J., Castle, R.D., Chen, L., Chierici, M., Currie, K., Evans, W., Featherstone, C., Feely, R.A., Fransson, A., Goyet, C., Greenwood, N., Gregor, L., Hankin, S., Hardman-Mountford, N.J., Harlay, J., Hauck, J., Hoppema, M., Humphreys, M.P., Hunt, C.W., Huss, B., Ibánhez, J.S.P., Johannessen, T., Keeling, R., Kitidis, V., Körtzinger, A., Kozyr, A., Krasakopoulou, E., Kuwata, A., Landschützer, P., Lauvset, S.K., Lefèvre, N., Lo Monaco, C., Manke, A., Mathis, J.T., Merlivat, L., Millero, F.J., Monteiro, P.M.S., Munro, D.R., Murata, A., Newberger, T., Omar, A.M., Ono, T., Paterson, K., Pearce, D., Pierrot, D., Robbins, L.L., Saito, S., Salisbury, J., Schlitzer, R., Schneider, B., Schweitzer, R., Sieger, R., Skjelvan, I., Sullivan, K.F., Sutherland, S.C., Sutton, A.J., Tadokoro, K., Telszewski, M., Tuma, M., van Heuven, S.M.A.C., Vandemark, D., Ward, B., Watson, A.J., Xu, S. (2016) A multi-decade record of high-quality fCO_2 data in version 3 of the Surface Ocean CO_2 Atlas (SOCAT). Earth Syst. Sci. Data 8, 383-413.

Battle, M., Mikaloff Fletcher, S., Bender, M.L., Keeling, R.F., Manning, A.C., Gruber, N., Tans, P.P., Hendricks, M.B., Ho, D.T., Simonds, C., Mika, R., Paplawsky, B. (2006) Atmospheric potential oxygen: New observations and their implications for some atmospheric and oceanic models. Global Biogeochemical Cycles 20, doi:10.1029/2005GB002534.

Bender, M., Ellis, T., Tans, P., Francey, R., Lowe, D. (1996) Variability in the O_2/N_2 ratio of southern hemisphere air, 1991-1994: Implications for the carbon cycle. Global Biogeochemical Cycles 10, 9-21, doi:10.1029/1095GB03295.

Bender, M.L., Battle, M., Keeling, R.F. (1998) The O_2 balance of the atmosphere: A tool for studying the fate of fossil-fuel CO_2. Annu. Rev. Energy Environ. 23, 207-223.

Bent, J.D., (2014) Airborne Oxygen Measurements over the Southern Ocean as an Integrated Constraint of Seasonal Biogeochemical Processes. Scripps Institution of Oceanography La Jolla, San Diego, California, U.S. .

Betts, R.A., Jones, C.D., Knight, J.R., Keeling, R.F., Kennedy, J.J. (2016) El Nino and a record CO_2 rise. Nature Clim. Change 6, 806-810.

Boden, T.A., G. Marland, and R.J. Andres. , (2009) Global, Regional, and National Fossil-Fuel CO_2 Emissions. , in: Center., C.D.I.A. (Ed.), Oak Ridge National Laboratory, U.S. Department of Energy, Oak Ridge, Tenn., U.S.A.

Bopp, L., Resplandy, L., Orr, J.C., Doney, S.C., Dunne, J.P., Gehlen, M., Halloran, P., Heinze, C., Ilyina, T., Séférian, R., Tjiputra, J., Vichi, M. (2013) Multiple stressors of ocean ecosystems in the 21st century: projections with CMIP5 models. Biogeosciences 10, 6225-6245.

Broecker, W.S., Peng, T.-H. (1974) Gas exchange rates between air and sea. Tellus 26, 21-35.

Broecker, W.S., Peng, T.H. (1982) Tracers in the Sea. Lamont Doherty Geological Observatory, Palisades, NY, USA.

Brown, P.J., Jullion, L., Landschützer, P., Bakker, D.C.E., Naveira Garabato, A.C., Meredith, M.P., Torres-Valdés, S., Watson, A.J., Hoppema, M., Loose, B., Jones, E.M., Telszewski, M., Jones, S.D., Wanninkhof, R. (2015) Carbon dynamics of the Weddell Gyre, Southern Ocean. Global Biogeochemical Cycles 29, 288-306.

Carslaw, D.C., Beevers, S.D., Ropkins, K., Bell, M.C. (2006) Detecting and quantifying aircraft and other on-airport contributions to ambient nitrogen oxides in the vicinity of a large international airport. Atmospheric Environment 40, 5424-5434.

Carslaw, D.C., Ropkins, K. (2012) openair — An R package for air quality data analysis. Environmental Modelling & Software 27–28, 52-61.

Cavalieri, D.J., Parkinson, C.L. (2008) Antarctic sea ice variability and trends, 1979–2006. Journal of Geophysical Research: Oceans 113, n/a-n/a.

Ciais, P., Rayner, P., Chevallier, F., Bousquet, P., Logan, M., Peylin, P., Ramonet, M. (2010) Atmospheric inversions for estimating CO_2 fluxes: methods and perspectives. Climatic Change 103, 69-92.

Doney, S.C., Glover, D.M., Najjar, R.G. (1996) A new coupled, one-dimensional biological-physical model for the upper ocean: Applications to the JGOFS Bermuda Atlantic Time-series Study (BATS) site. Deep Sea Research Part II: Topical Studies in Oceanography 43, 591-624.

Draxler, R.R., Hess, G.D. (1998) An overview of the HYSPLIT_4 modelling system for trajectories, dispersion, and deposition. Aust. Met. Mag. 47, 295-308.

Dunne, J.P., John, J.G., Shevliakova, E., Stouffer, R.J., Krasting, J.P., Malyshev, S.L., Milly, P.C.D., Sentman, L.T., Adcroft, A.J., Cooke, W., Dunne, K.A., Griffies, S.M., Hallberg, R.W., Harrison, M.J., Levy, H., Wittenberg, A.T., Phillips, P.J., Zadeh, N. (2013) GFDL's ESM2 Global Coupled Climate–Carbon Earth System Models. Part II: Carbon System Formulation and Baseline Simulation Characteristics. Journal of Climate 26, 2247-2267.

EDGAR, (2011) EDGAR4.2 Database: Emission Database for Global Atmospheric Research (EDGAR), release version 4.2 in: Joint Research Centre (JRC)/PBL Netherlands Environmental Assessment Agency (Ed.), European Commission. .

Evans, G.R., McDonagh, E.L., King, B.A., Bryden, H.L., Bakker, D.C.E., Brown, P.J., Schuster, U., Speer, K.G., van Heuven, S.M.A.C. (2017) South Atlantic interbasin exchanges of mass, heat, salt and anthropogenic carbon. Progress in Oceanography 151, 62-82.

Fleming, Z.L., Monks, P.S., Manning, A.J. (2012) Review: Untangling the influence of air-mass history in interpreting observed atmospheric composition. Atmospheric Research 104, 1-39.

Friedlingstein, P., Prentice, I.C. (2010) Carbon-climate feedbacks: a review of model and observation based estimates. Current Opinion in Environmental Sustainability 2, 251-257.

García, H.E., Keeling, R.F. (2001) On the global oxygen anomaly and air-sea flux. Journal of Geophysical Research-Oceans 106, 31155-31166.

Graven, H.D., Keeling, R.F., Piper, S.C., Patra, P.K., Stephens, B.B., Wofsy, S.C., Welp, L.R., Sweeney, C., Tans, P.P., Kelley, J.J., Daube, B.C., Kort, E.A., Santoni, G.W., Bent, J.D. (2013) Enhanced Seasonal Exchange of CO_2 by Northern Ecosystems Since 1960. Science 341, 1085-1089.

Griffies, S.M., Böning, C., Bryan, F.O., Chassignet, E.P., Gerdes, R., Hasumi, H., Hirst, A., Treguier, A.-M., Webb, D. (2000) Developments in ocean climate modelling. Ocean Modelling 2, 123-192.

Griffies, S.M., Winton, M., Anderson, W.G., Benson, R., Delworth, T.L., Dufour, C.O., Dunne, J.P., Goddard, P., Morrison, A.K., Rosati, A., Wittenberg, A.T., Yin, J., Zhang, R. (2015) Impacts on Ocean Heat from Transient Mesoscale Eddies in a Hierarchy of Climate Models. Journal of Climate 28, 952-977.

Gruber, N., Gloor, M., Fan, S.-M., Sarmiento, J.L. (2001) Air-sea flux of oxygen estimated from bulk data: Implications for the marine and atmospheric oxygen cycles. Global Biogeochemical Cycles 15, 783-803.

Heimann, M., Keeling, C.D., Tucker, C.J., (1989) A three dimensional model of atmospheric CO_2 transport based on observed winds: 3. Seasonal cycle and synoptic time scale variations, Aspects of Climate Variability in the Pacific and the Western Americas. American Geophysical Union, pp. 277-303.

Heimann, M., Körner, S, (2003) The global atmospheric tracer model TM3 (Technical Report 5). . Jena: Max-Planck-Institut für Biogeochemie.

Houghton, R.A. (2007) Balancing the global carbon budget. Annual Review of Earth and Planetary Sciences 35, 313-347.

Huang, C.J., Qiao, F., Dai, D. (2014) Evaluating CMIP5 simulations of mixed layer depth during summer. Journal of Geophysical Research: Oceans 119, 2568-2582.

Ishidoya, S., Morimoto, S., Aoki, S., Taguchi, S., Goto, D., Murayama, S., Nakazawa, T. (2012) Oceanic and terrestrial biospheric CO_2 uptake estimated from atmospheric potential oxygen observed at Ny-Ålesund, Svalbard, and Syowa, Antarctica. 2012 64.

Jacobson, A.R., Mikaloff Fletcher, S.E., Gruber, N., Sarmiento, J.L., Gloor, M. (2007) A joint atmosphere-ocean inversion for surface fluxes of carbon dioxide: 1. Methods and global-scale fluxes. Global Biogeochemical Cycles 21, n/a-n/a.

Jones, A.E., Wolff, E.W., Brough, N., Bauguitte, S.J.B., Weller, R., Yela, M., Navarro-Comas, M., Ochoa, H.A., Theys, N. (2013) The spatial scale of ozone depletion events derived from an autonomous surface ozone network in coastal Antarctica. Atmos. Chem. Phys. 13, 1457-1467.

Jones, A.E., Wolff, E.W., Salmon, R.A., Bauguitte, S.J.-B., Roscoe, H.K., Anderson, P.S., Ames, D., Clemitshaw, K.C., Flemming, Z.L., Bloss, W.J., Heard, D.E., Lee, J.D., Read, K.A., Hamer, P., Shallcross, D.E., Jackson, A.V., Walker, S.I., Lewis, A.C., Mills, G.P., Plane, J.M.C., Saiz-Lopez, A., Sturges, W.T., D.R., W. (2008) Chemistry of the Antarctic Boundary Layer and the Interface with Snow: an overview of the CHABLIS campaign. Atmospheric Chemistry and Physics, 3789-3803.

Jones, C.D., Collins, M., Cox, P.M., Spall, S.A. (2001) The Carbon Cycle Response to ENSO: A Coupled Climate–Carbon Cycle Model Study. Journal of Climate 14, 4113-4129.

Kalnay, E., Kanamitsu, M., Kistler, R., Collins, W., Deaven, D., Gandin, L., Iredell, M., Saha, S., White, G., Woollen, J., Zhu, Y., Leetmaa, A., Reynolds, R., Chelliah, M., Ebisuzaki, W., Higgins, W., Janowiak, J., Mo, K.C., Ropelewski, C., Wang, J., Jenne, R., Joseph, D. (1996) The NCEP/NCAR 40-Year Reanalysis Project. Bulletin of the American Meteorological Society 77, 437-471.

Keeling, C.D., Bacastow, R.B., Carter, A.F., Piper, S.C., Whorf, T.P., Heimann, M., Mook, W.G., Roeloffzen, H., (1989) A three-dimensional model of atmospheric CO_2 transport based on observed winds: 1. Analysis of observational data, Aspects of Climate Variability in the Pacific and the Western Americas. American Geophysical Union, pp. 165-236.

Keeling, R.F. (1988) Measuring correlations between atmospheric oxygen and carbon dioxide mole fractions: A preliminary study in urban air. Journal of Atmospheric Chemistry 7, 153-176.

Keeling, R.F., Najjar, R.P., Bender, M.L., Tans, P.P. (1993) What atmospheric oxygen measurements can tell us about the global carbon cycle. Global Biogeochemical Cycles 7, 37-67, doi:10.1029/1092GB02733.

Keeling, R.F., Shertz, S.R. (1992) Seasonal and interannual variations in atmospheric oxygen and implications for the global carbon cycle. Nature 358, 723-727, doi:710.1038/358723a358720.

Keeling, R.F., Stephens, B.B., Najjar, R.G., Doney, S.C., Archer, D., Heimann, M. (1998) Seasonal variations in the atmospheric O_2/N_2 ratio in relation to the kinetics of air-sea gas exchange. Global Biogeochemical Cycles 12, 141-163.

Krol, M., Houweling, S., Bregman, B., van den Broek, M., Segers, A., van Velthoven, P., Peters, W., Dentener, F., Bergamaschi, P. (2005) The two-way nested global chemistry-transport zoom model TM5: algorithm and applications. Atmos. Chem. Phys. 5, 417-432.

Kulmala, M., Petäjä, T., Mönkkönen, P., Koponen, I.K., Dal Maso, M., Aalto, P.P., Lehtinen, K.E.J., Kerminen, V.M. (2005) On the growth of nucleation mode particles: source rates of condensable vapor in polluted and clean environments. Atmos. Chem. Phys. 5, 409-416.

Landschützer, P., Gruber, N., Haumann, A., Rödenbeck, C., Bakker, D.C.E., van Heuven, S., Hoppema, M., Metzl, N., Sweeney, C., Takahashi, T., Tilbrook, B., Wanninkof, R. (2015) The reinvigoration of the Southern Ocean carbon sink. . Science 349, 1221-1224.

Law, R.M., Matear, R.J., Francey, R.J. (2008) Comment on "Saturation of the Southern Ocean CO_2 sink due to recent climate change". Science 319, 570.

Le Quéré, C., Andrew, R.M., Canadell, J.G., Sitch, S., Korsbakken, J.I., Peters, G.P., Manning, A.C., Boden, T.A., Tans, P.P., Houghton, R.A., Keeling, R.F., Alin, S., Andrews, O.D., Anthoni, P., Barbero, L., Bopp, L., Chevallier, F., Chini, L.P., Ciais, P., Currie, K., Delire, C., Doney, S.C., Friedlingstein, P., Gkritzalis, T., Harris, I., Hauck, J., Haverd, V., Hoppema, M., Klein Goldewijk, K., Jain, A.K., Kato, E., Körtzinger, A., Landschützer, P., Lefèvre, N., Lenton, A., Lienert, S., Lombardozzi, D., Melton, J.R., Metzl, N., Millero, F., Monteiro, P.M.S., Munro, D.R., Nabel, J.E.M.S., Nakaoka, S.I., O'Brien, K., Olsen, A., Omar, A.M., Ono, T., Pierrot, D., Poulter, B., Rödenbeck, C., Salisbury, J., Schuster, U., Schwinger, J., Séférian, R., Skjelvan, I., Stocker, B.D., Sutton, A.J., Takahashi, T., Tian, H., Tilbrook, B., van der Laan-Luijkx, I.T., van der Werf, G.R., Viovy, N., Walker, A.P., Wiltshire, A.J., Zaehle, S. (2016) Global Carbon Budget 2016. Earth Syst. Sci. Data 8, 605-649.

Le Quéré, C., Rödenbeck, C., Buitenhuis, E.T., Conway, T.J., Langenfelds, R., Gomez, A., Labuschagne, C., Ramonet, M., Nakazawa, T., Metzl, N., Gillett, N., Heimann, M. (2007) Saturation of the Southern Ocean CO_2 sink due to recent climate change. Science 316, 1735-1738, doi:1710.1126/science.1136188.

Le Quere, C., Roedenbeck, C., Buitenhuis, E.T., Conway, T.J., Langenfelds, R., Gomez, A., Labuschagne, C., Ramonet, M., Nakazawa, T., Metzl, N., Gillett, N.P., Heimann, M. (2008) Response to Comments on "Saturation of the Southern Ocean CO_2 sink due to recent climate change". Science 319.

Lin, J.C., Gerbig, C., Wofsy, S.C., Andrews, A.E., Daube, B.C., Davis, K.J., Grainger, C.A. (2003) A near-field tool for simulating the upstream influence of atmospheric observations: The Stochastic Time-Inverted Lagrangian Transport (STILT) model. Journal of Geophysical Research-Atmospheres 108.

Long, M.C., Lindsay, K., Peacock, S., Moore, J.K., Doney, S.C. (2013) Twentieth-Century Oceanic Carbon Uptake and Storage in CESM1(BGC). Journal of Climate 26, 6775-6800.

Lovenduski, N.S., Gruber, N., Doney, S.C., Lima, I.D. (2007) Enhanced CO_2 outgassing in the Southern Ocean from a positive phase of the Southern Annular Mode. Global Biogeochemical Cycles 21.

Manizza, M., Keeling, R.F., Nevison, C.D. (2012) On the processes controlling the seasonal cycles of the air–sea fluxes of O_2 and N_2O: A modelling study. Tellus B: Chemical and Physical Meteorology 64, 18429.

Manning, A.C., (2001) Temporal variability of atmospheric oxygen from both continuous measurements and a flask sampling network: Tools for studying the global carbon cycle, Scripps Institution of Oceanography. University of California, San Diego, La Jolla, California, U.S.A., p. 202.

McPhaden, M.J., Zebiak, S.E., Glantz, M.H. (2006) ENSO as an integrating concept in earth science. Science 314, 1740-1745.

Meals, D.W., Spooner,J., Dressing, S.A., Harcum, J.B., (2011) Statistical analysis for monotonic trends,, in: Agency, D.f.U.S.E.P. (Ed.). by Tetra Tech, Inc., Fairfax, VA, 23 p.

Metzl, N., Brunet, C., Jabaud-Jan, A., Poisson, A., Schauer, B. (2006) Summer and winter air–sea CO_2 fluxes in the Southern Ocean. Deep Sea Research Part I: Oceanographic Research Papers 53, 1548-1563.

Mikaloff Fletcher, S.E., Gruber, N., Jacobson, A.R., Gloor, M., Doney, S.C., Dutkiewicz, S., Gerber, M., Follows, M., Joos, F., Lindsay, K., Menemenlis, D., Mouchet, A., Muller, S.A., Sarmiento, J.L. (2007) Inverse estimates of the oceanic sources and sinks of natural CO_2 and the implied oceanic carbon transport. Global Biogeochemical Cycles 21.

Morrison, A.K., Frölichr, T., Sarmiento, J., (2015) Upwelling in the Southern Ocean Physics Today, pp. 27-32.

Munro, D.R., Lovenduski, N.S., Takahashi, T., Stephens, B.B., Newberger, T., Sweeney, C. (2015) Recent evidence for a strengthening CO_2 sink in the Southern Ocean from carbonate system measurements in the Drake Passage (2002–2015). Geophysical Research Letters 42, 7623-7630.

Naegler, T., Ciais, P., Orr, J.C., Aumont, O., RÖDenbeck, C. (2007) On evaluating ocean models with atmospheric potential oxygen. Tellus B 59, 138-156.

Nevison, C.D., Keeling, R.F., Kahru, M., Manizza, M., Mitchell, B.G., Cassar, N. (2012) Estimating net community production in the Southern Ocean based on atmospheric potential oxygen and satellite ocean color data. Global Biogeochemical Cycles 26.

Nevison, C.D., Keeling, R.F., Weiss, R.F., Popp, B.N., Jin, X., Fraser, P.J., Porter, L.W., Hess, P.G. (2005) Southern Ocean ventilation inferred from seasonal cycles of

atmospheric N_2O and O_2/N_2 at Cape Grim, Tasmania. Tellus Series B-Chemical and Physical Meteorology 57, 218-229.

Nevison, C.D., Mahowald, N.M., Doney, S.C., Lima, I.D., Cassar, N. (2008a) Impact of variable air-sea O_2 and CO_2 fluxes on atmospheric potential oxygen (APO) and land-ocean carbon sink partitioning. Biogeosciences 5, 875-889.

Nevison, C.D., Mahowald, N.M., Doney, S.C., Lima, I.D., van der Werf, G.R., Randerson, J.T., Baker, D.F., Kasibhatla, P., McKinley, G.A. (2008b) Contribution of ocean, fossil fuel, land biosphere, and biomass burning carbon fluxes to seasonal and interannual variability in atmospheric CO_2. Journal of Geophysical Research: Biogeosciences 113.

Nevison, C.D., Manizza, M., Keeling, R.F., Kahru, M., Bopp, L., Dunne, J., Tiputra, J., Ilyina, T., Mitchell, B.G. (2015) Evaluating the ocean biogeochemical components of Earth system models using atmospheric potential oxygen and ocean color data. Biogeosciences 12, 193-208.

Nevison, C.D., Manizza, M., Keeling, R.F., Stephens, B.B., Bent, J.D., Dunne, J., Ilyina, T., Long, M., Resplandy, L., Tjiputra, J., Yukimoto, S. (2016) Evaluating CMIP5 ocean biogeochemistry and Southern Ocean carbon uptake using atmospheric potential oxygen: Present-day performance and future projection. Geophysical Research Letters 43, 2077-2085.

ObsPack, (2016) Cooperative Global Atmospheric Data Integration Project; (2016): Multi-laboratory compilation of atmospheric carbon dioxide data for the period 1957-2015. , obspack_co2_1_GLOBALVIEWplus_v2.1_2016_09_02, 2.1 ed. NOAA Earth System Research Laboratory, Global Monitoring Division.

Pearman, G.I., Hyson, P. (1980) Activities of the global biosphere as reflected in atmospheric CO_2 records. Journal of Geophysical Research: Oceans 85, 4457-4467.

Pearman, G.I., Hyson, P. (1986) Global transport and inter-reservoir exchange of carbon dioxide with particular reference to stable isotopic distributions. Journal of Atmospheric Chemistry 4, 81-124.

Peters, W., Jacobson, A.R., Sweeney, C., Andrews, A.E., Conway, T.J., Masarie, K., Miller, J.B., Bruhwiler, L.M.P., Petron, G., Hirsch, A.I., Worthy, D.E.J., van der Werf, G.R., Randerson, J.T., Wennberg, P.O., Krol, M.C., Tans, P.P. (2007) An atmospheric perspective on North American carbon dioxide exchange:

CarbonTracker. Proceedings of the National Academy of Sciences of the United States of America 104, 18925-18930.

Peters, W., Krol, M.C., Van Der Werf, G.R., Houweling, S., Jones, C.D., Hughes, J., Schaefer, K., Masarie, K.A., Jacobson, A.R., Miller, J.B., Cho, C.H., Ramonet, M., Schmidt, M., Ciattaglia, L., Apadula, F., Heltai, D., Meinhardt, F., Di Sarra, A.G., Piacentino, S., Sferlazzo, D., Aalto, T., Hatakka, J., StrÖM, J., Haszpra, L., Meijer, H.A.J., Van Der Laan, S., Neubert, R.E.M., Jordan, A., RodÓ, X., MorguÍ, J.A., Vermeulen, A.T., Popa, E., Rozanski, K., Zimnoch, M., Manning, A.C., Leuenberger, M., Uglietti, C., Dolman, A.J., Ciais, P., Heimann, M., Tans, P.P. (2010) Seven years of recent European net terrestrial carbon dioxide exchange constrained by atmospheric observations. Global Change Biology 16, 1317-1337.

Peters, W., Miller, J.B., Whitaker, J., Denning, A.S., Hirsch, A., Krol, M.C., Zupanski, D., Bruhwiler, L., Tans, P.P. (2005) An ensemble data assimilation system to estimate CO_2 surface fluxes from atmospheric trace gas observations. Journal of Geophysical Research: Atmospheres 110, n/a-n/a.

Piao, S.L., Ciais, P., Friedlingstein, P., Peylin, P., Reichstein, M., Luyssaert, S., Margolis, H., Fang, J.Y., Barr, A., Chen, A.P., Grelle, A., Hollinger, D.Y., Laurila, T., Lindroth, A., Richardson, A.D., Vesala, T. (2008) Net carbon dioxide losses of northern ecosystems in response to autumn warming. Nature 451, 49-U43.

Pickers, P.A., Manning, A.C. (2015) Investigating bias in the application of curve fitting programs to atmospheric time series. Atmos. Meas. Tech. 8, 1469-1489.

Reinsch, C.H. (1967) Smoothing by spline functions. Numerische Mathematik 10, 177-183.

Rickard, G., Behrens, E. (2016) CMIP5 Earth System Models with biogeochemistry: A Ross Sea assessment. Antarctic Science 28, 327-346.

Riebesell, U., Körtzinger, A., Oschlies, A. (2009) Sensitivities of marine carbon fluxes to ocean change. Proceedings of the National Academy of Sciences 106, 20602-20609.

Rintoul, S.R. (2011) The Southern Ocean in the Earth System.

Rödenbeck, C., Le Quéré, C., Heimann, M., Keeling, R.F. (2008) Interannual variability in oceanic biogeochemical processes inferred by inversion of atmospheric O_2/N_2 and CO_2 data. Tellus B: Chemical and Physical Meteorology 60, 685-705.

Roscoe, H.K., Jones, A.E., Brough, N., Weller, R., Saiz-Lopez, A., Mahajan, A.S., Schoenhardt, A., Burrows, J.P., Fleming, Z.L. (2015) Particles and iodine

compounds in coastal Antarctica. Journal of Geophysical Research: Atmospheres 120, 7144-7156.

Roy, T., Rayner, P., Matear, R., Francey, R. (2003) Southern hemisphere ocean CO_2 uptake: reconciling atmospheric and oceanic estimates. Tellus Series B-Chemical and Physical Meteorology 55, 701-710.

Rutgers van der Loeff, M.M., Cassar, N., Nicolaus, M., Rabe, B., Stimac, I. (2014) The influence of sea ice cover on air-sea gas exchange estimated with radon-222 profiles. Journal of Geophysical Research: Oceans 119, 2735-2751.

Sabine, C.L., Feely, R.A., Gruber, N., Key, R.M., Lee, K., Bullister, J.L., Wanninkhof, R., Wong, C.S., Wallace, D.W.R., Tilbrook, B., Millero, F.J., Peng, T.-H., Kozyr, A., Ono, T., Rios, A.F. (2004) The oceanic sink for anthropogenic CO_2. Science 305, 367-371.

Sallee, J.-B., Matear, R.J., Rintoul, S.R., Lenton, A. (2012) Localized subduction of anthropogenic carbon dioxide in the Southern Hemisphere oceans. Nature Geosci 5, 579-584.

Sallée, J.B., Shuckburgh, E., Bruneau, N., Meijers, A.J.S., Bracegirdle, T.J., Wang, Z. (2013) Assessment of Southern Ocean mixed-layer depths in CMIP5 models: Historical bias and forcing response. Journal of Geophysical Research: Oceans 118, 1845-1862.

Simmonds, I., Keay, K., Lim, E.-P. (2003) Synoptic Activity in the Seas around Antarctica. Monthly Weather Review 131, 272-288.

Smith, R., Jones, P., Briegleb, B., Bryan, F., Danabasoglu, G., Dennis, J., Dukowicz, J., Eden, C., Fox-Kemper, B., Gent, P. (2010) The parallel ocean program (POP) reference manual ocean component of the community climate system model (CCSM) and community earth system model (CESM). Rep. LAUR-01853 141.

Stephens, B.B., Brailsford, G.W., Gomez, A.J., Riedel, K., Mikaloff Fletcher, S.E., Nichol, S., Manning, M. (2013) Analysis of a 39-year continuous atmospheric CO_2 record from Baring Head, New Zealand. Biogeosciences 10, 2683-2697.

Stephens, B.B., Keeling, R.F., Heimann, M., Six, K.D., Murnane, R., Caldeira, K. (1998) Testing global ocean carbon cycle models using measurements of atmospheric O_2 and CO_2 concentration. Global Biogeochemical Cycles 12, 213-230.

Takahashi, T., Sweeney, C., Hales, B., Chipman, D.W., Newberger, T., Goddard, J.G., Iannuzzi, R.A., Sutherland, S.C. (2012) The changing carbon cycle in the Southern Ocean. Oceanography 25, 26-37.

Taylor, K.E. (2001) Summarizing multiple aspects of model performance in a single diagram. Journal of Geophysical Research: Atmospheres 106, 7183-7192.

Taylor, K.E., Stouffer, R.J., Meehl, G.A. (2012) An Overview of CMIP5 and the Experiment Design. Bulletin of the American Meteorological Society 93, 485-498.

Thoning, K.W., Tans, P.P., Komhyr, W.D. (1989) Atmospheric carbon dioxide at Mauna Loa Observatory: 2. Analysis of the NOAA GMCC data, 1974–1985. Journal of Geophysical Research: Atmospheres 94, 8549-8565.

van der Laan-Luijkx, I.T., van der Velde, I.R., van der Veen, E., Tsuruta, A., Stanislawska, K., Babenhauserheide, A., Zhang, H.F., Liu, Y., He, W., Chen, H., Masarie, K.A., Krol, M.C., Peters, W. (2017) The CarbonTracker Data Assimilation Shell (CTDAS) v1.0: implementation and global carbon balance 2001–2015. Geosci. Model Dev. Discuss. 2017, 1-30.

van der Velde, I.R., Miller, J.B., Schaefer, K., van der Werf, G.R., Krol, M.C., Peters, W. (2014) Terrestrial cycling of $^{13}CO_2$ by photosynthes is, respiration, and biomass burning in SiBCASA. Biogeosciences 11, 6553-6571.

Varotsos, C.A., Tzanis, C.G., Sarlis, N.V. (2016) On the progress of the 2015–2016 El Niño event. Atmos. Chem. Phys. 16, 2007-2011.

Weller, R., Levin, I., Wagenbach, D., Minikin, A., (2007) The Air Chemistry Observatory at Neumayer Stations (GvN and NM-II) Antarctica. Alfred Wegener Institute for Polar and Marine Research & German Society of Polar Research, Bremerhaven, pp. 39-46.

Weller, R., Schmidt, K., Teinilä, K., Hillamo, R. (2015) Natural new particle formation at the coastal Antarctic site Neumayer. Atmospheric Chemistry and Physics 15, 11399-11410.

Wood, S. (2006) Generalized additive models: an introduction with R. CRC press.

Zickfeld, K., Fyfe, J.C., Eby, M., Weaver, A.J. (2008) Comment on "Saturation of the Southern Ocean CO_2 sink due to recent climate change". Science 319, -.

CHAPTER 5 A SEVEN-YEAR RECORD OF CONTINUOUS ATMOSPHERIC O_2 AND CO_2 MEASUREMENTS FROM WEYBOURNE ATMOSPHERIC OBSERVATORY, U.K.

5.1. Introduction

The over-arching aim of this thesis was investigate the processes that control the variability of atmospheric CO_2, O_2 and APO on different spatial and temporal scales at two contrasting coastal locations. The Weybourne Atmospheric Observatory (WAO) is an existing mid-latitude atmospheric O_2 and CO_2 measurement station in the northern hemisphere established in 2008 (Wilson, 2012). In this chapter, I revise and extend the current WAO record to 2015 to allow a thorough investigation of processes that influence the inter-annual variability of the seasonal cycles and the growth rates of CO_2, O_2 and APO in Chapter 6. In this chapter, I will present my revision of the WAO record and present the seasonal cycles and growth rates of the species. In doing so, I derive a unique method for extracting a baseline from continuous atmospheric observations. I then compare the seasonal cycles and growth rates to other northern hemisphere stations and examine the similarities and differences with respect to the influence of regional to hemispheric scale carbon cycle processes. Whilst I also briefly discuss trends in the seasonal cycles over the time period in this chapter, the analysis of the trends will be the focus of Chapter 6.

WAO is a Regional Global Atmospheric Watch (GAW) station located on the North Norfolk Coast, United Kingdom (52º57'02''N, 1º07'19''E, 20 m asl; **Figure 5.1**). Established in 1992 by the University of East Anglia (UEA) (Penkett et al., 1999b), it has been one of the United Kingdom's primary measurement facilities for understanding the reactive chemistry of the lower the troposphere (Allan et al., 1999; Fleming et al., 2006; Forster et al., 2012; Penkett et al., 1999a). The station currently collects high-precision, long-term *in situ* measurements of atmospheric carbon dioxide (CO_2), oxygen (O_2) (the focus of this chapter), carbon monoxide (CO), methane (CH_4), nitrous oxide (N_2O) sulphur hexafluoride (SF_6) tropospheric ozone (O_3) and molecular hydrogen (H_2), in addition to routine meteorological parameters. In 2016, the station became a part of the National Centre for Atmospheric Sciences (NCAS) Atmospheric Measurement Facility (AMF)[14].

The measurement building sits approximately 100m from the shoreline, 20m above mean sea level. Sample inlets are placed atop a 10m tall tower on the coastal facing

[14] https://www.ncas.ac.uk/en/about-amf

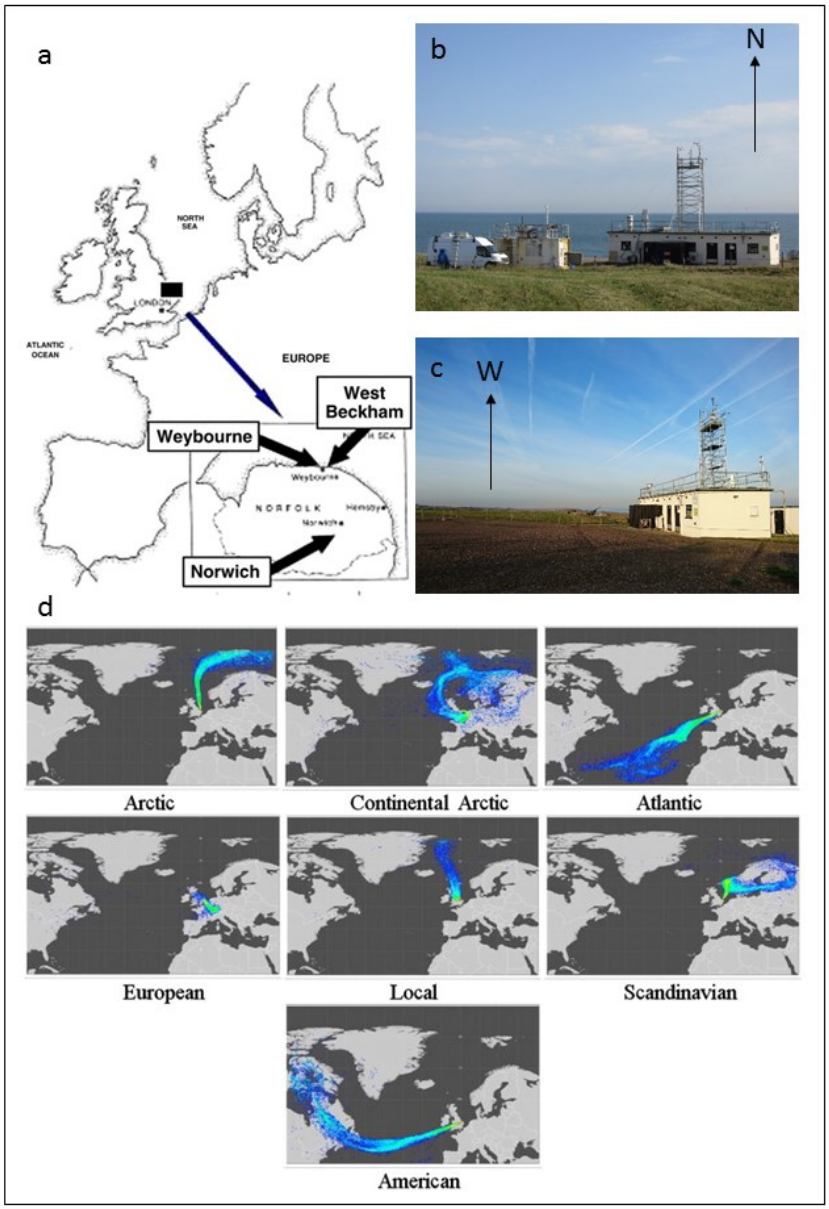

Figure 5.1. a: Location of the Weybourne Atmospheric Observatory (WAO) on the North Norfolk coast of the U.K (adapted from Fleming et al. (2012)). b: Northwards view from the observatory over the North Sea. c: Westward view from the observatory along the Norfolk coastline. d: Depiction of typical air masses arriving at the observatory. as determined by the NAME atmospheric dispersion model (adapted from Fleming et al. (2012)).

side of the building. Air is routinely sampled from Arctic, Atlantic, European, North Sea and UK air masses (**Figure 5.1**d) (Fleming et al., 2012) and so provides the ideal location to understand regional to hemispheric scale variations in tropospheric chemistry.

In 2008, Wilson (2012) installed a continuous, *in situ*, atmospheric O_2 and CO_2 measurement system that had been adapted for field station use from a previous shipboard system (Patecki and Manning, 2007b). This measurement system, and the knowledge gained from four years of continuous measurement, formed the blueprint for the

measurement system installed at the Halley Research Station (HBA) outlined in Chapters 2 and 3 of this thesis. During the construction and testing of the HBA system, much of my own knowledge and training came from working on the WAO system. Subsequently, from 2015, I became responsible for its maintenance and data quality control. It is from this work that I now present an extension to the WAO O_2 and CO_2 record originally presented by Wilson (2012).

Continuous, *in situ*, atmospheric O_2 and CO_2 observations at a site such as WAO allows investigation of many different carbon cycle processes at different spatial and temporal scales. For example, analysis of synoptic scale variability allows the separation of fossil fuel derived CO_2 from terrestrial biosphere processes (Pickers, 2016; Wilson, 2012). Regional scale atmospheric O_2 and CO_2 observation networks can lead to an understanding of fossil fuel emission gradients across highly populated areas such as Europe (van der Laan-Luijkx et al., 2010). Whilst, at the global scale, long term trends in O_2 and CO_2 allow one to quantify the global terrestrial and oceanic carbon sinks (Keeling et al., 1996b; Manning and Keeling, 2006a). However, whilst discussion and analysis of the inter-annual variability of the seasonal cycle of CO_2 and the inter-annual variability of the growth rate are discussed extensively in the literature (Bacastow, 1976; Bastos et al., 2013; Graven et al., 2013; Randerson et al., 1997) very few studies have applied such an analysis to O_2 and the related tracer Atmospheric Potential Oxygen (APO ~ $1.1O_2$ + CO_2, (Stephens et al., 1998)) (Bender et al., 1994a; Eddebbar et al., 2017; Hamme and Keeling, 2008; Rödenbeck et al., 2008). In Chapter 6 therefore, I analyse the variability in the seasonal cycles of O_2, CO_2 and APO over the full measurement period at WAO and frame this in the context of the inter-annual variability of the global cycle and its potential drivers. The scientific goals of such an analysis will therefore be introduced in Chapter 6. In this chapter however, I perform a thorough analysis of the WAO O_2, CO_2 and APO record in order for it to be reliably analysed in such a way, building upon the work of Wilson (2012).

In extending and reassessing the WAO O_2 and CO_2 record, I will compare to the original results for seasonal cycles and mean growth rates determined by Wilson (2012) shown in **Table 5.1**. Wilson (2012) identifies a number of caveats in both the derivation and interpretation of the seasonality and inter-annual variability of CO_2, O_2 and APO at WAO. Firstly, the shortness of the record. The data collection period ran from October 2007 to April 2012. However, owing to issues relating to the O_2 calibration scale of standards at the beginning of the record, only data collected in the 2009-2012 period were

used in the analysis (Wilson, 2012). In Chapter 4 of this thesis, I demonstrated the caveats of determining a mean climatological seasonal cycle from such a short data record. Consequently, in this work, I have extended the data record available for analysis back to June 2008 for O_2 and back to the initiation of the record for CO_2 at WAO. This was achieved through careful analysis of diagnostic data and manual observations recorded at the time of data collection. Moreover, at the time of writing, the quality controlled data record now extends through to the end of 2015, allowing 7 years of data to be used for analysis.

Secondly, Wilson (2012) made no attempt to extract a clean, background (or baseline) signal from the dataset before applying a curve fit to the data to decompose the time series into its respective seasonal and long-term trend components. Wilson (2012) did discuss this to be one of the main drawbacks of the analysis by demonstrating how the curve fit was computed through the middle of the data. Consequently, the resulting seasonal cycles and perceived inter-annual variations were likely to be unduly influenced by local sources and sinks of CO_2 and O_2 that impact the data record on diurnal to synoptic scale variability, such as local pollution and terrestrial biosphere fluxes. In this analysis therefore, I review the different techniques for deriving a baseline atmospheric signal from a time series, before assessing which are best suited for the WAO dataset and the proposed questions being asked of the data.

Finally, bringing together the above two points, the initial curve fitting routine used by Wilson (2012) ("HPspline", see Chapter 4, Section 4.2.5), may no longer be the most appropriate choice of curve fitting routine for the purpose of the following analysis. HPspline is good for extracting a climatological mean seasonal cycle, as was demonstrated in Chapter 4, and was therefore the most appropriate routine given the length of the record at the time. However, it may not be the most appropriate choice now given the extension of the data record and the type of analyses that can now be rigorously considered, such as the potential inter-annual variability in the growth rate and seasonal cycle. I therefore expand on my discussion of the appropriateness of different curve fitting routines for different datasets and scientific analyses introduced in Chapter 4.

By reassessing the curve fit and resulting time series decomposition in this chapter, I will do a full assessment of the variability in the seasonal cycles and the long terms growth rates of CO_2, O_2 and APO observed in Chapter 6. I will then investigate potential drivers of the variability observed.

Table 5.1. Seasonal amplitude and mean growth rate determined by Wilson (2012) at WAO for CO_2, $\delta(O_2/N_2)$ and APO for the period 2009-2012.

Species	Seasonal peak-to-peak amplitude	Mean growth rate
CO_2	14.9 ± 0.8 ppm	2.4 ppm yr^{-1}
$\delta(O_2/N_2)$	134.2 ± 7 per meg 8	-25 per meg yr^{-1}
APO	59.0 ± 5.6 per meg	-13 per meg yr^{-1}

5.1.1. Outline and objectives of this chapter

This chapter will present a revision and extension of the WAO O_2, CO_2 and APO data record (2008-2015) first presented by Wilson (2012). In Section 5.2, I discuss various methodological approaches to reliably determining a background (or baseline) signal at WAO before applying the most appropriate techniques to the dataset. I then go on to discuss the most appropriate curve fitting routines with respect to the goals of the analysis presented in Chapter 6. In Section 5.3, I discuss the seasonal cycle and inter-annual variability in the growth rate of each species and compare to the original results of Wilson (2012). Moreover, in contrast to Wilson (2012), I discuss WAO in the context of other northern hemisphere stations that are a part of the Scripps Institution of Oceanography (SIO) O_2 flask sampling network. This will highlight the additional insight into the spatial and temporal variability of global carbon cycle processes that can be gleaned from additional O_2 and CO_2 monitoring stations in distinct regions of the globe. Finally, I briefly discuss qualitatively the trends seen in the seasonal cycle and growth rates of CO_2, O_2 and APO over the measurement period (2008-2015) that will form the basis of a more quantitative analysis in Chapter 6.

5.2. Analysis methodology

5.2.1. Data collection

For those interested in a full description of the measurement system at WAO, readers are directed to Chapter 2 of Wilson (2012). However, there are only minor differences between the system installed at WAO and that installed at HBA. Readers wishing to understand the theory behind the measurements made at WAO are therefore directed to Chapter 2 of this thesis.

It is pertinent to briefly discuss the compatibility and reproducibility of the measurement system at WAO with respect to the World Meteorological Organisation

(WMO) goals introduced Chapter 3 of this thesis. From its inception up to June 2014, the WAO CO_2 data were declared on the SIO CO_2 scale and O_2 (expressed as the $\delta(O_2/N_2)$ ratio; see Chapter 2, Section 2.2.1) on the SIO O_2 S2 scale. After this date, however, we switched to the WMO X2007 scale with a new set of calibration standards. International efforts are afoot to reconcile these two scales (A. Manning, personal communication, 2017) and our own efforts to define the pre-June 2014 WAO standards on the WMO X2007 scale are also an ongoing task.

Nevertheless, cylinder inter-comparison exercises[15,16], whereby a cylinder of known atmospheric composition is circulated between different laboratories and field stations, show that WAO routinely achieves ± 0.1 ppm of the declared value for CO_2 and is comparable to other laboratories for $\delta(O_2/N_2)$ (Wilson, 2012). Furthermore, the internal reproducibility of the WAO system is shown in **Table 5.2**. Target Tank (TT) measurements (see Chapter 2, Section 2.4.4.2) show that the internal precision on CO_2 is below the internal reproducibility goal for the northern hemisphere (± 0.05 ppm) (Tans and Zellweger, 2016). For $\delta(O_2/N_2)$, we do not achieve the accepted internal reproducibility goal (± 2.5 per meg) determined by the O_2 measurement community (Tans and Zellweger, 2016). We are, however, comparable to other field station based $\delta(O_2/N_2)$ measurement systems (Kozlova and Manning, 2009; Pickers, 2016; Stephens et al., 2007; Thompson et al., 2007).

Table 5.2. Internal reproducibility of the Weybourne atmospheric O_2 and CO_2 measurement system as determined by repeated Target Tank measurements (run every 11 hours) over the entire measurement period (2008-2015). The final column also shows a second measure of internal reproducibility determined by Wilson (2012) from the 1σ standard deviation of successive ambient air measurements taken during a stable period when ambient variability was low.

Species	**Goal**	**Mean 1σ of all individual runs (2008-2015)**	**Mean 1σ of successive pairs of measurements (n= 30) (Wilson, 2012)**
CO_2 [ppm]	± 0.05	± 0.008 (n=5140)	± 0.03
$\delta(O_2/N_2)$ [per meg]	± 1.0 (± 2.5)	± 5.3 (n=5131)	± 2.0

[15] http://cucumbers.uea.ac.uk/

[16] http://gollum.uea.ac.uk/

5.2.2. Data filtering and baseline extraction

5.2.2.1. Background

The analysis of long term trends and seasonal variability of atmospheric gases, that are relevant to the carbon cycle, are typically done on datasets derived from either the United States (U.S.) National Oceanic and Atmospheric Administration (NOAA) Earth System Research Laboratory (ESRL) Global Monitoring Division (GMD) flask sampling network (e.g. Piao et al. (2008)) or the more widespread WMO GAW network (e.g. the World Data Centre for Greenhouse Gases (WDCGG)[17]). With respect to O_2, the SIO flask sampling network is the most widely used (Manning and Keeling, 2006a). The majority of the NOAA and SIO samples are collected once per week from sites deemed to sample only clean marine background air at a specific time of the day when the boundary layer is well mixed. In this way, each sample point from a particular flask is considered, for the most part, to represent a baseline signal (Masarie and Tans, 1995) upon which a time series decomposition can be performed.

WMO GAW stations, on the other hand, contain many more inland regional stations compared to NOAA/SIO and can therefore be more affected by local sources and sinks of a particular trace gas. To circumvent this, the WDCGG outlines their own method for deriving monthly mean data for global analyses. Briefly, this method requires monitoring stations that wish to be included to be within 3σ standard deviations of a latitudinal mean determined by fitting a loess model (Cleveland and Devlin, 1988) to all station data normalised to the South Pole (Masarie and Tans, 1995; Tsutsumi et al., 2009).

The WMO GAW stations, however, still only produce a monthly mean for data analysis which they take to represent a baseline signal upon which a time series decomposition can be performed without any additional filtering, in much the same way as the NOAA/SIO data. Extracting a baseline signal from a high frequency, continuous dataset from a regional site such as that at WAO on the other hand, requires a careful consideration of different extraction techniques that are appropriate to both the data and the station location.

Extraction of a baseline from high frequency data is typically done via a combination of filtering techniques that can be broadly characterised as either chemical, meteorological or statistical in their approach. Chemical filtering usually involves the

[17] http://ds.data.jma.go.jp/gmd/wdcgg/

examination of other trace gas concentrations to identify polluted air: using carbon monoxide (CO) to filter polluted periods in CO_2 for example (Tsutsumi et al., 2006).

Meteorological filters are perhaps the most widely used across the community and typically use knowledge of the local environment in combination with information on wind direction and wind speed to filter datasets. A trivial example is shown by Thoning et al. (1989) on continuous CO_2 from the Mauna Loa Observatory (MLO), Hawaii, whereby data are filtered out when the wind direction is such that the observatory is downstream of an active volcanic vent. A more rigorous meteorological approach considers air mass origin through the use of numerical transport models to determine when air may have advected over local source or sink regions (e.g. Ryall et al. (2001), Manning et al. (2011)).

Simple statistical filtering techniques typically consider the within hour and hour-to-hour variability by examination of the standard deviation over a particular averaging period for the raw data, with a high standard deviation indicating non background conditions (e.g. Thoning et al. (1989), Stephens et al. (2013)). A more rigorous methodology, however, was introduced by O'Doherty et al. (2001). To identify pollution on a particular day, a 2^{nd} order polynomial is fit to daily minima 60 days preceding and 60 following the day of investigation. The median of the difference between the data and the fit is then taken. The root mean square (RMS) of the difference of all data below this median is then calculated and any data that are more than 3σ standard deviations away from the median are flagged as polluted and removed, repeating the process for every single day in the dataset. The method is then repeated, but now data between 2σ and 3σ are flagged as possibly polluted. Those flagged as possibly polluted are deemed polluted if they are immediately adjacent to a polluted point (O'Doherty et al., 2001).

A different technique, but with a similar logic to the AGAGE method, was introduced by Novelli et al. (1998; 2003) and is built upon the curve-fitting procedure of Thoning et al. (1989). A 2^{nd} or 3^{rd} order polynomial, plus the sum of four harmonics, is fitted to the data. A low and high pass filter are then applied to the model residuals, adding those captured by the filter back into the function fit (see Chapter 4, Section 4.2.5). The resulting curve fit is then subtracted from the original data; any data points that lie more than 3σ of the residuals away from the curve are removed. This process is repeated until no more data points are removed.

More recently, Ruckstuhl et al. (2012) introduced a new method, based upon robust local regression (Cleveland, 1979) and modified from an existing technique to

remove baselines from chemical analytical spectra (Ruckstuhl et al., 2001). Termed the Robust Extraction of Baseline Signal (REBS), it is a non-parametric technique that assumes regional signals vary much more rapidly than the background signal and is comparable to the AGAGE method presented above. For more details see Ruckstuhl et al. (2012), however, briefly: Observed concentrations of a trace gas ($Y_{(ti)}$) are equal to the sum of the background concentration ($g_{(ti)}$), the contribution of a regionally polluted air mass ($m_{(ti)}$) and the measurement errors ($E_{(i)}$), which are assumed to be independent and Gaussian-distributed with a mean of zero and variance of σ^2. Non-background measurements ($Y_{(ti)}$) are therefore defined as those with $m_{(ti)} >> \sigma$ and assuming the regional signal is non negative ($m_{(ti)} \geq 0$), all of the outliers will be in the same direction and therefore a baseline can be derived. This is in contrast to the AGAGE method, which does not produce a baseline and is instead a method for identifying and removing polluted observations, typically assigning more data to be a non-background concentration than the REBS method (Ruckstuhl et al., 2012). In contrast to the Novelli et al. (1998; 2003) method, the REBS technique defines non-background conditions as those with residuals larger than the mode of the residual distribution. Whereas the Novelli et al. (1998; 2003) smooth curve fit considers the σ of all residuals and removes those that are more than 3σ away from the curve, which also leads to the lowest measurements being removed (Ruckstuhl et al., 2012).

Finally, a review of different filtering and baseline extraction techniques for CO_2 has been provided by Fang et al. (2015). Here, the authors compared and contrasted four different techniques that cover those discussed so far in this chapter: two that consider the concentration of other chemical species (methane (CH_4) and black carbon (BC)), one based on meteorological parameters and one using a statistical approach with REBS. The REBS method performed the least well of the four techniques, at least 1.7 ± 0.2 ppm higher in the baseline than the others. Furthermore, Fang et al. (2015) note two particular drawbacks of the REBS technique: (1) the baseline may be influenced by particularly noisy, raw data and (2) that REBS produces a high bias in the baseline during summer due to large nocturnal CO_2 values due to terrestrial biosphere respiration and is therefore not suitable for filtering at regional stations. The meteorological approach was found to be the most reasonable method for identifying non-background conditions. In this specific case, for example, Fang et al. (2015) excluded wind directions from the north due to a local village in this direction, rejected data when wind speeds were below 1.5 ms^{-1}, to minimise the influence of local sources and sinks and finally, only used data between

10:00 and 16:00 hours when the boundary layer was well mixed and to avoid diurnal influences.

Ultimately, there is no standard method for extracting a baseline from high frequency data sets. The choice of method eventually depends on the local conditions experienced at a particular station and the questions being asked of the data. The aim of the analysis presented here, both in this chapter and the next, is to investigate regional, hemispheric and global scale carbon cycle processes from the seasonal and long-term trend decomposition of the respective CO_2, $\delta(O_2/N_2)$ and APO time series at WAO. I will therefore use a variety of methods, as described in the following section.

5.2.2.2. Derivation of the Weybourne CO_2, $\delta(O_2/N_2)$ and APO baselines

To assess whether meteorological filtering would be feasible for the WAO time series and for the purpose of this analysis, I performed a bivariate analysis of concentration data with respect to wind direction and time of day (Carslaw et al., 2006) (Appendix C, **Figure 1.6**). Based on this analysis, clean background air for WAO could be defined as air arriving from the NW-NE. Although wind direction is not necessarily an indication of air mass origin (Fleming et al., 2012) it is likely that air originated from the north, potentially the Arctic, with a large amount of time spent over the North Sea. If the goal was to derive "clean marine background air" (such as in Stephens et al. (2013)) then it would be adequate to select data only from the NW to NE sector. However, for the purpose of this analysis, I feel that this would unfairly bias the interpretation of the WAO measurements. Data from this sector represents only 24.8% of the data. The goal is to investigate and explain the patterns of CO_2, O_2 and APO measured at WAO, be they global, hemispheric, or regional. Therefore for this analysis, I have chosen not to perform any metrological filtering.

Instead, I have chosen to determine a baseline using a combination of the statistical techniques discussed. Firstly, to remove very short term noise in the data, I average the two minute data points into 10 minute means. In order to remove the influence of both strong diurnal variability and pollution episodes, I extract the baseline using REBS method outlined above (Ruckstuhl et al., 2012). However, to compensate for the high bias seen in the baseline caused by high summer nocturnal CO_2 signals (and hence concurrent low O_2) (Fang et al., 2015; Ruckstuhl et al., 2012), I first filter the data following the method of Novelli et al. (1998; 2003) by applying a smooth curve fit to the

data consisting of a 3rd order polynomial plus the sum of 4 harmonics, with a low pass cut off value of 88 days and high pass cut off value of 667 days (Thoning et al., 1989) (See Chapter 4, Section 4.2.5). I then remove data that is more than 3σ standard deviations of the residuals away from the curve fit. I iteratively apply this until the standard deviation of the residuals changes by no more than 0.1 ppm, 0.5 per meg and 0.5 per meg (for CO_2, O_2 and APO, respectively; typically 3 to 4 passes).

Ruckstuhl et al. (2012) point out that the above mentioned method also removes the lowest observations, which in the case of their study, was not desirable as they were deriving baselines for CO and HFCs. For CO_2 and O_2 however, I would argue that this is desirable: A strong sink (source) signal for CO_2 (O_2) should not be considered as part of the baseline in much the same way that a strong source (sink) signal is not considered part of the baseline.

With the filtered data, I then take hourly means (applicable now, because the high bias has been removed) before applying the REBS method implanted by the RFBaseline function within the IDPMisc package in R (Ruckstuhl et al., 2009). I experimented with different values for the smoothing parameter (also known as the span) and the bi-weight function (b), which determines how much the function ignores high values. Each of the values used for the different species are shown in **Table 5.3**. The $\delta(O_2/N_2)$ and APO records, due to their negative values and trend, the "baseline" resides at the top of the data, rather than the bottom, and so, the data have to be inverted (made positive) before applying the technique.

Table 5.3. Parameters used in the implementation of the RFBaseline function to extract the baseline for each species.

Species	Span	Bi-weight function (b)	Number of Iterations
CO_2	0.005	0.01	(4,0)
$\delta(O_2/N_2)$	0.007	0.01	(4,0)
APO	0.008	0.01	(4,0)

5.2.3. Curve fitting and gap filling

The choice of curve fitting routine can significantly impact the interpretation of both the seasonal and long-term trend components of a data series (Pickers and Manning, 2015). It is therefore important to consider the choice of the routine in the context of the

data series and in the questions being asked of it. Two of the routines considered here, "CCGCRV" and "HPspline", are introduced in Chapter 4 Section 4.2.5. A third routine typically used in the atmospheric measurement community, "STL" (a procedure for Seasonal Trend decomposition using LOESS developed by Cleveland (1990)) is discussed in Pickers and Manning (2015), but not considered here for the reasons outlined below. The curve-fitting review paper of Pickers and Manning (2015) gives an extensive list of recommendations that I have considered when choosing the most appropriate routine for this analysis.

Firstly, it has been shown that typical curve fits derived from the HPspline routine are too stiff to capture short term variations and trends in the seasonal cycle if the shape and phasing of the data series are not relatively consistent. Instead, Pickers and Manning (2015) recommend using either CCGCRV or STL which have a particular skill in capturing short term variations in the seasonal cycle. Unfortunately, the current version of STL implemented in R cannot handle data gaps and there are significant gaps in the WAO time series in 2008-2009 and 2014. Some members of the greenhouse gas community consequently gap fill using HPspline before applying the STL routine (A. Manning, personal communication, 2016). However, I found the WAO APO time series to be too seasonally variable for HPspline to accurately fit a curve to the data (Appendix C, **Figure 1.7**). Consequently, I have opted to use the CCGCRV routine for all three species, which can handle data gaps and also captures the variability in seasonal trends that are the purpose of the analysis.

Secondly, Pickers and Manning (2015) argue against using the typical parameters used for any of the curve fitting routines and instead recommend choosing appropriate parameters based on the time series and the questions being asked of it. I have therefore not used the typical short and long term cut off values of 80 and 667, respectively, used by members of the community and chosen by Thoning et al. (1989). The 80 day short term cut off in particular, I would argue assigns too much variation to the seasonal component for my time series, owing to the shortness of the record (7 years). It may be applicable to longer data sets, where overall the seasonal cycle is likely to be relatively less variable, but not here. Instead, I have opted to use a value of 200 days to capture the seasonal component. This is more comparable to the "ideal" value found by Pickers and Manning (2015) for capturing seasonal variations in atmospheric time series. The choice in my long term cut off value, 720 days, on the other hand, is comparable to the typical value used and was chosen to so that long term trend values are captured on a time scale

of 2 years, which is more typical of the trend window used by NIWA colleagues applying the STL routine (P. Pickers, personal communication, 2016).

The results of the filtering, baseline and curve fitting are shown in **Figure 5.2**, along with the raw 2 minute data for each of the species considered at WAO. For O_2 and APO, I chose to omit data prior to June 2008 from the curve fitting routine as there were issues with the O_2 calibration scale during this period (Wilson, 2012). This visibly biases the result of the curve fit, resulting in a baseline that is inconceivably high biased compared to the baselines in the remaining years.

In the following section, I firstly discuss the carbon cycle processes behind the seasonality in each of the species and then go on to look at the inter-annual variability of the growth rate. I compare my results to that of Wilson (2012) whilst also discussing WAO in the context of three other northern hemisphere stations that span the tropics (20˚N) to the pole (82˚N). These are: Alert, Canada (ALT), Cold Bay, Alaska (CBA) and Mauna Loa Observatory, Hawaii (MLO). The data are provided by the SIO O_2 flask sampling network[18] and typically represent the measured mean of three flask replicates taken on given day, approximately twice a month. To extract the seasonal and long term trend components of the data I applied the CCGCRV curve fitting routine (Thoning et al., 1989) with low and high pass filters of 200 and 730 days, respectively, in order to compare them directly with the curve fit results of the WAO data. However, unlike the WAO data, no data filtering or baseline extraction was applied to the SIO data. This was deemed unnecessary since the flask samples are from clean marine background sampling sites that, by design, should avoid local pollution episodes and diurnal variability in the local terrestrial biosphere.

[18] http://scrippso2.ucsd.edu/data

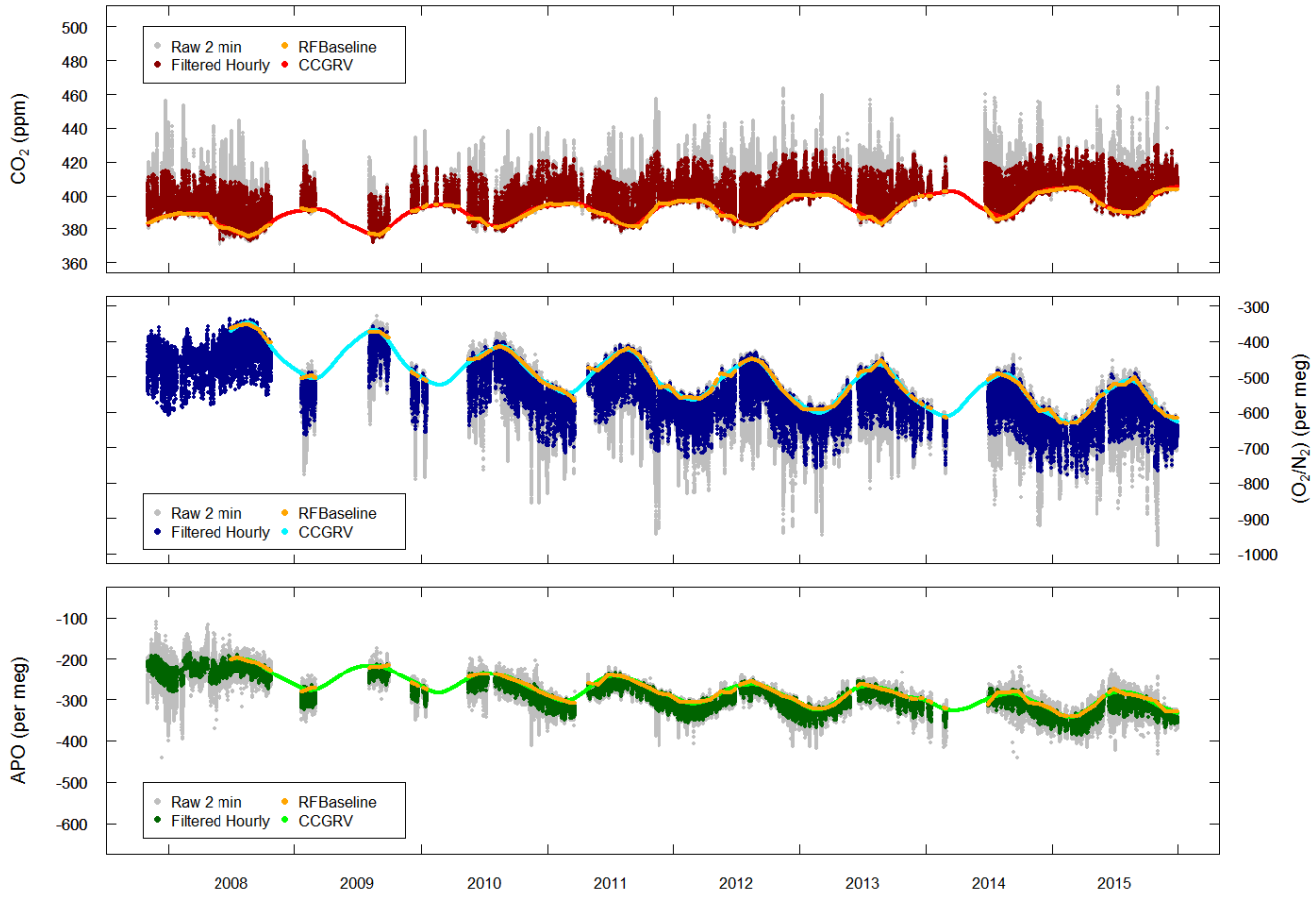

Figure 5.2. Results of the filtering, baseline extraction and curve fitting for CO_2, $\delta(O_2/N_2)$, and APO at WAO. Colours highlighting each stage are indicated in the figure. Raw 2 min: The original data recorded by the measurement system. Filtered Hourly: The Novelli et al. (1998; 2003) method applied to hourly means of the 2 minute data as outlined in the text. RFbaseline: The baseline signal extracted using the RFbaseline function of Ruckstuhl et al. (2012). CCGRV: the curve fit (Thoning et al., 1989) applied to the baseline signal as outlined in the text. Y-Axes are scaled so that CO_2, $\delta(O_2/N_2)$, and APO are visually comparable on a mole per mole basis.

5.3. Results and discussion

5.3.1. Seasonal cycles

5.3.1.1. Weybourne CO_2, $\delta(O_2/N_2)$ and APO seasonal cycle

Figure 5.3 shows the mean seasonal cyclse for CO_2, $\delta(O_2/N_2)$, and APO observed at WAO between 2008 and 2015. CO_2 has a mean amplitude of 15.2 ± 2.2 ppm with a broad, late winter-early spring maximum in February-March and a well-defined late

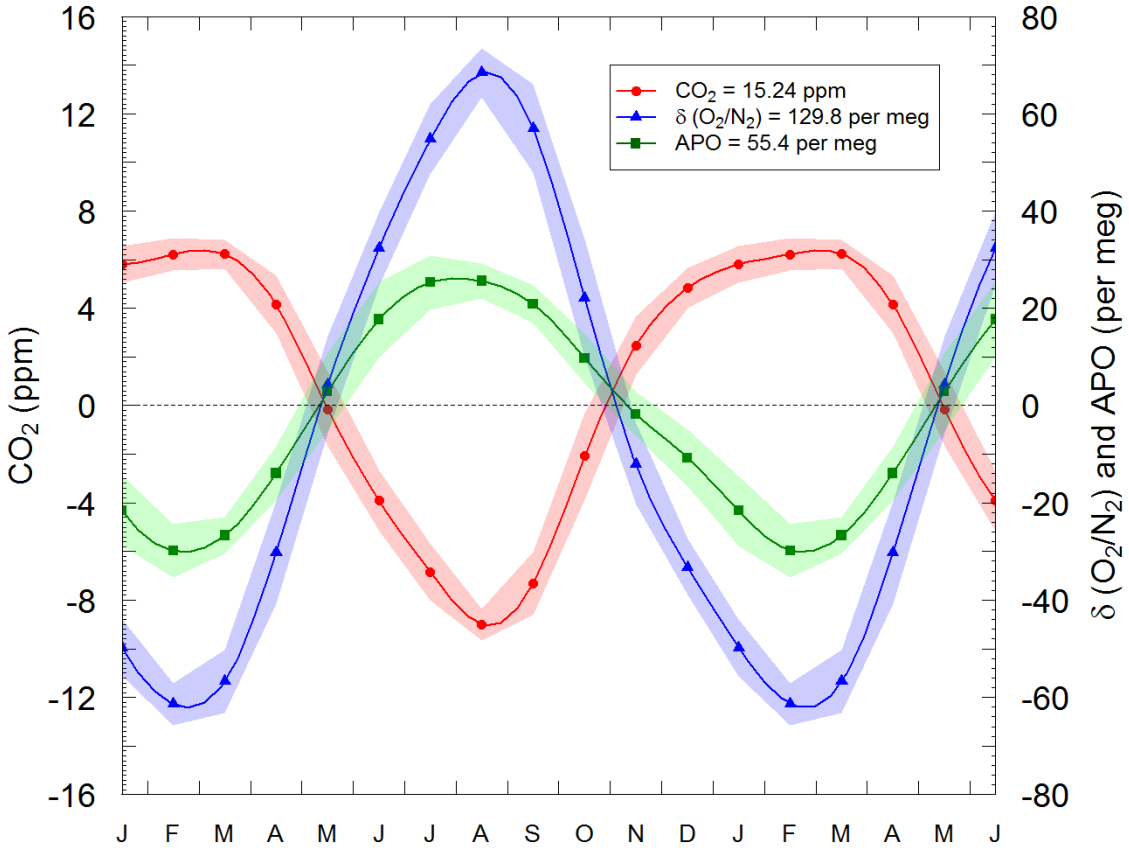

Figure 5.3. The seasonal cycle of atmospheric CO_2 (red points and lines, left y-axis), $\delta(O_2/N_2)$ (blue triangles and lines, right y-axis) and APO (green squares and lines, right y-axis) as determined from the CCGRV curve fit (see Section 0). The peak to peak amplitude of the seasonal cycles are shown in the key. Y-axes are scaled such that CO_2, $\delta(O_2/N_2)$ and APO are visually comparable on a mole per mole basis. The x-axis represents the first letter of individual months and the first 6 months are repeated to aid visual interpretation of the cycles. Individual points represent the monthly mean values of the curve fit. Lines represent a subsequent spline fit to the monthly data. Shaded error bands represent the 1σ standard deviation of the monthly mean value from all 7 years (2008-2015) and so represents real than month to month variability. The mean 1σ standard deviation from all months are: CO_2 = ± 1.1 ppm, $\delta(O_2/N_2)$ = ± 7.7 per meg and APO = ± 5.5 per meg.

summer minimum in August. Whereas $\delta(O_2/N_2)$ has a mean amplitude of 129.8 ± 15.4 per meg, with a well-defined late winter minimum in February and a well-defined late summer maximum in August. CO_2 and $\delta(O_2/N_2)$ are very well anti correlated and almost perfectly opposite in phase to each other.

The primary driver of the CO_2 seasonal cycle at WAO is the seasonally dependent competition between the photosynthesis and respiration reactions of the terrestrial biota in the northern hemisphere, particularly the northern boreal forests of Russia and Canada (Bolin and Keeling, 1963; Pearman and Hyson, 1980; Randerson et al., 1997). Since CO_2 is well mixed within the atmosphere (Carpenter, 1937), seasonal variability will largely be driven by hemispheric scale processes (Bolin and Keeling, 1963). From early spring until late summer, CO_2 is drawn down by the terrestrial biosphere with photosynthesis dominating over respiration due to the availability of light. As the season progresses, temperature has an increasing effect on respiration (Lloyd and Taylor, 1994) and, after the minimum in August, drives plant and soil respiration to dominate over plant photosynthesis, resulting in the release of CO_2 to the atmosphere. The rate of release, however, slows from November onwards due to cooler temperatures migrating south from the pole: Since temperature has a positive relationship with respiration (Lloyd and Taylor, 1994), its rate slows, resulting in the broad late winter peak seen in the CO_2 seasonal cycle. A small amount of the CO_2 seasonal cycle will be influenced by the CO_2 seasonality in the oceans (Heimann et al., 1989), however, since the timescales of air-sea gas exchange between the ocean and the atmosphere is on the order of 6 months to a year (Broecker and Peng, 1982b), the influence will be out of phase with respect to the terrestrial biosphere source and sink of CO_2 and relatively negligible (Heimann et al., 1989).

This is not the case for $\delta(O_2/N_2)$ on the other hand. The seasonal cycle is still predominantly driven by the terrestrial biosphere with O_2 release during the spring/summer months driven by photosynthesis, and O_2 drawdown in the autumn/winter months driven by respiration (Keeling et al., 1993; Keeling and Shertz, 1992). However, if the seasonal cycle was solely driven by the terrestrial biosphere, the cycle would be the same amplitude, phase and shape of the CO_2 seasonal cycle, but anti-correlated. Instead, on a mole per mole basis, the $\delta(O_2/N_2)$ seasonal amplitude is larger, by a factor of 1.78, than the CO_2 amplitude, implying that only 56% of the cycle is driven by the terrestrial biosphere. In contrast to CO_2, there is a significant ocean influence on the O_2 seasonal cycle (Keeling et al., 1993; Keeling and Shertz, 1992; Keeling et al., 1998b) due to the

short timescales for air-sea gas O_2 exchange (typically on the order of 6 weeks, (Broecker and Peng, 1982b)). During the spring/summer months, there is an outgassing of O_2 from the ocean to the atmosphere, driven by phytoplankton blooms responding to the increase in light availability and the shoaling of the mixed layer. During the autumn/winter months, the breakdown of the thermocline leads to mixing of the surface layer with deeper O_2 deficient waters, driving an in-gassing of O_2 from the atmosphere to the ocean (Keeling et al., 1993). This is entirely captured by the APO seasonal cycle which, by design, is conservative with respect to terrestrial biosphere processes and therefore represents the sum of CO_2 and O_2 ocean fluxes (Stephens et al., 1998). However, as mentioned previously, since the exchange of CO_2 between the ocean and the atmosphere is negligible on seasonal timescales (Broecker and Peng, 1982b), the APO seasonal cycle almost entirely represents ocean O_2 fluxes (Stephens et al., 1998).

The APO seasonal cycle has a mean amplitude of 55.4 ± 11.0 per meg and is characterised by a well-defined late winter minimum in February and a broad summer maximum in July-August. Summing the APO amplitude (~ocean O_2 fluxes) and the CO_2 seasonal amplitude (multiplied by the molar O_2:CO_2 exchange ratio for the terrestrial biosphere (O_2:CO_2 = 1.1, (Severinghaus, 1995)) (and dividing by the mean O_2 mole fraction: 0.2094 (Tohjima et al., 2005a)) gives: 55.4 + (15.2 * (1.1/0.2094)) = 135.5 per meg, which is within 4% of the actual $\delta(O_2/N_2)$ seasonal cycle observed at WAO. The reason why the actual $\delta(O_2/N_2)$ amplitude and the calculated $\delta(O_2/N_2)$ amplitude are not in 100% agreement is due to two important assumptions: Firstly, that the molar exchange ratio (O_2:CO_2) for the terrestrial biosphere is 1.1 (Severinghaus, 1995). Regionally however, this may change dependent on the vegetation type (Severinghaus, 1995). Secondly, summing the CO_2 and APO seasonal cycles assumes they are in phase with each other. Careful examination of the spring and autumn zero crossing (SZC, AZC, respectively) for the respective species shows this not to the case (**Figure 5.3** and **Table 5.4**). Moreover, the SZC and AZC days for each species do tell one information on the timing of the respective carbon cycle processes that drive the drawdown/release of each species to/from the atmosphere.

During spring, there is no significant difference between the zero crossings of CO_2 $\delta(O_2/N_2)$ and APO, although both $\delta(O_2/N_2)$ and APO very slightly precede that for CO_2 (**Figure 5.3**). In autumn on the other hand, there is a significant difference between CO_2 and $\delta(O_2/N_2)$ of approximately 5.5 days and the APO AZC is a further 10 days later than that for $\delta(O_2/N_2)$. However, caution must be applied in interpreting this since the $\delta(O_2/N_2)$

mean is within 1σ of the APO mean, which is comparatively large and there is therefore reflects more variability in APO AZC than in either CO_2 or $\delta(O_2/N_2)$. Nevertheless, the timings show that the ocean O_2 release period (defined by the APO release period) is longer than the terrestrial biosphere O_2 release period (as defined by the CO_2 uptake period) by ~ 17 days and that this difference is primarily driven by differences in the autumn.

To understand why the ocean exhibits a longer O_2 release period than the terrestrial biosphere, one must consider the individual factors that drive the carbon uptake period on land and the O_2 release period in the ocean. Firstly, both will equally be affected by the seasonal availability of light, therefore this cannot be driving the differences. On land, temperature is the primary driver behind the increase in respiration. This is also the case for the ocean biosphere. However, the length of the O_2 release period in the ocean will also depend on the timing of the breakdown in the seasonal thermocline. This will be dependent on temperature and on the amount of physical mixing induced by the increase in autumn/winter storms. Furthermore, the equilibration time for O_2 exchange between the ocean and the atmosphere is approximately 3 weeks (Broecker and Peng, 1982b). Therefore, I would propose that the ocean O_2 release period is longer than the terrestrial O_2 release period for three interacting reasons: Firstly, seasonal temperature changes are felt more rapidly on the land compared to the ocean due to the heat capacity of water, which results in a delayed ocean response to seasonal cooling, impacting the breakdown on the seasonal thermocline. Secondly, the breakdown on the thermocline and subsequent mixing with O_2 deficient waters is influenced by the amount of physical mixing induced by winter storms. Finally, the atmospheric signal of the above mentioned ocean processes will not be observed until the ocean-atmosphere system has equilibrated with respect to O_2, which will take approximately 3 weeks. This delay may not be apparent in comparison of the SZC for each species due to the prevalence of the snow pack ion the northern hemisphere, also delaying the drawdown of CO_2 and release of O_2.

The theory proposed is only speculation however, and may be influenced by the curve fitting procedure. To ascertain whether the mechanism I have proposed is robust, there are several strands of analysis which must be undertaken. Firstly, to determine whether the delayed APO AZC relative to O_2 and CO_2 is a reoccurring feature, a longer data record would be needed and a sensitivity analysis using different curve fitting routines with a range of parametrisations should be applied. Secondly, if the apparent staggering of the AZCs (and lack of in the SZCs) are due to the mechanisms described

above, one would need to examine years where (i) the northern hemisphere snow pack is more or less prevalent and (ii), winter mixing and stratification within the North Atlantic are more or less prevalent. This is deemed to be beyond the scope of the analysis presented in this thesis but will be examined in future work.

Table 5.4. The spring and autumn zero crossing days (SZC, AZC) for each species at WAO. The uptake/release period is determined by the difference between the respective crossing days. Errors are expressed as the 1σ standard deviation of the mean of zero crossing and uptake/release period of all years (n=7).

Species	Spring Crossing [Day of year]	Spring Crossing [Date]	Autumn Crossing [Day of year]	Autumn Crossing [Date]	Uptake/Release Period [Days]
CO_2	134.8 ± 5.5	15th May	301.0 ± 3.8	28th October	166.2 ± 6.7
$\delta(O_2/N_2)$	131.3 ± 2.9	11th May	306.6 ± 3.4	2nd November	175.3 ± 4.5
APO	132.8 ± 12.4	13th May	316.3 ± 15.3	12th November	183.5 ± 19.7

Table 5.5. Peak to peak amplitude of the climatological mean CO_2, $\delta(O_2/N_2)$ and APO seasonal cycles as determined by Wilson (2012), between 2009-2012, and in this study, determined over the period 2008-2015.

Species	Wilson (2012): 2009-2012	This study: 2008-2015
CO_2 [ppm]	14.9 ± 0.8	15.2 ± 1.1
$\delta(O_2/N_2)$ [per meg]	134.2 ± 7.8	129.8 ± 7.7
APO [per meg]	59.0 ± 5.6	50.7 ± 5.5

By examining the shape of the respective CO_2, $\delta(O_2/N_2)$ and APO seasonal cycles, one can qualitatively separate the terrestrial and oceanic influences on the O_2 seasonal cycle. Firstly, the well-defined late summer maximum of $\delta(O_2/N_2)$ has a correspondingly well-defined CO_2 minimum, whilst the APO maximum is relatively broad. This implies that the $\delta(O_2/N_2)$ maximum is predominantly driven by the terrestrial biosphere. Conversely, the well-defined O_2 minimum in late February has a correspondingly well-defined APO minimum, but a broad CO_2 maximum. If the $\delta(O_2/N_2)$ minimum were predominantly driven by the terrestrial biosphere, then one would expect a broad minimum, similar to the maximum of CO_2 caused by the slowdown of plant and soil respiration in northern hemisphere terrestrial biota driven by cold winter temperatures. Instead, the minimum follows that of APO and implies that ocean in-gassing of O_2 from

the atmosphere, driven by winter mixing of the surface layers, is the dominant process influencing the $\delta(O_2/N_2)$ minimum at WAO.

Finally, the amplitude of the respective seasonal cycles are shown in comparison to those determined by Wilson (2012) in **Table 5.5**. It is difficult to say whether the approach to applying a curve fit to the data without first determining a baseline would overestimate or underestimate the subsequent seasonal cycle. The curve fit will be equally biased by synoptic scale terrestrial biosphere and pollution fluxes in summer and winter, respectively. However, it is suffice to say that it would not be an accurate representation of the baseline seasonal cycle. Compared to this study, Wilson (2012) stated the amplitude of the CO_2 seasonal cycle as 0.3 ppm lower than that presented here, whilst the $\delta(O_2/N_2)$ and APO seasonal cycles were higher by 4.4 per meg and 8.3 per meg respectively. All are within the ± 1σ standard deviations declared here and so the differences are not significant.

5.3.1.2. Comparison with other northern hemisphere stations

The seasonal cycles for CO_2, $\delta(O_2/N_2)$, and APO, for all four stations are shown in **Figure 5.4**, respectively and are quantified in **Table 5.6**. Of the four stations, MLO is the most distinct. The CO_2 amplitude is < 40% of the amplitude of the other stations, whilst the $\delta(O_2/N_2)$ amplitude is < 35 % and the APO amplitude is < 30 %. With the exception of APO, MLO is out of phase by ~1-2 months with the other stations, with the CO_2 ($\delta(O_2/N_2)$) maximum (minimum) occurring in late spring and the CO_2 ($\delta(O_2/N_2)$) minimum (maximum) occurring in early autumn. I will first briefly discuss the reasons behind the shape and magnitude of the MLO seasonal cycles, before discussing WAO in the context of the other two, more similar, stations in more detail.

Table 5.6. Amplitude of the CO_2, $\delta(O_2/N_2)$ and APO seasonal cycles and the relative contribution of the ocean and terrestrial O_2 components recorded at each site. ALT = Alert, Canada; CBA = Cold Bay, Alaska; WAO = Weybourne, UK; MLO = Mauna Loa Observatory, Hawaii.

Station	Latitude	CO_2 amplitude [ppm]	$\delta(O_2/N_2)$ amplitude [per meg]	APO amplitude [per meg]	~ Ocean O_2 component (from APO) [%]	~ Land O_2 component (from CO_2) [%]
ALT	82˚N	15.82	130.4	47.2	36	64
CBA	55˚N	17.65	154.1	74.7	48	60
WAO	53˚N	15.24	129.8	50.7	39	62
MLO	20˚N	6.67	46.2	13.5	29	76

As discussed previously, the main driver of the CO_2, and to a lesser extent $\delta(O_2/N_2)$, seasonal cycles in the northern hemisphere is the terrestrial biosphere. However, there is very little seasonality in the tropical terrestrial biosphere (in contrast to mid to high latitudes) (Randerson et al., 1997), this is therefore reflected in the amplitude of the seasonal cycle of CO_2 and $\delta(O_2/N_2)$ at MLO. The remaining component of the $\delta(O_2/N_2)$, and all of the APO, seasonal cycle, is driven by marine productivity in summer and the breakdown of the thermocline and subsequent mixing in the winter. Again, the seasonality of these processes in the tropics is not well defined (Keeling et al., 1998b; Stephens et al., 1998). Additionally, the elevation of MLO (3397m) situates it above the marine boundary layer and so it is unlikely to sample surface fluxes.

The differences and similarities between the other three stations can inform us of the different carbon cycle processes occurring in three distinct areas of the mid to high latitude northern hemisphere. Broadly speaking, one can classify each of the remaining three stations as been representative of sampling (1). North Atlantic/Northern Europe air masses (WAO); (2). North Pacific/North American air masses (CBA) and (3). Arctic air masses (ALT). All stations broadly show the same shape and phasing, reflecting the mid to high latitude northern hemispheric influence on the seasonal cycles. However, subtle differences are apparent between the seasonal cycles which may reflect more regional influences defined by regional atmospheric transport which I will now discuss.

5.3.1.2.1. Timing of maxima, minima, and zero crossings

Of the three stations, WAO displays the earliest late winter-early spring CO_2 ($\delta(O_2/N_2)$) maximum (minimum) and SZC day in February-March and May, respectively (**Figure 5.4**). The CBA timings lag by approximately one month and ALT by another

month again. This implies an earlier onset of spring at WAO, followed by CBA and finally ALT. The late onset of spring at ALT is to be expected owing to Arctic seasonal irradiance and temperature patterns. However, both CBA and WAO are at similar latitude and so will receive the same seasonal irradiance. Instead, I propose this difference in the timing of spring between the two stations could be driven by their different climatology. Owing to the presence of the Gulf Stream in the North Atlantic, WAO is on average 4˚C warmer than CBA and hence drives an earlier spring in the terrestrial biosphere, since photosynthesis is both light and temperature dependent (Bryant and Frigaard, 2006). Contrastingly, the APO spring crossings are almost exactly in phase between WAO and CBA, whilst ALT lags by a month. This implies that light, rather than temperature, is the dominant driver of ocean productivity in all regions as one would expect, with WAO and CBA receiving the same seasonal irradiance and ALT receiving a seasonal irradiance pattern typical for its high latitude.

Furthermore, the timing of the late summer CO_2 ($\delta(O_2/N_2)$) minimum (maximum) for all three stations occur in August, again with WAO and CBA in phase but with ALT lagging by approximately 2 weeks. Moreover for the AZC, WAO and CBA cross almost simultaneously in October and ALT lags behind by almost a month. The earlier onset of spring at WAO, compared to CBA and the similar onset of autumn, indicate a longer terrestrial carbon uptake period at WAO compared to CBA (by 29 days), despite being located at a similar latitude. Again, I propose this is due to warmer annual temperatures at WAO. The later onset of spring and autumn at ALT would be expected owing to the seasonal temperature and irradiance profiles in Arctic locations.

Unlike WAO, the SZC for CO_2, $\delta(O_2/N_2)$ and APO are out of phase at CBA. APO zero crosses first at a similar time to CO_2, $\delta(O_2/N_2)$ and APO at WAO on day 130, followed by $\delta(O_2/N_2)$ on day 147, and finally CO_2 on day 167. This implies that, at CBA, the marine biosphere responds more quickly to the increase in the availability of light in spring than the terrestrial biosphere. Whereas, at WAO both respond at a similar time. I expect this reflects the cooler land temperatures and prevalence of the snowpack through late spring at CBA, compared to WAO.

The AZC on the other hand, all occur (approximately) on day 303 at CBA and is at similar time to that for CO_2 and $\delta(O_2/N_2)$ at WAO, but not APO, which lags CBA by approximately two weeks. Firstly, given the ocean-atmosphere three week equilibration timescale for O_2, (Broecker and Peng, 1982b) the simultaneous AZC for all three species actually implies that the marine biosphere responds sooner than does the terrestrial

biosphere. Secondly, the two week lag of autumn APO zero crossing at WAO implies the seasonal thermocline must breakdown sooner at CBA than at WAO, allowing the mixing of surface water with O_2 poor intermediate waters and hence stimulating O_2 drawdown from the atmosphere to the ocean. Again, I suspect this is due to differences in ocean temperatures between the two stations at this time of year caused by the presence of the Gulf Stream in the North Atlantic and evidenced by the differing climatology at the two stations.

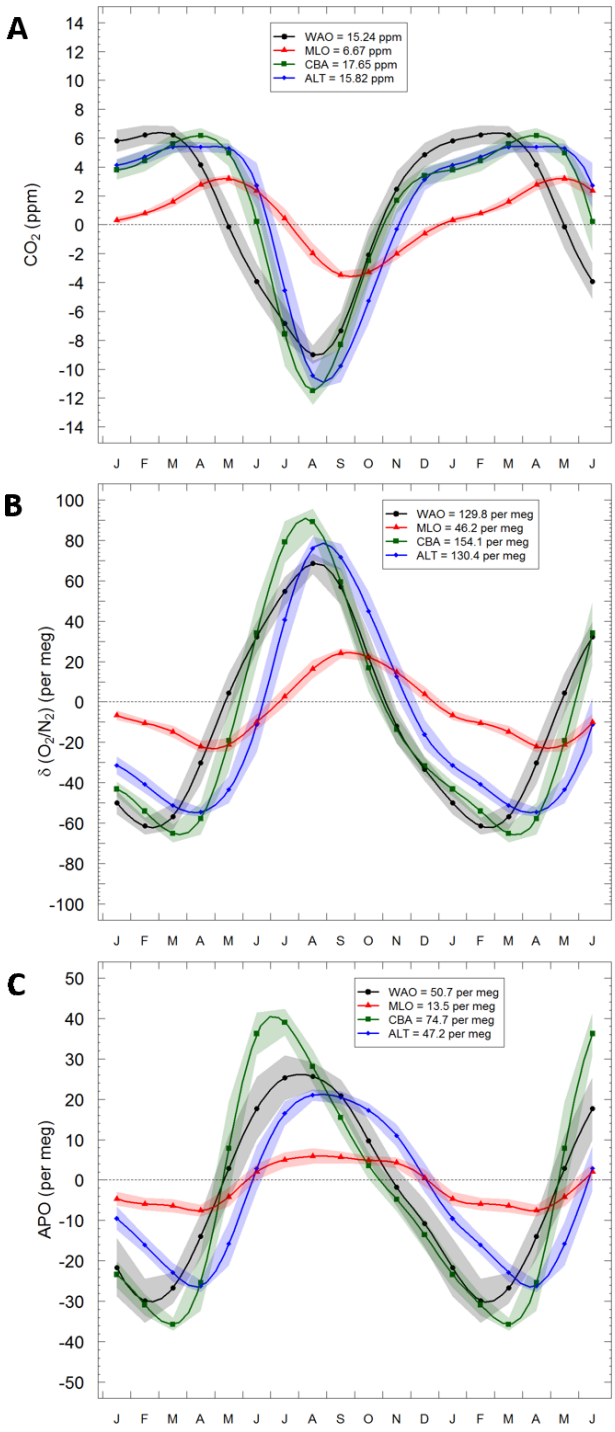

Figure 5.4. Seasonal cycles at each of the northern hemisphere stations considered in this analysis for (A) CO_2, (B) $\delta(O_2/N_2)$, and (C) APO. ALT = Alert (blue diamonds and lines), Canada; CBA = Cold Bay, Alaska (green squares and lines); WAO = Weybourne, UK (black points and lines); MLO = Mauna Loa Observatory, Hawaii (red triangles and lines). The peak to peak amplitude of the respective seasonal cycles are shown in the key. Y-axes are not scaled on a mole to mole basis. The x-axis represents the first letter of individual months and the first 6 months are repeated to aid visual interpretation of the cycles. Individual points represent the monthly mean values of the curve fit. Lines represent a subsequent spline fit to the monthly data. Shaded error bands represent the 1σ standard deviation of the monthly mean value from all 7 years (2008-2015) and so represent real than month to month variability.

5.3.1.2.2. Amplitude differences

Of the three stations, CBA has the largest amplitude in all three species. This implies both greater marine exchange (in APO) and greater terrestrial exchange (in CO_2 and O_2) compared to both ALT and WAO. Firstly, this reflects the proximity of CBA to the temperate northern boreal forests of Canada and Russia (Randerson et al., 1997). ALT on the other hand is much further north and will largely be influenced by the arctic tundra where the terrestrial biosphere is much less active and so the seasonal cycle will be attenuated. WAO, on the other hand, is much further from the equivalent northern boreal forests and will be more influenced by North Atlantic/European regional terrestrial signals. Secondly, the Bering Sea is known to be a region associated with strong seasonal air-sea gas exchange of O_2 (Battle et al., 2006; García and Keeling, 2001; Naegler et al., 2007) and CO_2 (Takahashi et al., 2002). Battle et al. (2006) suggest this is due to strong seasonal upwelling events stimulating phytoplankton blooms, subsequent drawdown of CO_2 and hence emission of O_2. This likely explains the large amplitude in APO displayed at CBA.

ALT and WAO show the most similar amplitude in the seasonal cycles of CO_2, $\delta(O_2/N_2)$ and APO, potentially because WAO also samples arctic air some of the time (**Figure 5.1c**) (Fleming et al., 2012) but they are out of phase for the late winter early spring CO_2 ($\delta(O_2/N_2)$) maximum (minimum), the spring and the autumn zero crossing, with ALT lagging WAO by 1-2 months. I expect that this reflects the later onset of spring expected at high northern latitude stations like ALT. The colder temperatures experienced by ALT in autumn would also delay the timing of terrestrial respiration becoming dominant over photosynthesis, compared to WAO with respect to the CO_2 and O_2 autumn crossing.

5.3.1.3. Inter-annual variability in the seasonal cycle at Weybourne

The seasonal cycle for each species in each year of the study period are shown in **Figure 5.5**. In contrast to the seasonal cycles shown in **Figure 5.3**, those in **Figure 5.5** represent hourly values from the de-trended curve fit, rather than monthly mean values centred on the middle of the month. As such, the finer details of the seasonal cycles can be drawn out and compared over different years. I will only give a brief qualitative discussion of the major features displayed in **Figure 5.5** in this chapter. This will form the basis of a more rigorous analysis in Chapter 6.

5.3.1.3.1. Qualitative assessment of the variability of Weybourne seasonal cycles

Figure 5.5A displays the evolution of the CO_2 seasonal cycle over the study period. The largest amount of variability between the years, as depicted by the 1σ standard deviation error bars about the monthly mean, is seen in October, close to the autumn zero crossing day. However, the longest, elevated amount of variability is seen during the spring drawdown period from April through to July. It also clear from **Figure 5.5**A that there is a trend towards an earlier autumn upward zero crossing day, particularly towards the end of the study period (2012-2015). Finally, of all of the years, 2011, appears to be the most anomalous, with a smaller winter peak compared to other years and a distinctly delayed timing in the spring downward zero crossing (~ 2 weeks later than the mean).

For $\delta(O_2/N_2)$ (**Figure 5.5**B) the variability mirrors that for CO_2, with the largest amount of variability seen in October, close to the autumn zero crossing day, whereas the longest elevated variability is seen during the spring-summer release period from April through to July. Again, there appears to be a trend towards an earlier autumn downward zero crossing, particularly towards the end of the study period, however, it does not appear to be as distinct as that seen for CO_2. Furthermore, there is a large amount of variability in the amplitude of the $\delta(O_2/N_2)$ cycle, with 2010 displaying the smallest amplitude and 2009 and 2013 displaying the largest.

Finally, for APO (**Figure 5.5**C), the largest amount of variability is seen from April through July, peaking in May. There is also elevated variability between December and February. The year 2013 almost displays a double peak, whilst 2014 is almost a month out of phase with the mean and displays a much smaller amplitude. However, the curve fit for 2014 may be unduly influenced by gaps in the data and so the bias in the curve fit, rather than ocean carbon cycle variability, may explain this particular anomalous year.

As discussed, analysis of the seasonal cycle of CO_2, $\delta(O_2/N_2)$ and APO can inform on the carbon cycle processes driving them: CO_2 is primarily driven by the terrestrial biosphere; APO is primarily driven by the air-sea gas exchange of O_2, driven by marine productivity and seasonal mixing of surface waters with deeper O_2 deficient waters; whilst $\delta(O_2/N_2)$ is driven by a combination of the two, in different proportions depending on the regional variability of the processes (see above). The qualitative assessment of the variability of the seasonal cycles over the study period highlights that there are clear trends in both the CO_2 and $\delta(O_2/N_2)$ autumn crossing days that may represent long term changes in the above mentioned carbon cycle processes. Moreover, it is clear that there

is a considerable amount of variability in the seasonal cycle of the individual species, with individual years identified as being anomalous. One of the aims of Chapter 6 is to provide a quantitative assessment of the variability of the phase, amplitude and shape of the seasonal cycle to ascertain how these processes may be changing with time.

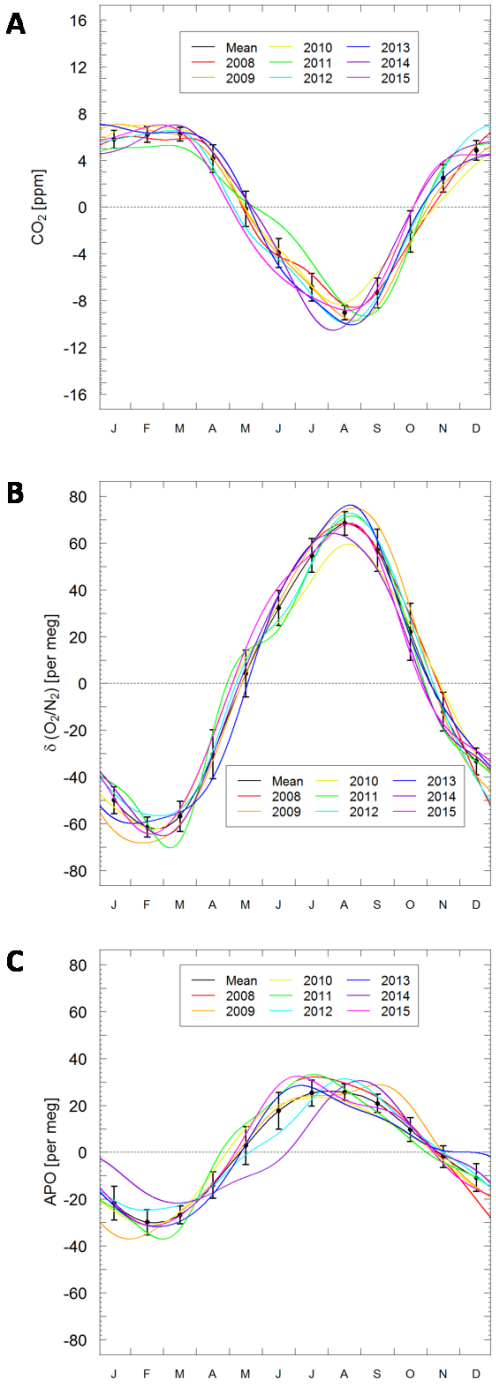

Figure 5.5. Annual seasonal cycles for CO_2, $\delta(O_2/N_2)$ and APO over the study period (2008-2015). The black points show the mean monthly seasonal cycle for all years with error bars denoting ± 1σ standard deviation. Colour coding for individual years are shown in the legend. Y axes are scaled so that they are visually comparable on a mole per mole basis. X-axes represent the first letter of the months of the year.

5.3.2. Inter-annual variability in the growth rate

5.3.2.1. General trends at WAO

The inter-annual variability in the growth rate, as determined by the derivative of the de-seasonalised curve fit to the data, for each species, are shown in **Figure 5.6** The long term, increasing trend in CO_2 (2.09 ppm yr^{-1}) and subsequent decreasing trend in $\delta(O_2/N_2)$ (-22.7 per meg yr^{-1}) and APO (-11.4 per meg yr^{-1}) are driven by fossil fuel burning, cement production land use change (Le Quéré et al., 2016). However, the inter-annual variability in the growth rate of these species are largely driven by the interaction of climate variability with both the land and ocean carbon sinks, with little impact from human emissions, which are relatively consistent over time (e.g. Le Quéré et al., 2016).

The growth rate in CO_2 and in $\delta(O_2/N_2)$ at WAO are very well anti-correlated, indicating the same carbon cycle process is likely to be responsible for the variability in both. However, the timing of the peaks and troughs in the growth rates are slightly out of phase in some instances. Although there will be little to no influence on the CO_2 growth rate from the ocean (Friedlingstein and Prentice, 2010; Jones et al., 2001) due to the timescales of air-sea CO_2 exchange (Broecker and Peng, 1982b), this is not the case for the $\delta(O_2/N_2)$ growth rate. For example, between 2008 to mid-2010, the trough and peak in CO_2 slightly precedes that for $\delta(O_2/N_2)$. Examination of the APO growth rate indicates that the $\delta(O_2/N_2)$ response is also responding to ocean changes which occur slightly later in time compared to CO_2. Conversely, in the period 2011-2013, the APO and consequently $\delta(O_2/N_2)$ peaks and troughs slightly precede that for CO_2, potentially indicative of a faster ocean response than the land to a particular process that may be driving the variability. Moreover, it is evident that the CO_2 and $\delta(O_2/N_2)$ growth rates becomes less variable from 2012 onwards, whereas APO maintain its variability.

Caution must be taken however, when interpreting the slight differences in the phasing between the respective growth rates. Differences in phasing may be due to errors

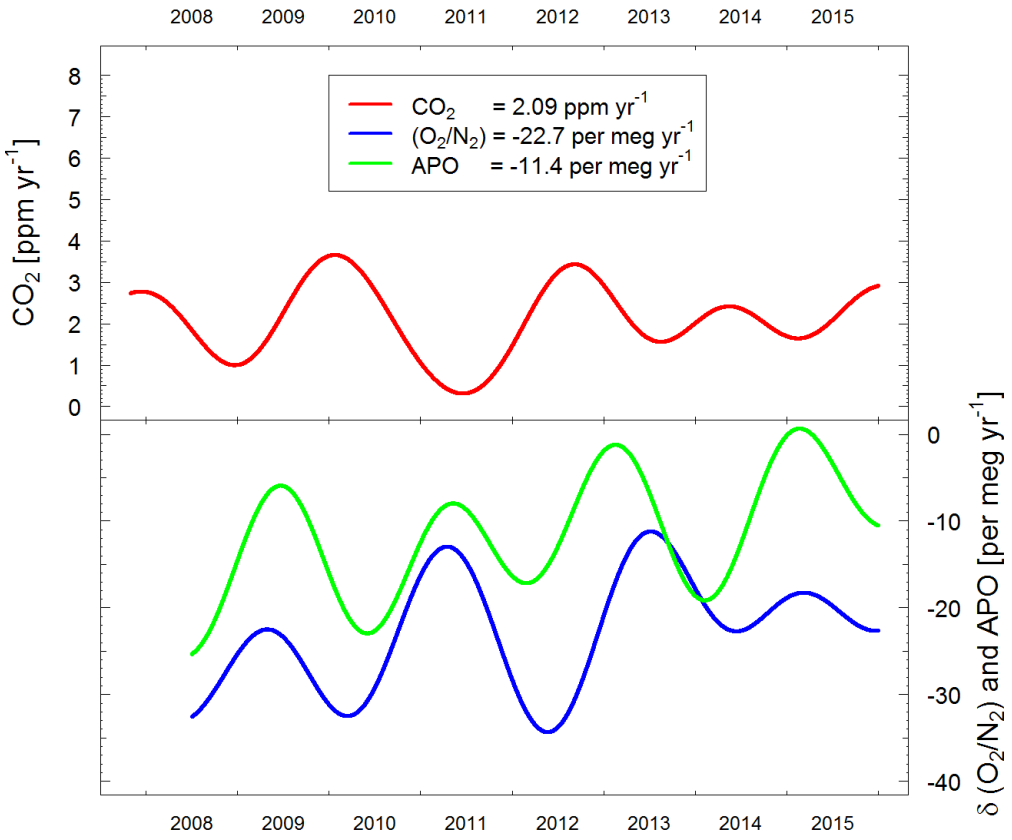

Figure 5.6. Inter-annual variability in the growth rate of CO_2 (top panel, left y-axis; red line), $\delta(O_2/N_2)$ (blue line) and APO (green line) (both on the bottom panel; right shared y-axis) observed at WAO over the study period (2008-2015). The key in the top panel depicts the mean growth rates observed over the study period for each species. Y-axes have been scaled so that they are visually comparable on a mole per mole basis. The x-axis represents the calendar year.

in the curve fitting procedure since each is treated individually and with individual baselines extractions. This is difficult to quantify however, and steps were taken to minimise curve fitting bias (Section 0)

5.3.2.2. Comparison with other northern hemisphere stations

To determine whether the inter-annual variability trends seen at WAO are reflective of hemispheric or regional scale phenomena, I have again compared the WAO results to that seen at the other the three other northern hemisphere stations introduced in Section 0 (**Figure 5.7**). For example, Wilson (2012), suggested the growth rates observed at WAO may have been driven by the variability in U.K. emissions. If this is true, then one would expect all three stations to display vastly different growth rates. On the hand, if hemispheric scale phenomenon are driving the trend in the growth rates, as shown by

Jones et al (2001), then one might expect the growth rates to be broadly similar across all four stations.

Up to 2012-2013, the CO_2 and $\delta(O_2/N_2)$ growth rates across all stations are in agreement, with only very slight phase offsets (on the order of a few months). This implies a hemispheric wide influence on the inter-annual variability of the growth rate observed

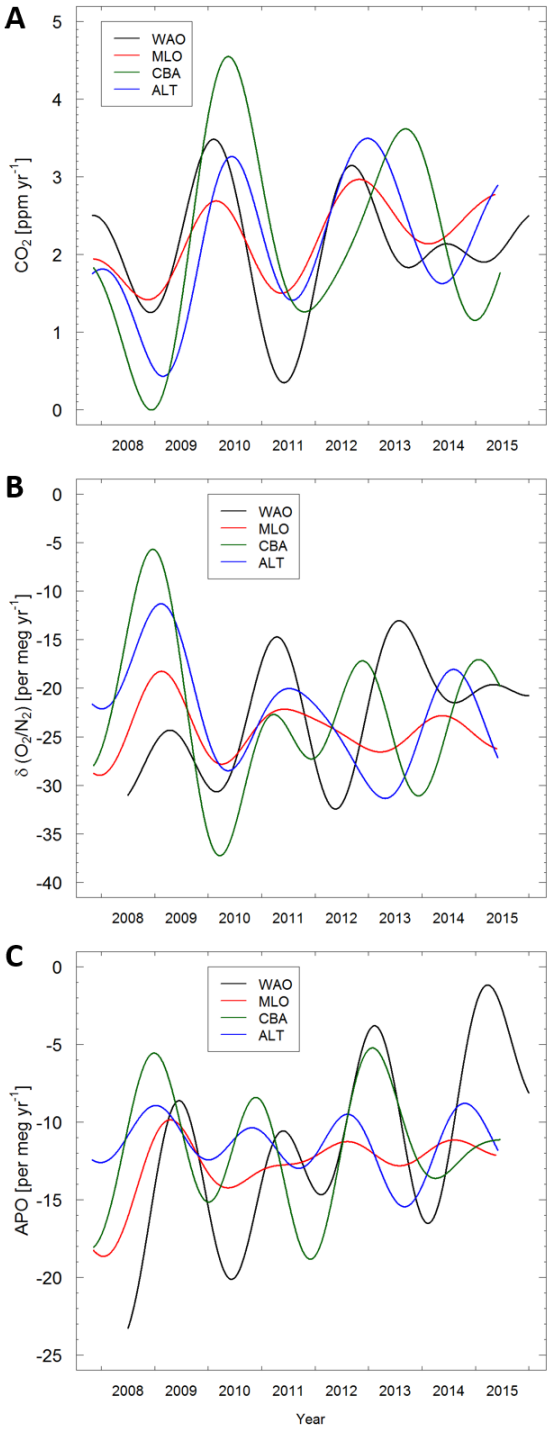

Figure 5.7. Inter-annual variability in the growth of (A) CO_2 (B) $\delta(O_2/N_2)$ and (C) observed at each of the four northern hemisphere stations considered for period (2008-2015).Note that y-axes are no longer visually comparable on a mole per mole basis. Each of the stations and their line colours are shown in the keys.

across the different stations which is to be expected due to the integration of carbon cycle process signals by atmospheric transport over the course of a year. However, after the beginning of 2013, each station becomes increasingly out of phase with one another. I therefore believe that strong hemispheric scale climate variability must be dominating the growth rate records of CO_2 and $\delta(O_2/N_2)$ up to 2012-2013. After this, however, the phasing disagrees more so, implying regional variability may play more of a role.

Contrastingly, the phasing in the APO inter-annual variability shows considerably more disagreement between stations. Although all stations, with the exception of MLO, show four peak/trough associations over the period, the phase offsets are considerable. Up to mid-2011, all stations show a clear peak in the growth rate between late-2008 and mid-2009, followed by a trough between late 2009-mid 2010, peaking again between late 2010 and mid-2011. This pattern is first recorded at CBA and ALT, followed by MLO and finally WAO, which lags CBA and ALT by ~6 months. Following this period, the subsequent peak between mid-2012 and early-2013 is first seen at ALT and MLO with CBA and WAO now in phase with each other, but lagging the other two stations by ~6 months. These phase offsets remain until the end of the record.

Unlike the CO_2 and $\delta(O_2/N_2)$ growth rates, APO likely reflects the combination of regional *and* global ocean responses to inter-annually varying regional and global phenomenon. For example, at the regional level, Battle et al. (2006) propose that the large amplitude in the APO seasonal cycle observed at CBA is due strong seasonal upwelling events stimulating phytoplankton blooms within the Bering Sea. The strength of these upwelling events is likely to vary from year to year which may help to explain the observed growth rate variability seen at APO at CBA. Moreover, Hamme and Keeling (2008) examined a globally integrated APO growth rate observed during the 1990s and proposed that much of the variations could be explained by the relative amount of convection, and hence deep water ventilation, in the North Atlantic and North Pacific basins in response to phenomenon such as the North Atlantic Oscillation (NAO. Finally, a recent study by Eddebbar et al. (2017) has highlighted the global response of APO to the El Niño–Southern Oscillation (ENSO. This should therefore also be considered when interpreting the growth rates at the individual stations presented here.

In the following chapter I will examine climatic phenomenon, such as the NAO and ENSO, influence on the CO_2, $\delta(O_2/N_2)$ and APO growth rates observed at WAO. It is beyond the scope of this thesis to extend this analysis to the other northern hemisphere stations considered above. Nevertheless, the CO_2 and $\delta(O_2/N_2)$ growth rates do display

broadly similar patterns across all four stations and therefore an analysis and explanation of the WAO record alone may be suffice to extend to the other stations. However, the same cannot be said for APO and this will be addressed in future work on the subject.

5.4. Summary and conclusions

The overarching aim of this thesis is to examine the variability of atmospheric CO_2, $\delta(O_2/N_2)$ and APO at different spatial and temporal scales. The primary aim of this chapter was to revise and extend the of the WAO continuous, *in situ*, atmospheric CO_2, $\delta(O_2/N_2)$ and APO record first presented by Wilson (2012). The record now represents seven years of data collected between 2008 and 2015 and can be used to investigate trends in the seasonal cycles and growth rates of the species. Chapter 6 examines these trends in detail. However, in this chapter I also discussed the seasonality and growth rates of the species observed at WAO in comparison with other northern hemisphere monitoring stations. I discussed the mechanisms behind the seasonality and the growth rates of each species and included a speculative discussion of the regional differences observed between the stations.

I began by discussing at length and implemented a rigorous method for baseline extraction in each of the respective species and subsequently decomposed the baselines using a curve fitting routine to extract seasonal and trend components. Using a combination of different techniques to extract the baseline has the merit of accounting for drawbacks associated with one particular technique. Filtering the data using the method of Novelli et al. (1998; 2003), by applying a smooth curve fit and then iteratively removing data that are more than 3σ away from the fit, removes the high bias that the REBS method is susceptible to. Applying the CCGCRV curve fitting routine to the baseline using a short term cut off value of 200 days and long term value of 720 days accurately captures the time series components that this analysis is interested in. I would recommend other researchers to follow this method for baseline extraction and encourage them to consider the type of curve fitting routine and it's parameterisation that is appropriate to the data analysis.

The seasonal cycles derived from the time series composition were then discussed. CO_2 has a mean amplitude of 15.2 ± 2.2 ppm with a broad, late winter-early spring maximum in February-March and a well-defined late summer minimum in August. Whereas $\delta(O_2/N_2)$ has a mean amplitude of 130 ± 15 per meg, with a well-defined late winter minimum in February and a well-defined late summer maximum in August. CO_2

and $\delta(O_2/N_2)$ are very well anti correlated and almost perfectly opposite in phase to each other and therefore broadly reflect the seasonally dependent competition between the photosynthesis and respiration reactions of the terrestrial biota in the northern hemisphere, particularly the northern boreal forests of Russia and Canada (Bolin and Keeling, 1963; Pearman and Hyson, 1980; Randerson et al., 1997). However, by examining the shape of the $\delta(O_2/N_2)$ seasonal cycle in the context of the observed APO (amplitude = 55 ± 11 per meg) and CO_2 seasonal cycles, I proposed that the $\delta(O_2/N_2)$ minimum at WAO is driven primarily by ocean exchange, whereas the maximum is characterised by terrestrial exchange. I did not examine whether this feature was true of other station seasonal data. This would be needed to determine whether the above assertion is true. For example, examining data sets with a similar balance of ocean and terrestrial influences to WAO and those that have a very different influence i.e. a predominantly ocean or a terrestrial influence.

I then compared the results of this analysis to the original analysis of Wilson (2012). The amplitudes of the seasonal cycles were within the error bounds stated of each analysis. Wilson (2012) did not attempt to extract a baseline for the data. This suggests that it may not be necessary to undergo the rigorous extraction method applied here before applying a curve fit. That said, a comparison of the different methods should be done across multiple stations and time periods before determining whether the baseline extraction is completely necessary for a time series decomposition. However, extraction of the baseline would help to more clearly define an event within synoptic scale data (not examined here).

Additionally I have compared the seasonal cycles observed at WAO to three other northern hemisphere atmospheric monitoring stations (ALT, CBA and MLO). CBA and WAO have a different amplitude and phase in the CO_2, $\delta(O_2/N_2)$ and APO cycles, despite being located at a similar latitude. I speculated that this reflects the proximity of each station to the drivers of the respective seasonal cycles (terrestrial biosphere and marine O_2 influences), and highlights the importance of atmospheric transport (in this case, the Gulf Stream) in modulating both the terrestrial and marine seasonal cycles of CO_2 and $\delta(O_2/N_2)$ at WAO compared to other northern hemisphere stations. Furthermore, ALT and WAO show a similar amplitude, despite different latitudes, but do show a lag in their phase. I speculated that ALT predominantly reflects the impact of the different irradiance regimes between the temperate and arctic latitudes.

To examine further the impact that regional atmospheric transport has on the seasonal cycles at the respective stations it would be beneficial to undertake a modelling analysis. Atmospheric transport could be controlled and varied at each of the stations. Predominant transport regimes could be "tagged" and atmospheric data filtered based on the air mass history. Examining the resultant seasonal cycles and their differences under different transport regimes could quantify this variable.

The application of a flexible curve fitting to the WAO CO_2, $\delta(O_2/N_2)$ and APO observation record has allowed the investigation of the variability in the seasonal cycle of each species over the study period. Here, I performed a qualitative assessment of the variability of the seasonal cycles over the study period and highlighted that there are clear trends in both the CO_2 and $\delta(O_2/N_2)$ autumn crossing days that may represent long term changes in the carbon cycle processes that drive them. Moreover, it is clear that there is a considerable amount of variability in the seasonal cycle of the individual species, with individual years identified as being anomalous. This analysis forms the basis of the analysis presented in the next chapter. The purpose of the Chapter 6, therefore, is to provide a quantitative assessment of the variability of the phase, amplitude and shape of the seasonal cycles at WAO to ascertain how these processes may be changing with time and what may be driving them.

Finally, I presented the inter-annual variability of the growth rate of CO_2, $\delta(O_2/N_2)$ and APO. The growth rate in CO_2 and in $\delta(O_2/N_2)$ at WAO are very well anti-correlated, indicating the same carbon cycle process is likely to be responsible for the variability in both. The timing of the peaks and troughs for CO_2 and $\delta(O_2/N_2)$, in addition to APO are potentially indicative of a differing terrestrial and ocean responses to a particular process that may be driving the variability. Moreover, it is evident that the CO_2 and $\delta(O_2/N_2)$ growth rates becomes less variable from 2012 onwards, whereas APO maintain its variability. This may be indicative of regional scale processes impacting APO and global scale processes impacting CO_2 and $\delta(O_2/N_2)$. To investigate this further I again compared the results observed at WAO to the other northern hemisphere stations discussed in this chapter. Up to 2012-2013, the CO_2 and $\delta(O_2/N_2)$ growth rates across all stations are in agreement, with only very slight phase offsets (on the order of a few months). However, after the beginning of 2013, each station becomes increasingly out of phase with one another. I proposed that strong hemispheric scale climate variability must be dominating the growth rate records of CO_2 and $\delta(O_2/N_2)$ up to 2012-2013. After this, however, the phasing disagrees more so, implying regional variability may play more of a role.

The results of this chapter will form the basis for the analysis in Chapter 6. In particular, I will attempt to answer the following questions: (1) How significant are the trends in the seasonal cycles of CO_2 and $\delta(O_2/N_2)$ observed at WAO and how do they compare to other northern hemisphere records? (2) What processes may be driving these trends? And finally (3) to what extent are the growth rates in CO_2, $\delta(O_2/N_2)$ and APO observed at WAO controlled by regional and hemispheric scale phenomenon such as the NAO and ENSO?

5.5. References

Allan, B.J., Carslaw, N., Coe, H., Burgess, R.A., Plane, J.M.C. (1999) Observations of the Nitrate Radical in the Marine Boundary Layer. Journal of Atmospheric Chemistry 33, 129-154.

Bacastow, R.B. (1976) Modulation of atmospheric carbon dioxide by southern oscillation. Nature 261, 116-118.

Bastos, A., Running, S.W., Gouveia, C., Trigo, R.M. (2013) The global NPP dependence on ENSO: La Niña and the extraordinary year of 2011. Journal of Geophysical Research: Biogeosciences 118, 1247-1255.

Battle, M., Mikaloff Fletcher, S., Bender, M.L., Keeling, R.F., Manning, A.C., Gruber, N., Tans, P.P., Hendricks, M.B., Ho, D.T., Simonds, C., Mika, R., Paplawsky, B. (2006) Atmospheric potential oxygen: New observations and their implications for some atmospheric and oceanic models. Global Biogeochemical Cycles 20, doi:10.1029/2005GB002534.

Bender, M., Ellis, T., Tans, P., (1994) Variability in the O_2/N_2 ratio of southern hemisphere air, 1991-1994: implications for the carbon cycle, Global Biogeochemical Cycles.

Bolin, B., Keeling, C.D. (1963) Large-scale atmospheric mixing as deduced from the seasonal and meridional variations of carbon dioxide. Journal of Geophysical Research 68, 3899-3920.

Broecker, W.S., Peng, T.H. (1982) Tracers in the Sea. Lamont Doherty Geological Observatory, Palisades, NY, USA.

Bryant, D.A., Frigaard, N.-U. (2006) Prokaryotic photosynthesis and phototrophy illuminated. Trends in Microbiology 14, 488-496.

Carpenter, T.M. (1937) The constancy of the atmosphere with respect to carbon dioxide and oxygen content. J. Amer. Chem. Soc. 59, 358-360.

Carslaw, D.C., Beevers, S.D., Ropkins, K., Bell, M.C. (2006) Detecting and quantifying aircraft and other on-airport contributions to ambient nitrogen oxides in the vicinity of a large international airport. Atmospheric Environment 40, 5424-5434.

Cleveland, R.B., Cleveland, W.S., McRae, J.E., Terpenning, I. (1990) STL: A seasonal-trend decomposition procedure based on loess. Journal of Official Statistics 6, 3-73.

Cleveland, W.S. (1979) Robust Locally Weighted Regression and Smoothing Scatterplots. Journal of the American Statistical Association 74, 829-836.

Cleveland, W.S., Devlin, S.J. (1988) Locally Weighted Regression: An Approach to Regression Analysis by Local Fitting. Journal of the American Statistical Association 83, 596-610.

Eddebbar, Y.A., Long, M.C., Resplandy, L., Rödenbeck, C., Rodgers, K.B., Manizza, M., Keeling, R.F. (2017) Impacts of ENSO on air-sea oxygen exchange: Observations and mechanisms. Global Biogeochemical Cycles 31, 901-921.

Fang, S.X., Tans, P.P., Steinbacher, M., Zhou, L.X., Luan, T. (2015) Comparison of the regional CO_2 mole fraction filtering approaches at a WMO/GAW regional station in China. Atmos. Meas. Tech. 8, 5301-5313.

Fleming, Z.L., Monks, P.S., Manning, A.J. (2012) Review: Untangling the influence of air-mass history in interpreting observed atmospheric composition. Atmospheric Research 104, 1-39.

Fleming, Z.L., Monks, P.S., Rickard, A.R., Bandy, B.J., Brough, N., Green, T.J., Reeves, C.E., Penkett, S.A. (2006) Seasonal dependence of peroxy radical concentrations at a Northern hemisphere marine boundary layer site during summer and winter: evidence for radical activity in winter. Atmos. Chem. Phys. 6, 5415-5433.

Forster, G.L., Sturges, W.T., Fleming, Z.L., Bandy, B.J., Emeis, S. (2012) A year of H_2 measurements at Weybourne Atmospheric Observatory, UK. Tellus B 64.

Friedlingstein, P., Prentice, I.C. (2010) Carbon-climate feedbacks: a review of model and observation based estimates. Current Opinion in Environmental Sustainability 2, 251-257.

García, H.E., Keeling, R.F. (2001) On the global oxygen anomaly and air-sea flux. Journal of Geophysical Research-Oceans 106, 31155-31166.

Graven, H.D., Keeling, R.F., Piper, S.C., Patra, P.K., Stephens, B.B., Wofsy, S.C., Welp, L.R., Sweeney, C., Tans, P.P., Kelley, J.J., Daube, B.C., Kort, E.A., Santoni,

G.W., Bent, J.D. (2013) Enhanced Seasonal Exchange of CO_2 by Northern Ecosystems Since 1960. Science 341, 1085-1089.

Hamme, R.C., Keeling, R.F. (2008) Ocean ventilation as a driver of interannual variability in atmospheric potential oxygen. Tellus Series B-Chemical and Physical Meteorology 60, 706-717.

Heimann, M., Keeling, C.D., Tucker, C.J., (1989) A three dimensional model of atmospheric CO_2 transport based on observed winds: 3. Seasonal cycle and synoptic time scale variations, Aspects of Climate Variability in the Pacific and the Western Americas. American Geophysical Union, pp. 277-303.

Jones, C.D., Collins, M., Cox, P.M., Spall, S.A. (2001) The Carbon Cycle Response to ENSO: A Coupled Climate–Carbon Cycle Model Study. Journal of Climate 14, 4113-4129.

Keeling, R.F., Najjar, R.P., Bender, M.L., Tans, P.P. (1993) What atmospheric oxygen measurements can tell us about the global carbon cycle. Global Biogeochemical Cycles 7, 37-67, doi:10.1029/1092GB02733.

Keeling, R.F., Piper, S.C., Heimann, M. (1996) Global and hemispheric CO_2 sinks deduced from changes in atmospheric O_2 concentration. Nature 381, 218-221.

Keeling, R.F., Shertz, S.R. (1992) Seasonal and interannual variations in atmospheric oxygen and implications for the global carbon cycle. Nature 358, 723-727, doi:710.1038/358723a358720.

Keeling, R.F., Stephens, B.B., Najjar, R.G., Doney, S.C., Archer, D., Heimann, M. (1998) Seasonal variations in the atmospheric O_2/N_2 ratio in relation to the kinetics of air-sea gas exchange. Global Biogeochemical Cycles 12, 141-163.

Kozlova, E.A., Manning, A.C. (2009) Methodology and calibration for continuous measurements of biogeochemical trace gas and O_2 concentrations from a 300-m tall tower in central Siberia. Atmospheric Measurement Techniques 2, 205-220.

Le Quéré, C., Andrew, R.M., Canadell, J.G., Sitch, S., Korsbakken, J.I., Peters, G.P., Manning, A.C., Boden, T.A., Tans, P.P., Houghton, R.A., Keeling, R.F., Alin, S., Andrews, O.D., Anthoni, P., Barbero, L., Bopp, L., Chevallier, F., Chini, L.P., Ciais, P., Currie, K., Delire, C., Doney, S.C., Friedlingstein, P., Gkritzalis, T., Harris, I., Hauck, J., Haverd, V., Hoppema, M., Klein Goldewijk, K., Jain, A.K., Kato, E., Körtzinger, A., Landschützer, P., Lefèvre, N., Lenton, A., Lienert, S., Lombardozzi, D., Melton, J.R., Metzl, N., Millero, F., Monteiro, P.M.S., Munro, D.R., Nabel, J.E.M.S., Nakaoka, S.I., O'Brien, K., Olsen, A., Omar, A.M., Ono,

T., Pierrot, D., Poulter, B., Rödenbeck, C., Salisbury, J., Schuster, U., Schwinger, J., Séférian, R., Skjelvan, I., Stocker, B.D., Sutton, A.J., Takahashi, T., Tian, H., Tilbrook, B., van der Laan-Luijkx, I.T., van der Werf, G.R., Viovy, N., Walker, A.P., Wiltshire, A.J., Zaehle, S. (2016) Global Carbon Budget 2016. Earth Syst. Sci. Data 8, 605-649.

Lloyd, J., Taylor, J.A. (1994) On the temperature dependence of soil respiration. Functional ecology 8, 315-323.

Manning, A.C., Keeling, R.F. (2006) Global oceanic and land biotic carbon sinks from the Scripps atmospheric oxygen flask sampling network. Tellus B 58, 95-116.

Manning, A.J., O'Doherty, S., Jones, A.R., Simmonds, P.G., Derwent, R.G. (2011) Estimating UK methane and nitrous oxide emissions from 1990 to 2007 using an inversion modeling approach. Journal of Geophysical Research: Atmospheres 116, n/a-n/a.

Masarie, K.A., Tans, P.P. (1995) Extension and integration of atmospheric carbon dioxide data into a globally consistent measurement record. Journal of Geophysical Research: Atmospheres 100, 11593-11610.

Naegler, T., Ciais, P., Orr, J.C., Aumont, O., RÖDenbeck, C. (2007) On evaluating ocean models with atmospheric potential oxygen. Tellus B 59, 138-156.

Novelli, P.C., Masarie, K.A., Lang, P.M. (1998) Distributions and recent changes of carbon monoxide in the lower troposphere. Journal of Geophysical Research-Atmospheres 103, 19015-19033.

Novelli, P.C., Masarie, K.A., Lang, P.M., Hall, B.D., Myers, R.C., Elkins, J.W. (2003) Reanalysis of tropospheric CO trends: Effects of the 1997–1998 wildfires. Journal of Geophysical Research: Atmospheres 108, n/a-n/a.

O'Doherty, S., Simmonds, P.G., Cunnold, D.M., Wang, H.J., Sturrock, G.A., Fraser, P.J., Ryall, D., Derwent, R.G., Weiss, R.F., Salameh, P., Miller, B.R., Prinn, R.G. (2001) In situ chloroform measurements at Advanced Global Atmospheric Gases Experiment atmospheric research stations from 1994 to 1998. Journal of Geophysical Research: Atmospheres 106, 20429-20444.

Patecki, M., Manning, A.C., (2007) First results from shipboard atmospheric O_2 and CO_2 measurements over the North Atlantic Ocean, Oceans 07. IEEE, Aberdeen, pp. 1-6, doi: 10.1109/OCEANSE.2007.4302351.

Pearman, G.I., Hyson, P. (1980) Activities of the global biosphere as reflected in atmospheric CO_2 records. Journal of Geophysical Research: Oceans 85, 4457-4467.

Penkett, S.A., Clemitshaw, K.C., Savage, N.H., Burgess, R.A., Cardenas, L.M., Carpenter, L.J., McFadyen, G.G., Cape, J.N. (1999a) Studies of Oxidant Production at the Weybourne Atmospheric Observatory in Summer and Winter Conditions. Journal of Atmospheric Chemistry 33, 111-128.

Penkett, S.A., Plane, J.M.C., Comes, F.J., Clemitshaw, K.C., Coe, H. (1999b) The Weybourne Atmospheric Observatory. Journal of Atmospheric Chemistry 33, 107-110.

Piao, S.L., Ciais, P., Friedlingstein, P., Peylin, P., Reichstein, M., Luyssaert, S., Margolis, H., Fang, J.Y., Barr, A., Chen, A.P., Grelle, A., Hollinger, D.Y., Laurila, T., Lindroth, A., Richardson, A.D., Vesala, T. (2008) Net carbon dioxide losses of northern ecosystems in response to autumn warming. Nature 451, 49-U43.

Pickers, P.A., (2016) New applications of continuous atmospheric O_2 measurements: meridional transects across the Atlantic Ocean, and improved quantification of fossil fuel-derived CO_2, School of Environmental Sciences. University of East anglia Norwich p. 291.

Pickers, P.A., Manning, A.C. (2015) Investigating bias in the application of curve fitting programs to atmospheric time series. Atmos. Meas. Tech. 8, 1469-1489.

Randerson, J.T., Thompson, M.V., Conway, T.J., Fung, I.Y., Field, C.B. (1997) The contribution of terrestrial sources and sinks to trends in the seasonal cycle of atmospheric carbon dioxide. Global Biogeochemical Cycles 11, 535-560.

Rödenbeck, C., Le Quéré, C., Heimann, M., Keeling, R.F. (2008) Interannual variability in oceanic biogeochemical processes inferred by inversion of atmospheric O_2/N_2 and CO_2 data. Tellus B: Chemical and Physical Meteorology 60, 685-705.

Ruckstuhl, A.F., Henne, S., Reimann, S., Steinbacher, M., Vollmer, M.K., O'Doherty, S., Buchmann, B., Hueglin, C. (2012) Robust extraction of baseline signal of atmospheric trace species using local regression. Atmos. Meas. Tech. 5, 2613-2624.

Ruckstuhl, A.F., Jacobson, M.P., Field, R.W., Dodd, J.A. (2001) Baseline subtraction using robust local regression estimation. Journal of Quantitative Spectroscopy and Radiative Transfer 68, 179-193.

Ruckstuhl, A.F., Unternaehrer, T., Locher, R., (2009) IDPmisc: Utilities of Institute of Data Analyses and Process Design, 2009 ed. available at: http://CRAN.R-project.org/package=, www.idp.zhaw.ch.

Ryall, D.B., Derwent, R.G., Manning, A.J., Simmonds, P.G., O'Doherty, S. (2001) Estimating source regions of European emissions of trace gases from observations at Mace Head. Atmospheric Environment 35, 2507-2523.

Severinghaus, J.P., (1995) Studies of the terrestrial O_2 and carbon cycles in sand dune gases and in Biosphere 2. Columbia University, New York, U.S.A., p. 148.

Stephens, B.B., Bakwin, P.S., Tans, P.P., Teclaw, R.M., Baumann, D.D. (2007) Application of a differential fuel-cell analyzer for measuring atmospheric oxygen variations. Journal of Atmospheric and Oceanic Technology 24, 82-94, doi:10.1175/JTECH1959.1171.

Stephens, B.B., Brailsford, G.W., Gomez, A.J., Riedel, K., Mikaloff Fletcher, S.E., Nichol, S., Manning, M. (2013) Analysis of a 39-year continuous atmospheric CO_2 record from Baring Head, New Zealand. Biogeosciences 10, 2683-2697.

Stephens, B.B., Keeling, R.F., Heimann, M., Six, K.D., Murnane, R., Caldeira, K. (1998) Testing global ocean carbon cycle models using measurements of atmospheric O_2 and CO_2 concentration. Global Biogeochemical Cycles 12, 213-230.

Takahashi, T., Sutherland, S.C., Sweeney, C., Poisson, A., Metzl, N., Tilbrook, B., Bates, N., Wanninkhof, R., Feely, R.A., Sabine, C., Olafsson, J., Nojiri, Y. (2002) Global sea-air CO_2 flux based on climatological surface ocean pCO_2, and seasonal biological and temperature effects. Deep-Sea Research Part II-Topical Studies in Oceanography 49, 1601-1622.

Tans, P.P., Zellweger, C., (2016) Report of the Eighteenth WMO/IAEA Meeting on Carbon Dioxide, Other Greenhouse Gases, and Related Measurement Techniques (GGMT-2015), in: Tans, P.P., Zellweger, C. (Eds.), San Diego, USA, pp. available at http://www.wmo.int/pages/prog/arep/gaw/gaw-reports.html.

Thompson, R.L., Manning, A.C., Lowe, D.C., Weatherburn, D.C. (2007) A ship-based methodology for high precision atmospheric oxygen measurements and its application in the Southern Ocean region. Tellus Series B-Chemical and Physical Meteorology 59, 643-653, doi:610.1111/j.1600-0889.2007.00292.x.

Thoning, K.W., Tans, P.P., Komhyr, W.D. (1989) Atmospheric carbon dioxide at Mauna Loa Observatory: 2. Analysis of the NOAA GMCC data, 1974–1985. Journal of Geophysical Research: Atmospheres 94, 8549-8565.

Tohjima, Y., Machida, T., Watai, T., Akama, I., Amari, T., Moriwaki, Y. (2005) Preparation of gravimetric standards for measurements of atmospheric oxygen and reevaluation of atmospheric oxygen concentration. Journal of Geophysical Research D: Atmospheres 110, 1-11.

Tsutsumi, Y., Mori, K., Hirahara, T., Ikegami, M., Conway, T.J., (2009) Technical Report of Global Analysis Method for Major Greenhouse Gases by the World Data Center for Greenhouse Gases, in: WATCH, W.M.O.G.A. (Ed.).

Tsutsumi, Y., Mori, K., Ikegami, M., Tashiro, T., Tsuboi, K. (2006) Long-term trends of greenhouse gases in regional and background events observed during 1998–2004 at Yonagunijima located to the east of the Asian continent. Atmospheric Environment 40, 5868-5879.

van der Laan-Luijkx, I.T., Karstens, U., Steinbach, J., Gerbig, C., Sirignano, C., Neubert, R.E.M., van der Laan, S., Meijer, H.A.J. (2010) CO_2, $\delta(O_2/N_2)$, and APO and APO: observations from the Lutjewad, Mace Head and F3 platform flask sampling network. Atmos. Chem. Phys. 10, 10691-10704.

Wilson, P., (2012) Insight into the Carbon Cycle from Continuous Measurements of Oxygen and Carbon Dioxide at Weybourne Atmospheric Observatory, UK, School of Environmental Sciences. Univeristy of East Anglia, Norwich, p. 155.

CHAPTER 6 EVIDENCE FOR CLIMATE DRIVEN VARIABILITY OF ATMOSPHERIC O_2 AND CO_2 FROM WEYBOURNE ATMOSPHERIC OBSERVATORY

6.1. Introduction

In Chapter 5, I presented a revision and extension of the atmospheric CO_2, $\delta(O_2/N_2)$ and APO record observed at the Weybourne Atmospheric Observatory (WAO), building upon the original work of Wilson (2012). From this analysis, there was a trend apparent in the autumn crossing day in both CO_2 and $\delta(O_2/N_2)$ observed over the measurement period (2008-2015). The purpose of this chapter was to therefore investigate the significance of this trend and determine what the drivers of such a trend may be.

Moreover, the inter-annual variability of the growth rate of all three species was considered, with CO_2 and $\delta(O_2/N_2)$ very well anti-correlated and therefore suggestive of a similar carbon cycle process driving the variability in both. This was also observed at three other northern hemisphere $\delta(O_2/N_2)$ and CO_2 monitoring stations and hence suggestive of a hemispheric scale response of the carbon cycle to a particular driving processes (or processes). APO, on the other hand, was more distinct in the inter-annual variability of its growth rate compared to $\delta(O_2/N_2)$ and CO_2 and was more variable across the three other stations considered. This was therefore suggestive of a combination of regional and hemispheric scale marine carbon cycle processes. Hence, the difference between the stations potentially reflected the spatial and temporal variability of global carbon cycle processes.

In the original analysis of Wilson (2012), the short data record (~4 years) precluded a thorough evaluation of changes in the either the amplitude or the zero crossing day (defined here in Section 6.2.3) of the seasonal cycle. Moreover, Wilson (2012) tentatively suggested that variability in the growth rate of CO_2 and $\delta(O_2/N_2)$ were down to the variability in U.K. fossil fuel emissions of CO_2. I demonstrated in the previous chapter that, since the variability in the growth rate of CO_2 and $\delta(O_2/N_2)$ observed at WAO was also observed at other northern hemisphere stations, I believe these will be more influenced by a larger scale response of the carbon cycle to a driving factor. However, the impact of fossil fuel CO_2 emissions will also be considered.

It has long been known that the variability in the CO_2 growth rate is largely influenced by climate variability, in particular the El Niño-Southern Oscillation (ENSO; defined in Section 6.2.5) (e.g. Bacastow, 1976; Bastos et al., 2013; Behrenfeld et al., 2001; McPhaden et al., 2006; Raupach et al., 2008). Bacastow (1976) first identified this link and found that in strong El Niño years the CO_2 growth rate was above average. At the time, Bacastow (1976) attributed this to variability in the ocean carbon cycle, however

it is now clear that this is in fact driven by changes in the terrestrial carbon cycle (Friedlingstein and Prentice, 2010; Jones et al., 2001). In particular, the warmer and drier conditions brought about by a strong El Niño result in decreased terrestrial productivity, an increase in plant and soil respiration and an increased occurrence of forest fires within the tropics. All of these responses simultaneously act to elevate the CO_2 growth rate above that driven by anthropogenic emissions alone (Jones et al., 2001; Raupach et al., 2008). The opposite is true during La Niña, the cooler and wetter conditions stimulate more carbon uptake by the terrestrial biosphere.

The dominance of the terrestrial carbon cycle response to ENSO therefore implies that the variability in the $\delta(O_2/N_2)$ growth rate, particularly in the northern hemisphere, will be driven by the same processes that drive the variability in CO_2, but will be the inverse of the CO_2 response due to the stoichiometric coupling between CO_2 and O_2 in the above mentioned carbon cycle processes.

Although much of the inter-annual variability in CO_2 and $\delta(O_2/N_2)$ will be driven by the response of the terrestrial carbon cycle to ENSO, the ocean carbon cycle still varies considerably in response to ENSO (Jones et al., 2001) and this will likely be reflected in the variability in the APO growth rate. During El Niño, decreased upwelling of carbon rich (and by extension O_2 poor) deep waters in the equatorial pacific results in the region becoming a sink for CO_2 (and therefore source of O_2) (Jones et al., 2001). During La Niña the reverse is true.

To date, there have only been three studies that have examined the global variability of APO (Eddebbar et al., 2017; Hamme and Keeling, 2008; Rödenbeck et al., 2008), the latter discussed most recently in Keeling and Manning (2014b). Rödenbeck et al. (2008) performed the first atmospheric inversion of global APO observations to assess the influence in the variability of ocean CO_2 and O_2 fluxes on the APO anomaly. The authors found that tropical APO fluxes were significantly correlated with the ESNO MEI index whereby ENSO induced changes in upwelling and therefore the ventilation of O_2 poor deep waters could explain the variability seen. Conversely, in a companion paper, Hamme and Keeling (2008) investigated the inter-annual variability of APO from observations and found them to be only weakly correlated with ENSO. However, the authors did find that a significant amount of the APO variability, particularly in the northern hemisphere, could be explained by ventilation of deep water masses within the North Atlantic and Western North Pacific Ocean basins (Hamme and Keeling, 2008). Moreover, the authors examined the variability in APO with the Arctic Oscillation (AO)

index and, although the variability was only weakly correlated, a large negative excursion in the AO index in 2001 corresponded with a negative excursion in the APO anomaly, indicative of ocean ventilation driven changes. Finally, a second atmospheric inversion of APO observations (Eddebbar et al., 2017) found a strong positive correlation with ENSO, thereby confirming the initial findings of Rödenbeck et al. (2008). Eddebbar et al. (2017) propose that APO variability is dominated by the ventilation effect in the central Pacific such that during El Niño anomalous O_2 outgassing is observed, whilst during La Niña anomalous ocean O_2 uptake is observed.

There has also been an extensive amount of work on the long term trends in the seasonal cycle in CO_2. All of these studies demonstrate an increase in in the peak to trough seasonal amplitude of CO_2 in northern latitudes (>45˚N) of up to 50% since the earliest records began in the 1960's (e.g. Graven et al., 2013; Keeling et al., 1996a). Two of these studies also reported an advance of the spring downward crossing of approximately 1 week since the 1950's, pointing to an increase in the length of the terrestrial biosphere growing season (or carbon uptake period) in response to spring warming (Keeling et al., 1996a; Myneni et al., 1997). However, Piao et al. (2008) demonstrated a trend towards an earlier autumn upward crossing day (-0.36 days yr^{-1}, 1980-2002) that was significantly negatively correlated with increasing autumn temperatures (-5.4 days $^{\circ}C^{-1}$, R= -0.61, $p = 0.002$) resulting in a shorter carbon uptake period, in contrast to the studies mentioned above. This work was corroborated by Barichivich et al. (2012), who note that despite the increase in the thermal growing season driven by an earlier spring onset and a later autumn termination, the increased temperatures in autumn actually lead to an earlier termination in the carbon uptake period.

Despite these early studies, more recent work has suggested a weakening temperature control, or at least a decoupling between increasing productivity and warmer spring temperatures (Piao et al., 2017; Piao et al., 2014). Forkel et al. (2016), assessed the different drivers of these trends in a modelling study and determined that they were driven by an interaction of climate (e.g. increased temperature) with vegetation dynamics (e.g. conversion of tundra shrub land to boreal forest). Clearly, different factors operating at different timescales appear to be controlling the response of the northern hemisphere terrestrial carbon cycle to current climatic change.

To date, no studies exist of the variability of the phase and amplitude in the seasonal cycle of $\delta(O_2/N_2)$ and APO over time. One would expect similar trends in the amplitude and phase shift of the $\delta(O_2/N_2)$ seasonal cycle to that for CO_2, given that a large

proportion of the $\delta(O_2/N_2)$ seasonal cycle is driven by the terrestrial biosphere at high northern latitudes (see Chapter 5) . However, it is yet to be seen if similar trends are evident in the marine carbon cycle, as demonstrated by the seasonal air-sea gas exchange of O_2 and captured in the variability of the APO seasonal cycle. Ocean temperatures have warmed in response to climate change (Levitus et al., 2005) and this may lead to increased stratification within the surface ocean (Capotondi et al., 2012). This may inhibit the breakdown of the seasonal thermocline in winter and subsequently impact productivity through a reduction in nutrient supply from depth in the spring and summer (Fu et al., 2016), hence influencing seasonal air-sea O_2 exchange.

Therefore, the WAO dataset, given that it is ideally placed in the northern hemisphere mid-to high latitude region, allows one to determine: firstly, whether there is a trend towards an earlier termination in the terrestrial carbon uptake period and an increase in the amplitude of CO_2 seasonal cycle. Secondly, whether these trends are also seen in the $\delta(O_2/N_2)$ seasonal cycle, and finally, whether similar trends are also occurring in the ocean carbon cycle as depicted by the seasonal cycle of APO.

6.1.1. Outline of this chapter

In this chapter, I will investigate the trends and drivers of behind the variability in the seasonal cycles and inter-annual growth rates of atmospheric CO_2, $\delta(O_2/N_2)$ and APO. Firstly, using the output from the curve fits to the WAO demonstrated in Chapter 5, I will extract the upwards and downwards zero crossing days (see Section 6.2.3) and the peak to peak amplitude of the respective seasonal cycles. I will then perform a simple regression of each of these metrics against various climatic variables and indices: temperature and precipitation at regional to hemispheric scales within the northern hemisphere, and the climate indices ENSO, AO and the North Atlantic Oscillation (NAO).

Secondly, in Section 6.3.2, I will perform a similar analysis of these indices against the growth rates for each species. I will investigate the drivers behind the variability in each of the species and therefore determine the carbon cycle response, as observed at WAO, to the various drivers.

6.2. Materials and methods

6.2.1. Atmospheric data

The WAO CO_2, $\delta(O_2/N_2)$ and APO data are described in Chapter 5 Section 5.2.1 and in Wilson (2012). In the station comparison in Section 6.3.1.2, I use data from the Scripps Institution of Oceanography (SIO) flask sampling network[19] at the following stations Alert, Canada (ALT), Cold Bay, Alaska (CBA) and Mauna Loa Observatory, Hawaii (MLO).

6.2.2. Curve fitting

The data filtering and subsequent curve fitting procedure applied to the WAO CO2, $\delta(O_2/N_2)$ and APO data are outlined in Section 0 of Chapter 5 and further details of the curve fit can be found in in Section 4.2.5 of Chapter 4. Briefly, however, the data were fit using the CCGCRV cure fitting routine (Thoning et al., 1989) using a short term (seasonal) cut off value of 200 days and a long term cut off (inter-annual variability) of 700 days.

6.2.3. Seasonal cycle metrics

The terminology for the quantifying aspects of the seasonal cycle have been referred to in previous chapter but are formally defined here. Firstly, the amplitude of the seasonal cycle is defined as the difference between the maximum and minimum values observed in the calendar year of the de-trended curve fit to the data. This is often referred to as the "peak-to-peak amplitude". Secondly, the spring and autumn zero crossing days (SZC and AZC, respectively) are defined as the day at which the de-trended curve fit to the data crosses the zero line (in the respective season within the calendar year) and values switch from being negative to positive or vice a versa, therefore indicating the switch between a source to, and sink from, the atmosphere. Finally, the carbon uptake or oxygen release period is defined as the difference between the SZC and AZC (over the summer months).

[19] http://scrippso2.ucsd.edu/data accessed 18th July 2017

6.2.4. Fossil fuel CO2 emissions data.

Annual, global fossil fuel CO_2 emissions data are from the Carbon Dioxide Information Analysis Center (CDIAC) (Boden, 2017)

6.2.5. Climate indices and variables

6.2.5.1. El Niño –Southern Oscillation (ENSO)

ENSO is the dominant mode of climate variability in the Pacific Ocean and represents and interaction between atmospheric winds and sea surface temperature (SST) trends within the region (Bjerknes, 1966) Under normal conditions, easterly trade winds push warm surface waters to the western Pacific, allowing the upwelling of deeper, cooler water in the east. The gradient in SST across the basin further drives a pressure gradient in the atmosphere resulting in winds that reinforce the initial state. During El Niño, however, the trade winds weaken and warm surface waters spread, via dowelling Kelvin waves, to the eastern basin where they deepen the thermocline and so suppress upwelling (McPhaden et al., 2006). During La Niña the reverse is true, the eastward trade winds are enhanced and a greater amount of upwelling is experienced across the eastern and equatorial Pacific.

To characterise the state of ENSO in this analysis I have used a monthly Multivariate ENSO index (MEI) (Wolter and Timlin, 1998), using data provided by the United States National Oceanic and Atmospheric Administration (NOAA)[20]. The MEI is based on six observed variables over the tropical Pacific: sea-level pressure, zonal and meridional components of the surface wind, SST, surface air temperature and total cloudiness fraction of the sky (Wolter and Timlin, 1998). The MEI is then calculated as the first Principal Component of all six observed fields combined for each of twelve bi-monthly seasons (Dec/Jan, Jan/Feb, etc). All seasonal values are then standardized with respect to each season and to a 1950-93 reference period (Wolter and Timlin, 1998).

6.2.5.2. Arctic Oscillation (AO)

The AO is the dominant mode of climate variability in the northern hemisphere and is characterised by the difference in pressure between the pole and ~45°N (Thompson et al., 2000). The positive phase is characterised from low pressure over the pole and higher pressure at 45°N, which results in strong winds circulating around the pole at 55°N

[20] (http://www.esrl.noaa.gov/psd/data/climateindices/list/)

that restricts cold air to the north. In its negative phase, this pressure difference decreases and the winds become weaker, allowing colder air to penetrate further south and results in increased storm tracks across the mid-latitudes (Thompson et al., 2000).

To characterise the phase of the AO, I have used the monthly AO index provided by NOAA[21]. This is defined as (described on the website link provided) the first leading mode of an Empirical Orthogonal Function analysis of monthly mean 1000 hPa height anomalies poleward of 20˚N.

6.2.5.3. North Atlantic Oscillation (NAO)

A similarly related, yet distinct mode of climate variability in the North Atlantic region to the AO, is the NAO (Ambaum et al., 2001; Zhou et al., 2001b). The NAO is characterised as the difference in sea-level pressure (SLP) between Iceland and the Azores and therefore determines the direction of low pressure weather systems across the North Atlantic (Hurrell, 1995). In its positive phase, when the SLP difference is high, northern Europe experiences warmer and wetter winters, whilst southern Europe experiences colder and drier conditions (Scaife et al., 2008). During the negative phase, when the SLP difference is low, the reverse is true.

To characterise the phase of the NAO, I have used the monthly NAO index provided by NOAA[22]. To determine this index, again as described in the website link provided, a Rotated Principal Component Analysis (Barnston and Livezey, 1987) is performed on monthly standardised 500 hPa height anomalies in the 20˚-90˚N region.

6.2.5.4. Temperature and precipitation data

The temperature and precipitation data are provided by the University of East Anglia's (UEA) Climate Research Unit (CRU) time series (TS) data set (CRU-TS 3.10)[23] with a 0.5˚ x 0.5˚ resolution (Harris et al., 2014). The data are compiled from the interpolation of global land-based meteorological observations (Harris et al., 2014). In the analysis presented here I have extracted mean values from the following regions: UK (local), North Atlantic (regional) and northern hemisphere (hemispheric). The latitude-

[21] http://www.cpc.ncep.noaa.gov/products/precip/CWlink/daily_ao_index/ao.shtml

[22] http://www.cpc.ncep.noaa.gov/products/precip/CWlink/pna/nao.shtml

[23] https://crudata.uea.ac.uk/cru/data/hrg/

longitude boundaries for each region are defined in **Table 6.1**. Data were provided up to the end of 2014 only.

Table 6.1. Definition of the regions of influence with respect to the CRU-TS 3.10 temperature and preciptiation data considered in this analysis.

Region	Latitude Range (˚N)	Longitude Range (˚E)
U.K.	50 to 60	-10 to 5
North Atlantic/Europe	40 to 80	-40 to 40
Northern hemisphere	30 to 90	-180 to 180

6.2.5.5. Data treatment

In the analysis of the seasonal cycle variability over the study period at WAO, only one data point per year for the SZC, AZC, uptake/release period and amplitude can be gathered. Thus, for the climatic data to be comparable, I must also distil each variable down to one annual data point. Therefore, for the temperature, precipitation and climatic indices data, I have derived the following means from the monthly datasets: annual, spring (March-April-May) and autumn (September-October-November).

In the analysis of the inter-annual growth rate variability against the climate indices, the monthly data are again not comparable to the derived growth rates, which are taken as the derivative of the trend, itself obtained by applying a high pass filter (700 days) (Thoning et al., 1989) to the original time series. Therefore, I have applied the curve fitting routine, described in Section 6.2.2, to the monthly indices data and extracted the long term trend, which is directly comparable to the growth rates. The same was applied to the fossil fuel emissions, except the first derivative of the trend was taken and therefore represents in the inter-annual variability in the growth rate of fossil fuel CO_2 emissions.

6.2.5.6. Statistical analyses

In the analysis of the seasonal cycle variability, I have opted to perform a monotonic trend analysis of each of the seasonal cycle metrics against time. In doing this, I am assuming that the data points are independent from one another and therefore not auto-correlated. I would argue each seasonal cycle is distinct from the preceding and succeeding cycles, particularly since there can only be one data point per year in the metrics described. In reality, however, this may not be strictly true.

In this analysis, the null hypothesis, H_0, is that no trend exists in each of the defined variables. The method of confirming this hypothesis and the level of significance

depends greatly on the characteristics of the data. Parametric tests, such as the Pearson correlation coefficient, R, are used when the data are normally distributed. The significance of the correlation or trend are then determined using a two tailed t-test. If the data are not normally distributed, then a non-parametric test is used, typically the Mann-Kendall test for significance, and the strength of the trend is expressed in terms of the Tau value (T) (which is analogous to the R value (Meals, 2011).

In the analysis of Piao et al. (2008), parametric tests were used to determine the trend with time and the correlation with climatic variables. The assumption of normality within the data is reasonable given the length of the data set (1980-2002) whereby variability in the seasonal cycle metrics will be normally distributed about the mean. Examination of the distribution of the AZC, SZC, uptake/release period and amplitudes at WAO, however, shows them to be non-normally distributed (not shown) and therefore the Mann-Kendall test for significance on the trend is more appropriate. This non-normality in the data can be expected given the short time period (2008-2015) and hence small number of data points (n=8).

However, in order to be directly comparable to the analysis of Piao et al (2008), I have discussed the WAO seasonal cycle trends and correlations with climatic variables in terms of the Pearson correlation coefficient, R, and its significance determined using the t-test. However, for transparency, I also state the strength of the relationships and its significance determined by the Mann-Kendall test. Hence, both R and Tau values and their respective P values are reported. I believe this is a useful exercise in demonstrating the pitfalls in choosing the correct statistical analyses with respect to short-term time series data as is common in the climate sciences.

In the second section, when correlating the growth rates with climatic indices, the assumption that there is no auto-correlation within the data is no longer valid. The growth rate of each species is derived from the trend, itself determined by applying a high pass filter to hourly data, whereby each data point will not be independent from the last or the next. The data will therefore be auto correlated. The same applies to each of the climate indices ENSO, AO, and NAO. Each of these are typically derived from daily atmospheric pressure anomalies (and others, with respect to ENSO, see Section 6.2.5.1), such that each observation will not be independent from the last or the next. Observing lagged correlations may also be significant, yet standard statistical tests are unable to handle this.

Ebisuzaki (1997) developed a non-parametric statistical test to determine the strength of a correlation between two auto-correlated time series which I will therefore

apply here. Briefly, 100000 synthetic time series are generated from the original with randomised phase lags upon which a regression is applied, via Monte Carlo simulations, and the correlation coefficients determined. Here, I use the function "surrogateCor" implemented in the "astrochron" R package (Meyers, 2014) originally designed for paleoclimate time series where autocorrelation is common (Baddouh et al., 2016). Furthermore, in applying the correct statistical test for the strength of the regression I have followed the same reasoning as in the seasonal analysis: The ENSO, NAO and AO indices over long periods of time would be expected to be normally distributed given that they are typically based on daily atmospheric pressure anomalies (see above) and so the parametric Pearson's correlation coefficient and the subsequent t-test for significance could be applied. However, as before, over a short time series such as presented here (2008-2015) and due to the smoothing of monthly values applied by the curve fitting routine, the data will be non-normally distributed and therefore the Mann-Kendall test would be more appropriate. Consequently, I report both the R and Tau values as before

Finally, I report P values at the ~1.5 σ standard deviation level, which corresponds to a 85% confidence level. ($p < 0.15$) with respect to the Pearson correlation coefficient and t-test for significance. True significance is typically determined at the 95% confidence level ($p < 0.05$). However, I consider all relationships with $p < 0.15$ here.

6.3. Results and discussion.

6.3.1. Inter-annual variability in the seasonal cycle at Weybourne

6.3.1.1. Phase shift

The extracted AZC, SZC and uptake/release period for $\delta(O_2/N_2)$ and CO_2 from the curve fits are displayed in **Figure 6.1**. The results vary considerably from year to year. At WAO, both CO_2 and $\delta(O_2/N_2)$ show negative trends in the SZC, AZC and the uptake/release period over the study period. APO, on the other hand, shows a positive

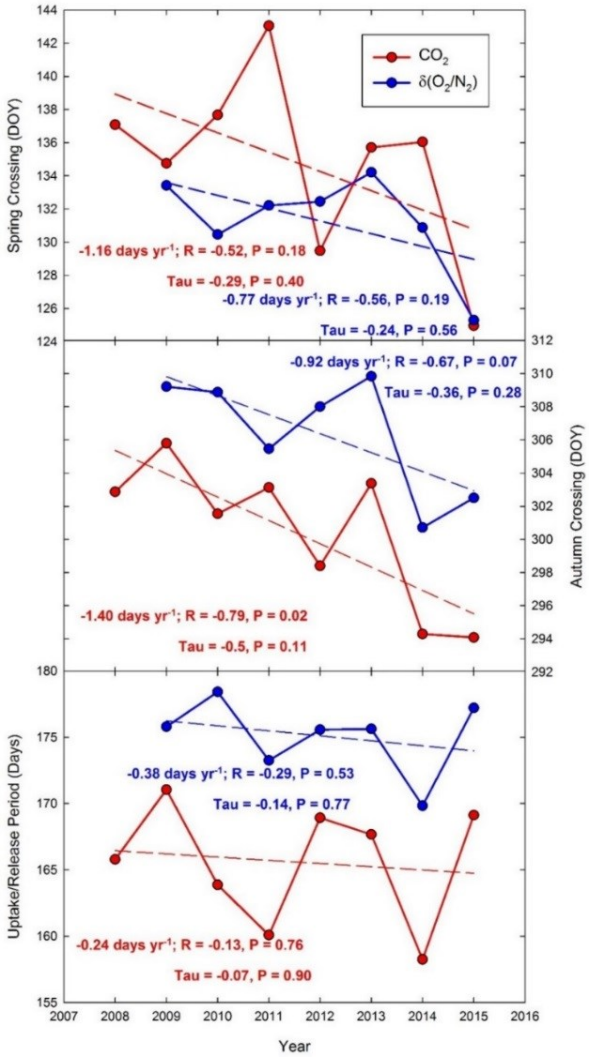

Figure 6.1. The spring zero crossing, (top panel) autumn zero crossing day (middle panel) and uptake/release period (defined as the difference between the SZC and AZC) for CO_2 (red points and lines) and $\delta(O_2/N_2)$ (blue points and lines) at WAO over the study period (2008-2015). The zero crossing days are reported as the Julian day of the year (DOY) and the uptake/release period in days. Dashed lines indicate the direction of the trend in the variable over the study period and its value, strength and significance are reported in the text within the respective plots.

trend in each of the respective measures (not shown), however, the trends in APO were not significant at the $p \leq 0.15$ level. The trend in both the SZC and AZC for CO_2 and $\delta(O_2/N_2)$ are significant however. In particular, the AZC for CO_2 and $\delta(O_2/N_2)$ show statistically significant negative trends of -1.40 days yr^{-1} ($R = -0.79$, $p = 0.02$; $Tau = -0.50$, $p = 0.11$) and -0.92 days yr^{-1} ($R = -0.67$, $p = 0.07$; $Tau = -0.36$, $p = 0.28$), respectively, indicating an earlier autumn termination to the terrestrial biosphere growing season. Furthermore, the earlier autumn termination of the terrestrial biosphere growing season has not significantly impacted the *length* of the growing season (carbon uptake period), which appears to be partially offset by the relatively parallel trend towards an earlier onset of spring. Despite this, it is clear that the stronger trend in the earlier autumn termination is significantly more robust than the earlier spring onset. If these trends hold, then it is not inconceivable that the trend towards a shorter carbon uptake period, currently at -0.24 days yr^{-1}, will become significant with a longer dataset, as was documented by Piao et al. (2008).

The rate of decrease in the trend of the AZC for CO_2 at WAO is typically much greater than those found in other studies. For example, Piao et al. (2008) found a mean CO_2 AZC trend of -0.36 ± 0.52 days yr^{-1} from 10 northern hemisphere stations with CO_2 records extending back >15 years, between 1980 and 2002 (only 4 of which were significant at the $p < 0.05$ level). Whereas Graven et al. (2013) observed a trend of -0.17 days yr^{-1} at Point Barrow, Alaska and -0.14 days yr^{-1} at the MLO over the period 1960-2010. The WAO data, are however, more comparable with the results of Barichivich et al. (2012) who found a mean trend of -0.83 ± 1.65 days yr^{-1} from four northern hemisphere stations over the period 1987-2009, although none of their trends were significant at the $p < 0.05$ level. In interpreting these results it is important to consider the different time periods of analysis given by the different authors. In particular, Barichivich et al. (2012) point to a strong autumn warming in the second half of the 2000s to explain the earlier termination (AZC) of the terrestrial biosphere uptake period. This could be significant in the interpretation of the faster rate of change in the AZC of the WAO data for the period 2008-2015.

In comparing the results of WAO presented here with that of other stations presented by different authors (Barichivich et al., 2012; Graven et al., 2013; Piao et al., 2008) it is important to note that each author applied a different curve-fitting routine (or the same routine with different parameterisations). The results are therefore not directly comparable. Moreover, the choice of routine may introduce a bias in each of the analyses.

I discussed at length in Chapter 5 the importance of selecting the right routine based on the analysis. In the following section I will highlight how using different routines or parametrisations can influence the results or the significance of them. To directly compare the results observed at WAO with those of the other authors would require the exact same methods to be applied.

6.3.1.2. Comparison with other Northern Hemisphere stations

To interpret the WAO trends in the context of potential hemispheric wide trends, I performed the same analysis on the other three selected northern hemisphere stations (ALT, CBA, and MLO), first presented in Chapter 5. The results are shown in **Figure 6.2**. The small negative but insignificant trend in the SZC and AZC at ALT agree well with the findings of Piao et al. (2008). As does the SZC for CO_2 at MLO, although in my analysis the trend is only significant at the $p \leq 0.15$ level. In contrast to the findings of Piao et al. (2008), I find the trend in the autumn crossing at MLO to be moderately positive (0.54 days yr^{-1}) but insignificant ($p = 0.66$). Similarly, I find the opposite trend in both the CO_2 spring and autumn zero crossing at CBA compared to Piao et al. (2008), who found a small, but insignificant, positive trend (< 0.25 days yr^{-1} for AZC and SZC). As a result, I find that the carbon uptake period has decreased (-0.71 days yr^{-1}) at CBA (R = -0.62, $p = 0.14$; *Tau* = -0.58, $p = 0.07$). Moreover, I find a negative trend in the $\delta(O_2/N_2)$ SZC (-0.74 days yr^{-1}, R = -0.66, $p = 0.11$; *Tau* = - 0.43, $p = 0.24$) and AZC (- 1.03 days yr^{-1}, R = -0.82, $p = 0.02$; *Tau* = -0.68, $p = 0.03$) crossing days, in contrast to that seen for CO_2, and has therefore resulted in a small, but insignificant increase in the O_2 release period (0.28 days yr^{-1}, R = 0.23, $p = 0.62$; *Tau* = -0.23, $p = 0.56$). Finally, I also found a large significant negative trend in the APO AZC at CBA (-2.07 days yr^{-1}, R = -0.78, $p = 0.02$; *Tau* = -0.50, $p = 0.11$).

I believe there are two reasons that could explain the discrepancy between the results of Piao et al. (2008) and my own analysis of the SZC and AZC trends seen at MLO and, in particular CBA. First of all, I used different values for the low and high pass filters compared to Piao et al. (2008). The authors there used the typical values of 80 and 667 days, whereas I used 200 and 730 days. The difference in the choice of settings is most apparent in the choice of the low pass filter. Smaller values attribute more short term variability to the seasonal cycle. Given the short time period, of my analysis, (7 years), a

small low pass filter value may unfairly bias the data set by attributing too much variability to the seasonal cycle compared to long term data sets (such as Piao et al. (2008)), where, over a longer time period, the shape and phase of the seasonal cycle is likely to be less variable.

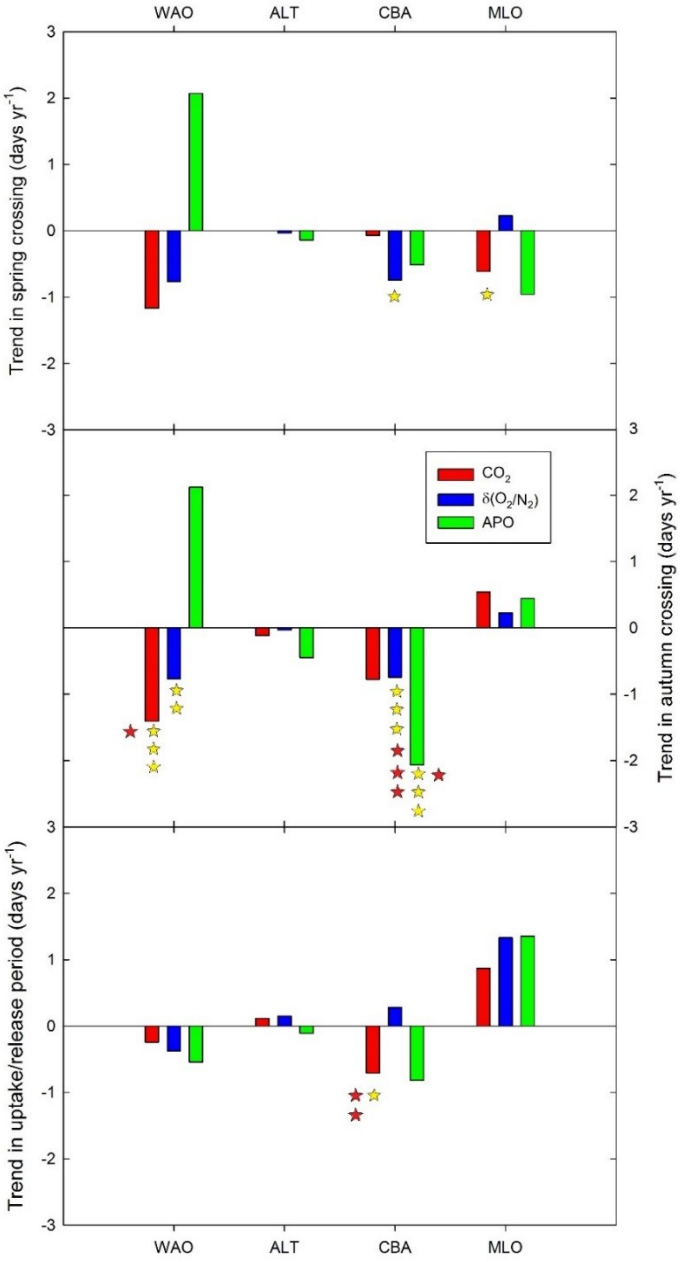

Figure 6.2 The trend in the spring and autumn crossing and in the uptake/release period for CO_2 (red), O_2 (blue) and APO (green) at all four northern hemisphere stations considered in this analysis. Stars represent levels of significance in the trend, with gold stars representing the significance of the Pearson's correlation coefficient and red stars indicating the Mann-Kendall test: 1 star = $p \leq 0.15$, 2 stars = $p \leq 0.10$, 3 stars = $p \leq 0.05$. ALT = Alert, Canada; CBA = Cold Bay, Alaska; WAO = Weybounre, UK; MLO = Mauna Loa Observatory, Hawaii.

However, in order to robustly test the significance the trends found in the WAO dataset, I repeated the extraction of AZC and SZC days from the curve fit firstly using the same values used by Piao et al. (2008) and secondly with a different curve fitting routine (HPspline), as is recommended by the curve fitting review paper of Pickers and Manning (2015). The results of this analysis are shown in **Table 6.2** with respect to the autumn crossing for CO_2 and $\delta(O_2/N_2)$ at WAO.

With the Piao et al. (2008) curve fitting parameters, both the trend in the CO_2 and $\delta(O_2/N_2)$ AZC increase drastically and become more significant (CO_2 AZC = -2.81 days yr^{-1}; R = -0.91, $p = 0.001$ and $\delta(O_2/N_2)$ AZC = -2.13 days yr^{-1}; R = -0.79; $p = 0.02$). This reinforces the findings of the original analysis. Although the trends are larger than that found by Piao et al. (2008) and Graven et al. (2013), it could signify either larger trends seen in the North Atlantic/Europe region and also a reflection of the increased warming detected in the late 2000s, as was noted Barichivich et al. (2012).

Table 6.2. Results of the sensitivity analysis of zero crossing days for WAO using a different curve fitting routine (HPSpline) and different user defined parameters for the short and long term cut off values (CCGCRV), defined in the first column. Tr = trend (days yr^{-1}); R = Pearson's correlation coefficient; p = significance level. Highlighted in bold are the trends that are significant at the $p < 0.10$, whilst those denoted by a star are significant at the $p < 0.05$ level.

Curve Fit; Settings	**CO_2 (Autumn crossing)**			**O_2 (Autumn crossing)**		
	Tr	R	*p*	Tr	R	*p*
CCGCRV; 200, 730	**-1.40***	**-0.79***	***0.02****	**-0.92**	**-0.67**	***0.07***
CCGCRV; 80, 667	**-2.81***	**-0.91***	***0.001****	**-2.13***	**-0.79***	***0.02****
Hpspline; 30	-0.06	-0.40	*0.33*	0.06	-0.37	*0.37*

Using HPSpline, there are no trends in any of the discussed parameters. This is likely due to the inflexibility of the spline used. Even with the most flexible *SD2* parameter (see Pickers and Manning (2015)), very little variability is allowed in the seasonal cycle (Pickers and Manning, 2015).

Secondly, the difference between the results of my analysis and Piao et al. (2008), could be, as was just allured to, the difference in study period. Piao et al. (2008) analysed data from 1980-2002, whereas I analysed from 2007-2015. It is not inconceivable that the trend in the autumn crossing found by Piao et al. (2008) is not linear with time and may vary from year to year or from decade to decade (Piao et al., 2017; Piao et al., 2014). Moreover, the main driver behind the trend seen may not be a simple linear autumn warming response as was proposed by Piao et al. (2008), but instead could be attributable to inter-annual and decadal climate variability, which will indirectly affect temperature,

such as variability in ENSO or NAO, for example. This will be investigated in the following section.

6.3.1.3. Amplitude

The results of the amplitude trend analysis are shown in **Figure 6.3**. There is a considerable amount variability in each of the species over the study period. No significant trend was found in the CO_2 and $\delta(O_2/N_2)$ amplitudes. However, a slight positive trend can be discerned in the CO_2 amplitude (0.12 ppm yr^{-1}, R = 0.31, *p = 0.46; Tau* = -0.21, *p = 0.54*) which is comparable with that found by Graven et al. (2013) at Point Barrow, Alaska (~0.10 ppm yr^{-1}). Although, the positive correlation between the CO_2 and $\delta(O_2/N_2)$ amplitudes is not significant (R = 0.59, *p = 0.16; Tau* = 0.43, *p = 0.24*), the largest amplitudes are observed in 2009 and 2013 for both species. Moreover, $\delta(O_2/N_2)$ and CO_2 display their smallest amplitudes in 2010 and 2011 respectively. This

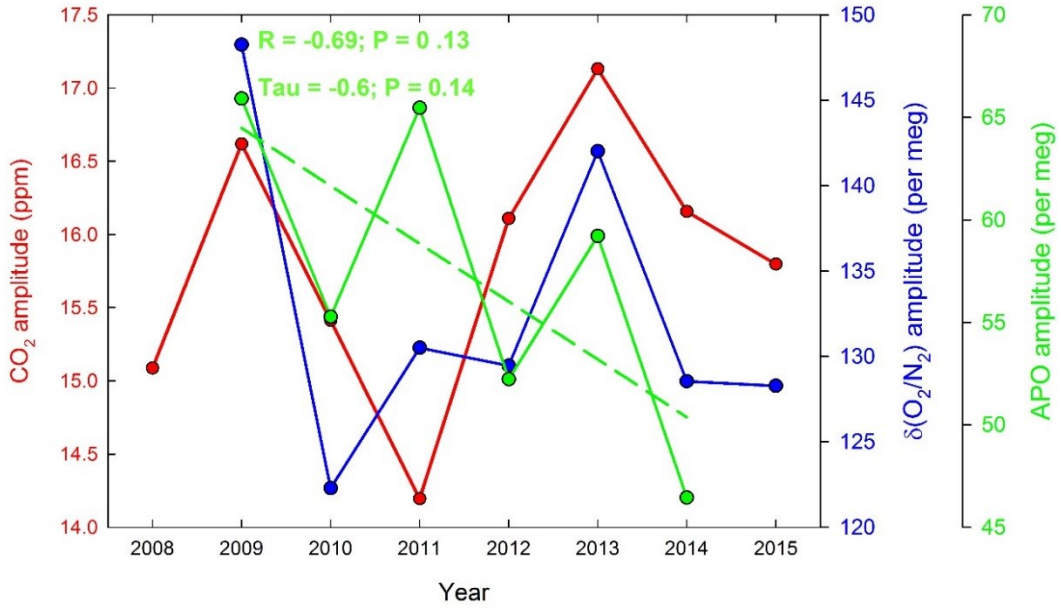

Figure 6.3. Variability in the annual amplitude of the seasonal cycle over the study period (2008-2015) for CO_2 (red points and lines, left y-axis), $\delta(O_2/N_2)$ (blue points and lines, first right y-axis), and APO (green points and lines, second y-axis) at WAO. Only the decreasing trend in the amplitude of the APO seasonal cycle is shown (dashed green line) and its strength and significance is shown by the text in the figure in green.

could indicate that the variability in the CO_2 and $\delta(O_2/N_2)$ amplitudes observed could be driven by the same process such as the terrestrial biosphere, which would be expected.

APO is not well correlated with either CO_2 or $\delta(O_2/N_2)$, however it does appear to show a similar trend $\delta(O_2/N_2)$ between 2012 and 2014. In contrast to the other two species, the APO amplitude does show a decreasing trend with time over the study period (R = -0.69, *p = 0.13; Tau* = -0.60, *p = 0.14*). If this trend is maintained, it implies a decrease in the seasonality of ocean carbon cycle processes observed at WAO. Increases in ocean stratification due to warming (Capotondi et al., 2012) would inhibit the breakdown in the seasonal thermocline in the upper ocean in the winter months, preventing the replenishment of nutrients required for productivity the following spring and summer (Capotondi et al., 2012). This would explain decrease in the seasonal amplitude of APO. However, analysis of only one APO time series is not adequate to ascertain whether this may be occurring globally, or even regionally. However the results shown here do merit further investigation.

6.3.1.4. Drivers of seasonal variability

I begin by looking at what may be driving the significant trend towards an early autumn upward crossing day for CO_2 and $\delta(O_2/N_2)$, before investigating the variability in the other defined variables for each species. Again, I have only reported correlations which are significant at the $p \leq 0.15$ level, whilst the following figures (**Figure 6.4** to **Figure 6.7**) only show the correlations which are significant at the $p \leq 0.05$ level with respect to the Pearson's correlation coefficient.

6.3.1.4.1. Autumn zero crossing in CO_2 and $\delta(O_2/N_2)$

In contrast to the findings of Piao et al. (2008) the AZC of CO_2 at WAO is not significantly correlated ($p > 0.15$) with autumn temperature trends within any of the three regions considered (U.K, North Atlantic/Europe and the northern hemisphere). However the AZC is negatively correlated with both the North Atlantic spring temperature (R = - 0.66, *p = 0.10; Tau = -0.42, p = 0.24*) and the northern hemisphere spring temperature (R = -0.71, *p = 0.07; Tau = -0.71, p = 0.03*) trends. The spring ENSO index is also negatively correlated with the CO_2 AZC crossing trend (R = -0.60, *p = 0.12; Tau = -0.57, p = 0.06*), as is the annual ENSO index (R = -0.67; *p = 0.07; Tau = -0.43, p = 0.18*).

The AZC of $\delta(O_2/N_2)$ at WAO (**Figure 6.4**) is also negatively correlated with spring temperatures, however, this is more so on the regional (North Atlantic: R = -0.80, *p = 0.03; Tau =-0.71, p = 0.03*) to local scale (UK: R = -0.68, *p = 0.09; Tau = -0.71, p = 0.03*), rather than the regional to hemispheric scale, as was the case for CO_2.

Furthermore, the $\delta(O_2/N_2)$ AZC is also negatively correlated with annual temperature trends in the North Atlantic (R = -0.73, *p = 0.06; Tau = -0.43, p = 0.24*) and the UK (R = -0.74, *p = 0.06; Tau = -0.43, p = 0.24*), whilst it is positively correlated with the North Atlantic autumn precipitation trend (R = 0.64; *p = 0.12; Tau = 0.33, p = 0.38*). Although the $\delta(O_2/N_2)$ AZC shows no correlation (*p > 0.15*) with the ENSO index, it does show a weak negative correlation with the annual NAO index (R = -0.56, *p = 0.14; Tau = - 0.21, p = 0.55*) and a strong negative correlation with the spring AO index (R = -0.71, *p = 0.05; Tau = -0.64, p = 0.03*).

The variability in the AZC for CO_2 and, to a lesser extent, the AZC in $\delta(O_2/N_2)$, will primarily be driven by the terrestrial biosphere's response to year to year variations

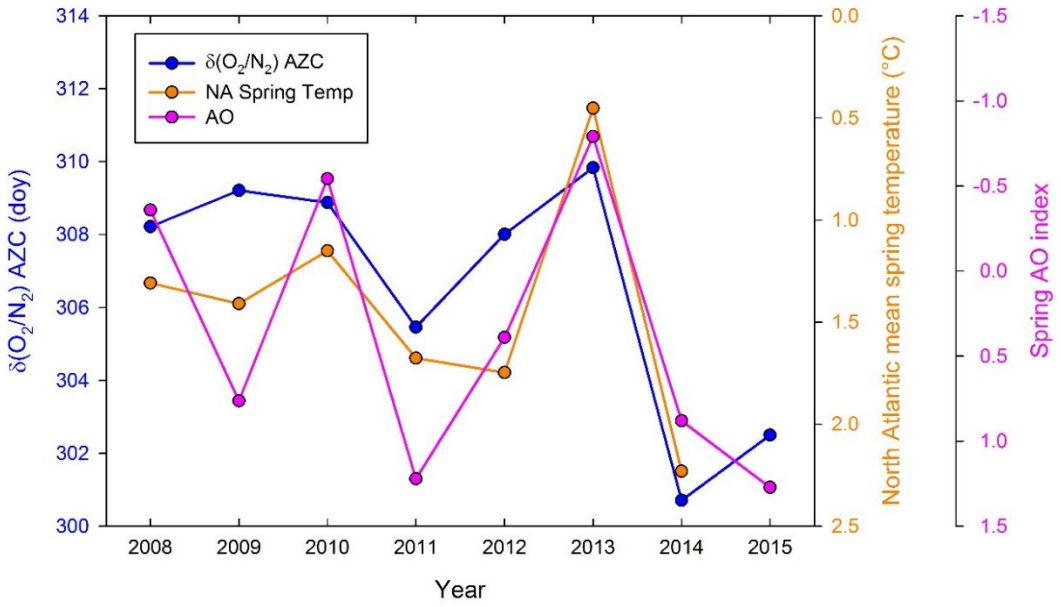

Figure 6.4. Covariation of the $\delta(O_2/N_2)$ autumn zero crossing day (AZC) expressed as the Julian day of the year (blue lines and points; left y-axis) with North Atlantic mean spring temperature (orange lines and points; first right y-axis) and the spring Arctic Oscillation index (pink lines and points; second right y-axis). Y-axes values on the right hand side (temperature and AO index) have been reversed to highlight the negative correlation seen between the variables.

in climate. However, instead of being linked to autumn temperatures (Barichivich et al., 2012; Piao et al., 2008), I find that the spring temperatures are more significant in affecting the autumn crossing. To explain this, I propose that a warm temperature anomaly in spring will stimulate more growth in the terrestrial biosphere in the early part of the growing season. This anomalous growth would then lead to increased respiration in the autumn, as there is simply more biomass to respire, resulting in an earlier AZC day.

Furthermore, the correlation with spring temperatures could be a symptom of larger climate variability, as is shown in the case for CO_2, by the correlation with both the spring and annual ENSO indices. Positive ENSO anomalies are associated with globally warmer and drier conditions (McPhaden et al., 2006) and this has trended towards a more positive phase over the final few years of the study period (~since 2012). These conditions would stimulate more respiration over growth (which is conversely favoured by cooler and wetter La Niña conditions) (Jones et al., 2001)

The strong, significant correlation in the AZC of $\delta(O_2/N_2)$ with both spring temperature and the AO, appears to be strongly influenced by the transition from a positive phase of the AO in 2011, to a strong negative phase in 2013, before returning to the positive state in 2014. Thus, the cooler and wetter conditions brought about by the negative AO in 2013 would have likely resulted in better growing conditions throughout the year (in much the same way that the terrestrial biosphere growth is favoured by cooler and wetter La Niña conditions), resulting in a much later $\delta(O_2/N_2)$ AZC day, as is seen in the WAO data. Although, the CO_2 AZC does not show a correlation with the AO, it does show a relatively late AZC day in 2013 (**Figure 6.1**).

It is interesting to note the slightly different climatic regions of influence on CO_2 and $\delta(O_2/N_2)$. CO_2 shows correlation with North Atlantic and northern hemisphere climatic variables, whilst also appears to be influenced by the global ENSO climatic phenomenon. $\delta(O_2/N_2)$ on the other hand, appears to be influenced more on the local to regional scale, showing correlations with UK and North Atlantic climatic variables and the more regional NAO and AO climate indices. This could reflect a more local/regional source and sink for oceanic $\delta(O_2/N_2)$, compared to CO_2, which appears to be reflecting hemispheric scale variations in the terrestrial biosphere. The APO data do not reflect this however.

6.3.1.4.2. Spring zero crossing in CO_2 and $\delta(O_2/N_2)$

The spring SZC trend of CO_2 (**Figure 6.5**) does not show any correlation with temperature or precipitation. It does however, show a very strong negative correlation with the annual ENSO index (R = -0.87, *p = 0.005; Tau = -0.64, p = 0.03)*, a strong negative correlation with the autumn ENSO index (R = -0.77, *p = 0.02; Tau = -0.71, p = 0.01*), and a slightly weaker negative correlation with the spring ENSO index (R = - 0.63, *p = 0.10; Tau = -0.36, p = 0.28*).

The $\delta(O_2/N_2)$ SZC, on the other hand, does show a negative correlation with northern hemisphere spring temperatures (R = -0.79, *p = 0.06; Tau = -0.2, p = 0.72*) and a positive correlation with northern hemisphere spring precipitation (R = 0.79, *p = 0.06; Tau = 0.7, p = 0.06*). The $\delta(O_2/N_2)$ SZC also negatively correlates well with the both the annual ENSO index (R = -0.69, *p = 0.08; Tau = -0.24, p = 0.56*) and the spring ENSO index (R = -0.65, *p = 0.11; Tau = -0.62, p = 0.07*).

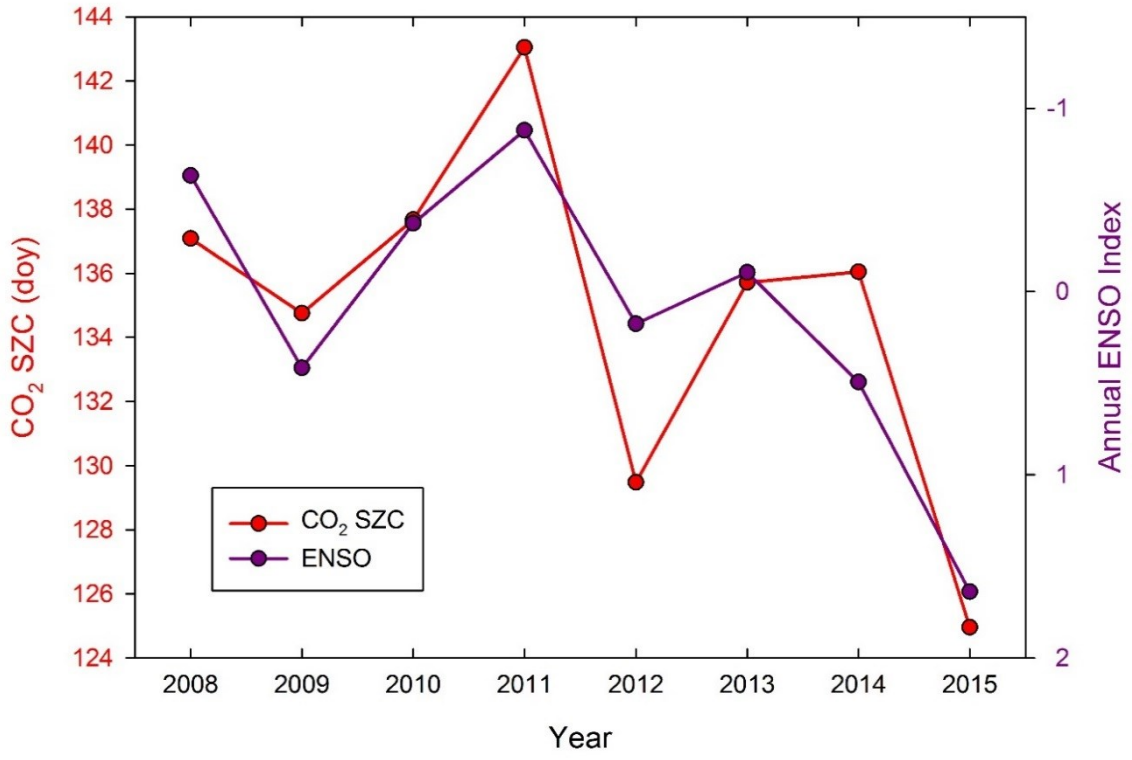

Figure 6.5. Covariation of the CO_2 spring zero crossing (SZC) day, expressed as the Julian day of the year (doy) (red points and lines) with the annual ENSO index (purple points and lines). Y-axes values on the right (ENSO) have been reversed to highlight the negative correlation observed between the variables.

As was discussed for the AZC for CO_2, ENSO clearly plays an important role in controlling the phase of the CO_2 and, to a lesser extent, the $\delta(O_2/N_2)$ seasonal cycles. The trend towards an earlier SZC for CO_2 is very well negatively correlated with the trend towards a more positive ENSO index over the study period, as is the SZC for $\delta(O_2/N_2)$, but to a lesser extent. Previously, I highlighted how the warmer conditions brought about by El Niño would favour respiration in the autumn, driving an earlier termination in the terrestrial biosphere growing season. In spring, at the start of the growing season, warmer conditions would also stimulate an earlier onset of spring. However, the CO_2 SZC shows no correlation with temperature and so this cannot be the driving cause of the correlation seen here. Instead, the relationship could be driven influenced by the increase in CO_2 caused by drought and fires related to warmer and drier conditions brought about by El-El Niño (Jones et al., 2001).

In addition to the ENSO index, the $\delta(O_2/N_2)$ SZC is also well correlated negatively with spring temperature (as would be expected from the above explanation), however it is also positively correlated with northern hemisphere precipitation. This is surprising, as wetter conditions may be expected to favour the onset of spring. However, I believe, the high precipitation values, for the whole northern hemisphere, at this time of year, may in fact represent snow fall which would act to delay the onset of spring. Thus cooler, wetter conditions in the northern hemisphere during the growing season may stimulate more terrestrial biosphere growth, however, cooler wetter conditions during late winter/early spring would act to delay the onset of spring, thus we see a later SZC day in $\delta(O_2/N_2)$ when precipitation is high and temperatures are low.

6.3.1.4.3. APO zero crossing trends

The APO SZC and AZC (**Figure 6.6**) do not show any correlation with temperature or with any of the climate indices at any of the regional levels considered. The variability in both of the zero crossing days is however, well correlated with precipitation. The AZC is positively correlated with precipitation at the hemispheric scale (annual: R = 0.70, *p = 0.08*; *Tau = 0.33, p = 0.38*. Autumn: R = 0.67, *p = 0.10; Tau = 0.33, p = 0.38*), particularly with the spring precipitation (R = 0.88, *p = 0.009; Tau = 0.52, p = 0.14*). Whereas the SZC is positively correlated with precipitation: Both with the UK spring (R = 0.74, *p = 0.09; Tau = 0.47, p = 0.27*) and annual (R = 0.78, *p = 0.06; Tau = 0.73, p = 0.06*) and with the annual North Atlantic precipitation (R = 0.67, *P = 0.14; Tau = 0.86, P = 0.02*).

I do not believe that precipitation is directly driving the variability in the APO AZC. For this to be true, then there would have to be a significant impact of riverine run

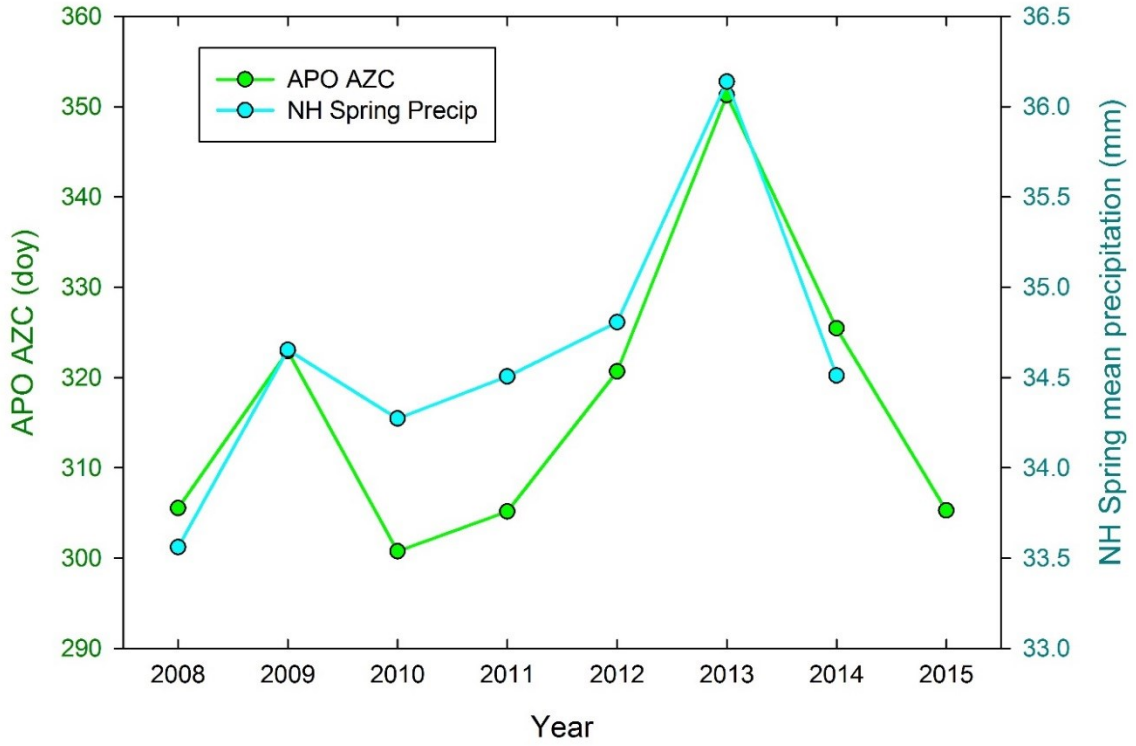

Figure 6.6. Covariation of the APO autumn zero crossing (AZC) day, expressed as the Julian day of the year, (green points and lines; left y-axis) and northern hemisphere mean spring precipitation (turquoise points and lines; right y-axis).

off on the seasonal breakdown of the thermocline in autumn in the North Atlantic, which, given the size of the basin, does not seem plausible. Instead, the precipitation could be correlated with a larger climate phenomena, which may in turn be also impacting the breakdown of the thermocline in the autumn, and the subsequent amount of mixing with O_2 depleted sub-surface waters. Although the APO AZC does not show any correlation with AO index, this might be due to both period of averaging for the AO index (a whole year to compare to one yearly AZC day), and also the shortness of the record (8 years).

6.3.1.4.4. Amplitude variability in CO_2, $\delta(O_2/N_2)$ and APO

Precipitation appears to play some role in modulating the CO_2 amplitude. The amplitude is positively correlated with northern hemisphere spring (R = 0.68, *p = 0.09; Tau = 0.62, p = 0.07*), autumn (R = 0.61, *p = 0.14; Tau = 0.43, p = 0.24*) and annual (R = 0.63, *p =0.13; Tau = 0.43, p = 0.24*) precipitation trends, whilst it is negatively correlated with the northern hemisphere spring temperature trends (R = -0.60; *p = 0.13, Tau = -0.24, p = 0.56*).

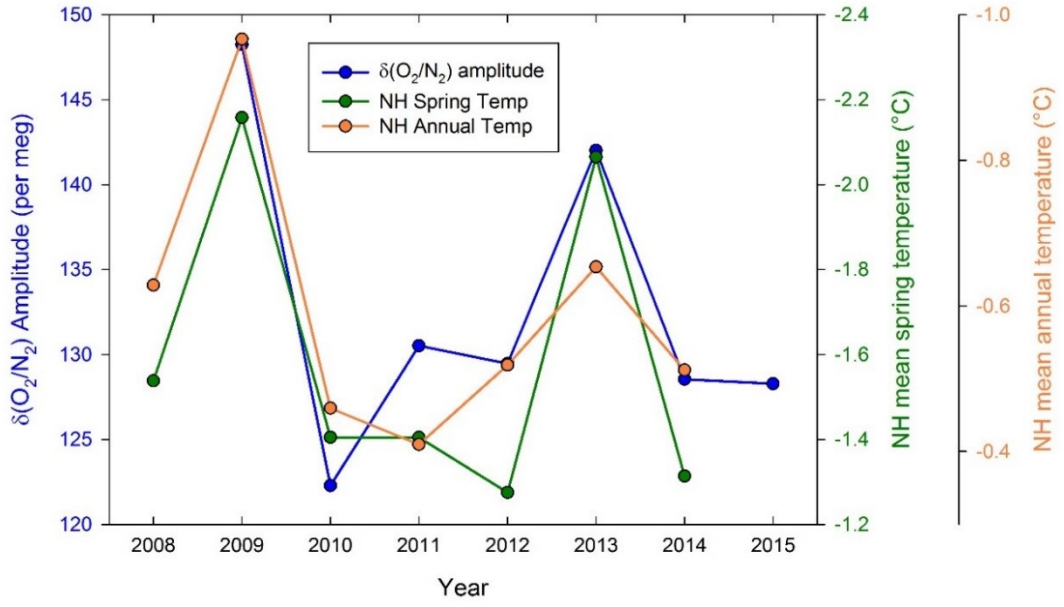

Figure 6.7. Covariation of the $\delta(O_2/N_2)$ seasonal cycle amplitude (blue points and lines; left y-axis) with the northern hemisphere mean spring temperature (green points and lines; first right y-axis) and northern hemisphere mean annual temperature (orange points and lines; second right y-axis). Y-axes values on the right hand side (temperature) have been reversed to highlight the negative correlation observed between the variables.

Conversely, the $\delta(O_2/N_2)$ amplitude does not appear to be modulated by precipitation. Instead, it shows a strong negative correlation with the northern hemisphere annual (R = -0.90; *p = 0.02, Tau = -0.60, p = 0.14*) and spring (R = -0.92, *p = 0.009; Tau = -0.47, p = 0.27*) temperatures.

The strong anti-correlation between the $\delta(O_2/N_2)$ amplitude and, to a lesser extent CO_2 amplitude, with temperature indicates cooler temperatures result in more uptake and release of the respective species during the growing season. Firstly, this corroborates the point made earlier that greater uptake is seen in the biosphere during cooler and wetter

periods (such as during La Niña conditions). Secondly, the cooler spring temperatures could be indicative of a larger amounts of snow fall. Whilst this would delay the onset of spring, it would also increase the soil moisture content upon melting, enhancing productivity during the summer (Bastos et al., 2013).

The APO amplitude again shows a weak negative correlation with the North Atlantic annual (R = -0.66, *p = 0.15; Tau = -0.60, p = 0.14*) and spring (R = -0.72, *p = 0.11; Tau = -0.33, p = 0.47*) precipitation. Whilst it is also negatively correlated with the spring ENSO index (R = -0.66, *p = 0.15; Tau = -0.60, p = 0.14*) and positively correlated with the autumn AO index (R = 0.69; *p = 0.13, Tau = 0.47, p = 0.27*).

6.3.1.5. Uncertainty in seasonal trends and their causes

Whilst I have presented the trends in the seasonal cycles and speculated as to what may causing them, this analysis is by no means complete. Although I have assigned a significance to the trends and the correlations, I have not presented any uncertainty based on how robust the curve fitting routine is. Uncertainty in the choice of the routine has been a common theme throughout this thesis and so I will not discuss it further here. However, quantifying this uncertainty should be the next step in this analysis. Moreover, the speculative discussion behind the causes of the trends could be examined further with further lines of inquiry. Examining northern hemisphere snow fall would be one such line of inquiry, whilst examining the impact of precipitation and temperature on the terrestrial biosphere could be examined within a dynamic global vegetation model.

6.3.2. Inter-annual variability of the growth rate

The inter-annual variability in the growth rate of atmospheric CO_2, $\delta(O_2/N_2)$ and APO first presented in Chapter 5 are shown in **Figure 6.8** compared to the variability in the ENSO, NAO and AO indices and the growth rate of fossil fuel emissions. Following the regression analysis of each of the metrics using the Mann-Kendall test for significance on auto correlated time series data, no significant relationship was found between the growth rate of fossil fuel emissions and the growth rate of any of the species ($p > 0.15$). Fossil fuel emissions are therefore unlikely to be the primary driver behind the variability in the growth rates first proposed by Wilson (2012).

Conversely, it is clear from **Figure 6.8** that the CO_2 growth rate is positively correlated with the ENSO, with the growth rate lagging the index by 3 to 6 months. Of all of the metrics considered, CO_2 showed the most significant relationship with ENSO

(R= 0.60, $p < 0.0001$; *Tau* = 0.39, $p < 0.0001$). Furthermore, a negative correlation is seen between ENSO and the growth rate in $\delta(O_2/N_2)$ (R = -0.48, $p < 0.0001$; *Tau* = -0.25, $p = 0.004$).

Strong transitions are apparent between La Niña conditions in 2008, a moderately strong El Niño in 2010, followed by a strong La Niña in 2011. However the variability in the ENSO index decreases after 2011, as it steadily trends towards a more positive, El Niño state, which peaked in early 2016 (Varotsos et al., 2016). As such, the relationship between ENSO, CO_2 and $\delta(O_2/N_2)$ appears to breakdown between 2012 and 2015. As discussed in Chapter 5 Section 5.3.2.2, this is mirrored by the increasing disagreement in

phase observed at northern hemisphere stations after this period, potentially indicating a less hemispheric scale influence.

This likely confirms that the inter-annual variability in CO_2 and $\delta(O_2/N_2)$ is, for the most part, driven by the response of the terrestrial biosphere to ENSO. The terrestrial

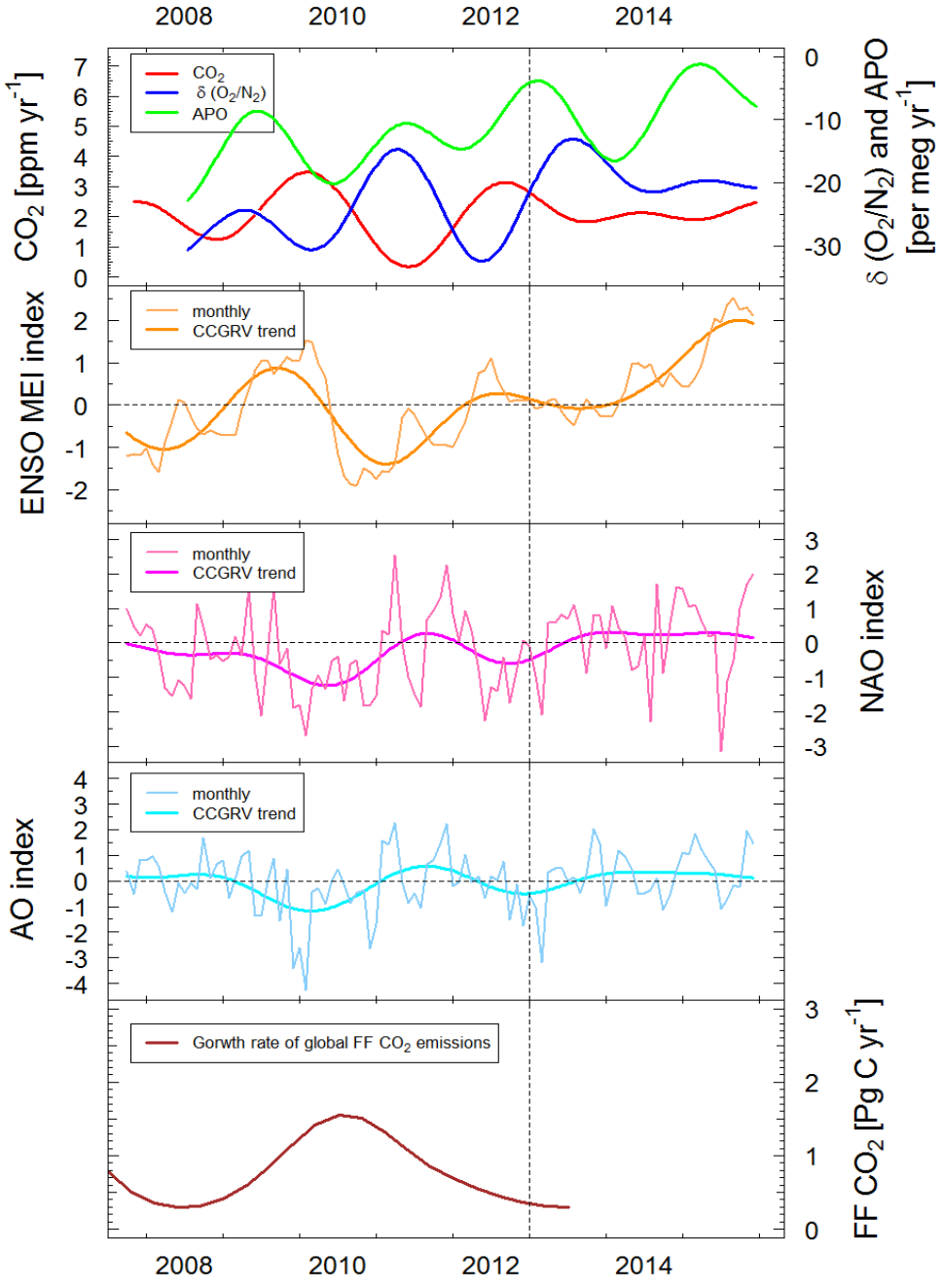

Figure 6.8. The inter-annual variability of atmospheric CO_2, $\delta(O_2/N_2)$ and APO observed at WAO over the study period (2008-2015) (top panel; CO_2 (red), left y-axis; $\delta(O_2/N_2)$ (blue) and APO (Green), right y-axis) in comparison to three climate indices: ENSO (second panel), NAO (third panel), AO (fourth panel) and the inter-annual variability in the growth rate of fossil fuel emissions (bottom panel). For ENSO, NAO and AO, the monthly data and the ~2 year smoothing (CCGRV trend) are shown in the respective keys.

carbon sink is enhanced in the tropics due to cooler and wetter conditions, whereas the opposite is true for El Niño, whereby warmer, drier conditions, result in more CO_2 loss from terrestrial ecosystems (Friedlingstein and Prentice, 2010; Jones et al., 2001).

Moreover, APO is weakly correlated with ESNO (R= 0.24, p = 0.05; *Tau* = 0.2, p = 0.01). This is weaker than the relationship found by Eddebbar et al. (2017). However, this relationship represents the tropical APO flux as determined by an atmospheric inversion of APO from a global network of monitoring stations. It is therefore not surprising, given the mid-latitude, North Atlantic location of WAO, that the relationship is weaker. Nevertheless, the relationship is still there and could be explained by the following mechanism: During El Niño, decreased upwelling of O_2 poor deep waters in the equatorial pacific results in the region becoming a small source of O_2, whereas during La Niña, enhanced upwelling results in anomalous in-gassing of O_2 from the atmosphere.(Eddebbar et al., 2017; Jones et al., 2001).

Hamme and Keeling (2008) proposed a small amount of the variability of APO in the northern hemisphere, at least the most anomalous excursions in the growth rate, could be explained by ventilation of deep water masses within the North Atlantic and North Pacific oceans in response to variations in the AO. However, I find no significant relationship between AO or NAO and the APO growth rate observed at WAO (*p > 0.15*).

The NAO index is, however, positively correlated with the $\delta(O_2/N_2)$ growth rate (R= 0.47, p = 0.03; *Tau = 0.34*, p = 0.02) and the CO_2 growth rate (R= 0.70, p = 0.12; Tau = 0.47, p = 0.15). Cooler and wetter conditions across the northern high latitudes during the negative phase of NAO has been shown to increase the productivity of northern terrestrial ecosystems (Bastos et al., 2013) and so therefore likely explains the relationships observed at WAO.

In conclusion, a marine carbon cycle response to ENSO is observed in the variability in APO at WAO. However, a much stronger terrestrial carbon cycle response to the different phases of ENSO and NAO is apparent in the growth rates of CO_2 and $\delta(O_2/N_2)$. Another factor that may influence the growth rates observed here that has not been considered is the impact of volcanism (Raupach et al., 2008). The emission of ash and sulphur dioxide into the stratosphere following an eruption acts to cool global temperatures and leads to more diffuse solar radiation that encourages plant productivity (Gu et al., 2003).Volcanic activity during the study period was low however (with respect to large, explosive eruptions that result in the above) ((NGDC/WDS), 2017), and so is unlikely to impact the variability of the growth rates seen.

6.4. Summary and conclusions

The aim of this chapter was firstly to quantify the inter-annual variability of the seasonal cycles and growth rates of atmospheric CO_2, $\delta(O_2/N_2)$ and APO observed at WAO over the 2008-2015 period. I then examined whether there were statistical relationships between the observed trends and variables that are related to seasonal and inter-annual climate variability on regional to hemispheric scales. I have further examined causal mechanisms behind the variability observed.

There is a significant shift towards an earlier autumn zero crossing at WAO in CO_2 (-1.40 days yr^{-1} (R = -0.79, p = 0.02*; Tau* = -0.50*, p* = 0.11) and, to a lesser extent, $\delta(O_2/N_2)$ (-0.92 days yr^{-1}; R= -0.67, p = 0.07; *Tau* =-0.36*, p* = 0.28) . I presented this finding in the context of other stations and showed the importance in the choice of curve fitting programme. In particular, I found a significant change in CBA trends compared to Piao *et al.* (2008), which could be a reflection of the different curve fitting parameters used and the different time periods of analysis. Moreover, the rate of decrease in the autumn zero crossing day at WAO is much higher compared to the results of Piao et al. (2008) and Graven et al. (2013), who analysed CO_2 over different time periods: 1980-2002 and 1960-2010, respectively. The larger trend seen at WAO could therefore be due to the different time period of analysis and/or could signify a response to greater autumn warming in the late 2000s, as was proposed by Barichivich et al. (2012).

I have demonstrated that the autumn zero crossing trend in CO_2 is well correlated with northern hemisphere spring temperatures (R = -0.71, *p = 0.07; Tau = -0.71, p = 0.03*), rather than autumn temperatures, in contrast to Piao *et al.* (2008). I speculated that a warmer spring would stimulate more growth during the start of the growing season, leading to an overall greater accumulation of biomass, that subsequently results in greater respiration in the autumn months, as there is simply more biomass to respire. The temperature trends could also be linked to the trend towards the more El Niño like conditions in recent years. However, this is not reflected in the amplitude of the CO_2 seasonal cycle. Conversely, there is a negative correlation between the CO_2 amplitude and the northern hemisphere spring temperature trends (R = -0.60; *p = 0.13, Tau = -0.24, p = 0.56*). Explaining the correlation between the AZC in CO_2 and northern hemisphere spring temperatures is challenging and merits further investigation.

The correlation with spring temperatures is also seen in the autumn zero crossing of $\delta(O_2/N_2)$ (e.g North Atlantic spring temperature: R = -0.80, *p = 0.03; Tau =-0.71,*

p = 0.03). However, in contrast to CO_2, I have shown this to be linked to the Arctic Oscillation (R = -0.71, *P = 0.05; Tau = -0.64, P = 0.03*), whereby a negative phase in 2013 in particular, drives a later crossing anomaly. 2013 was in contrast to the general trend towards a warmer spring, whereby cooler and wetter conditions associated with a negative AO phase in the mid latitudes, stimulates greater terrestrial biosphere growth in much same way as La Niña conditions do. The fact this is not also reflected in the CO_2 seasonal cycle casts doubt on this interpretation of the AO interaction with the terrestrial biosphere. It could be that the ocean is driving this trend, but again, this is not reflected in the APO AZC.

The spring zero crossing in CO_2, is very well correlated with the annual ENSO index (R = -0.87, *p = 0.005; Tau = -0.64, p = 0.03)*, and the trend towards an earlier onset of springs appears to be linked with the trend towards a more positive El Niño like state over this time period. These warmer conditions, stimulating earlier growth, are also seen in the $\delta(O_2/N_2)$ record.

The results presented here do indicate that climate variability influences seasonal variability within the WAO atmospheric CO_2, $\delta(O_2/N_2)$ and APO record. There is evidence that both regional and hemispheric climate variability influences the seasonal cycles, however, hemispheric scale climate variability appears to be the dominant driver. The analysis does merit further analysis with other northern hemisphere stations. Specifically, by performing the analysis on other atmospheric CO_2, $\delta(O_2/N_2)$ and APO monitoring stations the regional to hemispheric scale drivers could be separated further. For example, does the AO influence the seasonality of those stations north of 60˚N. Similarly, does the NAO influence North Atlantic stations more so than Pacific stations? To further increase the robustness of the conclusions, different curve fitting routines should be applied and those trends and correlations observed with all routines would be the most robust.

Finally, I examined the relationship between the growth rates of the species with climate indices. A marine carbon cycle response to ENSO is observed in the inter-annual variability in the APO growth rate at WAO. However, a much stronger terrestrial carbon cycle response to the different phases of ENSO and NAO is apparent in the growth rates of CO_2 and $\delta(O_2/N_2)$. The NAO index is positively correlated with the $\delta(O_2/N_2)$ growth rate (R= 0.47, $p = 0.03$; *Tau = 0.34*, $p = 0.02$) and the CO_2 growth rate (R= 0.70, $p = 0.12$; Tau = 0.47, $p = 0.15$). Moreover, the CO_2 growth rate was positively correlated with ENSO (R= 0.60, $p < 0.0001$; *Tau* = 0.39, $p < 0.0001$), whilst a negative correlation is seen

between ENSO and the growth rate in $\delta(O_2/N_2)$ (R=-0.48, $p < 0.0001$; *Tau* = -0.25, $p = 0.004$).

The results and their analysis represent a significant addition to the limited number of studies that have examined the inter-annual variability of $\delta(O_2/N_2)$ and APO. Enough O_2 monitoring stations now exist within the northern hemisphere to effectively quantify the role of variability driven by Atlantic and Pacific based climate indices. Moreover, the fundamental carbon cycle response mechanisms can be examined through the use of ocean biogeochemical models and global vegetation models coupled to different models of atmospheric transport.

6.5. References

(NGDC/WDS), N.G.D.C.W.D.S., (2017) Global Significant Volcanic Eruptions Database., in: Center., N.G.D. (Ed.). NOAA, U.S. .

Ambaum, M.H.P., Hoskins, B.J., Stephenson, D.B. (2001) Arctic Oscillation or North Atlantic Oscillation? Journal of Climate 14, 3495-3507.

Bacastow, R.B. (1976) Modulation of atmospheric carbon dioxide by southern oscillation. Nature 261, 116-118.

Baddouh, M.b., Meyers, S.R., Carroll, A.R., Beard, B.L., Johnson, C.M. (2016) Lacustrine 87Sr/86Sr as a tracer to reconstruct Milankovitch forcing of the Eocene hydrologic cycle. Earth and Planetary Science Letters 448, 62-68.

Barichivich, J., Briffa, K.R., Osborn, T.J., Melvin, T.M., Caesar, J. (2012) Thermal growing season and timing of biospheric carbon uptake across the Northern Hemisphere. Global Biogeochemical Cycles 26, n/a-n/a.

Barnston, A.G., Livezey, R.E. (1987) Classification, Seasonality and Persistence of Low-Frequency Atmospheric Circulation Patterns. Monthly Weather Review 115, 1083-1126.

Bastos, A., Running, S.W., Gouveia, C., Trigo, R.M. (2013) The global NPP dependence on ENSO: La Niña and the extraordinary year of 2011. Journal of Geophysical Research: Biogeosciences 118, 1247-1255.

Behrenfeld, M.J., Randerson, J.T., McClain, C.R., Feldman, G.C., Los, S.O., Tucker, C.J., Falkowski, P.G., Field, C.B., Frouin, R., Esaias, W.E., Kolber, D.D., Pollack, N.H. (2001) Biospheric Primary Production During an ENSO Transition. Science 291, 2594-2597.

Bjerknes, J. (1966) A possible response of the atmospheric Hadley circulation to equatorial anomalies of ocean temperature. Tellus 18, 820-829.

Boden, T.A., G. Marland, and R.J. Andres., (2017) Global, Regional, and National Fossil-Fuel CO2 Emissions., in: Carbon Dioxide Information Analysis Center (Ed.), Oak Ridge National Laboratory, U.S. Department of Energy, Oak Ridge, Tenn., U.S.A. .

Capotondi, A., Alexander, M.A., Bond, N.A., Curchitser, E.N., Scott, J.D. (2012) Enhanced upper ocean stratification with climate change in the CMIP3 models. Journal of Geophysical Research: Oceans 117, n/a-n/a.

Ebisuzaki, W. (1997) A Method to Estimate the Statistical Significance of a Correlation When the Data Are Serially Correlated. Journal of Climate 10, 2147-2153.

Eddebbar, Y.A., Long, M.C., Resplandy, L., Rödenbeck, C., Rodgers, K.B., Manizza, M., Keeling, R.F. (2017) Impacts of ENSO on air-sea oxygen exchange: Observations and mechanisms. Global Biogeochemical Cycles 31, 901-921.

Forkel, M., Carvalhais, N., Rödenbeck, C., Keeling, R., Heimann, M., Thonicke, K., Zaehle, S., Reichstein, M. (2016) Enhanced seasonal CO_2 exchange caused by amplified plant productivity in northern ecosystems. Science.

Friedlingstein, P., Prentice, I.C. (2010) Carbon-climate feedbacks: a review of model and observation based estimates. Current Opinion in Environmental Sustainability 2, 251-257.

Fu, W., Randerson, J.T., Moore, J.K. (2016) Climate change impacts on net primary production (NPP) and export production (EP) regulated by increasing stratification and phytoplankton community structure in the CMIP5 models. Biogeosciences 13, 5151-5170.

Graven, H.D., Keeling, R.F., Piper, S.C., Patra, P.K., Stephens, B.B., Wofsy, S.C., Welp, L.R., Sweeney, C., Tans, P.P., Kelley, J.J., Daube, B.C., Kort, E.A., Santoni, G.W., Bent, J.D. (2013) Enhanced Seasonal Exchange of CO_2 by Northern Ecosystems Since 1960. Science 341, 1085-1089.

Gu, L., Baldocchi, D.D., Wofsy, S.C., Munger, J.W., Michalsky, J.J., Urbanski, S.P., Boden, T.A. (2003) Response of a Deciduous Forest to the Mount Pinatubo Eruption: Enhanced Photosynthesis. Science 299, 2035-2038.

Hamme, R.C., Keeling, R.F. (2008) Ocean ventilation as a driver of interannual variability in atmospheric potential oxygen. Tellus Series B-Chemical and Physical Meteorology 60, 706-717.

Harris, I., Jones, P.D., Osborn, T.J., Lister, D.H. (2014) Updated high-resolution grids of monthly climatic observations – the CRU TS3.10 Dataset. International Journal of Climatology 34, 623-642.

Hurrell, J.W. (1995) Decadal Trends in the North Atlantic Oscillation: Regional Temperatures and Precipitation. Science 269, 676-679.

Jones, C.D., Collins, M., Cox, P.M., Spall, S.A. (2001) The Carbon Cycle Response to ENSO: A Coupled Climate–Carbon Cycle Model Study. Journal of Climate 14, 4113-4129.

Keeling, C.D., Chin, J.F.S., Whorf, T.P. (1996) Increased activity of northern vegetation inferred from atmospheric CO_2 measurements. Nature 382, 146-149.

Keeling, R.F., Manning, A.C., (2014) Studies of Recent Changes in Atmospheric O_2 Content, in: Turekian, K.K. (Ed.), Treatise on Geochemistry (Second Edition). Elsevier, Oxford, pp. 385-404.

Levitus, S., Antonov, J., Boyer, T. (2005) Warming of the world ocean, 1955-2003. Geophysical Research Letters 32.

McPhaden, M.J., Zebiak, S.E., Glantz, M.H. (2006) ENSO as an Integrating Concept in Earth Science. Science 314, 1740-1745.

Meals, D.W., Spooner,J., Dressing, S.A., Harcum, J.B., (2011) Statistical analysis for monotonic trends,, in: Agency, D.f.U.S.E.P. (Ed.). by Tetra Tech, Inc., Fairfax, VA, 23 p.

Meyers, S.R., (2014) Astrochron: an R package for astrochronology, http://cran.rproject.org/package=astrochron.

Myneni, R.B., Keeling, C.D., Tucker, C.J., Asrar, G., Nemani, R.R. (1997) Increased plant growth in the northern high latitudes from 1981 to 1991. Nature 386, 698-702.

Piao, S., Liu, Z., Wang, T., Peng, S., Ciais, P., Huang, M., Ahlstrom, A., Burkhart, J.F., Chevallier, F., Janssens, I.A., Jeong, S.-J., Lin, X., Mao, J., Miller, J., Mohammat, A., Myneni, R.B., Penuelas, J., Shi, X., Stohl, A., Yao, Y., Zhu, Z., Tans, P.P. (2017) Weakening temperature control on the interannual variations of spring carbon uptake across northern lands. Nature Clim. Change 7, 359-363.

Piao, S., Nan, H., Huntingford, C., Ciais, P., Friedlingstein, P., Sitch, S., Peng, S., Ahlström, A., Canadell, J.G., Cong, N., Levis, S., Levy, P.E., Liu, L., Lomas, M.R., Mao, J., Myneni, R.B., Peylin, P., Poulter, B., Shi, X., Yin, G., Viovy, N., Wang, T., Wang, X., Zaehle, S., Zeng, N., Zeng, Z., Chen, A. (2014) Evidence

for a weakening relationship between interannual temperature variability and northern vegetation activity. Nature Communications 5, 5018.

Piao, S.L., Ciais, P., Friedlingstein, P., Peylin, P., Reichstein, M., Luyssaert, S., Margolis, H., Fang, J.Y., Barr, A., Chen, A.P., Grelle, A., Hollinger, D.Y., Laurila, T., Lindroth, A., Richardson, A.D., Vesala, T. (2008) Net carbon dioxide losses of northern ecosystems in response to autumn warming. Nature 451, 49-U43.

Pickers, P.A., Manning, A.C. (2015) Investigating bias in the application of curve fitting programs to atmospheric time series. Atmos. Meas. Tech. 8, 1469-1489.

Raupach, M.R., Canadell, J.G., Le Quere, C. (2008) Anthropogenic and biophysical contributions to increasing atmospheric CO_2 growth rate and airborne fraction. Biogeosciences 5, 1601-1613.

Rödenbeck, C., Le Quéré, C., Heimann, M., Keeling, R.F. (2008) Interannual variability in oceanic biogeochemical processes inferred by inversion of atmospheric O_2/N_2 and CO_2 data. Tellus B: Chemical and Physical Meteorology 60, 685-705.

Scaife, A.A., Folland, C.K., Alexander, L.V., Moberg, A., Knight, J.R. (2008) European Climate Extremes and the North Atlantic Oscillation. Journal of Climate 21, 72-83.

Thompson, D.W., Wallace, J.M., Hegerl, G.C. (2000) Annular modes in the extratropical circulation. Part II: Trends. Journal of Climate 13, 1018-1036.

Thoning, K.W., Tans, P.P., Komhyr, W.D. (1989) Atmospheric carbon dioxide at Mauna Loa Observatory: 2. Analysis of the NOAA GMCC data, 1974–1985. Journal of Geophysical Research: Atmospheres 94, 8549-8565.

Varotsos, C.A., Tzanis, C.G., Sarlis, N.V. (2016) On the progress of the 2015–2016 El Niño event. Atmos. Chem. Phys. 16, 2007-2011.

Wilson, P., (2012) Insight into the Carbon Cycle from Continuous Measurements of Oxygen and Carbon Dioxide at Weybourne Atmospheric Observatory, UK, School of Environmental Sciences. Univeristy of East Anglia, Norwich, p. 155.

Wolter, K., Timlin, M.S. (1998) Measuring the strength of ENSO events: How does 1997/98 rank? Weather 53, 315-324.

Zhou, S., Miller, A.J., Wang, J., Angell, J.K. (2001) Trends of NAO and AO and their associations with stratospheric processes. Geophysical Research Letters 28, 4107-4110.

CHAPTER 7 SUMMARY AND CONCLUSIONS

7.1. Introduction

The over-arching aim of this thesis was to investigate the carbon cycle processes that control the variability of atmospheric CO_2, O_2 and APO on different spatial and temporal scales at two contrasting coastal locations from continuous observations. In Chapter 1, I discussed the applicability of atmospheric CO_2, O_2, and APO observations for use as a tool for understanding the global carbon cycle, with a particular focus on the terrestrial biosphere and the Southern Ocean.

The Southern Ocean is a key component of the global carbon cycle and there is much debate as to the efficiency of this region as a sink for anthropogenic CO_2 (e.g. Landschützer et al., 2015; Le Quéré et al., 2007). Due to compounding physical and biogeochemical factors, it is very difficult to investigate ocean carbon cycle processes from atmospheric CO_2 observations alone. APO, on the other hand, has a distinct oceanic signal. APO has been shown to be a useful tool when investigating the current state and future evolution of the Southern Ocean carbon cycle through model-observation comparisons (e.g. Nevison et al., 2012; Nevison et al., 2016). However, there are a limited number of APO monitoring stations in the region, exemplified by the current O_2 or APO "observational gap" in the South Atlantic and Weddell Sea sector of the Southern Ocean. This region is an important area of carbon export from the surface to the deep ocean, as well as a key region of atmosphere-ocean carbon exchange (e.g. Bakker et al., 2008; Brown et al., 2015).

There has been very little research on the similarities and differences of the APO seasonal cycle in the vicinity of the Southern Ocean, which could inform about regional carbon cycle processes and/or atmospheric transport patterns. Furthermore, the APO monitoring stations that do exist in the region are, for the most part, flask sampling sites; only two continuous measurement systems exist (Syowa Station, Antarctica (Ishidoya et al., 2012) and Baring Head, New Zealand (Manning, 2001)). Continuous measurements have the advantage of being able to capture synoptic scale variability in APO, driven by the combination of regional carbon cycle processes and atmospheric transport, which may otherwise be missed by flask measurements.

Consequently, the largest body of work in this thesis attempted to address the above points. I have built, tested and installed a continuous atmospheric O_2 and CO_2 measurements system at the Halley Research Station (Chapters 2 and 3). Atmospheric observations were collected for one year successfully before and unprecedented station

closure forced the instrumentation to be dismantled. However, one year of data did allow comparison of the seasonal cycle with other Southern Ocean APO stations and with modelled APO observations from two ocean circulation plus biogeochemistry model's (OCBMs) coupled to an atmospheric transport model (ATM). This was the focus of the research in Chapter 4.

Whilst Chapter 4 primarily focused on atmospheric CO_2, O_2 and APO variability on seasonal timescales across the Southern Ocean, Chapters 5 and 6 focused on the variability of atmospheric CO_2, O_2 and APO on inter-annual timescales from an existing monitoring station in the U.K.: the Weybourne Atmospheric Observatory (WAO). The proximity of WAO to the boreal forests of the northern hemisphere and to the North Atlantic Ocean makes it ideally placed to improve understanding of both the ocean and terrestrial carbon cycles of the northern hemisphere.

There has been a significant amount of research using northern hemisphere atmospheric CO_2 observations to characterise the current state of the terrestrial carbon cycle and it's response to current climate change through analysis of the inter-annual variability of the seasonal cycle and the growth rate (e.g. Keenan et al., 2016; Piao et al., 2008). However, no such research has been undertaken with respect to the variability of the O_2 and APO seasonal cycles, which may infer changes to the ocean carbon cycle (APO) in addition to the terrestrial carbon cycle (O_2). Moreover, there is a limited amount of research on the inter-annual variability of the O_2 and APO growth rate (e.g. Eddebbar et al., 2017; Rödenbeck et al., 2008). These existing studies have focused on stations within the Scripps Institution of Oceanography (SIO) network that have a bias towards the Pacific Ocean owing to their location. By revising and extending the WAO atmospheric CO_2, O_2 and APO record in Chapter 5, I have reduced these geographic gaps by examining the inter-annual variability of the seasonal cycle and growth rate of the species. In Chapter 6, I examined whether statistical relationships exist between the trends seen and measures of the climate (temperature, precipitation and climate indices).

In this final chapter, I summarise and review the work undertaken in each chapter, discuss the implications of the work and comment on future areas of research. I assess whether the work has addressed the knowledge gaps outlined above and met the objectives set out in Chapter 1 of this thesis.

7.2. The atmospheric O_2 and CO_2 measurement system

In Chapter 2, I explained the theory and design of the measurement system built for the purpose of addressing the O_2 observational gap in the South Atlantic and Weddell Sea sector of the Southern Ocean. The requirement for the measurements to capture synoptic scale variability of the species in the region meant that a continuous system was required, whereas personnel time demands at HBA also meant the system needed to be almost entirely automated. Consequently, the system was based on a similar set up that has been collecting data at WAO since 2008 (Wilson, 2012). Although the system was based on this blueprint (as many other continuous O_2 and CO_2 measurement systems are (e.g. Pickers, 2016; Thompson et al., 2007; van der Laan-Luijkx, 2010)), a large amount of work (1.5 years) was necessary to build what is largely a custom, homemade system, and to achieve the required precision and accuracy demanded for O_2 measurements (Tans and Zellweger, 2016). Nevertheless, during this period I did implement modifications to the system. These included the removal of the first stage drying component (which was not necessary for Antarctic work) and the implementation of a new position of the "fast purge" line which allowed key components of the gas handling system to maintain the conditioning achieved under a constant 100 ml min^{-1} flow rate. In addition, the major improvement I implemented was a reduction in the sample and reference gas switching time.

Having a faster sample and reference fuel cell switching time (30 seconds compared to 60 seconds) improved the O_2 measurement precision by a factor of 1.4. This is due to the reduction in the signal to noise ratio imparted by the averaging period of the measurement. Whilst the ideal switching time was found to be 2.6 seconds (see Section 2.4.2), the current fuel cell's response time (Maxtec MAX-250; 15 seconds) and the constraints imparted by the software control, meant that this could not be achieved. However, using the Maxtec 250 ESF fuel cell, which has a response time of 5 seconds, would allow a switching time of 7.6 seconds - closer to the ideal switching time of 2.6 seconds. Software control constraints would also have to be overcome. However, if this were achieved, then the measurement precision would theoretically improve by a factor of 2.2 upon that achieved with a 60 second switching time. Future O_2 measurement system builds should therefore consider this if they are to use the fuel cell measurement technique.

Following the construction period at UEA, the measurement system was installed at HBA in February 2016 and performed very well for a period of ~11 months with minimal downtime. The internal reproducibility of the ambient air measurements during this period were $\delta(O_2/N_2)$ of ± 6.1 per meg and ± 0.007 ppm for CO_2, which is comparable to other fuel cell based O_2 measurement systems and meets the World Meteorological Organization's (WMO) Global Atmosphere Watch (GAW) programme goals (Tans and Zellweger, 2016). However, the reproducibility of the system determined from repeat measurements of a Target Tank highlighted issues that were not apparent in the analysis of the precision of ambient air measurements. Whilst the O_2 measurement precision was not impacted, the precision of the CO_2 measurements deteriorated as a consequence of the poor laboratory temperature stability over the winter months. Although more stable CO_2 analysers do exist, such as the Picarro, the vacuum based measurement principle and the higher flow rate are not compatible with the O_2 fuel cell based measurement principle. As such, O_2 and CO_2 cannot be measured simultaneously. This is necessary in order to correct for the CO_2 dilution effect on the O_2 mole fraction. Temperature control within the lab must therefore improve if the measurement precision of CO_2 is to be improved at HBA.

7.3. Analysis of atmospheric CO_2, O_2 and APO observations at Halley Research Station

The aim of Chapter 4 was to investigate the processes that control atmospheric CO_2, O_2 and APO variability on different spatial and temporal scales from the measurement system installed at HBA. This work contributed to the O_2 measurement gap in the South Atlantic and Weddell Sea sector of the Southern Ocean.

I began by investigating what could be learnt from historical flask measurements of atmospheric CO_2 collected at HBA for the 2000-2015 period. Specifically, I set out to determine which carbon cycle processes control the seasonality of atmospheric CO_2 depicted by the flask observations using the CarbonTracker Europe 2016 (CTE2016) atmospheric inversion scheme (van der Laan-Luijkx et al., 2017).

The analysis indicated that the modelled CO_2 seasonal cycle at HBA appears to be largely controlled by the terrestrial biosphere, particularly the amplitude. However, the timing of the upwards and downwards zero crossing days (UZC, DZC, respectively) of the modelled CO_2 seasonal cycle, although primarily determined by the phase (timing of

UZC and DZC) of the terrestrial biosphere fluxes, appeared to be modulated somewhat by (1) the magnitude of the late summer-early autumn ocean outgassing and (2) the combined influence of ocean CO_2 uptake and the decrease in biomass burning plus fossil emissions in the late spring-early summer (UZC).

However, although the results were statistically conclusive, the analysis is likely to be biased by uncertainties inherent within the CTE2016 mode1. In particular, the sparseness of the datasets that fed into the model, both in the *a prior* fluxes and the optimised *a posterior* fluxes, likely resulted in larger uncertainties than would otherwise be found in regions of more dense data coverage. No attempt was made to quantify these uncertainties and should therefore be the focus of future work.

Furthermore, I highlighted how the choice of curve fitting routine and its parametrisation used in this analysis will also influence the results. Although much consideration was given to the choice of curve fitting routine and the selection of the parametrisation values, it would be advisable to carry out a sensitivity analysis using a range of parametrisation values and by selection of a different curve fitting routine, as was demonstrated by Pickers and Manning (2015).

The use of the CTE2016 atmospheric inversion scheme at HBA represents the first such use of the model at an Antarctic coastal station and the first time this iteration of the model has been used to understand the processes that control the atmospheric CO_2 seasonal cycle at high southern latitudes. Future work should extend the analysis to other Southern Ocean CO_2 monitoring stations. Moreover, whilst the results are not conclusive, given the uncertainties, they do merit further investigation. For example, the *a prior* ocean flux fields could be improved from those of Jacobson et al. (2007). A more novel technique for interpolating sparse datasets, such as using the flux fields from the neural network approach of Landschützer et al. (2013), could be used to more accurately determine the *a prior* ocean fluxes.

The second objective of the research presented in Chapter 4 was to investigate synoptic scale variability of atmospheric O_2, CO_2 and APO to ascertain to what extent the variability observed could be explained by local to regional scale carbon cycle processes.

This objective was not fulfilled within the time frame of the Ph.D. A significant event within the continuous observation record was defined by deviation of the observations from the curve fit by > 2σ. Only one such event was found in the record (in February 2016). This was briefly explored in Appendix B. The large positive excursion in APO and negative excursion in CO_2 may have been explained by air deriving from a

region of intense productivity in the Southern Ocean to the east of South America, but was not explored further than this. The remainder of the observation record was not forthcoming with events and so this analysis was abandoned. It may not be surprising that the winter record did not exhibit events of the magnitude observed in February. This may be due to the increased distance from the ocean that HBA is due to the winter sea ice extent. This analysis should still be pursued however. A longer dataset may be more forthcoming with events.

Defining the magnitude of a significant event is difficult and the more one scrutinises the variability, the more an explanation for the variability seen is needed. Atmospheric transport plays a key role in whether an event, which could be regarded as an instantaneous carbon cycle event in space and time (such as a phytoplankton bloom), is detected. That said, whether such an instantaneous event can be detected, or whether it is more prudent to consider events as regions of the ocean where these instantaneous events happen, whereby atmospheric transport actually defines the magnitude of the event detected, still needs to be explored.

In future work, I would suggest that satellite productivity data be examined and a net O_2 flux to the atmosphere could be derived based on the O_2:C exchange ratio for phytoplankton. Other factors influencing the O_2 flux, such as the temperature solubility effect and ocean circulation, would also need to be considered. This flux could then be fed into a transport model with air subsequently sampled at HBA. The magnitude of the event detected in the modelled atmospheric observations and the role atmospheric transport plays in defining the strength of the event could be investigated.

The third objective of Chapter 4 was to compare the seasonal cycle of APO observed at HBA to that observed at other Southern Ocean stations and assess what could be learnt about the spatial and temporal variability of carbon cycle processes within the Southern Ocean region. However, before specifically addressing this objective, I presented the seasonal cycle of each of the species observed at HBA over the measurement period. Examination of the CO_2 seasonal cycle observed from the continuous data, compared to the climatological seasonal cycle observed from flask observations (2000-2015), allowed me to assess whether the seasonal cycle observed for APO was likely to be a typical seasonal cycle – a key assumption when comparing to other climatological APO seasonal cycles at other monitoring stations.

The CO_2 seasonal cycle observed from the continuous measurement system has an amplitude of 1.71 ± 0.13 ppm. Compared to the flask observations, in terms of the

seasonal peak to peak amplitude and the autumn zero crossing day, 2016 is comparable to other years in the 2000-2015 period, yet it is still not a typical year in comparison to the climatological mean. Secondly, the spring zero crossing day appears to be anomalous. These differences could potentially be explained by the poor data coverage in January 2017 and February 2016 due to decommissioning and installation of the measurement system, respectively. However, the differences may also be explained by the moderate to strong El Niño event that occurred in 2016 (Betts et al., 2016). The influence of El Niño on the seasonal cycle of atmospheric CO_2 should be examined further by extending the analysis of the flask record back to include the 1998 El Niño event. This would likely ascertain whether this could be a casual factor in the difference observed between the climatological seasonal cycle and that observed in 2016.

The $\delta(O_2/N_2)$ and APO seasonal cycles have an amplitude of 77 ± 11 and 73 ± 11 per meg, respectively. In comparison to other Southern Ocean APO monitoring stations (Palmer Station, Antarctica (PSA), South Pole Observatory (SPO) and Cape Grim Observatory (CGO)), HBA exhibited the largest amplitude (73 ± 11 per meg) of all stations. However, the HBA mean overlaps with the errors associated with the means of the other stations, with the exception of SPO. The absolute differences in the amplitude observed at HBA, CGO and PSA are therefore not significant. This would therefore suggest a basin wide carbon cycle influence on all stations. However, improvements in measurement precision and in the quality of the curve fit could reduce the errors on the amplitude. If this were possible, then the absolute differences could suggest that HBA, in comparison to the other stations, is either influenced by large local seasonal oceanic O_2 fluxes, from the Weddell Sea for example, or similarly, samples air deriving from a larger region that exhibits large seasonal fluxes, such as the South Atlantic sector of the Southern Ocean. If the synoptic scale variability showed large events that were attributed to this region, then this would support this speculation. However, as already discussed, the synoptic data presented in this research do not suggest this in the time period presented.

By plotting the amplitude observed at each station against the station's latitude, a small gradient was observed from HBA (75˚S) towards CGO (40˚S) of -2.4 per meg/10˚ latitude. The gradient is within the uncertainty of the stated errors on each station's amplitude. However, unpublished data from a continuous atmospheric O_2 and CO_2 measurement system on-board the Laurence M. Gould Research ship, which continuously sails between South America and PSA, displays a seasonal amplitude gradient of ~ -20 per meg/10˚ latitude over the 55-65 ˚S latitude range (B. Stephens, *personal*

communication). Averaging this over the latitude range presented here would result in -5.7 per meg/10˚ latitude gradient. I speculated that this gradient could imply that the magnitude of seasonal O_2 exchange is largest at the southern boundary of the Southern Ocean, where it meets Antarctica, and that the magnitude of the seasonal fluxes decreases at lower latitudes in the Southern Ocean.

This work should be pursued further. Increasing the number of APO monitoring stations across the latitude range, although difficult, could help to confirm this on inter-annual timescales, with variations in the gradient possibly indicative of inter-annual variability in the Southern Ocean carbon cycle. Moreover, as demonstrated by the Laurence M. Gould research vessel, installing measurement systems on polar going vessels is a good way of making repeat measurements over a significant latitude range. Aircraft measurement campaigns also have this advantage (Stephens et al., 2018), however, they are limited in that they provide only a snapshot in time. Finding the necessary funding to make such repeat aircraft campaigns would be difficult, yet the data, as is beginning to be shown (Stephens et al., 2018), could be invaluable.

Furthermore, I discussed the similarities and differences between the phasing of the seasonal cycle observed at each of the stations considered in this analysis. HBA was most similar to SPO in terms of its phasing and I speculated that this was due to a similar air mass history, which was supported by a cluster analysis of HYSPLIT transport model back trajectories (Draxler and Hess, 1998). However, further work would be needed to confirm the similar air mass history, which could be easily confirmed using a larger dataset of atmospheric circulation reanalysis data. I speculated that if the air mass history were similar, then the difference in the amplitude observed at HBA and SPO could represent an important test for atmospheric transport models with respect to the vigour of vertical mixing.

Although the conclusions made in this section of Chapter 4 are limited somewhat by the uncertainties in the analysis. HBA does represent a vital addition to the APO monitoring network in the Southern Ocean. Reducing the uncertainties associated with characterising the seasonal cycle at each of the stations could further highlight regional differences in the Southern Ocean carbon cycle that I have discussed. However, at this time, it is only possible to confirm that the stations depict a relatively homogeneous atmospheric APO response to processes that influence the seasonality of the Southern Ocean carbon cycle.

The final objective of the research presented in Chapter 4 was to determine whether APO observations in the Southern Ocean, with the addition of HBA, highlight deficiencies or strengths in OCBMs that are otherwise overlooked with fewer stations to compare against.

Two OCBM's (MOM4 (Dunne et al., 2013) and CESM (Long et al., 2013)) coupled to an ATM (TM3 (Heimann, 2003)) were used to generate modelled APO observations at each of the stations in the analysis. The results were then compared to the measured observations. Whilst MOM4+TM3 reproduced the amplitude well at PSA and SPO, it slightly underestimated it at HBA, and even more so at CGO. Overall however, MOM4+TM3 performed better than CESM+TM3 at reproducing the APO amplitude observed at the stations considered. Furthermore, in terms of the phasing, MOM4+TM3 is the most consistent across all stations. Whilst CESM+TM3 displays the best phasing agreement seen across all stations and models at CGO and SPO, it performs the worst at HBA and PSA. In general, CESM+TM3 appears to be overestimating the APO fluxes and, in terms of phasing, performs least well at the two coastal Antarctic stations.

The inter-model and inter-station model differences could be due to a combination of the way in which the models characterise net ecosystem production and the physical mixing of the surface waters with more intermediate layers, either locally or basin wide. A local assesment of the models within the Ross Sea (Rickard and Behrens, 2016) found that CESM slightly overestimates cholorphyll concentrations whilst MOM4 displays a slight underestimation between November-March with respect to satellite SeaWiFS data, which agrees with the results of the analysis presented here. However, with respecct to the seasonal MLD, both models display a shallow bias across the Southern Ocean compared to observations (Huang et al., 2014; Sallée et al., 2013). This would act to dampen air-sea fluxes during winter but increase them during summer, which in turn implies, that if a model does well at recreating the observed seasonal cycle, then the biological component of the O_2 flux could be underestimated in summer and overestimated in the winter and/or vertical mixing in the ocean circulation model is too large.

The analysis presented here does demonstrate the value of having an additonal coastal Antarctic APO monitoring station in different oceanic regions to those already established when testing OCBMs coupled to an ATM. Whilst the models' general skill at recreating the APO seasonal cycle across stations is indicative of basin wide model differences. The relative skill of each model at recreating the seasonal cycle at individual

stations does indicate regional heterogenity within the models. To assess why these differences exist, the next logical step would be to investigate the dissolved O_2 profiles within the different regions: the South Atlantic, Pacific and Indian Ocean sectors of the Southern Ocean. The seasonal variability of dissolved O_2 in the surface ocean will control the seasoanl O_2 flux to or from the atmosphere. Understanding whether the models accurately capture the dissolved O_2 profiles in each of the Southern Ocean regions, by comparison with measursed profiles would further indicate how well the models are respresenting physcial mixing and net community production at a regional level.

7.4. Analysis of atmospheric CO_2, O_2 and APO observations at the Weybourne Atmospheric Observatory

The overarching aim of Chapters 5 and 6 was to examine the variability of atmospheric CO_2, O_2 and APO at different spatial and temporal scales from the Weybourne Atmospheric Observatory on the north Norfolk coast of the U.K. The WAO O_2 and CO_2 measurement system was installed by Wilson (2012) in 2008. The primary aim of Chapter 5 was to revise and extend the WAO continuous, *in situ*, atmospheric CO_2, O_2 and APO record. The record now represents seven years of data collected between 2008 and 2015 and can be used to investigate trends in the seasonal cycles and growth rates of the species. Chapter 5 focused on the seasonality and growth rates of the species observed at WAO in comparison with other northern hemisphere monitoring stations. I discussed the mechanisms behind the seasonality and the growth rates of each species and included a speculative discussion of the regional differences observed between the stations. Chapter 6 examined these trends in detail.

I began by implementing a rigorous method for baseline extraction in each of the respective species and subsequently decomposed the baselines using a curve fitting routine to extract the seasonal and trend components. Using a combination of different techniques to extract the baseline has the merit of accounting for drawbacks associated with one particular technique. I would recommend other researchers to follow this method for baseline extraction and encourage them to consider the type of curve fitting routine and it's parameterisation that is appropriate to the data analysis.

CO_2 has a mean amplitude of 15.2 ± 2.2 ppm, whilst $\delta(O_2/N_2)$ has a mean amplitude of 130 ± 15 per meg. By examining the shape of the $\delta(O_2/N_2)$ seasonal cycle in the context of the observed APO (55 ± 11 per meg) and CO_2 seasonal cycles, I proposed

that the $\delta(O_2/N_2)$ minimum at WAO is driven primarily by ocean exchange, whereas the maximum is characterised by terrestrial exchange. However, I did not examine whether this feature was true of other northern hemisphere station seasonal data. This would be needed to determine whether the above assertion is true. For example, examining data sets with a similar balance of ocean and terrestrial influences to WAO and those that have a very different influence i.e. a predominantly ocean or a terrestrial influence.

The amplitude of the seasonal cycles from this analysis were within the error bounds stated by Wilson (2012). Wilson (2012) did not attempt to extract a baseline for the data in his analysis. This therefore suggests that it may not be necessary to undergo the rigorous extraction method applied here before applying a curve fit. That said, a comparison of the different methods should be done across multiple stations and time periods before determining whether a baseline extraction is completely necessary for a time series decomposition. However, extraction of the baseline would help to more clearly define an event within synoptic scale data (not examined here).

Regional differences were observed between the seasonality of the species observed at WAO and at other northern hemisphere monitoring stations (Mauna Loa Observatory, Hawaii (MLO), Cold Bay, Alaska (CBA) and Alert, Canada (ALT). The different amplitude and phase observed at CBA and WAO, which are at a similar latitude, likely indicates the importance of atmospheric transport in modulating both the terrestrial and marine seasonal cycles of CO_2 and $\delta(O_2/N_2)$ across the northern hemisphere. ALT, on the other hand, given its high latitude Arctic location, displayed a seasonality that is likely explained by the seasonal irradiance regime. To examine further the impact that regional atmospheric transport has on the seasonal cycles at the respective stations it would be beneficial to undertake a modelling analysis. Atmospheric transport could be controlled and varied at each of the stations. Predominant transport regimes could be "tagged" and atmospheric data filtered based on the air mass history. Examining the resultant seasonal cycles and their differences under different transport regimes could quantify this variable.

The atmospheric growth rates of each of the species observed at WAO were also compared to the other northern hemisphere stations discussed in Chapter 5. The observed differences and similarities between the stations indicated a spatial and temporal variability in the processes that drive the variability of the growth rates. Up to 2012-2013, the CO_2, $\delta(O_2/N_2)$ and APO growth rates across all stations were in agreement, with only very slight phase offsets. However, after the beginning of 2013, each station becomes

increasingly out of phase with one another. I speculated that this could indicate a hemispheric wide carbon cycle response to a particular driving force, whilst after 2013 regional processes may be playing more of a role. This analysis was taken further in Chapter 6. Finally, the analyses undertaken in Chapter 5 also indicated there was a significant amount of variability in the seasonal cycle of the species, as has been observed in atmospheric CO_2 by other authors (e.g. Graven et al., 2013; Piao et al., 2008).

The aim of Chapter 6 was to investigate the inter-annual variability of the seasonal cycles and growth rates of atmospheric CO_2, O_2 and APO at WAO, discussed in Chapter 5, and assess whether a statistical relationship exists with the variability of the climate.

There is a significant shift towards an earlier autumn zero crossing (AZC) at WAO in CO_2 (-1.40 days yr^{-1}) and, to a lesser extent, $\delta(O_2/N_2)$ (-0.92 days yr^{-1}). I presented this finding in the context of other stations and showed the importance in the choice of curve fitting programme. In particular, I found the opposite CBA trend compared to Piao et al. (2008), which could be a reflection of the different curve fitting parameters used and the different time periods of analysis. Moreover, the rate of decrease in the autumn zero crossing day at WAO is much higher compared to the results of Piao et al. (2008) and Graven et al. (2013), who analysed CO_2 over different time periods: 1980-2002 and 1960-2010, respectively, of a global CO_2 dataset that did not include WAO. The larger trend seen at WAO could therefore be due to the different time period of analysis and/or could signify a response to greater autumn warming in the late 2000s, as was proposed by Barichivich et al. (2012)

The analysis indicated that the AZC trend in CO_2 is well correlated with northern hemisphere spring temperatures ($R = -0.71$, *$p = 0.07$; Tau = -0.71, $p = 0.03$*), rather than autumn temperatures, in contrast to Piao *et al.* (2008). I speculated that a warmer spring stimulates more growth during the start of the growing season, leading to an overall greater accumulation of biomass, which subsequently results in greater respiration in the autumn months, as there is simply more biomass to respire. However, for this to be true, one would also expect a positive correlation between the amplitude of the seasonal cycle and the northern hemisphere spring temperature. Conversely, there is a negative correlation between the CO_2 amplitude and the northern hemisphere spring temperature trends ($R = -0.60$; *$p = 0.13$, Tau = -0.24, $p = 0.56$*). Explaining the correlation between the AZC in CO_2 and northern hemisphere spring temperatures is challenging and merits further investigation. It could be that the spring temperature trends could also be linked to the trend towards the more El Niño like conditions in recent years.

The correlation with spring temperatures is also seen in the AZC of $\delta(O_2/N_2)$ (e.g. North Atlantic spring temperature: R = -0.80, *p = 0.03; Tau =-0.71, p = 0.03).* However, in contrast to CO_2, I have shown this to be linked to the Arctic Oscillation (AO) (R = -0.71, *P = 0.05; Tau = -0.64, P = 0.03*), whereby a negative phase in 2013 in particular, drives a later crossing anomaly. 2013 was in contrast to the general trend towards a warmer spring, whereby cooler and wetter conditions associated with a negative AO phase in the mid latitudes, stimulates greater terrestrial biosphere growth in much same way as La Niña conditions do. However, if this is the mechanism, then AO signal should also be correlated with the CO_2, which it is not. There could be an ocean response within the $\delta(O_2/N_2)$ AZC, however this should be apparent in the APO AZC also, which it is not.

The spring zero crossing (SZC) in CO_2, is very well correlated with the annual El Niño Southern Oscillation (ENSO) index (R = -0.87, *p = 0.005; Tau = -0.64, p = 0.03)*, and the trend towards an earlier onset of springs appears to be linked with the trend towards a more positive El Niño like state over this time period. Thus warmer conditions stimulating earlier growth, is also supported by the $\delta(O_2/N_2)$ trends.

Whilst statistical trends in the AZC of the CO_2 and O_2 seasonal cycle are indicative of changes within the terrestrial biosphere, no such phase shifts are observed in the APO seasonal cycle. Conversely, the APO amplitude does show a decreasing trend over the time period (3 per meg yr^{-1}), whilst the CO_2 and O_2 and amplitudes show no evidence of the trend found by other authors for CO_2. If the decrease in the APO amplitude is a response of the ocean carbon cycle to current climate change, then this should be investigated further. More stations should be examined, particularly in the North Atlantic.

The results presented here do indicate that there is a statistical relationship between climate variability and the seasonal variability within the WAO atmospheric CO_2, $\delta(O_2/N_2)$ and APO record. There is evidence that both regional and hemispheric climate variability influences the seasonal cycles, however, hemispheric scale climate variability appears to be the dominant driver. Moreover, clear casual mechanisms are not forthcoming. The explanations proposed for terrestrial biosphere responses to the climate should be apparent in both the CO_2 and O_2 trends. Here, they are often at odds with each other.

Finally, a marine carbon cycle response to ENSO is observed in the inter-annual variability in the APO growth rate at WAO (R= 0.24, p = 0.05; *Tau* = 0.2, p = 0.01). However, a much stronger terrestrial carbon cycle response to the different phases of

ENSO and North Atlantic Oscillation (NAO) is apparent in the growth rates of CO_2 and $\delta(O_2/N_2)$. The NAO index is positively correlated with the $\delta(O_2/N_2)$ growth rate (R= 0.47, p = 0.03; *Tau = 0.34*, p = 0.02) and the CO_2 growth rate (R= 0.70, p = 0.12; Tau = 0.47, p = 0.15). Moreover, the CO_2 growth rate is positively correlated with ENSO (R= 0.60, $p < 0.0001$; *Tau* = 0.39, $p < 0.0001$), whilst a negative correlation is seen between ENSO and the growth rate in $\delta(O_2/N_2)$ (R=-0.48, $p < 0.0001$; *Tau* = -0.25, p = 0.004).

The link between the CO_2 growth rate and ENSO is well known and is predominantly due to the response of the terrestrial biosphere to the phases of ENSO (e.g. Jones et al., 2001). Given that the O_2 growth rate will also be driven by the same processes, the correlation between O_2 and ENSO is not surprising. Conversely, there is a strong positive correlation between the NAO and the CO_2 observed at WAO. This implies that regional climate variability does impact the CO_2 growth rate and is indicative of a regional terrestrial carbon cycle response to the climate mode, supporting the work of Bastos et al. (2016). However, O_2 should be negatively correlated to support the terrestrial biosphere response interpretation, but instead shows a positive correlation. That said, the O_2 growth rate will have an ocean influence in addition to the terrestrial biosphere influence which may be masking the terrestrial biosphere response. APO does not show any correlation with the NAO however.

This work does represent a significant addition to the small amount of research that exists on the inter-annual variability of APO. Whilst a response to ENSO is observed in the APO growth rate at WAO, it is not as strong as the relationship observed by Eddebbar et al. (2017). This likely represents the remoteness of WAO to the Pacific Ocean compared to the SIO sites used by Eddebbar et al. (2017).

7.5. Conclusions

The research presented in this thesis has demonstrated some of the insight that atmospheric O_2 and CO_2 observations can give with respect to understanding carbon cycle processes in two distinct regions of the globe. Establishing a new atmospheric O_2 monitoring at HBA allowed investigation of the spatial variability of carbon cycle processes in the Southern Ocean region by comparison to other O_2 monitoring stations within the region. Conversely, the revision and extension of the WAO observation record

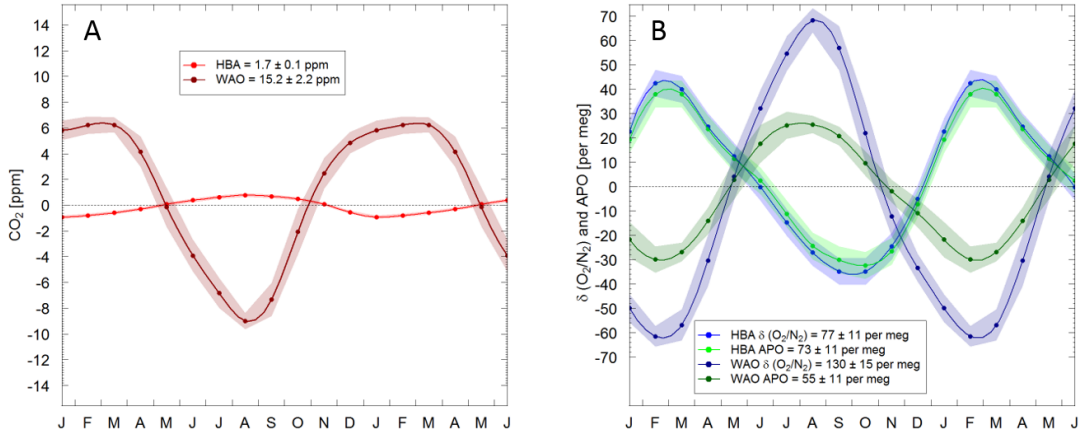

Figure 1.1. The seasonal cycle of atmospheric CO_2 (A), $\delta(O_2/N_2)$ and APO (B) observed at WAO and HBA (see key) .The peak to trough seasonal amplitude for each species are shown in the key. Y-axes are scaled such that CO_2, $\delta(O_2/N_2)$ and APO are visually comparable on a mole per mole basis. The x-axis represents the first letter of individual months and the first 6 months are repeated to aid visual interpretation of the cycles. Individual points represent the monthly mean values of the curve fit. Lines represent a subsequent spline fit to the monthly data. Shaded error bands represent the 1σ standard deviation of the residuals of the curve fit and so represents closeness of the fit to the measured data, rather than month to month variability as is often shown.

allowed the investigation of the inter-annual variability of the seasonal cycles and growth rates that were primarily related to terrestrial biosphere variability.

A comparison of the atmopsheric CO_2, O_2, and APO observations at HBA and WAO (**Figure 1.1**) demonstrates the different carbon cycle influences at each location. WAO shows a much larger seasonal cycle in CO_2 and O_2 than HBA. This is due to the different proximity of the stations to terrestrial carbon cyle processes. WAO samples air masses that exchange CO_2 and O_2 with the terrestrial biosphere of the northern hemisphere, where as HBA samples air masses that exchange with the Southern Ocean, as exmplified by the larger APO seasoanl cycle.

Although the WAO atmospheric CO_2 seasonal cycle is much larger than that displayed at HBA, the CTE2016 model analysis of atmospheric CO_2 flask observations at HBA indicated that the CO_2 seasonal cycle is largely controlled by the terrestrial biosphere rather than the ocean, with the ocean CO_2 flux modulating the timing of the phase and magnitude of the amplitude. How much of the terrestrial biosphere influence is from the northern and southern hemispheres was not determined and should be addressed in future work Moreover, uncertainty within the CTE2016 model due to the sparseness of observation sites that are used in the derivation of *a prior* fluxes and in the optimization of *a posterior* fluxes also needs to be addressed.

The comparison of the HBA APO seasonal cycle with other stations in the region did indicate some regional variability of the processes that control the seasonal cycle. I speculated that HBA captures large O_2 fluxes in the South Atlantic and Weddell Sea sectors of the Southern Ocean, in comparison to other stations. However, the conclusions were limited by the uncertainty assigned to the seasonal cycles. This was primarily due to measurement uncertainty and the quality of the curve fits to the data. Reducing these uncertainties must be the focus of future work if the differences between the stations, and the speculative reasons behind them, are to be investigated further.

The examination of the two OCBM's ability to recreate the seasonal cycle of APO observed at Southern Ocean stations allowed the interrogation of the mechanisms within the models that control atmosphere-ocean O_2 fluxes. Inter-model and inter-station differences highlighted both basin-wide model differences and a regional heterogenity in the models' characterisation of the processes. Future work should focus on this regional heterogenity within the models. Examination of dissolved O_2 profiles within the different ocean basins of the Southern Ocean would be a prudent next step.

Whislt the HBA research focused on the seasonaility of atmospheric CO_2, O_2, and APO, the WAO research focused more on longer term trends in the seasonal cycles and growth rates of the species. However, I began by comapring the WAO seasoanl cycles to other observations in the northern hemisphere, in much the same way as I did for the APO seasoanl cycle across the Southern Ocean. In comaprison to the Southern Ocean, APO in the northern hemiphere, as well as CO_2 and O_2, displayed much more regional heterogenity. Furthermore, the comparison of the seasonal cycles and growth rates in the northern hemisphere highlighted the regional variability of carbon cycle processes that result in the exchange of atmopsheric O_2 and CO_2 with air masses that are sampled by the different stations. In particular, the comparison in the growth rates potentially indicated a

shift from hemispheric scale driving processes to more regional scale driving processes over the time period analysed (2008-2015).

By quantifying the trends in the seasonal cycles of the species at WAO, I discovered that the WAO CO_2 seasonal cycle displays a shift towards an earlier AZC that has been seen by other authors (Graven et al., 2013; Piao et al., 2008). However, the rate of decrease in the AZC at WAO is much higher compared to the results of Piao et al. (2008) and Graven et al. (2013).

A statistical relationship between climate variability and the seasonal variability within the WAO atmospheric CO_2, $\delta(O_2/N_2)$ and APO record was found. However, explanations for the relationships, whilst speculated, were not found. Future work should therefore focus on understanding these relationships. Isolating the terrestrial biosphere and ocean response to variations in climate could be examined with subsequent model runs. For example, by using a coupled terrestrial biosphere-climate model, parameters such as precipitation and temperature could be held constant whilst the other was allowed to vary. The same could be done with respect to coupled climate-ocean carbon cycle models.

Investigating the growth rate variability at WAO showed that the CO_2 and O_2 growth rates have a strong relationship with ENSO. However, whilst APO also showed a relationship with ENSO, it was much weaker than that found by Eddebbar et al. (2017). This is likely due to the remoteness of WAO to the Pacific Ocean compared to the SIO stations analysed by Eddebbar et al. (2017). Furthermore, a relationship was also found between the NAO and the CO_2 growth rate, likely indicating a terrestrial biosphere response to the climate mode. The O_2 growth rate also displayed a relationship with NAO, however this was opposite in sign to what should be expected from a terrestrial biosphere response.

Finally, whilst the research presented in this thesis has, for the most part, answered the research questions set out in Chapter 1, many questions and uncertainties remain, many of which have been discussed throughout this final chapter. Maintaining O_2 and CO_2 measurement stations in remote regions of the globe is difficult, however, the research into the long term trends observed at WAO highlights why this work is valuable. Furthermore, a significant amount of research has gone into characterising the northern terrestrial biosphere and it's response to current climate change. Conversely, there is a lack of research investigating the variability of atmospheric O_2, CO_2 and APO observations due to Southern Ocean carbon cycle variability. The additional insight that

APO has on ocean carbon cycle processes compared to atmospheric CO_2 observations alone has been demonstrated in this thesis. Future APO work needs to characterise the gradients that have been observed in this thesis. However, the gradients are at the limit of the measurement uncertainty and reducing these uncertainties on measurement systems that need to be mobile, such as on aircraft or on research vessels, should be a primary focus of the APO measurement community.

7.6. References

(NGDC/WDS), N.G.D.C.W.D.S., (2017) Global Significant Volcanic Eruptions Database., in: Center., N.G.D. (Ed.). NOAA, U.S. .

Allan, B.J., Carslaw, N., Coe, H., Burgess, R.A., Plane, J.M.C. (1999) Observations of the Nitrate Radical in the Marine Boundary Layer. Journal of Atmospheric Chemistry 33, 129-154.

Ambaum, M.H.P., Hoskins, B.J., Stephenson, D.B. (2001) Arctic Oscillation or North Atlantic Oscillation? Journal of Climate 14, 3495-3507.

Anav, A., Friedlingstein, P., Kidston, M., Bopp, L., Ciais, P., Cox, P., Jones, C., Jung, M., Myneni, R., Zhu, Z. (2013) Evaluating the Land and Ocean Components of the Global Carbon Cycle in the CMIP5 Earth System Models. Journal of Climate 26, 6801-6843.

Anderson, L.A. (1995) On the hydrogen and oxygen content of marine phytoplankton. Deep Sea Research Part I: Oceanographic Research Papers 42, 1675-1680.

Arrhenius, S. (1896) On the influence of carbonic acid in the air upon the temperature of the ground. Philosophical Magazine 41, 237-276.

Bacastow, R.B. (1976) Modulation of atmospheric carbon dioxide by southern oscillation. Nature 261, 116-118.

Bacastow, R.B., Keeling, C.D., Whorf, T.P. (1985) Seasonal amplitude increase in atmospheric CO_2 concentration at Mauna Loa, Hawaii, 1959-1982. Journal of Geophysical Research-Atmospheres 90, 10529-10540.

Baddouh, M.b., Meyers, S.R., Carroll, A.R., Beard, B.L., Johnson, C.M. (2016) Lacustrine 87Sr/86Sr as a tracer to reconstruct Milankovitch forcing of the Eocene hydrologic cycle. Earth and Planetary Science Letters 448, 62-68.

Bakker, D.C.E., Hoppema, M., Schröder, M., Geibert, W., De Baar, H.J.W. (2008) A rapid transition from ice covered CO_2-rich waters to a biologically mediated CO_2 sink in the eastern Weddell Gyre. Biogeosciences Discussions 5, 1205-1235.

Bakker, D.C.E., Pfeil, B., Landa, C.S., Metzl, N., O'Brien, K.M., Olsen, A., Smith, K., Cosca, C., Harasawa, S., Jones, S.D., Nakaoka, S.I., Nojiri, Y., Schuster, U., Steinhoff, T., Sweeney, C., Takahashi, T., Tilbrook, B., Wada, C., Wanninkhof, R., Alin, S.R., Balestrini, C.F., Barbero, L., Bates, N.R., Bianchi, A.A., Bonou, F., Boutin, J., Bozec, Y., Burger, E.F., Cai, W.J., Castle, R.D., Chen, L., Chierici, M., Currie, K., Evans, W., Featherstone, C., Feely, R.A., Fransson, A., Goyet, C., Greenwood, N., Gregor, L., Hankin, S., Hardman-Mountford, N.J., Harlay, J., Hauck, J., Hoppema, M., Humphreys, M.P., Hunt, C.W., Huss, B., Ibánhez, J.S.P., Johannessen, T., Keeling, R., Kitidis, V., Körtzinger, A., Kozyr, A., Krasakopoulou, E., Kuwata, A., Landschützer, P., Lauvset, S.K., Lefèvre, N., Lo Monaco, C., Manke, A., Mathis, J.T., Merlivat, L., Millero, F.J., Monteiro, P.M.S., Munro, D.R., Murata, A., Newberger, T., Omar, A.M., Ono, T., Paterson, K., Pearce, D., Pierrot, D., Robbins, L.L., Saito, S., Salisbury, J., Schlitzer, R., Schneider, B., Schweitzer, R., Sieger, R., Skjelvan, I., Sullivan, K.F., Sutherland, S.C., Sutton, A.J., Tadokoro, K., Telszewski, M., Tuma, M., van Heuven, S.M.A.C., Vandemark, D., Ward, B., Watson, A.J., Xu, S. (2016) A multi-decade record of high-quality fCO_2 data in version 3 of the Surface Ocean CO_2 Atlas (SOCAT). Earth Syst. Sci. Data 8, 383-413.

Barichivich, J., Briffa, K.R., Osborn, T.J., Melvin, T.M., Caesar, J. (2012) Thermal growing season and timing of biospheric carbon uptake across the Northern Hemisphere. Global Biogeochemical Cycles 26, n/a-n/a.

Barnola, J.M., Anklin, M., Porcheron, J., Raynaud, D., Schwander, J., Stauffer, B. (1995) CO_2 evolution during the last millennium as recorded by Antarctic and Greenland ice. Tellus B 47, 264-272.

Barnston, A.G., Livezey, R.E. (1987) Classification, Seasonality and Persistence of Low-Frequency Atmospheric Circulation Patterns. Monthly Weather Review 115, 1083-1126.

Bastos, A., Janssens, I.A., Gouveia, C.M., Trigo, R.M., Ciais, P., Chevallier, F., Peñuelas, J., Rödenbeck, C., Piao, S., Friedlingstein, P., Running, S.W. (2016) European land CO2 sink influenced by NAO and East-Atlantic Pattern coupling. Nature Communications 7, 10315.

Bastos, A., Running, S.W., Gouveia, C., Trigo, R.M. (2013) The global NPP dependence on ENSO: La Niña and the extraordinary year of 2011. Journal of Geophysical Research: Biogeosciences 118, 1247-1255.

Battle, M., Mikaloff Fletcher, S., Bender, M.L., Keeling, R.F., Manning, A.C., Gruber, N., Tans, P.P., Hendricks, M.B., Ho, D.T., Simonds, C., Mika, R., Paplawsky, B. (2006) Atmospheric potential oxygen: New observations and their implications for some atmospheric and oceanic models. Global Biogeochemical Cycles 20, doi:10.1029/2005GB002534.

Behrenfeld, M.J., Falkowski, P.G. (1997) Photosynthetic rates derived from satellite-based chlorophyll concentration. Limnology and Oceanography 42, 1-20.

Behrenfeld, M.J., Randerson, J.T., McClain, C.R., Feldman, G.C., Los, S.O., Tucker, C.J., Falkowski, P.G., Field, C.B., Frouin, R., Esaias, W.E., Kolber, D.D., Pollack, N.H. (2001) Biospheric Primary Production During an ENSO Transition. Science 291, 2594-2597.

Bender, M., Ellis, T., Tans, P., (1994a) Variability in the O_2/N_2 ratio of southern hemisphere air, 1991-1994: implications for the carbon cycle, Global Biogeochemical Cycles.

Bender, M., Ellis, T., Tans, P., Francey, R., Lowe, D. (1996) Variability in the O_2/N_2 ratio of southern hemisphere air, 1991-1994: Implications for the carbon cycle. Global Biogeochemical Cycles 10, 9-21, doi:10.1029/1095GB03295.

Bender, M.L., Battle, M., Keeling, R.F. (1998) The O_2 balance of the atmosphere: A tool for studying the fate of fossil-fuel CO_2. Annu. Rev. Energy Environ. 23, 207-223.

Bender, M.L., Battle, M.O. (1999) Carbon cycle studies based on the distribution of O_2 in air. Tellus Series B-Chemical and Physical Meteorology 51, 165-169.

Bender, M.L., Tans, P.P., Ellis, J.T., Orchardo, J., Habfast, K. (1994b) A high precision isotope ratio mass spectrometry method for measuring the O_2/N_2 ratio of air. Geochimica et Cosmochimica Acta 58, 4751-4758.

Benedict, F.G. (1912) The composition of the atmosphere with special reference to its oxygen content. Carnegie Institution of Washington.

Bent, J.D., (2014) Airborne Oxygen Measurements over the Southern Ocean as an Integrated Constraint of Seasonal Biogeochemical Processes. Scripps Institution of Oceanography La Jolla, San Diego, California, U.S. .

Bergamaschi, P., Lowe, D.C., Manning, M.R., Moss, R., Bromley, T., Clarkson, T.S. (2001) Transects of atmospheric CO, CH_4, and their isotopic composition across the Pacific: Shipboard measurements and validation of inverse models. Journal of Geophysical Research-Atmospheres 106, 7993-8011.

Berner, R.A. (1998) The Carbon Cycle and Carbon Dioxide over Phanerozoic Time: The Role of Land Plants. Philosophical Transactions of the Royal Society B: Biological Sciences 353, 75–82.

Betts, R.A., Jones, C.D., Knight, J.R., Keeling, R.F., Kennedy, J.J. (2016) El Nino and a record CO_2 rise. Nature Clim. Change 6, 806-810.

Bjerknes, J. (1966) A possible response of the atmospheric Hadley circulation to equatorial anomalies of ocean temperature. Tellus 18, 820-829.

Blaine, T.W., Keeling, R.F., Paplawsky, W.J. (2005) An improved inlet for precisely measuring the atmospheric Ar/N_2 ratio. Atmos. Chem. Phys. Discuss. 5, 11899-11910.

Boden, T.A., G. Marland, and R.J. Andres., (2017) Global, Regional, and National Fossil-Fuel CO2 Emissions., in: Carbon Dioxide Information Analysis Center (Ed.), Oak Ridge National Laboratory, U.S. Department of Energy, Oak Ridge, Tenn., U.S.A. .

Boden, T.A., G. Marland, and R.J. Andres. , (2009) Global, Regional, and National Fossil-Fuel CO_2 Emissions. , in: Center., C.D.I.A. (Ed.), Oak Ridge National Laboratory, U.S. Department of Energy, Oak Ridge, Tenn., U.S.A.

Bolin, B., Keeling, C.D. (1963) Large-scale atmospheric mixing as deduced from the seasonal and meridional variations of carbon dioxide. Journal of Geophysical Research 68, 3899-3920.

Bopp, L., Le Quéré, C., Heimann, M., Manning, A.C., Monfray, P. (2002) Climate-induced oceanic oxygen fluxes: Implications for the contemporary carbon budget. Global Biogeochemical Cycles 16, 6-1-6-13.

Bopp, L., Resplandy, L., Orr, J.C., Doney, S.C., Dunne, J.P., Gehlen, M., Halloran, P., Heinze, C., Ilyina, T., Séférian, R., Tjiputra, J., Vichi, M. (2013) Multiple stressors of ocean ecosystems in the 21st century: projections with CMIP5 models. Biogeosciences 10, 6225-6245.

Broecker, W.S. (1970) Mans Oxygen Reserves. Science 168, 1537-1538.

Broecker, W.S., Peng, T.-H. (1974) Gas exchange rates between air and sea. Tellus 26, 21-35.

Broecker, W.S., Peng, T.-H. (1982a) Tracers in the Sea. Lamont-Doherty Geological Observatory, Columbia University, Palisades, New York.

Broecker, W.S., Peng, T.H. (1982b) Tracers in the Sea. Lamont Doherty Geological Observatory, Palisades, NY, USA.

Broecker, W.S., Takahashi, T., Simpson, H.J., Peng, T.-H. (1979) Fate of fossil fuel carbon dioxide and the global carbon budget. Science 206, 409-418.

Brown, P.J., Jullion, L., Landschützer, P., Bakker, D.C.E., Naveira Garabato, A.C., Meredith, M.P., Torres-Valdés, S., Watson, A.J., Hoppema, M., Loose, B., Jones, E.M., Telszewski, M., Jones, S.D., Wanninkhof, R. (2015) Carbon dynamics of the Weddell Gyre, Southern Ocean. Global Biogeochemical Cycles 29, 288-306.

Bryant, D.A., Frigaard, N.-U. (2006) Prokaryotic photosynthesis and phototrophy illuminated. Trends in Microbiology 14, 488-496.

Butler, A.H., Thompson, D.W.J., Gurney, K.R. (2007) Observed relationships between the Southern Annular Mode and atmospheric carbon dioxide. Global Biogeochemical Cycles 21, -.

Capotondi, A., Alexander, M.A., Bond, N.A., Curchitser, E.N., Scott, J.D. (2012) Enhanced upper ocean stratification with climate change in the CMIP3 models. Journal of Geophysical Research: Oceans 117, n/a-n/a.

Carpenter, T.M. (1937) The constancy of the atmosphere with respect to carbon dioxide and oxygen content. J. Amer. Chem. Soc. 59, 358-360.

Carslaw, D.C., Beevers, S.D., Ropkins, K., Bell, M.C. (2006) Detecting and quantifying aircraft and other on-airport contributions to ambient nitrogen oxides in the vicinity of a large international airport. Atmospheric Environment 40, 5424-5434.

Carslaw, D.C., Ropkins, K. (2012) openair — An R package for air quality data analysis. Environmental Modelling & Software 27–28, 52-61.

Cavalieri, D.J., Parkinson, C.L. (2008) Antarctic sea ice variability and trends, 1979–2006. Journal of Geophysical Research: Oceans 113, n/a-n/a.

Ciais, P., Rayner, P., Chevallier, F., Bousquet, P., Logan, M., Peylin, P., Ramonet, M. (2010) Atmospheric inversions for estimating CO_2 fluxes: methods and perspectives. Climatic Change 103, 69-92.

Cleveland, R.B., Cleveland, W.S., McRae, J.E., Terpenning, I. (1990) STL: A seasonal-trend decomposition procedure based on loess. Journal of Official Statistics 6, 3-73.

Cleveland, W.S. (1979) Robust Locally Weighted Regression and Smoothing Scatterplots. Journal of the American Statistical Association 74, 829-836.

Cleveland, W.S., Devlin, S.J. (1988) Locally Weighted Regression: An Approach to Regression Analysis by Local Fitting. Journal of the American Statistical Association 83, 596-610.

Doney, S.C., Fabry, V.J., Feely, R.A., Kleypas, J.A. (2009) Ocean Acidification: The Other CO2 Problem. Annual Review of Marine Science 1, 169-192.

Doney, S.C., Glover, D.M., Najjar, R.G. (1996) A new coupled, one-dimensional biological-physical model for the upper ocean: Applications to the JGOFS Bermuda Atlantic Time-series Study (BATS) site. Deep Sea Research Part II: Topical Studies in Oceanography 43, 591-624.

Draxler, R.R., Hess, G.D. (1998) An overview of the HYSPLIT_4 modelling system for trajectories, dispersion, and deposition. Aust. Met. Mag. 47, 295-308.

Dunne, J.P., John, J.G., Shevliakova, E., Stouffer, R.J., Krasting, J.P., Malyshev, S.L., Milly, P.C.D., Sentman, L.T., Adcroft, A.J., Cooke, W., Dunne, K.A., Griffies, S.M., Hallberg, R.W., Harrison, M.J., Levy, H., Wittenberg, A.T., Phillips, P.J., Zadeh, N. (2013) GFDL's ESM2 Global Coupled Climate–Carbon Earth System Models. Part II: Carbon System Formulation and Baseline Simulation Characteristics. Journal of Climate 26, 2247-2267.

Ebisuzaki, W. (1997) A Method to Estimate the Statistical Significance of a Correlation When the Data Are Serially Correlated. Journal of Climate 10, 2147-2153.

Eddebbar, Y.A., Long, M.C., Resplandy, L., Rödenbeck, C., Rodgers, K.B., Manizza, M., Keeling, R.F. (2017) Impacts of ENSO on air-sea oxygen exchange: Observations and mechanisms. Global Biogeochemical Cycles 31, 901-921.

EDGAR, (2011) EDGAR4.2 Database: Emission Database for Global Atmospheric Research (EDGAR), release version 4.2 in: Joint Research Centre (JRC)/PBL Netherlands Environmental Assessment Agency (Ed.), European Commission. .

Evans, G.R., McDonagh, E.L., King, B.A., Bryden, H.L., Bakker, D.C.E., Brown, P.J., Schuster, U., Speer, K.G., van Heuven, S.M.A.C. (2017) South Atlantic interbasin exchanges of mass, heat, salt and anthropogenic carbon. Progress in Oceanography 151, 62-82.

Fang, S.X., Tans, P.P., Steinbacher, M., Zhou, L.X., Luan, T. (2015) Comparison of the regional CO_2 mole fraction filtering approaches at a WMO/GAW regional station in China. Atmos. Meas. Tech. 8, 5301-5313.

Fleming, Z.L., Monks, P.S., Manning, A.J. (2012) Review: Untangling the influence of air-mass history in interpreting observed atmospheric composition. Atmospheric Research 104, 1-39.

Fleming, Z.L., Monks, P.S., Rickard, A.R., Bandy, B.J., Brough, N., Green, T.J., Reeves, C.E., Penkett, S.A. (2006) Seasonal dependence of peroxy radical concentrations

at a Northern hemisphere marine boundary layer site during summer and winter: evidence for radical activity in winter. Atmos. Chem. Phys. 6, 5415-5433.

Forkel, M., Carvalhais, N., Rödenbeck, C., Keeling, R., Heimann, M., Thonicke, K., Zaehle, S., Reichstein, M. (2016) Enhanced seasonal CO_2 exchange caused by amplified plant productivity in northern ecosystems. Science.

Forster, G.L., Sturges, W.T., Fleming, Z.L., Bandy, B.J., Emeis, S. (2012) A year of H_2 measurements at Weybourne Atmospheric Observatory, UK. Tellus B 64.

Fourier, J. (1827) Mémoire Sur Les Températures Du Globe Terrestre Et Des Espaces Planétaires. Mémoires de l'Académie Royale des Sciences 7, 569-604.

Friedlingstein, P., Prentice, I.C. (2010) Carbon-climate feedbacks: a review of model and observation based estimates. Current Opinion in Environmental Sustainability 2, 251-257.

Fu, W., Randerson, J.T., Moore, J.K. (2016) Climate change impacts on net primary production (NPP) and export production (EP) regulated by increasing stratification and phytoplankton community structure in the CMIP5 models. Biogeosciences 13, 5151-5170.

García, H.E., Keeling, R.F. (2001) On the global oxygen anomaly and air-sea flux. Journal of Geophysical Research-Oceans 106, 31155-31166.

Gloor, M., Sarmiento, J.L., Gruber, N. (2010) What can be learned about carbon cycle climate feedbacks from the CO_2 airborne fraction? Atmospheric Chemistry and Physics 10, 7739-7751.

Graven, H.D., Keeling, R.F., Piper, S.C., Patra, P.K., Stephens, B.B., Wofsy, S.C., Welp, L.R., Sweeney, C., Tans, P.P., Kelley, J.J., Daube, B.C., Kort, E.A., Santoni, G.W., Bent, J.D. (2013) Enhanced Seasonal Exchange of CO_2 by Northern Ecosystems Since 1960. Science 341, 1085-1089.

Griffies, S.M., Böning, C., Bryan, F.O., Chassignet, E.P., Gerdes, R., Hasumi, H., Hirst, A., Treguier, A.-M., Webb, D. (2000) Developments in ocean climate modelling. Ocean Modelling 2, 123-192.

Griffies, S.M., Winton, M., Anderson, W.G., Benson, R., Delworth, T.L., Dufour, C.O., Dunne, J.P., Goddard, P., Morrison, A.K., Rosati, A., Wittenberg, A.T., Yin, J., Zhang, R. (2015) Impacts on Ocean Heat from Transient Mesoscale Eddies in a Hierarchy of Climate Models. Journal of Climate 28, 952-977.

Gruber, N., Gloor, M., Fan, S.-M., Sarmiento, J.L. (2001) Air-sea flux of oxygen estimated from bulk data: Implications for the marine and atmospheric oxygen cycles. Global Biogeochemical Cycles 15, 783-803.

Gruber, N., Sarmiento, J.L., Stocker, T.F. (1996) An improved method for detecting anthropogenic CO_2 in the oceans. Global Biogeochemical Cycles 10, 809-837.

Gu, L., Baldocchi, D.D., Wofsy, S.C., Munger, J.W., Michalsky, J.J., Urbanski, S.P., Boden, T.A. (2003) Response of a Deciduous Forest to the Mount Pinatubo Eruption: Enhanced Photosynthesis. Science 299, 2035-2038.

Hamme, R.C., Keeling, R.F. (2008) Ocean ventilation as a driver of interannual variability in atmospheric potential oxygen. Tellus Series B-Chemical and Physical Meteorology 60, 706-717.

Hansen, J., Lacis, A., Rind, D., Russell, G., Stone, P., Fung, I., Ruedy, R., Lerner, J., (1984) Climate Sensitivity: Analysis of Feedback Mechanisms, Climate Processes and Climate Sensitivity. American Geophysical Union, pp. 130-163.

Hansen, J., Sato, M., Ruedy, R., Lacis, A., Asamoah, K., Beckford, K., Borenstein, S., Brown, E., Cairns, B., Carlson, B., Curran, B., deCastro, S., Druyan, L., Etwarrow, P., Ferede, T., Fox, M., Gaffen, D., Glascoe, J., Gordon, H., Hollandsworth, S., Jiang, X., Johnson, C., Lawrence, N., Lean, J., Lerner, J., Lo, K., Logan, J., Luckett, A., McCormick, M.P., McPeters, R., Miller, R., Minnis, P., Ramberran, I., Russell, G., Russell, P., Stone, P., Tegen, I., Thomas, S., Thomason, L., Thompson, A., Wilder, J., Willson, R., Zawodny, J. (1997) Forcings and chaos in interannual to decadal climate change. Journal of Geophysical Research-Atmospheres 102, 25679-25720.

Hansen, J., Sato, M., Ruedy, R., Lo, K., Lea, D.W., Medina-Elizade, M. (2006) Global temperature change. Proceedings of the National Academy of Sciences 103, 14288-14293.

Harris, I., Jones, P.D., Osborn, T.J., Lister, D.H. (2014) Updated high-resolution grids of monthly climatic observations – the CRU TS3.10 Dataset. International Journal of Climatology 34, 623-642.

Heimann, M. (1995) The global atmospheric tracer model TM2. DKRZ.

Heimann, M., Keeling, C.D., Tucker, C.J., (1989) A three dimensional model of atmospheric CO_2 transport based on observed winds: 3. Seasonal cycle and synoptic time scale variations, Aspects of Climate Variability in the Pacific and the Western Americas. American Geophysical Union, pp. 277-303.

Heimann, M., Körner, S, (2003) The global atmospheric tracer model TM3 (Technical Report 5). . Jena: Max-Planck-Institut für Biogeochemie.

Heinze, C., Meyer, S., Goris, N., Anderson, L., Steinfeldt, R., Chang, N., Le Quéré, C., Bakker, D.C.E. (2015) The ocean carbon sink – impacts, vulnerabilities and challenges. Earth Syst. Dynam. 6, 327-358.

Houghton, R.A. (2007) Balancing the global carbon budget. Annual Review of Earth and Planetary Sciences 35, 313-347.

Huang, C.J., Qiao, F., Dai, D. (2014) Evaluating CMIP5 simulations of mixed layer depth during summer. Journal of Geophysical Research: Oceans 119, 2568-2582.

Hurrell, J.W. (1995) Decadal Trends in the North Atlantic Oscillation: Regional Temperatures and Precipitation. Science 269, 676-679.

Imbrie, J., Boyle, E.A., Clemens, S.C., Duffy, A., Howard, W.R., Kukla, G., Kutzbach, J., Martinson, D.G., McIntyre, A., Mix, A.C., Molfino, B., Morley, J.J., Peterson, L.C., Pisias, N.G., Prell, W.L., Raymo, M.E., Shackleton, N.J., Toggweiler, J.R. (1992) On the Structure and Origin of Major Glaciation Cycles 1. Linear Responses to Milankovitch Forcing. Paleoceanography 7, 701-738.

Indermuhle, A., Stocker, T.F., Joos, F., Fischer, H., Smith, H.J., Wahlen, M., Deck, B., Mastroianni, D., Tschumi, J., Blunier, T., Meyer, R., Stauffer, B. (1999) Holocene carbon-cycle dynamics based on CO_2 trapped in ice at Taylor Dome, Antarctica. Nature 398, 121-126.

IPCC (2001) Climate Change 2001: Impacts, Adaptation and Vulnerability. Contribution of Working Group II to the Third Assessment Report of the Intergovernmental Panel on Climate Change, 2001. Cambridge University Press, Cambridge, United Kingdom and New York, NY, USA.

IPCC (2007a) Climate Change 2007: Impacts, Adaptation and Vulnerability. Contribution of Working Group II to the Fourth Assessment Report of the Intergovernmental Panel on Climate Change, 2007. Cambridge University Press, Cambridge, United Kingdom and New York, NY, USA.

IPCC (2007b) Climate Change 2007: The Physical Science Basis. Contribution of Working Group I to the Fourth Assessment Report of the Intergovernmental Panel on Climate Change. Cambridge University Press, Cambridge, United Kingdom and New York, NY, USA.

IPCC (2013) Climate Change 2013: The Physical Science Basis. Contribution of Working Group I to the Fifth Assessment Report of the Intergovernmental Panel on Climate

Change Cambridge University Press, Cambridge, United Kingdom and New York, NY, USA.

IPCC (2014) Climate Change 2014: Impacts, Adaptation, and Vulnerability. Part A: Global and Sectoral Aspects. Contribution of Working Group II to the Fifth Assessment Report of the Intergovernmental Panel on Climate Change. Cambridge University Press, Cambridge, United Kingdom and New York, NY, USA. .

Ishidoya, S., Morimoto, S., Aoki, S., Taguchi, S., Goto, D., Murayama, S., Nakazawa, T. (2012) Oceanic and terrestrial biospheric CO_2 uptake estimated from atmospheric potential oxygen observed at Ny-Ålesund, Svalbard, and Syowa, Antarctica. 2012 64.

Jacob, D. (1999) Introduction to Atmospheric Chemistry. Princeton University Press.

Jacobson, A.R., Mikaloff Fletcher, S.E., Gruber, N., Sarmiento, J.L., Gloor, M. (2007) A joint atmosphere-ocean inversion for surface fluxes of carbon dioxide: 1. Methods and global-scale fluxes. Global Biogeochemical Cycles 21, n/a-n/a.

Jones, A.E., Wolff, E.W., Brough, N., Bauguitte, S.J.B., Weller, R., Yela, M., Navarro-Comas, M., Ochoa, H.A., Theys, N. (2013) The spatial scale of ozone depletion events derived from an autonomous surface ozone network in coastal Antarctica. Atmos. Chem. Phys. 13, 1457-1467.

Jones, A.E., Wolff, E.W., Salmon, R.A., Bauguitte, S.J.-B., Roscoe, H.K., Anderson, P.S., Ames, D., Clemitshaw, K.C., Flemming, Z.L., Bloss, W.J., Heard, D.E., Lee, J.D., Read, K.A., Hamer, P., Shallcross, D.E., Jackson, A.V., Walker, S.I., Lewis, A.C., Mills, G.P., Plane, J.M.C., Saiz-Lopez, A., Sturges, W.T., D.R., W. (2008) Chemistry of the Antarctic Boundary Layer and the Interface with Snow: an overview of the CHABLIS campaign. Atmospheric Chemistry and Physics, 3789-3803.

Jones, C.D., Collins, M., Cox, P.M., Spall, S.A. (2001) The Carbon Cycle Response to ENSO: A Coupled Climate–Carbon Cycle Model Study. Journal of Climate 14, 4113-4129.

Kalnay, E., Kanamitsu, M., Kistler, R., Collins, W., Deaven, D., Gandin, L., Iredell, M., Saha, S., White, G., Woollen, J., Zhu, Y., Leetmaa, A., Reynolds, R., Chelliah, M., Ebisuzaki, W., Higgins, W., Janowiak, J., Mo, K.C., Ropelewski, C., Wang, J., Jenne, R., Joseph, D. (1996) The NCEP/NCAR 40-Year Reanalysis Project. Bulletin of the American Meteorological Society 77, 437-471.

Keeling, C.D. (1960) The concentration and isotopic abundance of carbon dioxide in the atmosphere. Tellus 12, 200-203.

Keeling, C.D., Bacastow, R.B., Carter, A.F., Piper, S.C., Whorf, T.P., Heimann, M., Mook, W.G., Roeloffzen, H., (1989) A three-dimensional model of atmospheric CO_2 transport based on observed winds: 1. Analysis of observational data, Aspects of Climate Variability in the Pacific and the Western Americas. American Geophysical Union, pp. 165-236.

Keeling, C.D., Chin, J.F.S., Whorf, T.P. (1996a) Increased activity of northern vegetation inferred from atmospheric CO_2 measurements. Nature 382, 146-149.

Keeling, R.F., (1988a) Development of an interferometric oxygen analyzer for precise measurement of the atmospheric O_2 mole fraction, Division of Applied Sciences. Harvard University, Cambridge, Massachusetts, U.S.A., p. 178.

Keeling, R.F. (1988b) Measuring correlations between atmospheric oxygen and carbon dioxide mole fractions: A preliminary study in urban air. Journal of Atmospheric Chemistry 7, 153-176.

Keeling, R.F., Manning, A.C., (2014a) 5.15 - Studies of Recent Changes in Atmospheric O2 Content, in: Turekian, H.D.H.K. (Ed.), Treatise on Geochemistry (Second Edition). Elsevier, Oxford, pp. 385-404.

Keeling, R.F., Manning, A.C., (2014b) Studies of Recent Changes in Atmospheric O_2 Content, in: Turekian, K.K. (Ed.), Treatise on Geochemistry (Second Edition). Elsevier, Oxford, pp. 385-404.

Keeling, R.F., Manning, A.C., McEvoy, E.M., Shertz, S.R. (1998a) Methods for measuring changes in atmospheric O_2 concentration and their applications in southern hemisphere air. Journal of Geophysical Research-Atmospheres 103, 3381-3397.

Keeling, R.F., Manning, A.C., Paplawsky, W.J., Cox, A.C., (2006) On the long-term stability of reference gases for high precision measurements of O_2/N_2 ratio, Journal of Atmospheric and Oceanic Technology.

Keeling, R.F., Manning, A.C., Paplawsky, W.J., Cox, A.C. (2007) On the long-term stability of reference gases for atmospheric O_2/N_2 measurements. Tellus Series B-Chemical and Physical Meteorology 59, 3-14, doi:10.1111/j.1600-0889.2006.00228.x.

Keeling, R.F., Najjar, R.P., Bender, M.L., Tans, P.P. (1993) What atmospheric oxygen measurements can tell us about the global carbon cycle. Global Biogeochemical Cycles 7, 37-67, doi:10.1029/1092GB02733.

Keeling, R.F., Piper, S.C., Heimann, M. (1996b) Global and hemispheric CO_2 sinks deduced from changes in atmospheric O_2 concentration. Nature 381, 218-221.

Keeling, R.F., Shertz, S.R. (1992) Seasonal and interannual variations in atmospheric oxygen and implications for the global carbon cycle. Nature 358, 723-727, doi:710.1038/358723a358720.

Keeling, R.F., Stephens, B.B., Najjar, R.G., Doney, S.C., Archer, D., Heimann, M. (1998b) Seasonal variations in the atmospheric O_2/N_2 ratio in relation to the kinetics of air-sea gas exchange. Global Biogeochemical Cycles 12, 141-163.

Keenan, T.F., Prentice, I.C., Canadell, J.G., Williams, C.A., Wang, H., Raupach, M., Collatz, G.J. (2016) Recent pause in the growth rate of atmospheric CO2 due to enhanced terrestrial carbon uptake. 7, 13428.

Knox, F., McElroy, M.B. (1984) Changes in atmospheric CO_2: Influence of the marine biota at high latitude. Journal of Geophysical Research: Atmospheres 89, 4629-4637.

Kozlova, E.A., Manning, A.C. (2009) Methodology and calibration for continuous measurements of biogeochemical trace gas and O_2 concentrations from a 300-m tall tower in central Siberia. Atmospheric Measurement Techniques 2, 205-220.

Krol, M., Houweling, S., Bregman, B., van den Broek, M., Segers, A., van Velthoven, P., Peters, W., Dentener, F., Bergamaschi, P. (2005) The two-way nested global chemistry-transport zoom model TM5: algorithm and applications. Atmos. Chem. Phys. 5, 417-432.

Kulmala, M., Petäjä, T., Mönkkönen, P., Koponen, I.K., Dal Maso, M., Aalto, P.P., Lehtinen, K.E.J., Kerminen, V.M. (2005) On the growth of nucleation mode particles: source rates of condensable vapor in polluted and clean environments. Atmos. Chem. Phys. 5, 409-416.

Landschützer, P., Gruber, N., Bakker, D.C.E., Schuster, U., Nakaoka, S., Payne, M.R., Sasse, T.P., Zeng, J. (2013) A neural network-based estimate of the seasonal to inter-annual variability of the Atlantic Ocean carbon sink. Biogeosciences 10, 7793-7815.

Landschützer, P., Gruber, N., Haumann, A., Rödenbeck, C., Bakker, D.C.E., van Heuven, S., Hoppema, M., Metzl, N., Sweeney, C., Takahashi, T., Tilbrook, B.,

Wanninkof, R. (2015) The reinvigoration of the Southern Ocean carbon sink. . Science 349, 1221-1224.

Law, R.M., Matear, R.J., Francey, R.J. (2008) Comment on "Saturation of the Southern Ocean CO_2 sink due to recent climate change". Science 319, 570.

Laws, E. (2004) Export flux and stability as regulators of community composition in pelagic marine biological communities: Implications for regime shifts. Progress in Oceanography 60, 343-354.

Le Quéré, C., Andrew, R.M., Canadell, J.G., Sitch, S., Korsbakken, J.I., Peters, G.P., Manning, A.C., Boden, T.A., Tans, P.P., Houghton, R.A., Keeling, R.F., Alin, S., Andrews, O.D., Anthoni, P., Barbero, L., Bopp, L., Chevallier, F., Chini, L.P., Ciais, P., Currie, K., Delire, C., Doney, S.C., Friedlingstein, P., Gkritzalis, T., Harris, I., Hauck, J., Haverd, V., Hoppema, M., Klein Goldewijk, K., Jain, A.K., Kato, E., Körtzinger, A., Landschützer, P., Lefèvre, N., Lenton, A., Lienert, S., Lombardozzi, D., Melton, J.R., Metzl, N., Millero, F., Monteiro, P.M.S., Munro, D.R., Nabel, J.E.M.S., Nakaoka, S.I., O'Brien, K., Olsen, A., Omar, A.M., Ono, T., Pierrot, D., Poulter, B., Rödenbeck, C., Salisbury, J., Schuster, U., Schwinger, J., Séférian, R., Skjelvan, I., Stocker, B.D., Sutton, A.J., Takahashi, T., Tian, H., Tilbrook, B., van der Laan-Luijkx, I.T., van der Werf, G.R., Viovy, N., Walker, A.P., Wiltshire, A.J., Zaehle, S. (2016) Global Carbon Budget 2016. Earth Syst. Sci. Data 8, 605-649.

Le Quéré, C., Raupach, M.R., Canadell, J.G., Marland, G., Bopp, L., Ciais, P., Conway, T.J., Doney, S.C., Feely, R.A., Foster, P., Friedlingstein, P., Gurney, K., Houghton, R.A., House, J.I., Huntingford, C., Levy, P.E., Lomas, M.R., Majkut, J., Metzl, N., Ometto, J.P., Peters, G.P., Prentice, I.C., Randerson, J.T., Running, S.W., Sarmiento, J.L., Schuster, U., Sitch, S., Takahashi, T., Viovy, N., van der Werf, G.R., Woodward, F.I. (2009) Trends in the sources and sinks of carbon dioxide. Nature Geoscience 2, 831-836.

Le Quéré, C., Rödenbeck, C., Buitenhuis, E.T., Conway, T.J., Langenfelds, R., Gomez, A., Labuschagne, C., Ramonet, M., Nakazawa, T., Metzl, N., Gillett, N., Heimann, M. (2007) Saturation of the Southern Ocean CO_2 sink due to recent climate change. Science 316, 1735-1738, doi:1710.1126/science.1136188.

Le Quere, C., Roedenbeck, C., Buitenhuis, E.T., Conway, T.J., Langenfelds, R., Gomez, A., Labuschagne, C., Ramonet, M., Nakazawa, T., Metzl, N., Gillett, N.P.,

Heimann, M. (2008) Response to Comments on "Saturation of the Southern Ocean CO_2 sink due to recent climate change". Science 319.

Lenton, A., Matear, R.J. (2007) Role of the Southern Annular Mode (SAM) in Southern Ocean CO2 uptake. Global Biogeochemical Cycles 21.

Levitus, S., Antonov, J., Boyer, T. (2005) Warming of the world ocean, 1955-2003. Geophysical Research Letters 32.

Lin, J.C., Gerbig, C., Wofsy, S.C., Andrews, A.E., Daube, B.C., Davis, K.J., Grainger, C.A. (2003) A near-field tool for simulating the upstream influence of atmospheric observations: The Stochastic Time-Inverted Lagrangian Transport (STILT) model. Journal of Geophysical Research-Atmospheres 108.

Lloyd, J., Taylor, J.A. (1994) On the temperature dependence of soil respiration. Functional ecology 8, 315-323.

Long, M.C., Lindsay, K., Peacock, S., Moore, J.K., Doney, S.C. (2013) Twentieth-Century Oceanic Carbon Uptake and Storage in CESM1(BGC). Journal of Climate 26, 6775-6800.

Lovenduski, N.S., Gruber, N., Doney, S.C. (2008) Toward a mechanistic understanding of the decadal trends in the Southern Ocean carbon sink. Global Biogeochemical Cycles 22.

Lovenduski, N.S., Gruber, N., Doney, S.C., Lima, I.D. (2007) Enhanced CO_2 outgassing in the Southern Ocean from a positive phase of the Southern Annular Mode. Global Biogeochemical Cycles 21.

Lumpkin, R., Speer, K. (2007) Global Ocean Meridional Overturning. Journal of Physical Oceanography 37, 2550-2562.

Machta, L., (1980a) Oxygen depletion, in: Jacoby, G.C. (Ed.), Proceedings of the International Meeting on Stable Isotopes in Tree Ring Research, pp. 125-127.

Machta, L., Hughes, E. (1970) Atmospheric oxygen in 1967 to 1970. Science 168, 1582-1584.

Machta, L.E., (1980b) Oxygen depletion, in: Jacoby (Ed.), Carbon Dioxide Effcts Research and Assessment Program: Proceedings of the International Meeting on Stable isotopes in Tree-Ring Research. U.S. Department of Energy, pp. 125-127.

Mahowald, N.M., Rasch, P.J., Eaton, B.E., Whittlestone, S., Prinn, R.G. (1997) Transport of ^{222}radon to the remote troposphere using the Model of Atmospheric Transport and Chemistry and assimilated winds from ECMWF and the National Center for

Environmental Prediction/NCAR. Journal of Geophysical Research: Atmospheres 102, 28139-28151.

Manizza, M., Keeling, R.F., Nevison, C.D. (2012) On the processes controlling the seasonal cycles of the air–sea fluxes of O_2 and N_2O: A modelling study. Tellus B: Chemical and Physical Meteorology 64, 18429.

Manning, A.C., (2001) Temporal variability of atmospheric oxygen from both continuous measurements and a flask sampling network: Tools for studying the global carbon cycle, Scripps Institution of Oceanography. University of California, San Diego, La Jolla, California, U.S.A., p. 202.

Manning, A.C., Keeling, R.F. (2006a) Global oceanic and land biotic carbon sinks from the Scripps atmospheric oxygen flask sampling network. Tellus B 58, 95-116.

Manning, A.C., Keeling, R.F. (2006b) Global oceanic and land biotic carbon sinks from the Scripps atmospheric oxygen flask sampling network. Tellus-B 58B, 95-116, doi:110.1111/j.1600-0889.2006.00175.x.

Manning, A.C., Keeling, R.F., Severinghaus, J.P. (1999) Precise atmospheric oxygen measurements with a paramagnetic oxygen analyzer. Global Biogeochemical Cycles 13, 1107-1115.

Manning, A.J., O'Doherty, S., Jones, A.R., Simmonds, P.G., Derwent, R.G. (2011) Estimating UK methane and nitrous oxide emissions from 1990 to 2007 using an inversion modeling approach. Journal of Geophysical Research: Atmospheres 116, n/a-n/a.

Marshall, J., Speer, K. (2012) Closure of the meridional overturning circulation through Southern Ocean upwelling. Nature Geoscience 5, 171.

Masarie, K.A., Tans, P.P. (1995) Extension and integration of atmospheric carbon dioxide data into a globally consistent measurement record. Journal of Geophysical Research: Atmospheres 100, 11593-11610.

McPhaden, M.J., Zebiak, S.E., Glantz, M.H. (2006) ENSO as an Integrating Concept in Earth Science. Science 314, 1740-1745.

Meals, D.W., Spooner,J., Dressing, S.A., Harcum, J.B., (2011) Statistical analysis for monotonic trends,, in: Agency, D.f.U.S.E.P. (Ed.). by Tetra Tech, Inc., Fairfax, VA, 23 p.

Metzl, N., Brunet, C., Jabaud-Jan, A., Poisson, A., Schauer, B. (2006) Summer and winter air–sea CO_2 fluxes in the Southern Ocean. Deep Sea Research Part I: Oceanographic Research Papers 53, 1548-1563.

Meyers, S.R., (2014) Astrochron: an R package for astrochronology, http://cran.rproject.org/package=astrochron.

Mikaloff Fletcher, S.E., Gruber, N., Jacobson, A.R., Gloor, M., Doney, S.C., Dutkiewicz, S., Gerber, M., Follows, M., Joos, F., Lindsay, K., Menemenlis, D., Mouchet, A., Muller, S.A., Sarmiento, J.L. (2007) Inverse estimates of the oceanic sources and sinks of natural CO_2 and the implied oceanic carbon transport. Global Biogeochemical Cycles 21.

Milankovitch, M.R. (1941) Kanon der Erdbestrahlung. (Canon of insolation and the ice-age problem, English translation by Israel Program for Scientific Translations, Jerusalem, 1969). Royaal Serbian Academy Specialist Publication 132.

Morrison, A.K., Frölichr, T., Sarmiento, J., (2015) Upwelling in the Southern Ocean Physics Today, pp. 27-32.

Munro, D.R., Lovenduski, N.S., Takahashi, T., Stephens, B.B., Newberger, T., Sweeney, C. (2015) Recent evidence for a strengthening CO_2 sink in the Southern Ocean from carbonate system measurements in the Drake Passage (2002–2015). Geophysical Research Letters 42, 7623-7630.

Myneni, R.B., Keeling, C.D., Tucker, C.J., Asrar, G., Nemani, R.R. (1997) Increased plant growth in the northern high latitudes from 1981 to 1991. Nature 386, 698-702.

Naegler, T., Ciais, P., Orr, J.C., Aumont, O., RÖDenbeck, C. (2007) On evaluating ocean models with atmospheric potential oxygen. Tellus B 59, 138-156.

Nemani, R.R., Keeling, C.D., Hashimoto, H., Jolly, W.M., Piper, S.C., Tucker, C.J., Myneni, R.B., Running, S.W. (2003) Climate-Driven Increases in Global Terrestrial Net Primary Production from 1982 to 1999. Science 300, 1560-1563.

Nevison, C.D., Keeling, R.F., Kahru, M., Manizza, M., Mitchell, B.G., Cassar, N. (2012) Estimating net community production in the Southern Ocean based on atmospheric potential oxygen and satellite ocean color data. Global Biogeochemical Cycles 26.

Nevison, C.D., Keeling, R.F., Weiss, R.F., Popp, B.N., Jin, X., Fraser, P.J., Porter, L.W., Hess, P.G. (2005) Southern Ocean ventilation inferred from seasonal cycles of atmospheric N_2O and O_2/N_2 at Cape Grim, Tasmania. Tellus Series B-Chemical and Physical Meteorology 57, 218-229.

Nevison, C.D., Mahowald, N.M., Doney, S.C., Lima, I.D., Cassar, N. (2008a) Impact of variable air-sea O_2 and CO_2 fluxes on atmospheric potential oxygen (APO) and land-ocean carbon sink partitioning. Biogeosciences 5, 875-889.

Nevison, C.D., Mahowald, N.M., Doney, S.C., Lima, I.D., van der Werf, G.R., Randerson, J.T., Baker, D.F., Kasibhatla, P., McKinley, G.A. (2008b) Contribution of ocean, fossil fuel, land biosphere, and biomass burning carbon fluxes to seasonal and interannual variability in atmospheric CO_2. Journal of Geophysical Research: Biogeosciences 113.

Nevison, C.D., Manizza, M., Keeling, R.F., Kahru, M., Bopp, L., Dunne, J., Tiputra, J., Ilyina, T., Mitchell, B.G. (2015) Evaluating the ocean biogeochemical components of Earth system models using atmospheric potential oxygen and ocean color data. Biogeosciences 12, 193-208.

Nevison, C.D., Manizza, M., Keeling, R.F., Stephens, B.B., Bent, J.D., Dunne, J., Ilyina, T., Long, M., Resplandy, L., Tjiputra, J., Yukimoto, S. (2016) Evaluating CMIP5 ocean biogeochemistry and Southern Ocean carbon uptake using atmospheric potential oxygen: Present-day performance and future projection. Geophysical Research Letters 43, 2077-2085.

Novelli, P.C., Masarie, K.A., Lang, P.M. (1998) Distributions and recent changes of carbon monoxide in the lower troposphere. Journal of Geophysical Research-Atmospheres 103, 19015-19033.

Novelli, P.C., Masarie, K.A., Lang, P.M., Hall, B.D., Myers, R.C., Elkins, J.W. (2003) Reanalysis of tropospheric CO trends: Effects of the 1997–1998 wildfires. Journal of Geophysical Research: Atmospheres 108, n/a-n/a.

O'Doherty, S., Simmonds, P.G., Cunnold, D.M., Wang, H.J., Sturrock, G.A., Fraser, P.J., Ryall, D., Derwent, R.G., Weiss, R.F., Salameh, P., Miller, B.R., Prinn, R.G. (2001) In situ chloroform measurements at Advanced Global Atmospheric Gases Experiment atmospheric research stations from 1994 to 1998. Journal of Geophysical Research: Atmospheres 106, 20429-20444.

ObsPack, (2016) Cooperative Global Atmospheric Data Integration Project; (2016): Multi-laboratory compilation of atmospheric carbon dioxide data for the period 1957-2015. , obspack_co2_1_GLOBALVIEWplus_v2.1_2016_09_02, 2.1 ed. NOAA Earth System Research Laboratory, Global Monitoring Division.

Olbers, D., Borowski, D., Volker, C., Wolff, J. (2004) The dynamical balance, transport and circulation of the Antarctic Circumpolar Current. Antarctic Science 16, 439-470.

Patecki, M., Manning, A.C., (2007a) First results from shipboard atmospheric O_2 and CO_2 measurements over the North Atlantic Ocean, Oceans 2007 - Europe. doi: 10.1109/OCEANSE.2007.4302351, IEEE, Aberdeen, Scotland, UK.

Patecki, M., Manning, A.C., (2007b) First results from shipboard atmospheric O_2 and CO_2 measurements over the North Atlantic Ocean, Oceans 07. IEEE, Aberdeen, pp. 1-6, doi: 10.1109/OCEANSE.2007.4302351.

Pearman, G.I., Hyson, P. (1980) Activities of the global biosphere as reflected in atmospheric CO_2 records. Journal of Geophysical Research: Oceans 85, 4457-4467.

Pearman, G.I., Hyson, P. (1981) The annual variation of atmospheric CO2 concentration observed in the northern hemisphere. Journal of Geophysical Research: Oceans 86, 9839-9843.

Pearman, G.I., Hyson, P. (1986) Global transport and inter-reservoir exchange of carbon dioxide with particular reference to stable isotopic distributions. Journal of Atmospheric Chemistry 4, 81-124.

Penkett, S.A., Clemitshaw, K.C., Savage, N.H., Burgess, R.A., Cardenas, L.M., Carpenter, L.J., McFadyen, G.G., Cape, J.N. (1999a) Studies of Oxidant Production at the Weybourne Atmospheric Observatory in Summer and Winter Conditions. Journal of Atmospheric Chemistry 33, 111-128.

Penkett, S.A., Plane, J.M.C., Comes, F.J., Clemitshaw, K.C., Coe, H. (1999b) The Weybourne Atmospheric Observatory. Journal of Atmospheric Chemistry 33, 107-110.

Pepper, W. (1992) Emission scenarios for the IPCC, an update, assumptions, methodology, and results. Prepared for the Intergovernmental Panel on Climate Change, Working Group 1.

Peters, W., Jacobson, A.R., Sweeney, C., Andrews, A.E., Conway, T.J., Masarie, K., Miller, J.B., Bruhwiler, L.M.P., Petron, G., Hirsch, A.I., Worthy, D.E.J., van der Werf, G.R., Randerson, J.T., Wennberg, P.O., Krol, M.C., Tans, P.P. (2007) An atmospheric perspective on North American carbon dioxide exchange: CarbonTracker. Proceedings of the National Academy of Sciences of the United States of America 104, 18925-18930.

Peters, W., Krol, M.C., Van Der Werf, G.R., Houweling, S., Jones, C.D., Hughes, J., Schaefer, K., Masarie, K.A., Jacobson, A.R., Miller, J.B., Cho, C.H., Ramonet, M., Schmidt, M., Ciattaglia, L., Apadula, F., Heltai, D., Meinhardt, F., Di Sarra, A.G., Piacentino, S., Sferlazzo, D., Aalto, T., Hatakka, J., StrÖM, J., Haszpra, L., Meijer, H.A.J., Van Der Laan, S., Neubert, R.E.M., Jordan, A., RodÓ, X., MorguÍ, J.A., Vermeulen, A.T., Popa, E., Rozanski, K., Zimnoch, M., Manning, A.C., Leuenberger, M., Uglietti, C., Dolman, A.J., Ciais, P., Heimann, M., Tans, P.P. (2010) Seven years of recent European net terrestrial carbon dioxide exchange constrained by atmospheric observations. Global Change Biology 16, 1317-1337.

Peters, W., Miller, J.B., Whitaker, J., Denning, A.S., Hirsch, A., Krol, M.C., Zupanski, D., Bruhwiler, L., Tans, P.P. (2005) An ensemble data assimilation system to estimate CO_2 surface fluxes from atmospheric trace gas observations. Journal of Geophysical Research: Atmospheres 110, n/a-n/a.

Petit, J.R., Jouzel, J., Raynaud, D., Barkov, N.I., Barnola, J.M., Basile, I., Bender, M., Chappellaz, J., Davis, M., Delaygue, G., Delmotte, M., Kotlyakov, V.M., Legrand, M., Lipenkov, V.Y., Lorius, C., Pepin, L., Ritz, C., Saltzman, E., Stievenard, M. (1999) Climate and atmospheric history of the past 420,000 years from the Vostok ice core, Antarctica. Nature 399, 429-436.

Peylin, P., Law, R.M., Gurney, K.R., Chevallier, F., Jacobson, A.R., Maki, T., Niwa, Y., Patra, P.K., Peters, W., Rayner, P.J., Rödenbeck, C., van der Laan-Luijkx, I.T., Zhang, X. (2013) Global atmospheric carbon budget: results from an ensemble of atmospheric CO₂ inversions. Biogeosciences 10, 6699-6720.

Piao, S., Liu, Z., Wang, T., Peng, S., Ciais, P., Huang, M., Ahlstrom, A., Burkhart, J.F., Chevallier, F., Janssens, I.A., Jeong, S.-J., Lin, X., Mao, J., Miller, J., Mohammat, A., Myneni, R.B., Penuelas, J., Shi, X., Stohl, A., Yao, Y., Zhu, Z., Tans, P.P. (2017) Weakening temperature control on the interannual variations of spring carbon uptake across northern lands. Nature Clim. Change 7, 359-363.

Piao, S., Nan, H., Huntingford, C., Ciais, P., Friedlingstein, P., Sitch, S., Peng, S., Ahlström, A., Canadell, J.G., Cong, N., Levis, S., Levy, P.E., Liu, L., Lomas, M.R., Mao, J., Myneni, R.B., Peylin, P., Poulter, B., Shi, X., Yin, G., Viovy, N., Wang, T., Wang, X., Zaehle, S., Zeng, N., Zeng, Z., Chen, A. (2014) Evidence for a weakening relationship between interannual temperature variability and northern vegetation activity. Nature Communications 5, 5018.

Piao, S.L., Ciais, P., Friedlingstein, P., Peylin, P., Reichstein, M., Luyssaert, S., Margolis, H., Fang, J.Y., Barr, A., Chen, A.P., Grelle, A., Hollinger, D.Y., Laurila, T., Lindroth, A., Richardson, A.D., Vesala, T. (2008) Net carbon dioxide losses of northern ecosystems in response to autumn warming. Nature 451, 49-U43.

Pickers, P.A., (2016) New applications of continuous atmospheric O_2 measurements: meridional transects across the Atlantic Ocean, and improved quantification of fossil fuel-derived CO_2, School of Environmental Sciences. University of East anglia Norwich p. 291.

Pickers, P.A., Manning, A.C. (2015) Investigating bias in the application of curve fitting programs to atmospheric time series. Atmos. Meas. Tech. 8, 1469-1489.

Plattner, G.K., Joos, F., Stocker, T.F., (2002) Revision of the global carbon budget due to changing air-sea oxygen fluxes, GBC.

Popa, E.M., (2008) Contunuous tall tower multispecies measurements in Europe for quantifying and understanding land-atmosphere carbon exchange.

Randerson, J.T., Thompson, M.V., Conway, T.J., Fung, I.Y., Field, C.B. (1997) The contribution of terrestrial sources and sinks to trends in the seasonal cycle of atmospheric carbon dioxide. Global Biogeochemical Cycles 11, 535-560.

Rasch, P.J., Mahowald, N.M., Eaton, B.E. (1997) Representations of transport, convection, and the hydrologic cycle in chemical transport models: Implications for the modeling of short-lived and soluble species. Journal of Geophysical Research: Atmospheres 102, 28127-28138.

Raupach, M.R., Canadell, J.G., Le Quere, C. (2008) Anthropogenic and biophysical contributions to increasing atmospheric CO_2 growth rate and airborne fraction. Biogeosciences 5, 1601-1613.

Redfield, A.C., Ketchum, B.H., Richards, F.A., (1963) The influence of organisms on the composition of sea-water, in: Hill, M.N. (Ed.), The Sea. Wiley Interscience, New York, pp. 26-77.

Reinsch, C.H. (1967) Smoothing by spline functions. Numerische Mathematik 10, 177-183.

Revelle, R., Suess, H.E. (1957) Carbon dioxide exchange between atmosphere and ocean and the question of an increase of atmospheric CO_2 during the past decades. Tellus 9, 18-27.

Rickard, G., Behrens, E. (2016) CMIP5 Earth System Models with biogeochemistry: A Ross Sea assessment. Antarctic Science 28, 327-346.

Riebesell, U., Körtzinger, A., Oschlies, A. (2009) Sensitivities of marine carbon fluxes to ocean change. Proceedings of the National Academy of Sciences 106, 20602-20609.

Rintoul, S.R. (2011) The Southern Ocean in the Earth System.

Rödenbeck, C., Le Quéré, C., Heimann, M., Keeling, R.F. (2008) Interannual variability in oceanic biogeochemical processes inferred by inversion of atmospheric O_2/N_2 and CO_2 data. Tellus B: Chemical and Physical Meteorology 60, 685-705.

Roscoe, H.K., Jones, A.E., Brough, N., Weller, R., Saiz-Lopez, A., Mahajan, A.S., Schoenhardt, A., Burrows, J.P., Fleming, Z.L. (2015) Particles and iodine compounds in coastal Antarctica. Journal of Geophysical Research: Atmospheres 120, 7144-7156.

Roy, T., Rayner, P., Matear, R., Francey, R. (2003) Southern hemisphere ocean CO_2 uptake: reconciling atmospheric and oceanic estimates. Tellus Series B-Chemical and Physical Meteorology 55, 701-710.

Ruckstuhl, A.F., Henne, S., Reimann, S., Steinbacher, M., Vollmer, M.K., O'Doherty, S., Buchmann, B., Hueglin, C. (2012) Robust extraction of baseline signal of atmospheric trace species using local regression. Atmos. Meas. Tech. 5, 2613-2624.

Ruckstuhl, A.F., Jacobson, M.P., Field, R.W., Dodd, J.A. (2001) Baseline subtraction using robust local regression estimation. Journal of Quantitative Spectroscopy and Radiative Transfer 68, 179-193.

Ruckstuhl, A.F., Unternaehrer, T., Locher, R., (2009) IDPmisc: Utilities of Institute of Data Analyses and Process Design, 2009 ed. available at: http://CRAN.R-project.org/package=, www.idp.zhaw.ch.

Rutgers van der Loeff, M.M., Cassar, N., Nicolaus, M., Rabe, B., Stimac, I. (2014) The influence of sea ice cover on air-sea gas exchange estimated with radon-222 profiles. Journal of Geophysical Research: Oceans 119, 2735-2751.

Ryall, D.B., Derwent, R.G., Manning, A.J., Simmonds, P.G., O'Doherty, S. (2001) Estimating source regions of European emissions of trace gases from observations at Mace Head. Atmospheric Environment 35, 2507-2523.

Sabine, C.L., Feely, R.A., Gruber, N., Key, R.M., Lee, K., Bullister, J.L., Wanninkhof, R., Wong, C.S., Wallace, D.W.R., Tilbrook, B., Millero, F.J., Peng, T.-H., Kozyr, A., Ono, T., Rios, A.F. (2004) The oceanic sink for anthropogenic CO_2. Science 305, 367-371.

Sallee, J.-B., Matear, R.J., Rintoul, S.R., Lenton, A. (2012) Localized subduction of anthropogenic carbon dioxide in the Southern Hemisphere oceans. Nature Geosci 5, 579-584.

Sallée, J.B., Shuckburgh, E., Bruneau, N., Meijers, A.J.S., Bracegirdle, T.J., Wang, Z. (2013) Assessment of Southern Ocean mixed-layer depths in CMIP5 models: Historical bias and forcing response. Journal of Geophysical Research: Oceans 118, 1845-1862.

Sarmiento, J.L., Murnane, R., Le Quéré, C. (1995) Air-sea CO_2 transfer and the carbon budget of the North Atlantic. Philosophical Transactions of the Royal Society of London B 348, 211-219.

Scaife, A.A., Folland, C.K., Alexander, L.V., Moberg, A., Knight, J.R. (2008) European Climate Extremes and the North Atlantic Oscillation. Journal of Climate 21, 72-83.

Schimel, D., Stephens, B.B., Fisher, J.B. (2015) Effect of increasing CO₂ on the terrestrial carbon cycle. Proceedings of the National Academy of Sciences 112, 436-441.

Schulze, E.D. (2006) Biological control of the terrestrial carbon sink. Biogeosciences 3, 147-166.

Severinghaus, J.P., (1995) Studies of the terrestrial O_2 and carbon cycles in sand dune gases and in Biosphere 2. Columbia University, New York, U.S.A., p. 148.

Severinghaus, J.P., Bender, M.L., Keeling, R.F., Broecker, W.S. (1996) Fractionation of soil gases by diffusion of water vapor, gravitational settling, and thermal diffusion. Geochimica et Cosmochimica Acta 60, 1005-1018.

Shindell, D.T., Schmidt, G.A. (2004) Southern Hemisphere climate response to ozone changes and greenhouse gas increases. Geophysical Research Letters 31.

Siegenthaler, U., Stocker, T.F., Monnin, E., Lüthi, D., Schwander, J., Stauffer, B., Raynaud, D., Barnola, J.-M., Fischer, H., Masson-Delmotte, V., Jouzel, J. (2005) Stable Carbon Cycle Climate Relationship During the Late Pleistocene. Science 310, 1313-1317.

Siegenthaler, U., Wenk, T. (1984) Rapid atmospheric CO_2 variations and ocean circulation. Nature 308, 624-626.

Sigman, D.M., Boyle, E.A. (2000) Glacial/interglacial variations in atmospheric carbon dioxide. Nature 407, 859-869.

Simmonds, I., Keay, K., Lim, E.-P. (2003) Synoptic Activity in the Seas around Antarctica. Monthly Weather Review 131, 272-288.

Six, K.D., Maier-Reimer, E. (1996) Effects of plankton dynamics on seasonal carbon fluxes in an ocean general circulation model. Global Biogeochemical Cycles 10, 559-583.

Smith, R., Jones, P., Briegleb, B., Bryan, F., Danabasoglu, G., Dennis, J., Dukowicz, J., Eden, C., Fox-Kemper, B., Gent, P. (2010) The parallel ocean program (POP) reference manual ocean component of the community climate system model (CCSM) and community earth system model (CESM). Rep. LAUR-01853 141.

Spreen, G., Kaleschke, L., Heygster, G. (2008) Sea ice remote sensing using AMSR-E 89-GHz channels. Journal of Geophysical Research: Oceans 113, n/a-n/a.

Stephens, B.B., Bakwin, P.S., Tans, P.P., Teclaw, R.M., Baumann, D.D. (2007) Application of a differential fuel-cell analyzer for measuring atmospheric oxygen variations. Journal of Atmospheric and Oceanic Technology 24, 82-94, doi:10.1175/JTECH1959.1171.

Stephens, B.B., Brailsford, G.W., Gomez, A.J., Riedel, K., Mikaloff Fletcher, S.E., Nichol, S., Manning, M. (2013) Analysis of a 39-year continuous atmospheric CO_2 record from Baring Head, New Zealand. Biogeosciences 10, 2683-2697.

Stephens, B.B., Keeling, R.F., Heimann, M., Six, K.D., Murnane, R., Caldeira, K. (1998) Testing global ocean carbon cycle models using measurements of atmospheric O_2 and CO_2 concentration. Global Biogeochemical Cycles 12, 213-230.

Stephens, B.B., Keeling, R.F., Paplawsky, W.J. (2003) Shipboard measurements of atmospheric oxygen using a vacuum-ultraviolet absorption technique. Tellus Series B-Chemical and Physical Meteorology 55, 857-878.

Stephens, B.B., Long, M.C., Keeling, R.F., Kort, E.A., Sweeney, C., Apel, E.C., Atlas, E.L., Beaton, S., Bent, J.D., Blake, N.J., Bresch, J.F., Casey, J., Daube, B.C., Diao, M., Diaz, E., Dierssen, H., Donets, V., Gao, B.-C., Gierach, M., Green, R., Haag, J., Hayman, M., Hills, A.J., Hoecker-Martínez, M.S., Honomichl, S.B., Hornbrook, R.S., Jensen, J.B., Li, R.-R., McCubbin, I., McKain, K., Morgan, E.J., Nolte, S., Powers, J.G., Rainwater, B., Randolph, K., Reeves, M., Schauffler, S.M., Smith, K., Smith, M., Stith, J., Stossmeister, G., Toohey, D.W., Watt, A.S. (2018) The O2/N2 Ratio and CO2 Airborne Southern Ocean Study. Bulletin of the American Meteorological Society 99, 381-402.

Sturm, P., Leuenberger, M., Sirignano, C., Neubert, R.E.M., Meijer, H.A.J., Langenfelds, R., Brand, W.A., Tohjima, Y. (2004) Permeation of atmospheric gases through polymer O-rings used in flasks for air sampling. Journal of Geophysical Research-Atmospheres 109.

Takahashi, T., Sutherland, S.C., Sweeney, C., Poisson, A., Metzl, N., Tilbrook, B., Bates, N., Wanninkhof, R., Feely, R.A., Sabine, C., Olafsson, J., Nojiri, Y. (2002) Global sea-air CO_2 flux based on climatological surface ocean pCO_2, and seasonal biological and temperature effects. Deep-Sea Research Part II-Topical Studies in Oceanography 49, 1601-1622.

Takahashi, T., Sutherland, S.C., Wanninkhof, R., Sweeney, C., Feely, R.A., Chipman, D.W., Hales, B., Friederich, G., Chavez, F., Sabine, C., Watson, A., Bakker, D.C.E., Schuster, U., Metzl, N., Yoshikawa-Inoue, H., Ishii, M., Midorikawa, T., Nojiri, Y., Kortzinger, A., Steinhoff, T., Hoppema, M., Olafsson, J., Arnarson, T.S., Tilbrook, B., Johannessen, T., Olsen, A., Bellerby, R., Wong, C.S., Delille, B., Bates, N.R., de Baar, H.J.W. (2009) Climatological mean and decadal change in surface ocean pCO_2, and net sea-air CO_2 flux over the global oceans. Deep-Sea Research Part II -Topical Studies in Oceanography 56, 554-577.

Takahashi, T., Sweeney, C., Hales, B., Chipman, D.W., Newberger, T., Goddard, J.G., Iannuzzi, R.A., Sutherland, S.C. (2012) The changing carbon cycle in the Southern Ocean. Oceanography 25, 26-37.

Tans, P.P., Zellweger, C., (2014) Report of the Seventeeth WMO/IAEA Meeting on Carbon Dioxide, Other Greenhouse Gases, and Related Measurement Techniques (GGMT-2013), in: Tans, P.P., Zellweger, C. (Eds.), Beijing, China, pp. available at http://www.wmo.int/pages/prog/arep/gaw/gaw-reports.html.

Tans, P.P., Zellweger, C., (2016) Report of the Eighteenth WMO/IAEA Meeting on Carbon Dioxide, Other Greenhouse Gases, and Related Measurement Techniques (GGMT-2015), in: Tans, P.P., Zellweger, C. (Eds.), San Diego, USA, pp. available at http://www.wmo.int/pages/prog/arep/gaw/gaw-reports.html.

Taylor, K.E. (2001) Summarizing multiple aspects of model performance in a single diagram. Journal of Geophysical Research: Atmospheres 106, 7183-7192.

Taylor, K.E., Stouffer, R.J., Meehl, G.A. (2012) An Overview of CMIP5 and the Experiment Design. Bulletin of the American Meteorological Society 93, 485-498.

Thomas, R.T., Prentice, I.C., Graven, H., Ciais, P., Fisher, J.B., Hayes, D.J., Huang, M., Huntzinger, D.N., Ito, A., Jain, A., Mao, J., Michalak, A.M., Peng, S., Poulter, B., Ricciuto, D.M., Shi, X., Schwalm, C., Tian, H., Zeng, N. (2016) Increased light-use efficiency in northern terrestrial ecosystems indicated by CO_2 and greening observations. Geophysical Research Letters 43, 11,339-311,349.

Thompson, D.W., Wallace, J.M., Hegerl, G.C. (2000) Annular modes in the extratropical circulation. Part II: Trends. Journal of Climate 13, 1018-1036.

Thompson, D.W.J., Solomon, S. (2002) Interpretation of Recent Southern Hemisphere Climate Change. Science 296, 895-899.

Thompson, R.L., (2005) Variations in Atmospheric O_2 and CO_2 in the Southern Ocean Region from Continuous Ship-based Measurements. Victoria University of Wellington, Wellington, p. 184.

Thompson, R.L., Manning, A.C., Lowe, D.C., Weatherburn, D.C. (2007) A ship-based methodology for high precision atmospheric oxygen measurements and its application in the Southern Ocean region. Tellus Series B-Chemical and Physical Meteorology 59, 643-653, doi:610.1111/j.1600-0889.2007.00292.x.

Thoning, K.W., Tans, P.P., Komhyr, W.D. (1989) Atmospheric carbon dioxide at Mauna Loa Observatory: 2. Analysis of the NOAA GMCC data, 1974–1985. Journal of Geophysical Research: Atmospheres 94, 8549-8565.

Toggweiler, J.R. (1999) Variation of atmospheric CO_2 by ventilation of the ocean's deepest water. Paleoceanography 14, 571-588.

Toggweiler, J.R., Samuels, B. (1995) Effect of drake passage on the global thermohaline circulation. Deep Sea Research Part I: Oceanographic Research Papers 42, 477-500.

Tohjima, Y. (2000) Method for measuring changes in the atmospheric O_2/N_2 ratio by a gas chromatograph equipped with a thermal conductivity detector. Journal of Geophysical Research-Atmospheres 105, 14575-14584.

Tohjima, Y., Machida, T., Watai, T., Akama, I., Amari, T., Moriwaki, Y. (2005a) Preparation of gravimetric standards for measurements of atmospheric oxygen and reevaluation of atmospheric oxygen concentration. Journal of Geophysical Research D: Atmospheres 110, 1-11.

Tohjima, Y., Mukai, H., Machida, T., Nojiri, Y., Gloor, M. (2005b) First measurements of the latitudinal atmospheric O_2 and CO_2 distributions across the western Pacific. Geophysical Research Letters 32, 1-4.

Tohjima, Y., Mukai, H., Nojiri, Y., Yamagishi, H., Machida, T. (2008) Atmospheric O_2/N_2 measurements at two Japanese sites: estimation of global oceanic and land biotic carbon sinks and analysis of the variations in atmospheric potential oxygen (APO). Tellus Series B-Chemical and Physical Meteorology 60, 213-225.

Tsutsumi, Y., Mori, K., Hirahara, T., Ikegami, M., Conway, T.J., (2009) Technical Report of Global Analysis Method for Major Greenhouse Gases by the World Data Center for Greenhouse Gases, in: WATCH, W.M.O.G.A. (Ed.).

Tsutsumi, Y., Mori, K., Ikegami, M., Tashiro, T., Tsuboi, K. (2006) Long-term trends of greenhouse gases in regional and background events observed during 1998–2004 at Yonagunijima located to the east of the Asian continent. Atmospheric Environment 40, 5868-5879.

Tyndall, J. (1864) On the Absorption and Radiation of Heat by Gaseous and Liquid Matter. Fourth Memoir. Philosophical Transactions of the Royal Society of London 154, 201-225.

van der Laan-Luijkx, I.T., (2010) Atmospheric oxygen and the global carbon cycle: Observations from the new F3 North Sea platform monitoring station and 6 additional locations in Europe and Siberia, Centre for Isotope Research. University of Groningen, Groningen, The Netherlands.

van der Laan-Luijkx, I.T., Karstens, U., Steinbach, J., Gerbig, C., Sirignano, C., Neubert, R.E.M., van der Laan, S., Meijer, H.A.J. (2010) CO_2, $\delta(O_2/N_2)$, and APO and APO: observations from the Lutjewad, Mace Head and F3 platform flask sampling network. Atmos. Chem. Phys. 10, 10691-10704.

van der Laan-Luijkx, I.T., van der Velde, I.R., van der Veen, E., Tsuruta, A., Stanislawska, K., Babenhauserheide, A., Zhang, H.F., Liu, Y., He, W., Chen, H., Masarie, K.A., Krol, M.C., Peters, W. (2017) The CarbonTracker Data Assimilation Shell (CTDAS) v1.0: implementation and global carbon balance 2001–2015. Geosci. Model Dev. Discuss. 2017, 1-30.

van der Velde, I.R., Miller, J.B., Schaefer, K., van der Werf, G.R., Krol, M.C., Peters, W. (2014) Terrestrial cycling of $^{13}CO_2$ by photosynthes is, respiration, and biomass burning in SiBCASA. Biogeosciences 11, 6553-6571.

Varotsos, C.A., Tzanis, C.G., Sarlis, N.V. (2016) On the progress of the 2015–2016 El Niño event. Atmos. Chem. Phys. 16, 2007-2011.

Verdy, A., Dutkiewicz, S., Follows, M.J., Marshall, J., Czaja, A. (2007) Carbon dioxide and oxygen fluxes in the Southern Ocean: Mechanisms of interannual variability. Global Biogeochemical Cycles 21.

Wanninkhof, R., Asher, W.E., Ho, D.T., Sweeney, C., McGillis, W.R. (2009) Advances in Quantifying Air-Sea Gas Exchange and Environmental Forcing*. Annual Review of Marine Science 1, 213-244.

Watson, A.J., Naveira Garabato, A.C. (2006) The role of Southern Ocean mixing and upwelling in glacial-interglacial atmospheric CO_2 change. Tellus B 58, 73-87.

Weller, R., Levin, I., Wagenbach, D., Minikin, A., (2007) The Air Chemistry Observatory at Neumayer Stations (GvN and NM-II) Antarctica. Alfred Wegener Institute for Polar and Marine Research & German Society of Polar Research, Bremerhaven, pp. 39-46.

Weller, R., Schmidt, K., Teinilä, K., Hillamo, R. (2015) Natural new particle formation at the coastal Antarctic site Neumayer. Atmospheric Chemistry and Physics 15, 11399-11410.

Wenzel, S., Cox, P.M., Eyring, V., Friedlingstein, P. (2016) Projected land photosynthesis constrained by changes in the seasonal cycle of atmospheric CO_2. Nature 538, 499-501.

Wilson, P., (2012) Insight into the Carbon Cycle from Continuous Measurements of Oxygen and Carbon Dioxide at Weybourne Atmospheric Observatory, UK, School of Environmental Sciences. Univeristy of East Anglia, Norwich, p. 155.

Wolter, K., Timlin, M.S. (1998) Measuring the strength of ENSO events: How does 1997/98 rank? Weather 53, 315-324.

Wood, S. (2006) Generalized additive models: an introduction with R. CRC press.

Zachos, J., Pagani, M., Sloan, L., Thomas, E., Billups, K. (2001) Trends, Rhythms, and Aberrations in Global Climate 65 Ma to Present. Science 292, 686-693.

Zhou, L., Tucker, C.J., Kaufmann, R.K., Slayback, D., Shabanov, N.V., Myneni, R.B. (2001a) Variations in northern vegetation activity inferred from satellite data of vegetation index during 1981 to 1999. Journal of Geophysical Research: Atmospheres 106, 20069-20083.

Zhou, S., Miller, A.J., Wang, J., Angell, J.K. (2001b) Trends of NAO and AO and their associations with stratospheric processes. Geophysical Research Letters 28, 4107-4110.

Zickfeld, K., Fyfe, J.C., Eby, M., Weaver, A.J. (2008) Comment on "Saturation of the Southern Ocean CO_2 sink due to recent climate change". Science 319, -.

APPENDICES

Appendix A

UEA Atmospheric O_2 and CO_2 Observations at Halley Research Station, Antarctica

Operating Manual

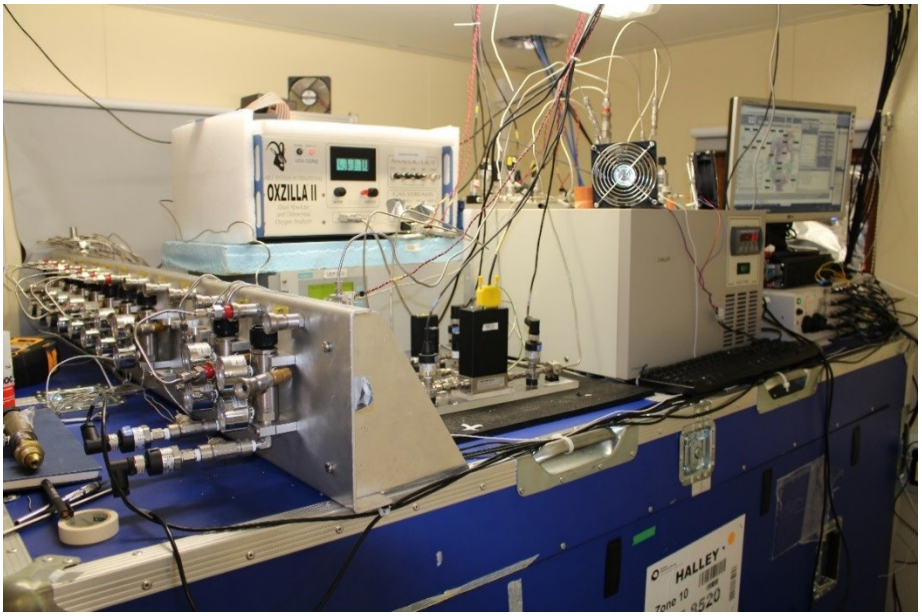

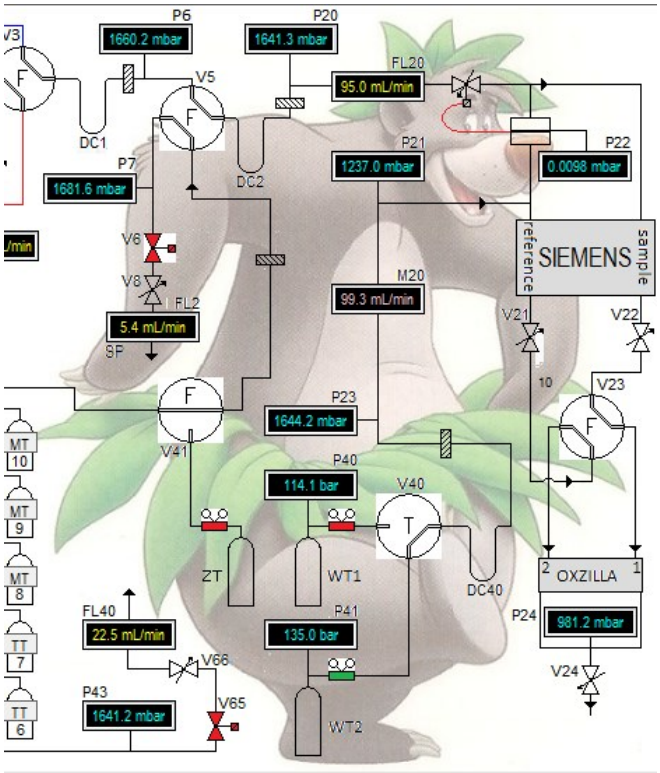

Welcome to Baloo! The only bear in Antarctica….

I have only included the title page of the User Manual here since it is a 48-page document that would be inappropriate to include at this stage. The full version can be found as a separate PDF document submitted with this thesis.

Appendix B .

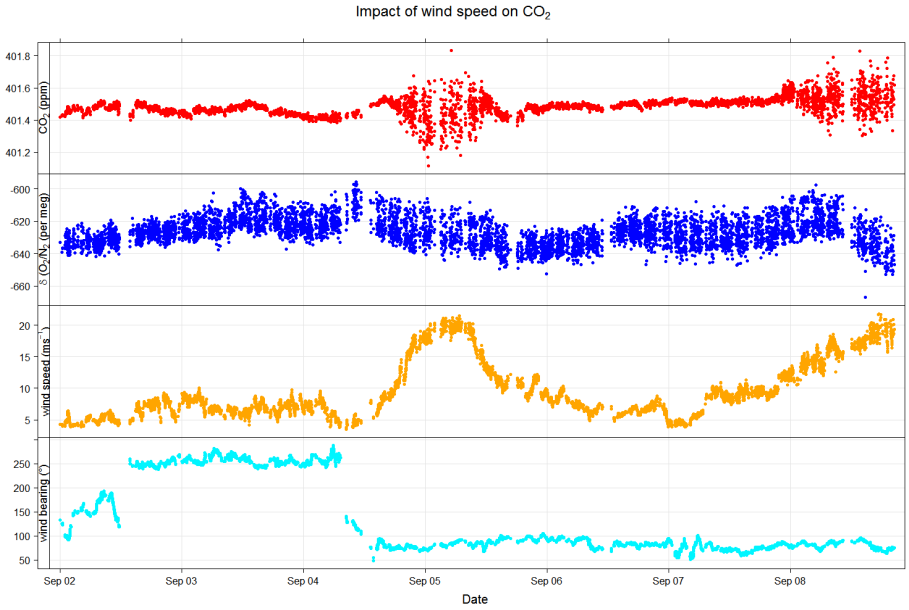

Figure 1.2. Example of the increase in variability of CO_2 when wind speeds was high (i.e. above 15 ms^{-1}. Top panel: CO_2; red points; Second panel: $\delta(O_2/N_2)$, blue points; Third panel: wind speed, orange points; Bottom panel: wind direction, turquoise points. The increase in CO_2 variability when the wind speed is high is believed to be a result of the oscillating of the suspended laboratory the measurement system is housed in, thereby impacting the stability of the laser inside the Siemens CO_2 analyser

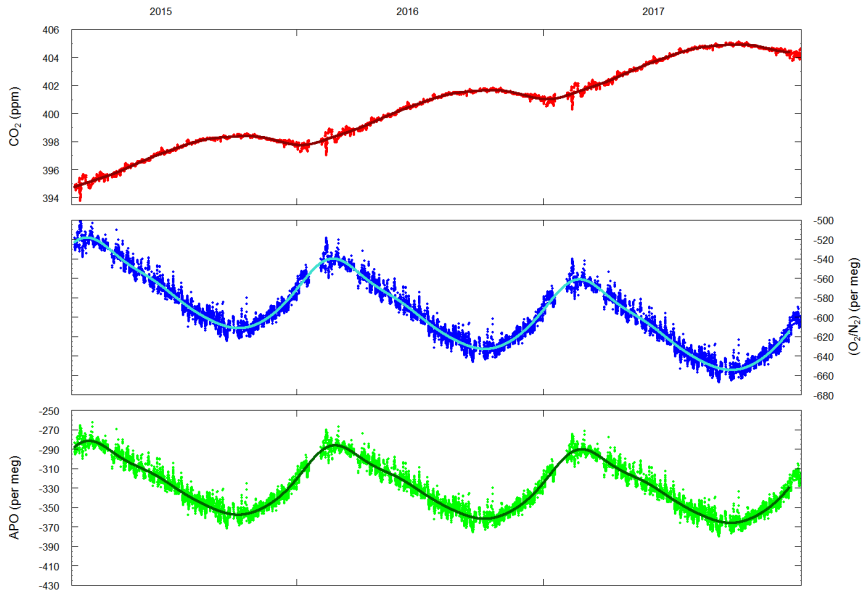

Figure 1.3. The HPspline curve fit to the replicated data observed at HBA. Real data is shown in 2016. Data in 2015 and 2017 are the 2016 data but with the assumed growth rates applied (either subtracted or added from the corresponding 2016 date. Top panel: CO_2 (red points) Hppline curve fit (dark red line). Middle Panel: $\delta(O_2/N_2)$ (blue points), HPspline curve fit (turquoise line). Bottom panel: APO (green points) HPspline curve fit (dark green line).

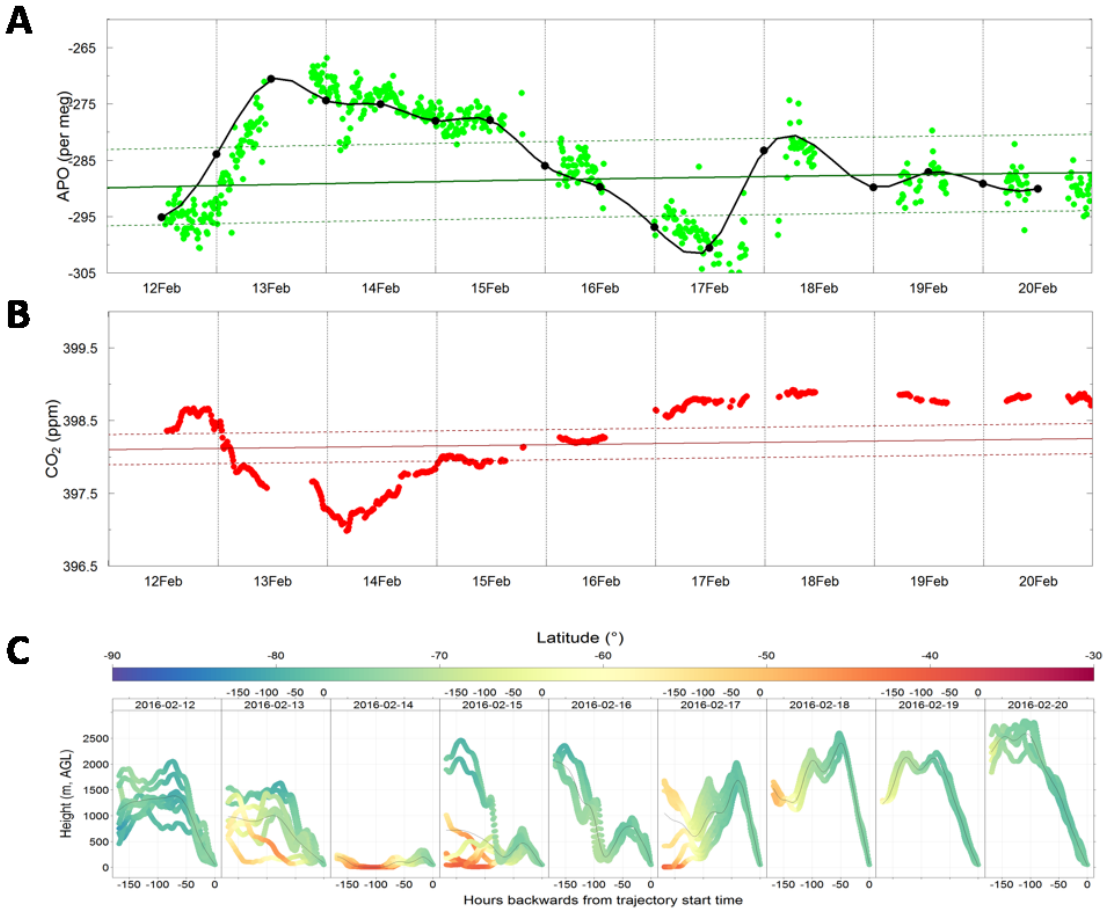

Figure 1.4. Example of a short-term, synoptic scale event observed at HBA during February 2016. A: APO (green points), black points represent 12 hourly means of the data and the dark black lines are a spline between the 12 hour points, shown to highlight the event. The dark green line represents the curve fit to the data, with the dashed green lines representing ± 1 σ standard deviation of the curve fit residuals. B. CO_2 (red points), the dark red line and dashed lines are as in in A, but for the CO_2 curve fit. C. Daily back trajectories generated by the Hysplit model; a total of 8 trajectories per day are visible (released every 3 hours) and trajectories run backwards for 7 days (or 168 hours; x-axis)). The y-axes represents the height of the trajectory at a particular time. Trajectories are coloured by the latitude as shown by the colour bar in the figure. The mean trajectory for each day is shown by the think black line in each panel

Figure 1.4. Example of a short-term, synoptic scale event observed at HBA during February 2016. A: APO (green points), black points represent 12 hourly means of the data and the dark black lines are a spline between the 12 hour points, shown to highlight the event. The dark green line represents the curve fit to the data, with the dashed green lines representing ± 1 σ standard deviation of the curve fit residuals. B. CO_2 (red points), the dark red line and dashed lines are as in in A, but for the CO_2 curve fit. C. Daily back trajectories generated by the Hysplit model; a total of 8 trajectories per day are visible (released every 3 hours) and trajectories run backwards for 7 days (or 168 hours; x-axis)). The y-axes represents the height of the trajectory at a particular time. Trajectories are coloured by the latitude as shown by the colour bar in the figure. The

mean trajectory for each day is shown by the think black line in each panel depicts the event observed in February within the APO and CO_2 observations. There is a positive excursion of APO that is mirrored by a negative excursion in CO_2 between the 12th and 15th of February. Back trajectories in **Figure 1.5**C show that during this event, air was being sampled from the surface (0-500m) at a relatively low latitude (40-50˚S).

In **Figure 1.5**, it is evident that the air mass originated over a productive area of the ocean at the lower latitudes mentioned, which would explain the higher APO O_2 emission from the ocean) and lower CO_2 (CO_2 uptake from the ocean).

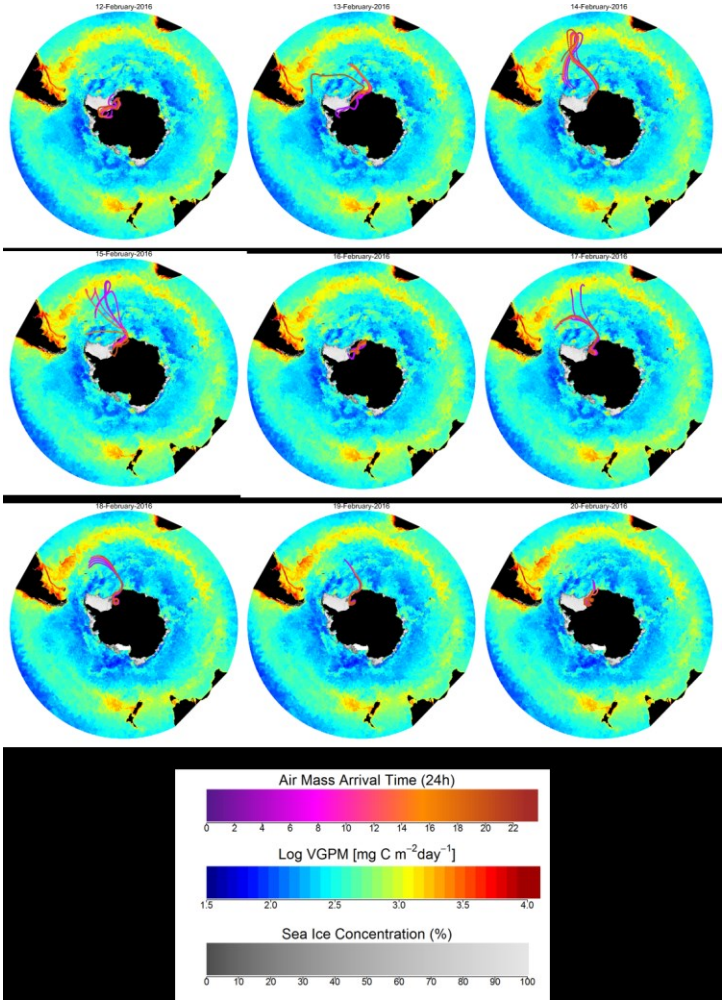

Figure 1.5. Progression of the event depicted in **Figure 1.4** as shown by the trajectory evolution (coloured by the time of the day) over a map of Net Primary Productivity from the Vertically Generalised Productive model of Behrenfeld and Falkowski (1997), based on satellite seaWifs chlorophyll concentration. Also shown is the sea-ice concentration from satellite data (Spreen et al., 2008). Colour bar scale for each are shown in the figure. Note the origin of trajectories on the 14th and 15th February.

Appendix C ..

C.1 Meteorological filtering of WAO data.

To assess whether meteorological filtering would be feasible for the WAO time series and for the purpose of this analysis, I performed a bivariate analysis of concentration data with respect to wind direction and time of day (Carslaw et al., 2006). The function to provide this analysis was provided by the OpenAir package (Carslaw and Ropkins, 2012) and is freely available in the open source R programming language. The analysis first de-seasonalises the data before taking mean mixing ratios/concentrations for the hour of the day and by wind direction. The results are shown in **Figure 1.6**

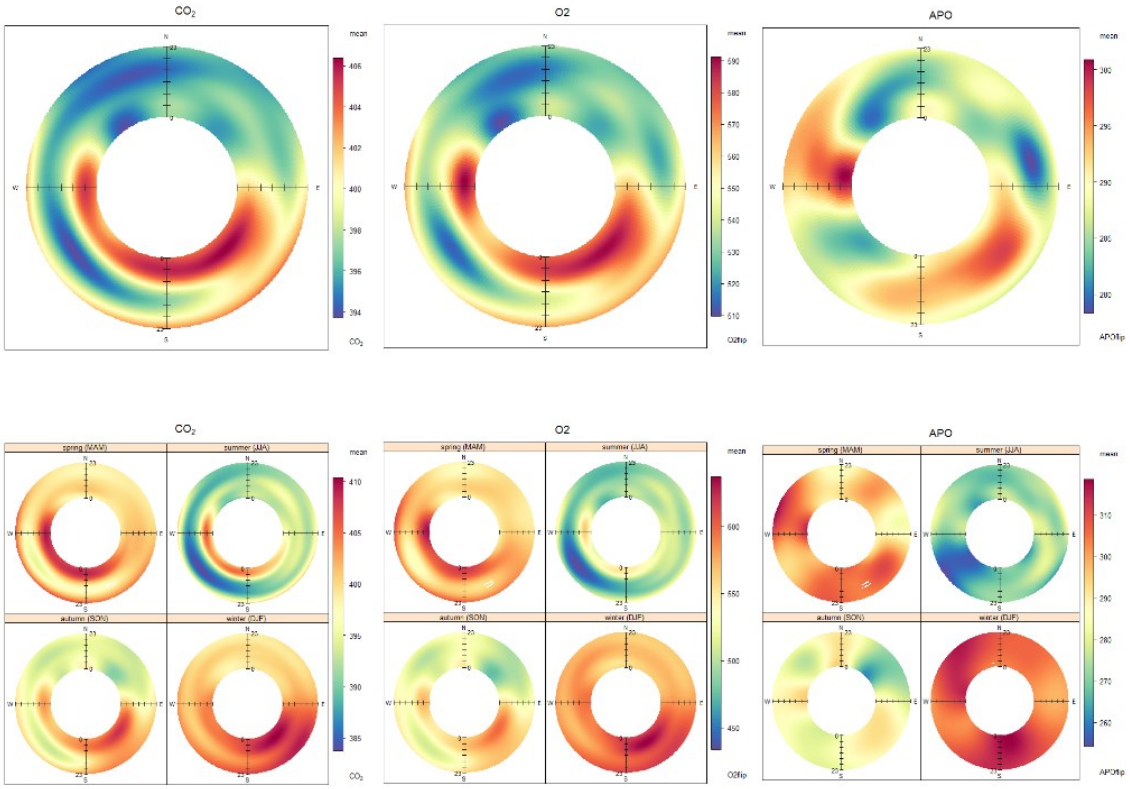

Figure 1.6. Bivariate analysis of concentration data with respect to wind direction and time of day at WAO. The top row represents the annual mean for each species, whilst the second row splits the data by season. O2 and APO data have been inverted (made positive), therefore depleted values are represented by red on the colour scale.

Figure 1.6 depicts a strong diurnal cycle in both CO_2 and O_2 when winds are derived from the south west. Since there is no diurnal change in APO, this strongly suggests the signal is from the local terrestrial biosphere. The south east quadrant however, is both depleted O_2, APO and elevated in CO_2, suggesting a local pollution source - likely to be the urban areas to the ESE, such as Sheringham and Cromer. Based on this analysis, clean background air for WAO could be defined as air arriving from the

NW-NE. Although wind direction is not necessarily an indication of air mass it is likely that air originated from the North, potentially the Arctic, with a large amount of time spent over the North Sea. If the goal was to derive "clean marine background air" (such as in Stephens *et al.* (2013)) then it would be adequate to select data only from the NW to NE sector. However, for the purpose of this analysis, I feel that this would unfairly bias the interpretation of the WAO measurements. Data from this sector represents only 24.8% of the data. The goal is to investigate and explain the patterns of CO_2, O_2 and APO measured at WAO, be they global, hemispheric, or regional. Therefore for this analysis, I have chosen not to perform any metrological filtering.

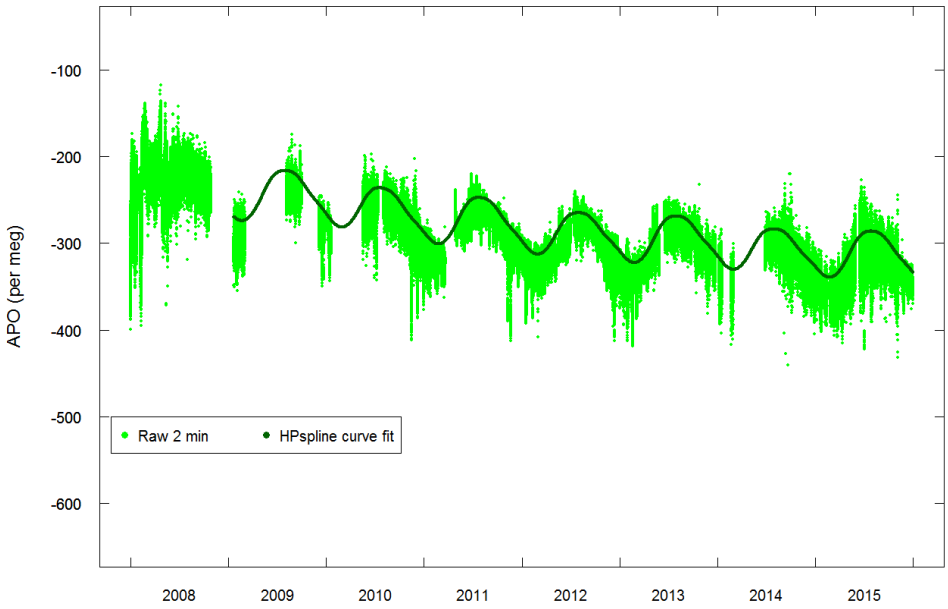

Figure 1.7. The HPspline curve fit (dark green points) against the raw 2 minute APO data at WAO (green points). Note how the curve does not represent baseline APO concentrations at different periods in the record.